

Design, Synthesis, and Evaluation of Dual Inhibitors of β -secretase and Acetylcholinesterase

THESIS

Submitted in partial fulfilment
of the requirements for the degree of

DOCTOR OF PHILOSOPHY

by

AMIT SHARMA

ID. No. 2019PHXF0050P

Under the Supervision of

PROF. HEMANT R. JADHAV

&

Co-supervision of

PROF. SANTOSH RUDRAWAR



BITS Pilani
Pilani | Dubai | Goa | Hyderabad

BIRLA INSTITUTE OF TECHNOLOGY & SCIENCE, PILANI

2024

***Dedicated to Almighty and
My Family!!***

DECLARATION

I hereby declare that the thesis work entitled “**Design, Synthesis, and Evaluation of Dual Inhibitors of β -secretase and Acetylcholinesterase**” is an original piece of research work carried out under the supervision of Prof. Hemant R. Jadhav and co-supervision of Dr. Santosh Rudrawar in the Department of Pharmacy, Birla Institute of Technology and Sciences (BITS PILANI), Pilani campus. This thesis has not been submitted by me for the award of any other degree of any other University/Institute.



Amit Sharma

2019PHXF0050P

Ph.D. Research scholar

BITS PILANI, Pilani campus

BIRLA INSTITUTE OF TECHNOLOGY AND SCIENCE, PILANI

CERTIFICATE

This is to certify that the thesis entitled “Design, Synthesis, and Evaluation of Dual Inhibitors of β -secretase and Acetylcholinesterase,” submitted by Amit Sharma, ID No 2019PHXF0050P for award of Ph.D. of the Institute, embodies original work done by him under my supervision.



Signature of the Supervisor:

Name in capital letters:

PROF. HEMANT R. JADHAV

Designation:

Professor,

Department of Pharmacy

Birla Institute of Technology and Science

Pilani, Pilani Campus

Signature of the Co-supervisor:

Name in capital letters:

PROF. SANTOSH RUDRAWAR

Designation:

Senior Lecturer

School of Pharmacy and Medical Sciences,

Griffith University, Gold Coast, Australia

ACKNOWLEDGEMENTS

Throughout my Ph.D. journey, I encountered a diverse range of experiences that encompassed numerous highs and lows, which I consider integral to the process of personal and academic refinement. The successful culmination of this doctoral dissertation owes much to the invaluable support extended by numerous individuals. I firstly thank almighty GOD for giving me the strength to fight and not letting me give up throughout my tenure. Another deepest gratitude towards my real god, i.e. my parents. Without the steadfast assistance of these individuals, this achievement would not have been possible.

First and foremost, I would like to express sincere gratitude to my supervisor Prof. Hemant R Jadhav, Department of Pharmacy, Birla Institute of Technology and Science, Pilani and my co-supervisor Dr. Santosh Rudrawar, School of Pharmacy and Medical Science, Institute for Glycomics, Griffith University for providing me an excellent platform to pursue research under their skilled guidance. We have achieved our expected research goals; in addition to this, they helped me become a good human being. They never spooned me with the procedures but surely helped me to develop the skills to solve the problems. They always given us the freedom to carry research, and I really appreciate it. I am grateful for their persistent counsels throughout the duration of my research work. Under their guidance, I have immensely improved my research aptitude and teaching skills and their diligent approach has always kept me motivated to work harder. I would also like to thank them, for encouraging me to attend international conferences, which gave me opportunities to acquire more knowledge and interact with eminent scientists and researchers working in our field of interest, which will be extremely helpful in future endeavours.

I am grateful to Prof. V. Ramgopal Rao (Vice-Chancellor, BITS, Pilani), Prof. Sudhir Kumar Barai (Director, BITS Pilani, Pilani Campus), Prof. Souvik Bhattacharyya (Former Vice-Chancellor, BITS, Pilani), Prof. Ashoke K. Sarkar (Ex-Director, BITS Pilani, Pilani Campus), Prof. S. K. Verma (Dean, Administration), and Prof. Shamik Chakraborty (Associate Dean, AGSRD) for their academic administration support of this research work. Besides my advisor, I would like to thank my Doctoral Advisory Committee members Prof. S. Murugesan (Ex. Head, Department of Pharmacy) and Prof. Atish T. Paul (Ex. Head, Department of Pharmacy). Their insightful comments and suggestions always broaden the perspectives related to research.

My whole-hearted gratitude to, Prof. Anil Gaikwad (Head, Department of Pharmacy), Dr. Anil Jindal, (Convener, Departmental Research Committee, Department of Pharmacy, BITS Pilani, Pilani Campus), Prof. R. Mahesh (Ex. Dean, Faculty affairs division) for their support and encouragement.

My sincere thanks to Prof. Rajeev Taliyan, Dr. Deepak Chitkara, Dr. Anupama Mittal, Dr. Gautam Singhvi, Dr. Aniruddha Roy, Dr. Murali Manohar Pandey, Dr. Sandeep Sundriyal, Dr. Richa Shrivastava and Dr. Vaibhav A. Dixit for their encouragement throughout my association with Department of Pharmacy, BITS, Pilani.

I always believe that good friends always have a great influential role in my life, and I thankful for all the moments spent with my friends-cum-batchmates Dr. Prashant S. Auti, Mr. Mukesh, Dr. Atharva Bhide, Ms. Manisha Chaudhary, Dr. Ajinath Kale, Mr. Shivam Kumar Vyas, Ms. Reena, Mr. Sai Bhargava, Mr. Ravi Kant, Ms. Shreya Das, Mrs. Nisha Yadav, Mrs. Sriravali, Dr. Kavya Shree and Dr. Sharyu Kesarwani etc.

Also, another true relation, without her I can't imagine my life in BITS, thank you so much my better half Mrs. Propanna B. Sharma, who came as a friend and became my life partner. Really thank you to stand positively as a pillar in every situation. Thank you is really not enough for her support.

True energetic senior-cum-friends, Mr. Imran K. Ansari, Dr. Rupesh Jain, Dr. Samrat Majumdar, Dr. Saurabh Sharma, Dr. Amritansh Bhanot, Dr. Sudeep Pukale, Dr. Rajesh Pradhan and Dr. Ginson George who were always there to look towards me. Thank you all for supporting me in research activities and for taking care of me.

I would like particularly to acknowledge the contribution of my lab senior Dr. Pankaj Wadhwa for his kind support and friendly gesture.

I am extremely lucky to have a great company of research scholars of the Department of pharmacy and chemistry. It was a great opportunity to observe and learn a lot from them and I sincerely acknowledge to all.

I am thankful to the administrative staff, Mr. Tarachand Saini, Mr. Puran Singh, Mr. Vikas Kumar Agrawal, Mr. Laxman Kumar, Mr. Ram Suthar, Mr. Naveen Rana, Mr. Mahender, Mr. Abhishek and Mr. Sandeep Ruidas for their continuous support.

AMIT SHARMA

Table of Contents

Content	Title	Page No.
	<i>Certificate</i>	
	<i>Acknowledgements</i>	<i>iii-iv</i>
	<i>List of Figures</i>	<i>vi- viii</i>
	<i>List of Tables</i>	<i>ix- x</i>
	<i>List of Schemes</i>	<i>xi</i>
	<i>List of Abbreviations and Symbols</i>	<i>xii-xiv</i>
Chapter 1	Introduction	1-68
Chapter 2	Objective of the work	69-72
Chapter 3	Materials and Methods	73-82
Chapter 4	Results and Discussion	83-181
Chapter 5	Summary and Conclusion	182-186
Chapter 6	References	187-203
	<i>List of publications</i>	205
<i>Appendixes</i>	<i>List of Workshops/ Symposium attended</i>	206
	<i>Brief Biographies</i>	207-208

List of Figures

S.No.	Title	Page
Fig. 1	Pathogenesis of AD summarizing the central role of amyloid beta plaques	3
Fig. 2	The cholinergic hypothesis of AD with their reported inhibitors	5
Fig. 3	Effect of normal synaptic transmission and long-term potentiation of the glutamatergic network in the brain	6
Fig. 4	Amyloid plaques interacting with ghrelin receptors	8
Fig. 5	USFDA-approved therapy for improving cognitive symptoms	10
Fig. 6	Downstream events of APP cleavage and therapeutic options being explored	11
Fig. 7	A few representative β -Secretase inhibitors for AD	18
Fig. 8	Structures of some of the representative dual inhibitors	27
Fig. 9	Structures of some of the representative multi-target-directed ligands	31
Fig. 10	Important considerations in the design of dual inhibitors	56
Fig. 11	Design strategy using molecular hybridization approach	71
Fig. 12	Docking validation of 4EY7 and 6UWP (A) Redocked pose of Donepezil (red) in 4EY7 (AChE) superimposed on the co-crystallized ligand (yellow) (RMSD: 0.14 Å, Glide score: -14.56 Kcal/mol); (B) Redocked pose of QKA (red) in 6UWP (BACE 1) superimposed on the co-crystallized ligand (green) (RMSD: 0.08Å, Glide score: -9.64 Kcal/mol)	84
Fig. 13	(A) and (B) show overlapping of all of the docked compounds within the active site of 4EY7 and 6UWP, respectively	85
Fig. 14	(A) 2D interaction plot of compound 1h in AChE (Glide score-12.26 kcal/mol); (B) 2D interaction plot of compound 1h in BACE 1 (Glide score-8.03 kcal/mol)	87
Fig. 15	(A) 2D interaction plot of compound 2o in 4EY7 (Glide score-12.59 kcal/mol); (B) 2D interaction plot of compound 2o in BACE 1 (Glide score-7.94 kcal/mol)	89

S.No.	Title	Page
Fig. 16	(A) 2D interaction plot of compound 3l in 4EY7 (Glide score-11.47 kcal/mol); (B) 2D interaction plot of compound 3l in BACE 1 (Glide score-9.87 kcal/mol)	90
Fig. 17	(A) and (B) show overlapping of all of the docked compounds within the active site of 4EY7 and 6UWP, respectively	98
Fig. 18	(A) 2D interaction plot of compound 4o in AChE (Glide score -11.08 kcal/mol); (B) 2D interaction plot of compound 4o in BACE 1 (Glide score -10.98 kcal/mol)	101
Fig. 19	(A) 2D interaction plot of compound 5f in 4EY7 (Glide score -11.05 kcal/mol); (B) 2D interaction plot of compound 5f in BACE 1 (Glide score -7.87 kcal/mol)	102
Fig. 20	(A) 2D interaction plot of compound 6q in 4EY7 (Glide score -12.05 kcal/mol); (B) 2D interaction plot of compound 6q in BACE 1 (Glide score -6.89 kcal/mol)	104
Fig. 21	Molecular dynamics studies of 3l -AChE (4EY7) docked complex. [A] Comparative RMSD of AChE (protein backbone) and compound 3l in the protein-ligand complex throughout the simulation period of 100 ns. [B] Graphical representation showing protein RMSF throughout the simulation period of 100 ns. [C] Histogram showing interaction fractions with active amino acid residues. [D and E] Timeline representation showing interaction with all the amino acid residues at each time frame	176
Fig. 22	Molecular dynamics studies of 3l -BACE 1 (6UWP) docked complex [A] Comparative RMSD of BACE 1 (protein backbone) and compound 3l in the protein-ligand complex throughout the simulation period of 100 ns. [B] Graphical representation showing protein RMSF throughout the simulation period of 100 ns. [C] Histogram showing interaction fractions with active amino acid residues; [D, E] Timeline representation showing interaction with all the amino acid residues at each time frame	178

S.No.	Title	Page
Fig. 23	Molecular dynamics studies of compound 4o -AChE (4EY7) docked complex. [A] Comparative RMSD of AChE (protein backbone) and compound 4o in the protein-ligand complex throughout the simulation period of 100 ns. [B] Graphical representation showing interactions with active site amino acid residues of PAS and CAS; [C] Histogram showing interaction fractions with active amino acid residues; [D and E] Timeline representation showing interaction with all the amino acid residues at each time frame	180
Fig. 24	Molecular dynamics studies of compound 4o -BACE 1 (6UWP) docked complex. [A] Comparative RMSD of BACE 1 (protein backbone) and compound 4o in the protein-ligand complex throughout the simulation period of 100 ns. [B] Graphical representation showing interactions with active site amino acid residues (Aspartate dyad); [C] Histogram showing interaction fractions with active amino acid residues; [D, E] Timeline representation showing interaction with all the amino acid residues at each time frame	181

List of Tables

S.No.	Title	Page
Table 1	Important events in developing the amyloid cascade hypothesis and practical implementations	4
Table 2	A β -targeting small molecules in clinical trials	11-14
Table 3	List of α - Secretase activators/enhancers in clinical trials	15-16
Table 4	γ -Secretase inhibitors for AD in clinical trials	19-21
Table 5	Clinically approved small molecule-based chelating agents in metal chelation therapy	21-22
Table 6	Drugs under clinical trial for AD treatment	31-53
Table 7	<i>In silico</i> docking results of Series-I derivatives	85-86
Table 8	<i>In silico</i> docking results of Series-II derivatives	87-88
Table 9	<i>In silico</i> docking results of Series-III derivatives	89-90
Table 10	Interactions of the representative compounds in the active site of BACE 1 (6UWP)	91-92
Table 11	Interactions of the representative compounds in the active site of AChE (4EY7)	92-93
Table 12	<i>In silico</i> Predicted Drug-likeness and ADME characteristics of series-1 as determined by QikProp	94-96
Table 13	<i>In silico</i> Predicted Drug-likeness and ADME characteristics of series-II as determined by QikProp	96-97
Table 14	<i>In silico</i> Predicted Drug-likeness and ADME characteristics of series-III as determined by QikProp	97-98
Table 15	<i>In silico</i> docking results of Series-IV (4a-4z, 4aa-4af) derivatives	99-100
Table 16	<i>In silico</i> docking results of Series-V (5a-x) derivatives	101-102
Table 17	<i>In silico</i> docking results of Series-VI (6a-u) derivatives	103-104
Table 18	Interactions of the representative compounds in the active site of BACE 1 (6UWP)	105-107
Table 19	Interactions of the representative compounds in the active site of AChE (4EY7)	107-110
Table 20	<i>In-silico</i> Predicted Drug-likeness and ADME characteristics of series-IV as determined by QikProp	110-111

S.No.	Title	Page
Table 21	<i>In-silico</i> Predicted Drug-likeness and ADME characteristics of Series-V as determined by QikProp	112
Table 22	<i>In-silico</i> Predicted Drug-likeness and ADME characteristics of Series-VI as determined by QikProp	113
Table 23	Inhibitory potential of compounds 1a-1a , 1aa-1ak (Series I) against AChE and BACE 1	161-163
Table 24	Inhibitory activities of compounds 2a-2y (Series-II) against AChE and BACE 1	163-165
Table 25	Inhibitory activities of compounds 3a-3s (Series-III) against AChE and BACE 1	165-166
Table 26	Inhibitory activities of compounds 4a-4z , 4aa-4af (Series-IV) against AChE and BACE 1	169-171
Table 27	Inhibitory activities of compounds 5a-5x (Series-V) against AChE and BACE 1	171-172
Table 28	Inhibitory activities of compounds 6a-6u (Series-VI) on AChE and BACE 1	173-174

List of Schemes

S.No.	Title	Page
Scheme 1	Synthesis of series-I,II,III analogues (1a-1z, 1aa-1ak), (2a-2y), (3a- 3s)	77
Scheme 2	Synthesis of series-IV,V,VI analogues (4a-4z, 4aa-4af), (5a-5x), (6a-6u)	79

List of Abbreviations and Symbols

°C	degree centigrade
µl	micro liters
AChE	Acetylcholinestrase
AD	Alzheimer's disease
ADAM	A Disintegrin and Metalloprotease domain protein
AICD	APP Intracellular Domain
Ala	Alanine
Aph-I	Anterior Pharynx-I
ApoE	Apolipoprotein E
APP	Amyloid Precursor Protein
Arg	Arginine
Asn	Asparagine
Asp	Aspartic acid
Aβ	Amyloid-β peptide
BACE 1	Beta site APP Cleaving Enzyme- 1
CNS	Central Nervous System
CSF	Cerebrospinal Fluid
Cys	Cysteine
Da	Dalton
DAPT	<i>N</i> -[<i>N</i> -(3,5-difluorophenacetyl)- <i>L</i> -alanyl]- <i>S</i> -phenylglycine t-butyl ester
DCM	Dichloromethane
DRAP	Down's Region Aspartic Protease
EDC-HCl	<i>N</i> -(3-Dimethylaminopropyl)- <i>N</i> '-ethylcarbodiimide hydrochloride
EtOH	Ethanol
Ex/Em	Excitation/Emission
FAD	Familial Alzheimer's disease
FBDD	Fragment-based Drug Discovery
FRET	Fluorescence Resonance Energy Transfer
GSK	Glaxosmithkline
HBA	Hydrogen Bond Acceptor

HBD	Hydrogen Bond Donor
HE	Hydroxyethylene
HOBt	Hydroxybenzotriazole
hr	hour
HTS	High-Throughput Screening
i.v.	Intravenous
IC ₅₀	Concentration at which there is 50% inhibition
IR	Infra Red
kcal	kilocalorie
LE	Ligand Efficiency
Leu	Leucine
LogP	Log partition coefficient
Lys	Lysine
MCI	Mild Cognitive Impairment
Met	Methionine
mg	Milligram
ml	Milli Litres
mM	Milli Moles
MM2	Molecular Mechanics 2
mol	Mole
MP	Melting Point
MR	Molar Refractivity
MW	Molecular Weight
Na ₂ CO ₃	Sodium Carbonate
NaHCO ₃	Sodium Bicarbonate
NaNO ₂	Sodium Nitrite
NaOH	Sodium Hydroxide
Nct	Nicestrin
NFTs	Neurofibrillary Tangles
NMDA	<i>N</i> -methyl-D-aspartate
NMR	Nuclear Magnetic Resonance
NSAID	Non-Steroidal Anti-Inflammatory Drugs
OPLS	Optimized Potentials for Liquid Simulations

PDAPP	PDGF Promoter Expressing Amyloid Precursor Protein
PDB	Protein Data Bank
Pen-2	Presenilin Enhancer-2
Phe	Phenylalanine
PKC	Protein Kinase C
ppm	Part Per Million
PS	Presenilin
PSA	Polar Surface Area
RMSD	Root Mean Square Deviation
SAR	Structure Activity Relationship
SnCl ₂	Stannous chloride
Sol	Solubility
TACE	Tumour Necrosis Factor-Alpha Converting Enzyme
TEA	Triethylamine
Tg	Transgenic
TGN	Trans-Golgi network
THF	Tetrahydrofuran
Thr	Threonine
TLC	Thin Layer Chromatography
TM	Transmembrane
TMS	Trimethylsilane
Tyr	Tyrosine
Val	Valine
WHO	World Health Organization
XP	Extra Precision
GSK	Glaxosmithkline
HBA	Hydrogen Bond Acceptor
HBD	Hydrogen Bond Donor
HE	Hydroxyethylene
HOBt	Hydroxybenzotriazole
hr	hour
HTS	High-Throughput Screening
i.v.	Intravenous

CHAPTER 1. INTRODUCTION

1. Introduction

1.1. Alzheimer's disease

AD is a progressive neurodegenerative condition, particularly in those 65 years or older, and is a leading cause of dementia [1]. It gradually erodes cognitive abilities and interpersonal engagement due to brain cell degeneration. As of 2023, about 55 million people worldwide have dementia, with AD accounting for 60-70% of these cases. By 2050, this number is expected to reach 139 million due to the aging global population. Females are at a higher risk of AD. In India, over 4 million individuals have various forms of dementia, with Alzheimer's as the most widespread type [2].

A century since AD's discovery, the disease's precise pathogenesis remains elusive and not fully comprehended. A combination of factors, encompassing the abnormal folding and aggregation of proteins, frequently associated with oxidative stress and the generation of free radicals, result in AD [3]. Further, bioenergetics, irregularities in mitochondrial function, and neuroinflammation processes are involved in its complications. Understanding these factors, aided by the latest research on AD pathogenesis, has laid the foundation for research into potential treatments. However, the absence of animal models accurately mirroring the human AD pathogenesis remains a significant hurdle [4]. Given the multifaceted nature of the disease, concentrating solely on one causative factor has proven ineffective or comparatively less impactful. Also, designing selective drugs that target causative factors is a significant challenge. Developing multi-target directed ligands (MTDLs) is another challenge, as it can lead to various side effects [5]. Biologicals have also been explored, such as Aducanumab and Lecanemab, which are the sole approved disease-modifying drugs for Alzheimer's. These human monoclonal antibodies are specifically designed to target aggregated beta-amyloid proteins found in the brain lesions associated with AD. Other available treatments, mainly cholinergic drugs such as galantamine, rivastigmine, and donepezil, primarily focus on managing symptoms, as the degeneration of brain cells in Alzheimer's is irreversible. The inability to reverse brain cell damage remains a significant task in Alzheimer's therapy [6].

1.2. Pathogenesis of AD

AD has been linked to various symptoms and pathological features that include the formation of neurofibrillary tangles (NFTs) within brain cells, the accumulation of amyloid- β ($A\beta$) in the form of senile plaques, increased oxidative stress, inflammation within neurons, and a decline in the acetylcholine, etc. The interplay and precise sequence of events leading to the disease are still under active investigation. A comprehensive understanding

of AD's pathogenesis is crucial for the development of effective treatments and interventions for this devastating condition [7]. The following are the proposed hypotheses based on the current understanding of AD (**figure 1**).

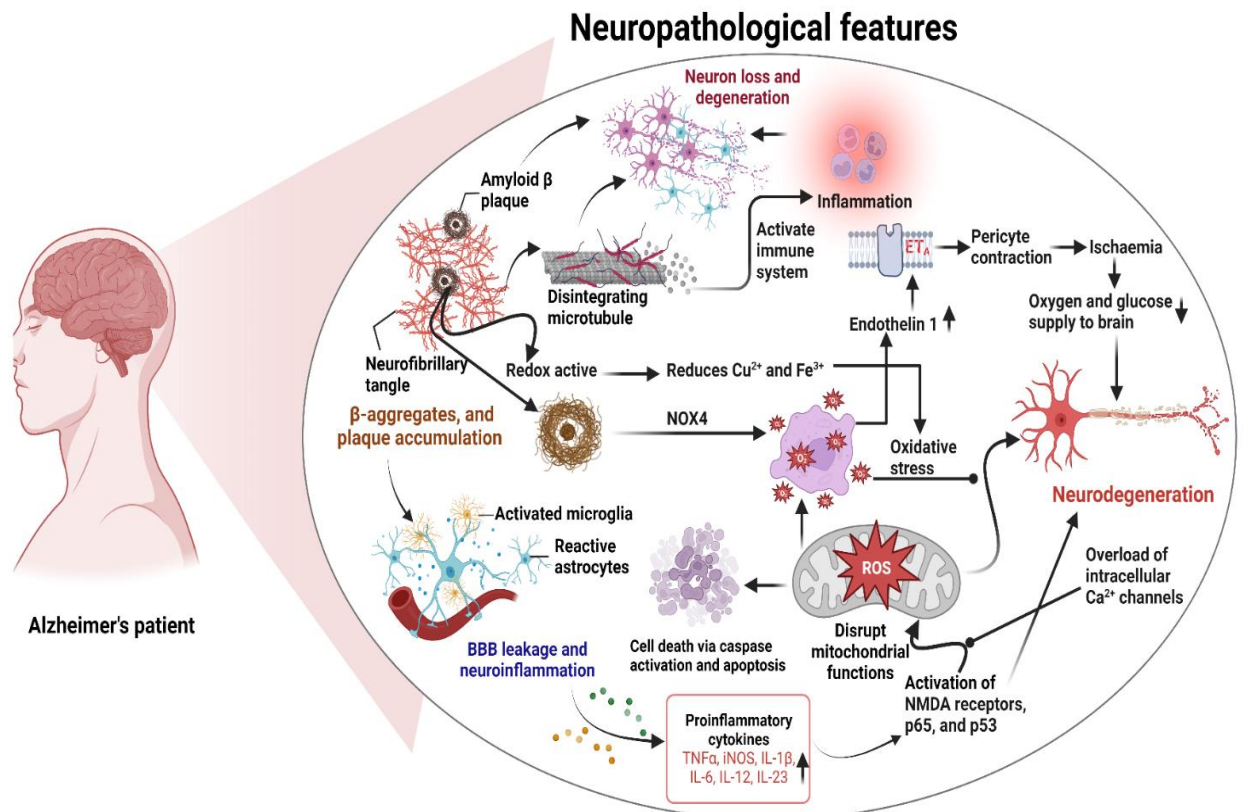


Figure 1: Pathogenesis of AD summarizing the central role of amyloid beta plaques

1.2.1 The amyloid hypothesis

The widely accepted hypothesis for AD is the amyloid-cascade pathway, centered around the Amyloid Precursor Protein (APP). Under normal conditions, amyloid precursor protein (APP) is cleaved by α -secretase, followed by γ -secretase, yielding harmless fragments [8]. In AD, cleavage by β -secretase (BACE 1) followed by γ -secretase leads to the formation of amyloid β ($A\beta$) peptides, which aggregate and accumulate as extracellular plaques. $A\beta$ is a hallmark of AD and comprises 37 to 43 amino acids, with the isoform $A\beta_{42}$ being the most problematic. β -amyloid peptides aggregate into plaques, triggering inflammation, brain damage, synaptic dysfunction, and Tau protein hyperphosphorylation, leading to neurofibrillary tangle formation (**figure 1**) [9]. BACE 1 is a key target for therapies aiming to reduce amyloid plaque production to slow AD progression [10]. The important milestones in the development of the amyloid cascade hypothesis and its practical utilization are presented in **Table 1**.

Table 1. Important events in developing the amyloid cascade hypothesis and practical implementations [11].

Year	Key research findings
1906	Senile plaques were first established.
1984	Amyloid β protein ($A\beta$) was isolated as the principal constituent found within the plaques in the brains of individuals with AD.
1987	The observation that the formation of $A\beta$ resulted from the processing of amyloid precursor proteins.
1990	Evidence of the neurotoxic properties of $A\beta$ aggregates was presented.
1992	The hypothesis of the amyloid cascade was put forward.
1995	AD patients exhibit a significant decrease in CSF $A\beta_{42}$ levels, revealing an established connection between $A\beta$ and inflammation.
1997	The discovery of the ability of $A\beta_{42}$ to inhibit Long-Term Potentiation
1998	The primary instigator of neuronal damage was identified as $A\beta$ oligomers.
2001	Evidence was provided to establish a connection between $A\beta$ and the formation of neurofibrillary tangles.
2004	The inaugural amyloid PET tracer, Pittsburgh compound-B (PIB), was formulated.
2016	Light therapy led to a reduction in $A\beta$ accumulation in both animal models of AD and patients.
2017	The transfer of $A\beta$ from the periphery through the blood-brain barrier into the brain is reported.
2018	The ultrasensitive technology, Simoa, was devised for quantifying $A\beta$ at sub-femtomolar concentrations.
2021	Aducanumab became the inaugural FDA-approved medication for diminishing $A\beta$ plaques.
2023	FDA approval has been granted to Lecanemab for the treatment of AD.

1.2.2 The Tau (τ) protein hypothesis

The τ -protein is essential for microtubule stabilization, provides structural support, aids axonal transport, and promotes neuronal growth. Senile plaques trigger τ -protein hyperphosphorylation, leading to its aggregation with cytoskeletal proteins and reduced microtubule interaction. It elevates free τ -protein levels, promoting self-aggregation and fibril formation. Consequently, axonal transport is impaired, resulting in axonal

degeneration due to disruption of nutrient transport. The compromised neurons eventually form neurofibrillary tangles (NTs), contributing to neurodegeneration (Figure 1) [12].

1.2.3 The cholinergic deficit hypothesis

The cholinergic hypothesis posits that AD progression is primarily linked to the loss of cholinergic neurons and reduced acetyltransferase activity, resulting in decreased acetylcholine (ACh) (**Figure 2**). As per the hypothesis, loss of limbic and neocortical cholinergic innervations due to neurofibrillary degeneration in the basal forebrain and associated loss of cholinergic neurotransmission results in decreased cognitive function. This degeneration primarily affects memory and cognition-related regions, like the hippocampus and frontal cortex, leading to compromised choline uptake, impaired ACh release, receptor imbalances, and disrupted neurotrophin support [13].

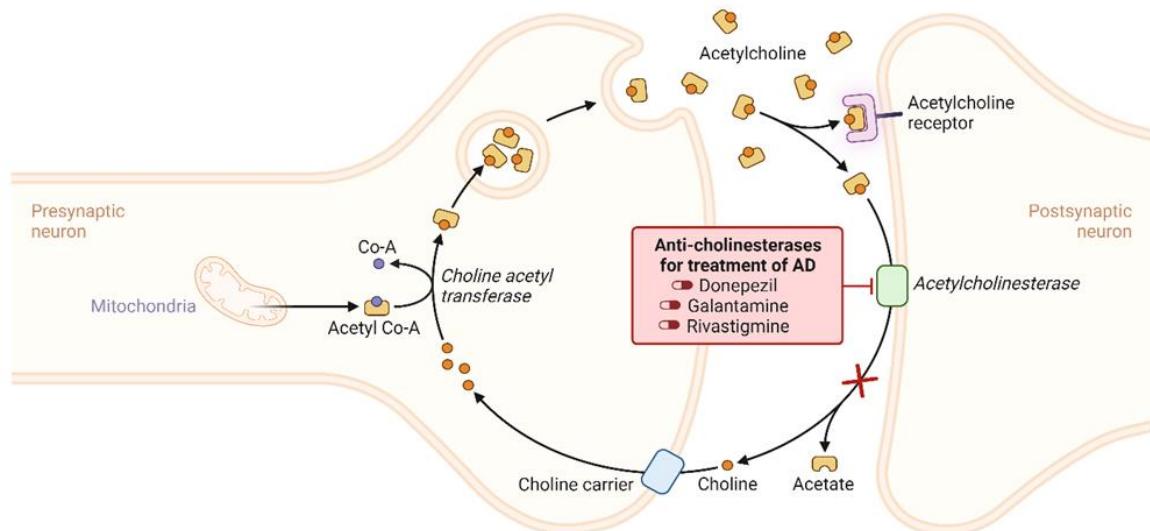


Figure 2. The cholinergic hypothesis of AD with their reported inhibitors

1.2.4 Adrenergic hypothesis

In advanced AD, significant degeneration of noradrenergic neurons occurs in the locus coeruleus (LC), with a 30% loss during the transition to amnesic mild cognitive impairment (MIC) and an additional 25% reduction in AD progression. AD patients display variable adrenergic receptor expression, including decreased $\alpha 1$ adrenergic receptors ($\alpha 1$ ARs) in the prefrontal cortex, hippocampus, and cerebellar hemisphere. Also, increased $\alpha 1$ AR binding sites in specific layers, decreased $\alpha 2$ adrenergic receptors ($\alpha 2$ ARs) in the nucleus basalis of Meynert, reduced $\beta 1$ adrenergic receptors ($\beta 1$ ARs) in the cortex, and increased $\beta 2$ adrenergic receptors ($\beta 2$ ARs) in the cortex and hippocampus. The role of beta-adrenergic receptor alterations in AD is still controversial. However, clinical investigations indicate that

Amyloid beta peptide ($A\beta$) initiates subtle modifications in synaptic function during AD. Specifically, $A\beta$ interacts with $\beta 2$ adrenergic receptors within the central noradrenergic system, influencing synaptic functions in prefrontal cortical neurons. This interaction leads to the internalization and degradation of $\beta 2$ -adrenergic receptors, subsequently impairing adrenergic and glutamatergic activities and impacting cognitive function in AD [14]

1.2.5 Glutamatergic hypothesis

Glutamatergic networks in the hippocampal regions are essential for cognitive function, with N-methyl D-aspartate receptors (NMDARs) playing a pivotal role in synaptic strength and long-term potentiation (LTP) crucial for memory. AD patients exhibit lower levels of vesicular glutamate transporters (VGLUT-1 and VGLUT-2) in the prefrontal cortex, indicating disrupted glutamatergic synapses. Soluble $A\beta$ oligomers further disrupt glutamatergic networks, inhibiting LTP and inducing NMDAR hyperactivation. It also causes activation of ligand-gated or ionotropic glutamate receptors (iGluRs), predominantly the α -amino-3-hydroxy-5-methyl-4-isoxazolepropionic acid (AMPA) receptor subtype. The excess NMDAR activity raises intracellular Ca^{++} levels, triggering nitric oxide synthesis, free radical generation, oxidative stress (OS), apoptosis, and excitotoxic neuronal death. These changes further the AD pathogenesis caused by $A\beta$ plaques by disrupting synaptic plasticity and neuronal function [15]. **Figure 3** illustrates the effect of normal synaptic transmission and long-term potentiation of the glutamatergic network in the brain.

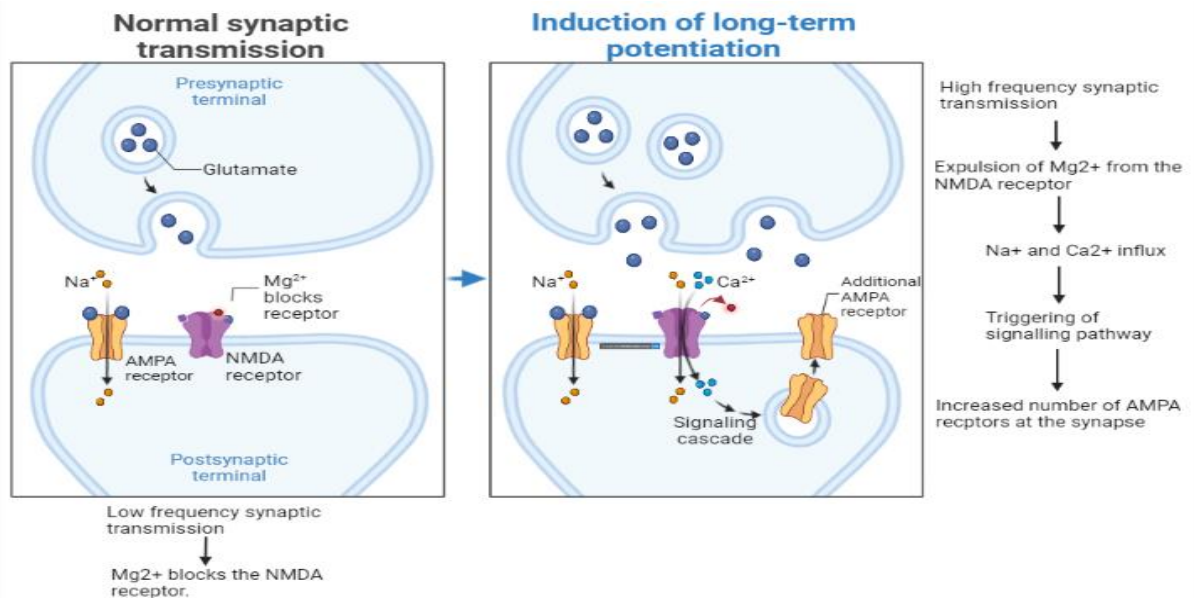


Figure 3. Effect of normal synaptic transmission and long-term potentiation of the glutamatergic network in the brain

1.2.6 Calcium homeostasis hypothesis

Calcium serves as a crucial intracellular messenger and is important in vital physiological processes. Its precise control relies on complex mechanisms, with mitochondria and the endoplasmic reticulum (ER) playing central roles. ATPase Ca^{2+} pumps and the $\text{Na}^{+}\text{-Ca}^{2+}$ exchanger aid calcium efflux, while the ER membrane facilitates calcium exchange. Disruptions in these processes can lead to harmful intracellular calcium buildup, triggering protein cleavage, oxidative stress, energy disruption, and activation of proteins like β -amyloid and τ -protein. $\text{A}\beta$ exacerbates calcium overload in AD by inducing oxidative stress and membrane pore formation, linking calcium dysregulation to AD pathology (**figure 1**) [16].

1.2.7 Oxidative stress hypothesis

Neurodegenerative disorders often involve an imbalance between reactive oxygen species (ROS) generation and antioxidant availability, resulting in cellular damage. AD exhibits disturbances in antioxidant enzyme activity, driven by $\text{A}\beta$'s activation of NMDA receptors, which fosters ROS production. OS also contributes, in turn, to increased $\text{A}\beta$ production and aggregation, as well as τ -protein hyperphosphorylation and polymerization (**figure 1**) [17].

1.2.8 Microgliosis

Microglia are the immune cells residing within the brain and are activated by β -amyloid plaques (**figure 1**). Upon activation, microglial cells release pro-inflammatory mediators, ROS, proteases, and complements, and secondly, as a defense mechanism, break down amyloid plaques. Though clusters of microglial cells gather around β -amyloid plaques, these are unable to break down the plaques effectively. This phenomenon, referred to as "frustrated phagocytosis," contributes to neurodegenerative alterations [18].

1.2.9 Metal chelation hypothesis

β -amyloid precipitates at low Zn^{+2} concentrations, Cu^{+2} and Fe^{+3} enhance aggregation, especially at slightly acidic pH (6.8). Elevated Cu^{+2} and Zn^{+2} levels in Alzheimer's patients are linked to apoE4 allele induction. β -amyloid also possesses redox activity, reducing Cu^{+2} and Fe^{+3} , generating H_2O_2 , leading to ROS formation, exacerbating the pathology (**figure 1**) [19].

1.2.10 Prion-like behavior of plaques

Prions are self-propagating proteins linked to neurodegenerative disorders like Creutzfeldt–Jakob disease (CJD), Gerstmann–Sträussler–Scheinker syndrome (GSS), and fatal familial insomnia (FFI) [44]. $\text{A}\beta$ takes on a pathogenic conformation akin to prions, spreading in a cross-synaptic manner from specific brain regions. Tau protein also follows the same pattern

with initially formed neurofibrillary tangles (NFTs), which are linked to cognitive decline [20].

1.2.11 Ghrelin/GHSR1 α signaling

GHSR1 α , the ghrelin receptor in the hippocampus, regulates learning and memory through unique signaling involving Ca²⁺/calmodulin-dependent protein kinase II (CaMKII) and dopamine receptor D1 (DRD1). AD involves early hippocampal damage, possibly related to GHSR1 α loss, leading to synaptic stress and memory problems. AD patients have been reported to have increased hippocampal GHSR1 α , possibly as an A β defense mechanism (figure 4) [21].

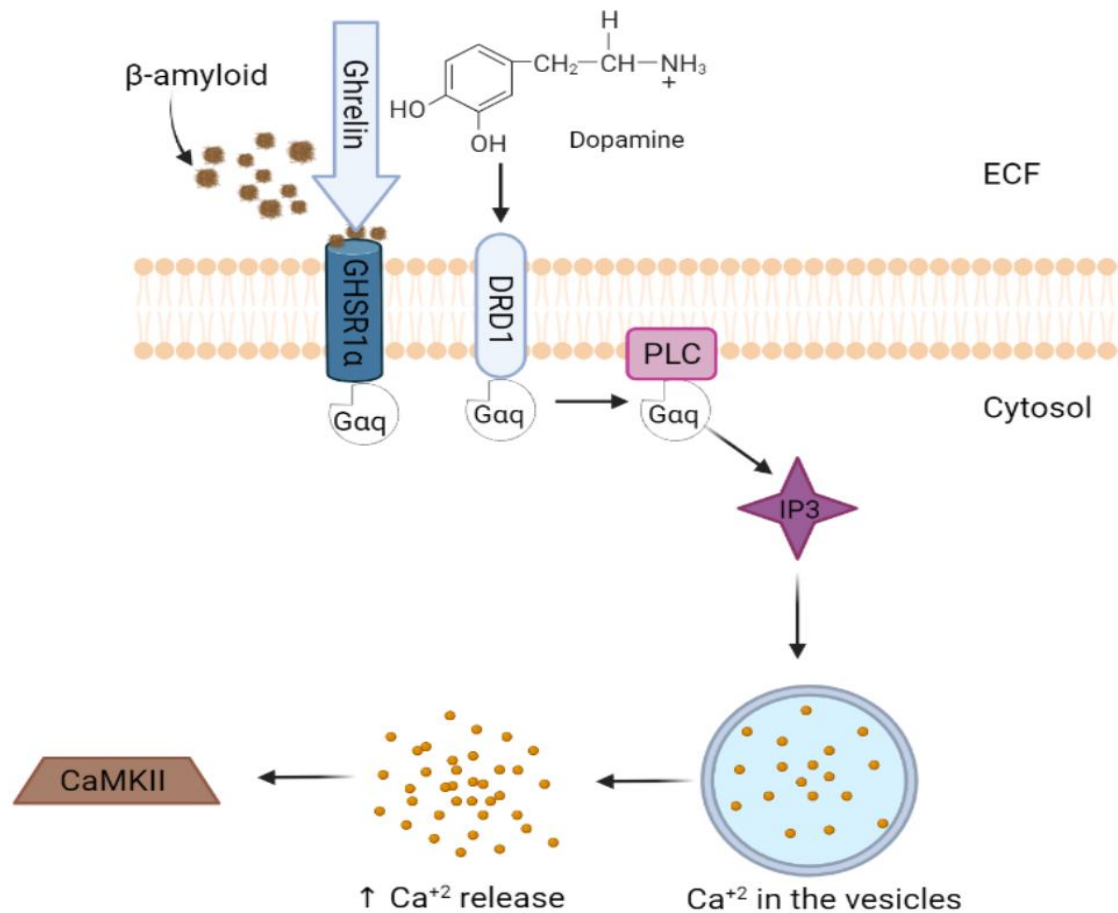


Figure 4. Amyloid plaques interacting with ghrelin receptors

1.2.12 Cerebral capillaries constriction

Cerebrovascular disorders can lead to brain function alterations, and early signs of AD include angiogenesis damage and reduced cerebral blood flow. AD patients exhibit abnormal capillary constriction. Animal studies showed that introducing exogenous A β can lower cerebral blood flow in rats, triggering A β production. A β presence generates ROS via

NOX, releasing endothelin (ET), which contracts pericytes via ETA receptors. This contraction causes pericyte necrosis, sustaining capillary constriction and resulting in ischemia. Crucially, A β oligomers are central to this complex process, linking vascular dysfunction to AD pathology (**figure 1**) [22].

2. Therapeutic approaches for the treatment of AD

2.1 Current therapeutic strategies

The current treatment options for AD are focused on preventing disease progression via monoclonal antibodies and on providing symptomatic relief to the patients.

2.1.1 Drugs that may change disease progression

Aducanumab and Lecanemab are anti-amyloid antibodies that remove amyloid plaques from the brain. Aducanumab was approved by the US- Food and Drug Administration (USFDA) in 2021 for mild cognitive impairment or mild dementia of Alzheimer's. However, it has not been approved in Europe due to a lack of strong evidence of its efficacy. It is an IgG1 antibody binding to the A β at amino acids 3–7. Lecanemab also acts on amyloid plaques, albeit differently, by inhibiting aggregated soluble and insoluble forms of A β peptide with high selectivity to A β protofibrils. US-FDA approved it in July 2023 for patients with early Alzheimer's disease. The common side effects of these antibodies include amyloid-related imaging abnormalities (ARIA), which can lead to swelling and bleeding in the brain, as well as swelling of the face, headaches, infusion-related reactions, and vision changes [23-26].

2.1.2 Drugs that may mitigate some of the symptoms of the disease

2.1.2.1 Cognitive Symptoms

These alleviate memory and thinking symptoms without affecting the progression of the disease. They offer temporary relief by targeting neurotransmitters or receptors, enhancing patient comfort, dignity, and independence. These include cholinesterase inhibitors (donepezil, galantamine, and rivastigmine) and the NMDA receptor antagonist memantine (**figure 5**). Cholinesterase inhibitors preserve acetylcholine levels, which decline in AD and contribute to cognitive loss [27]. Memantine blocks excessive glutamate receptor activation, preventing neuronal death caused by glutamate excess. These medications address cognitive symptoms and temporarily improve AD patients' quality of life. The cholinesterase inhibitors have been approved for use in mild to severe dementia due to Alzheimer's, whereas memantine is approved for moderate to severe dementia. A combination of donepezil with memantine is also approved for moderate to severe dementia due to Alzheimer's [28-29].

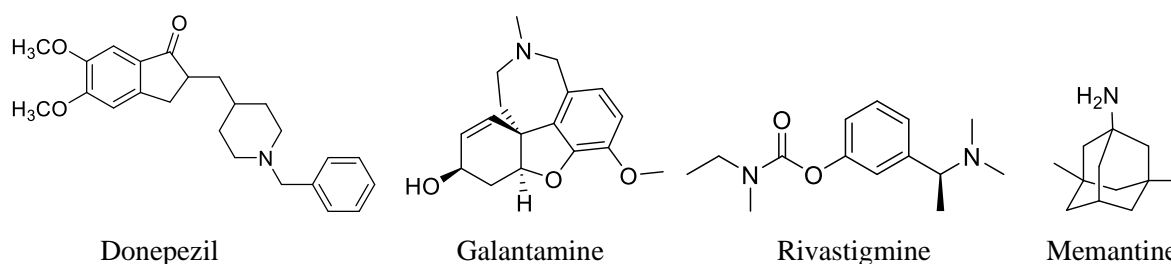


Figure 5: USFDA-approved therapy for improving cognitive symptoms [30]

2.1.2.2 Non-cognitive (behavioral and psychological) symptoms

In AD patients, sleep changes such as difficulty in sleeping, taking longer daytime naps, changes in sleep cycle, etc, may aggravate mood swings. Suvorexant, a potent dual orexin receptor (OXR1 and OXR2) antagonist, is recommended for treating sleep changes in AD patients. It promotes sleep by binding to the receptors and blocking the binding of orexin A and B, neuropeptides that promote wakefulness, to the receptors. Recently, Suvorexant has been found to decrease tau phosphorylation and A β in humans [31].

2.2 Therapeutic strategies based on hypotheses proposed

AD drug development aims at disease modification or symptom management by targeting A β and Tau protein [32]. Developing new central nervous system (CNS) drugs is challenging but vital to finding more effective AD treatments [57]. Most of the drugs that reached phase II trials failed to show promising results in phase III, like BIIB092, Crenezumab, TRx0237, Azeliragon, Verubecestat, Atabecestat, BI 409306, etc [33]. The following section discusses various therapeutic options based on the understanding of proposed hypotheses and also lists developmental candidates, particularly in clinical trials.

2.2.1 A β -based approach

Targeting A β with vaccines and antibodies is a promising approach for halting AD progression, exemplified by the recent entry of monoclonal antibodies into the market and ongoing clinical trials [34]. **Figure 6** illustrates the downstream events of APP processing and the possible therapeutic interventions being considered for drug development. Some small molecules targeting A β peptide for AD treatment are in clinical trials (**Table 2**).

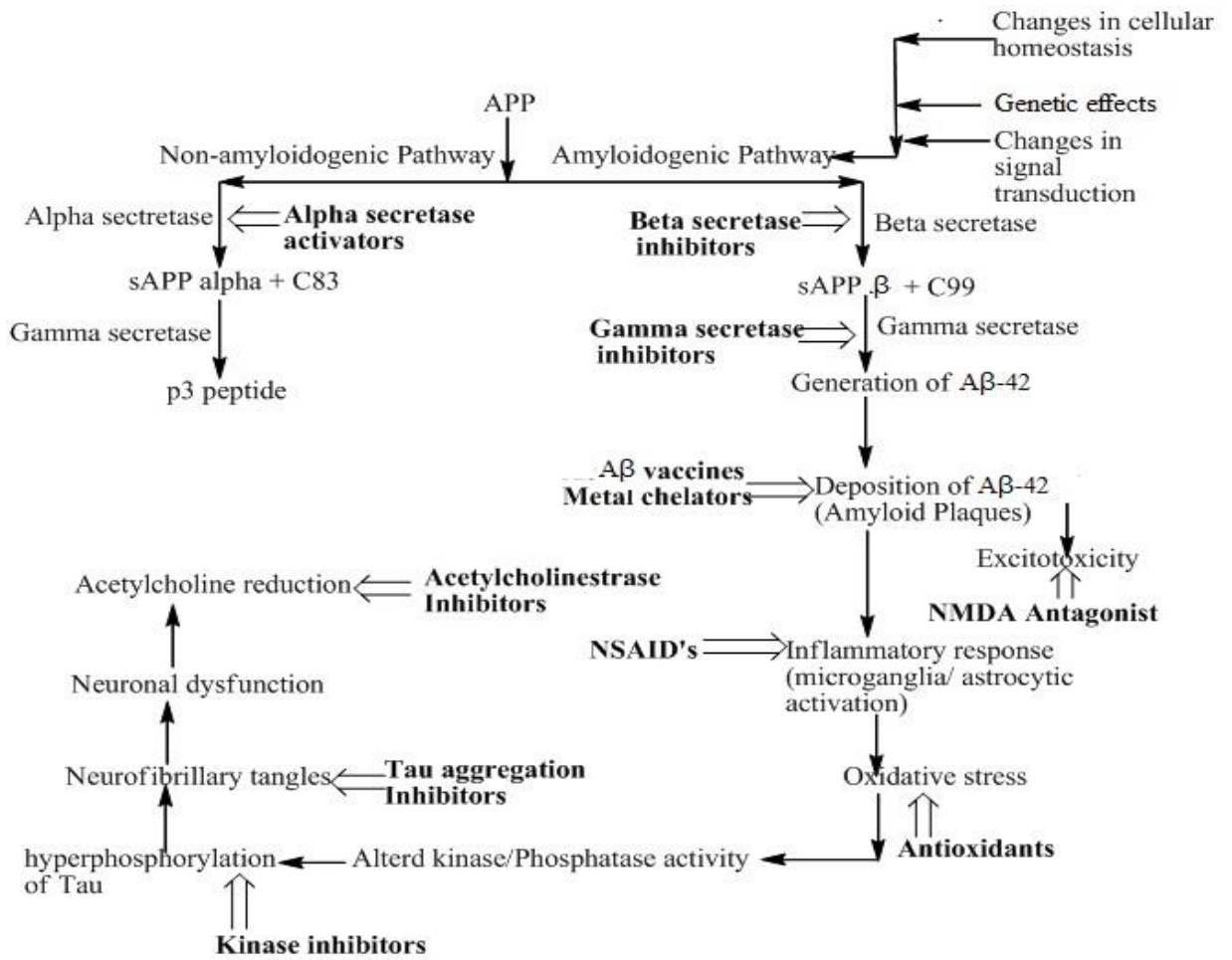
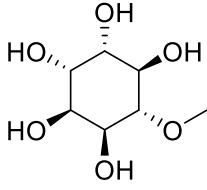
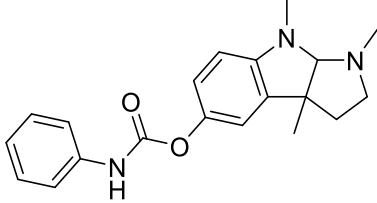
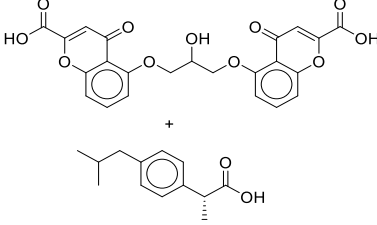
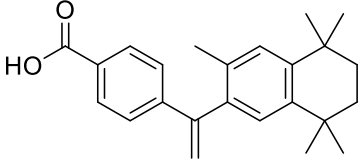
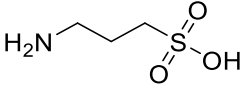
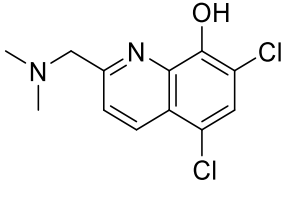
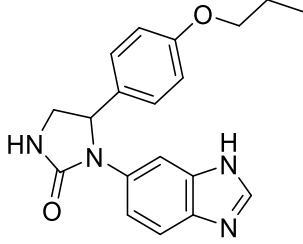
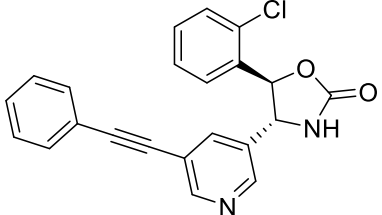


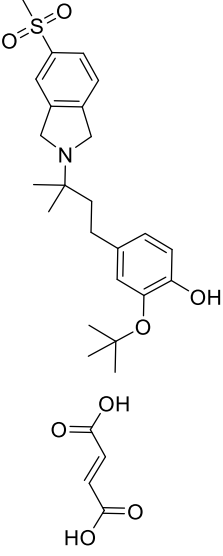
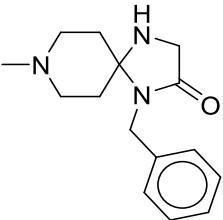
Figure 6: Downstream events of APP cleavage and therapeutic options being explored

Table 2. Aβ-targeting small molecules in clinical trials (<https://clinicaltrials.gov/>)

Drug Name	Structure	Mode of Action	Route	Status	Reference
Acitretin	<chem>CC1=C(C)C(=C(C)C=C1C/C=C/C/C=C/C/C=C/C(=O)O)OC</chem>	Reduces Aβ generation	Oral	Phase II	[35]
Lenalidomide	<chem>NC1=CC=C2C(=C1)C(=O)N2C3CC(=O)NCC3=O</chem>	BACE1 inhibitor	Oral	Phase II	[36]
Levetiracetam	<chem>CC[C@H](C(=O)N)N1CCOC1=O</chem>	Reduce Aβ generation	Oral	Phase II	[37]

<p>NIC5-15 (1R,2S,3R,4S,5S,6S)-6-methoxy cyclohexane-1,2,3,4,5-pentaol</p>		<p>Modulator of γ-secretase</p>	<p>Oral</p>	<p>Phase II</p>	<p>[38]</p>
<p>Posiphen</p>		<p>Hinders the translation of the APP</p>	<p>Oral</p>	<p>Phase II</p>	<p>[39]</p>
<p>ALZT-OP1 [Cromolyn + (R)-Ibuprofen]</p>		<p>Facilitate the elimination of $A\beta$ or its aggregates</p>	<p>Oral</p>	<p>Phase III</p>	<p>[40]</p>
<p>Bexarotene</p>		<p>Facilitate the elimination of $A\beta$ or its aggregates</p>	<p>Oral</p>	<p>Phase II</p>	<p>[41]</p>
<p>ALZ-801 3-aminopropane-1-sulfonic acid</p>		<p>Disrupt or hinder the formation of $A\beta$ aggregates</p>	<p>Oral</p>	<p>Phase II</p>	<p>[42]</p>
<p>Contraloid</p>	<p>Peptide (all D enantiomeric) sequence: PTLHTHNRRRRR</p>	<p>Terminates toxic and replicating amyloid beta ($A\beta$) oligomer prions by disassembling aggregates into non-toxic $A\beta$ monomers</p>	<p>Oral</p>	<p>Phase I</p>	<p>[43]</p>

<p>PBT2 5,7-dichloro-2- ((dimethylamino) methyl)quinolin- 8-ol</p>		<p>Decreasing metal- facilitated Aβ aggregation.</p>	<p>Oral</p>	<p>Phase II</p>	<p>[44]</p>
<p>Varoglutamstat</p>		<p>Prevents the formation of a particularly toxic and aggregation- prone variant of Aβ known as pGlu-Aβ.</p>	<p>Oral</p>	<p>Phase II</p>	<p>[45]</p>
<p>ALX-001 (4R,5R)-5-(2- chlorophenyl)-4- (5- (phenylethynyl)p yridin-3- yl)oxazolidin-2- one</p>		<p>Designed to block the pathogenic binding of toxic amyloid-β oligomers and cellular prion protein to glutamate receptor</p>	<p>Oral</p>	<p>Phase II</p>	<p>[46]</p>

<p>CT1812 2-(tert-butoxy)-4-(3-methyl-3-(5-(methylsulfonyl)isoindolin-2-yl)butyl)phenol fumarate</p>		<p>Prevents the interaction between oligomeric Aβ and its receptors, leading to a reduction in synaptic toxicity caused by Aβ</p>	<p>Oral</p>	<p>Phase I</p>	<p>[47]</p>
<p>Nasal insulin</p>	<p>Restructuring of synapses and utilization of glucose</p>		<p>Intranasal</p>	<p>Phase III</p>	<p>[48]</p>
<p>Simufilam</p>		<p>Diminishes tau buildup, decreases neuroinflammation</p>	<p>Oral</p>	<p>Phase III</p>	<p>[49]</p>

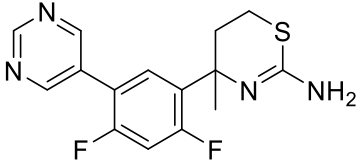
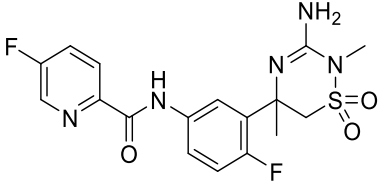
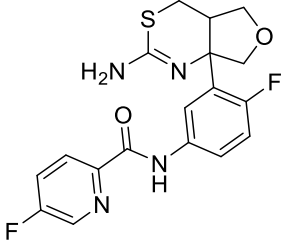
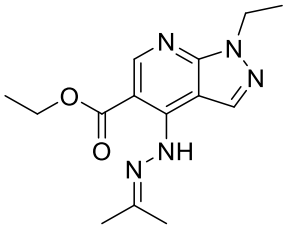
2.2.2 Secretase inhibitors

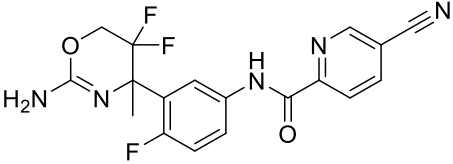
Secretases are a group of proteolytic enzymes responsible for processing APP. Three key secretases, namely α -secretase, γ -secretase, and β -secretase, are involved in this process. In healthy conditions, APP undergoes cleavage by α - and γ -secretases. However, the cleavage pattern in AD involves β - and γ -secretases [50].

α -secretase:

Activation of α -secretase is represented by the metalloprotease ADAM10, which cleaves APP within the A β domain, inhibiting A β generation and yielding neuroprotective APP fragments. Therefore, α -secretase cleavage of APP is beneficial by impeding the formation of A β peptides and protecting against neurotoxic agents. It has led to the proposal of enhancing α -secretase activity as a treatment strategy to shift the balance towards the nonamyloidogenic pathway, potentially influencing the progression of AD (**Table 3**) [51].

Table 3. List of α - Secretase activators/enhancers in clinical trials [52].

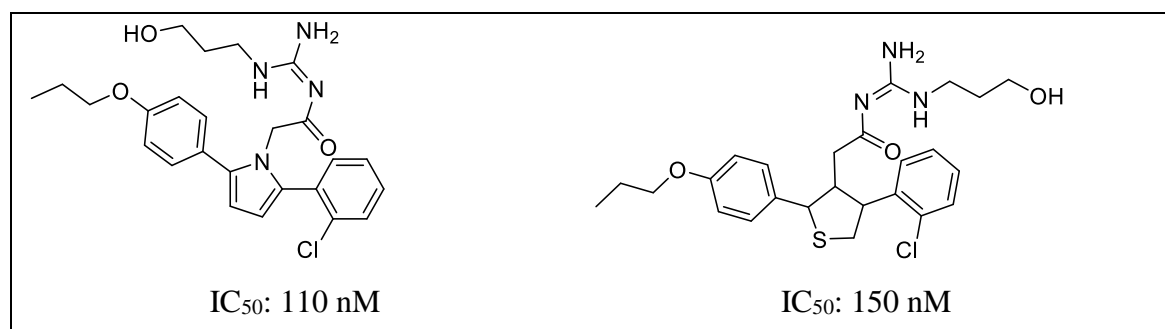
Compound Name	Structure	Status
LY2811376 4-(2,4-difluoro-5-(pyrimidin-5-yl)phenyl)-4-methyl-5,6-dihydro-4H-1,3-thiazin-2-amine		Phase I
MK-8931 N-(3-(3-amino-2,5-dimethyl-1,1-dioxido-5,6-dihydro-2H-1,2,4-thiadiazin-5-yl)-4-fluorophenyl)-5-fluoropicolinamide		Phase I
LY2886721 N-(3-(2-amino-4a,5-dihydro-4H-furo[3,4-d][1,3]thiazin-7a(7H)-yl)-4-fluorophenyl)-5-fluoropicolinamide		Phase I
Etazolate		Phase II

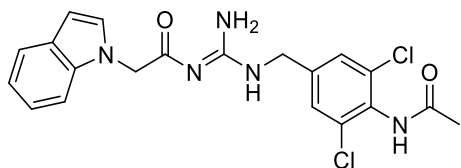
<p>AZ-4217</p> <p>N-(3-(2-amino-5,5-difluoro-4-methyl-5,6-dihydro-4H-1,3-oxazin-4-yl)-4-fluorophenyl)-5-cyanopicolinamide</p>		<p>Phase II</p>
<p>APH1105</p>	<p>A bryostatin analog</p>	<p>Phase II</p>

β -secretase:

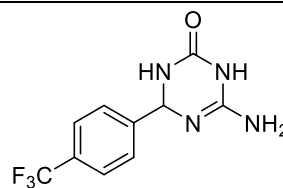
The 1999 discovery of β -secretase (BACE) was pivotal in AD research, identified independently by five research groups using various names like BACE, β -secretase, Asp2, or memapsin 2 [53]. BACE, a type 1 transmembrane aspartic protease with 501 amino acids, functions optimally under low pH conditions in intracellular compartments. It is predominantly expressed in brain neurons, and modulating its expression directly impacts A β production [54]. BACE's discovery led to the identification of its homolog, BACE2. Still, due to its low expression in brain neurons and distinct APP cleavage activity, BACE1 remains the main β -secretase, a potential therapeutic target to reduce cerebral A β levels in AD [55].

Despite several drugs developed to inhibit BACE activity, such as elenbecestat, atabecestat, lanabecestat, and verubecestat, failing to reach the market, researchers remain committed to the pursuit of BACE-inhibitory drugs due to the critical role it has in the disease development [56]. The structures of some of the representative β -Secretase inhibitors are given in **Figure 7**, indicating the use of various scaffolds.

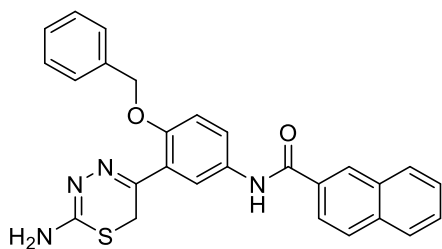




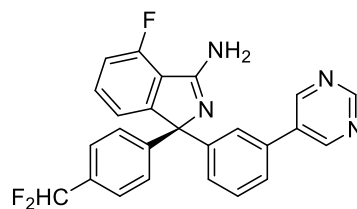
IC₅₀: 0.079 μM



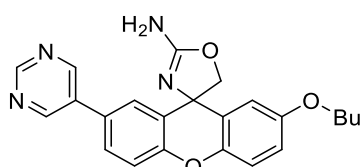
IC₅₀: 18.03 μM



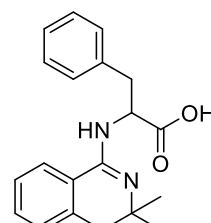
IC₅₀: 9.9 μM



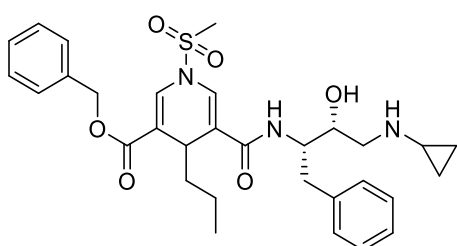
IC₅₀: 26 nM



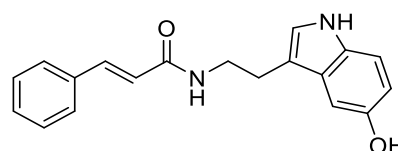
IC₅₀: 8 nM



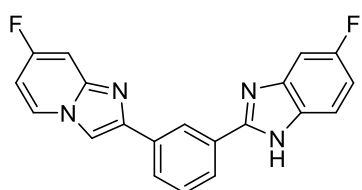
IC₅₀: 27.2 μM



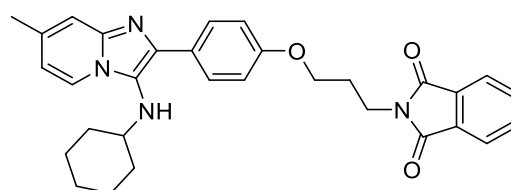
IC₅₀: 8.1 μM



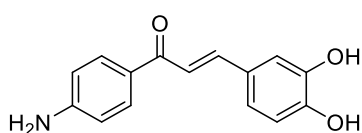
IC₅₀: 86.7 μM



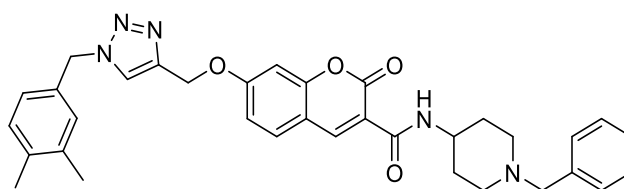
IC₅₀: 18.0 nM



IC₅₀: 2.84 μM



IC₅₀: 17.7 μM



IC₅₀: 21.13 μM

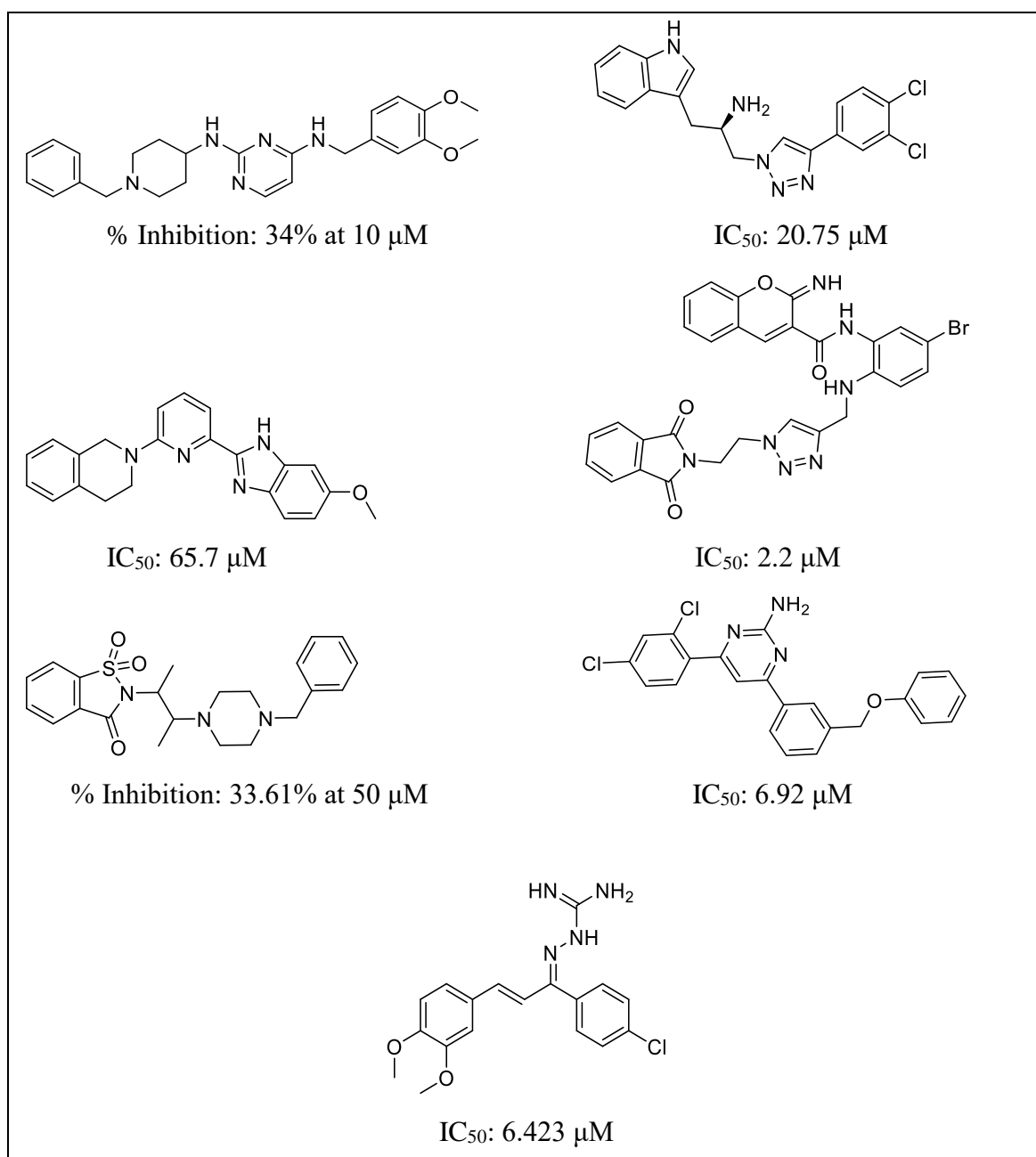


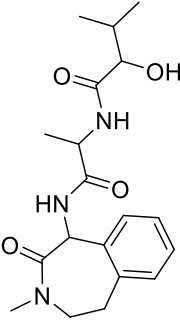
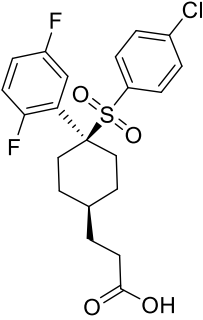
Figure 7. A few representative β -Secretase inhibitors for AD [57,58].

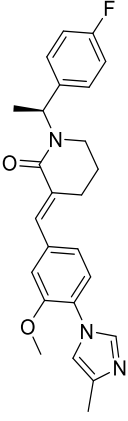
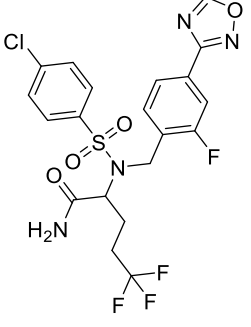
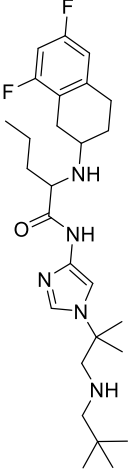
γ -secretase:

γ -secretase, composed of Presenilin-I (PS-I), Nicastrin, Anterior Pharynx-I, and Presenilin enhancer-2, plays a pivotal role in AD as it executes the final intramembrane cleavage of APP [59]. γ -secretase cleavage, which follows cleavage by α -secretase, yields the C99 fragment, leading to a minor fraction of A β -42. Mutations in presenilins, the catalytic core of γ -secretase, contribute to elevated A β -42 levels in familial AD (FAD). However, γ -secretase influences other substrates like Notch, Delta, and Tumor necrosis factor-alpha converting enzyme (TACE) [60]. Targeting γ -secretase to reduce A β formation is

challenging due to the potential disruption of vital functions of these substrates [61]. As a result, drugs designed as γ -secretase modulators (such as avagacestat, semagacestat, and flurizan) have faced setbacks during clinical trials [62]. The status of different γ -Secretase inhibitors is shown in **Table 4**.

Table 4. γ -Secretase inhibitors for AD in clinical trials

Drug Name	Structure	Mode of Action	Remarks	Status	Reference
Semagacestat		Reduces A β levels in AD and induces changes in the peptidome of human cerebrospinal fluid	In phase III trials, the outcome was inferior to placebo	Terminated in Phase III.	[62]
MK-0752 3-((1s,4r)-4-((4-chlorophenyl)sulfonyl)-4-(2,5-difluorophenyl)cyclohexyl)propanoic acid		Lowers A β 1-40 levels in healthy participants, and currently undergoing testing for its potential in cancer treatment.	The medication was linked to gastrointestinal discomfort and feelings of fatigue.	Terminated in Phase I	[63]

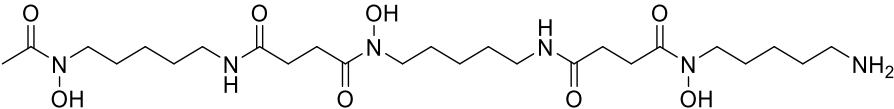
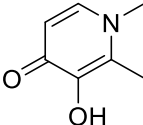
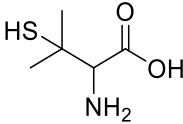
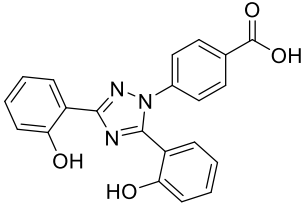
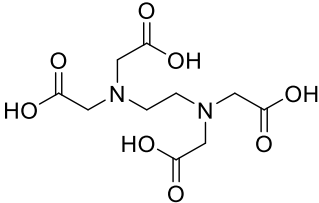
<p>E 2012 (S,E)-1-(1-(4-fluorophenyl)ethyl)-3-(3-methoxy-4-(4-methyl-1H-imidazol-1-yl)benzylidene)piperidin-2-one</p>		<p>A gamma-secretase inhibitor/modulator that preserves Notch function without impacting Notch processing</p>	<p>Lenticular opacity</p>	<p>Terminated in Phase I</p>	<p>[64]</p>
<p>Avagacestat, BMS-708163, 2-((4-chloro-N-(2-fluoro-4-(1,2,4-oxadiazol-3-yl)benzyl)phenyl)sulfonamido)-5,5,5-trifluoropentanamide</p>		<p>Preserving Notch function leads to a reduction in Aβ levels in the cerebrospinal fluid of healthy participants</p>	<p>Amyloid-related imaging abnormalities (ARIA)</p>	<p>Terminated in Phase II</p>	<p>[64]</p>
<p>Nirogacestat, PF-3084014 2-((6,8-difluoro-1,2,3,4-tetrahydronaphthalen-2-yl)amino)-N-(1-(2-methyl-1-</p>		<p>Reversible, orally bioavailable, noncompetitive, and selective γ-secretase inhibitor</p>	<p>Aβ1-40 levels show no decline in the cerebrospinal fluid of patients with AD.</p>	<p>US FDA has approved its use for desmoid tumors. Terminated</p>	<p>[64]</p>

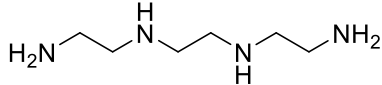
(neopentylamino)propan-2-yl)-1H-imidazol-4-yl)pentanamide				ated in Phase II for AD patients
---	--	--	--	----------------------------------

2.2.3 Metal Chelators

Metal ions, such as Zn^{+2} , Cu^{+2} , and Fe^{+3} , promote the aggregation of β -amyloid. Zn^{+2} can lead to aggregation even at low physiological concentrations, while Cu^{+2} and Fe^{+3} enhance aggregation under mildly acidic conditions. Elevated Cu^{+2} and Zn^{+2} levels have been linked to developing the apoE4 allele associated with AD. β -amyloid also participates in redox reactions mediated by metal ions, generating ROS [65]. To counteract metal interactions with $A\beta$, strategies like using iron-chelating agents are under investigation (**Table 5**) [66].

Table 5. Clinically approved small molecule-based chelating agents in metal chelation therapy

Name	Structure
Deferoxamine	
Deferiprone	
D-Penicillamine	
Deferasirox	
Ethylenediaminetetraacetic acid	

Triethylenetetramine (TETA)	
-----------------------------	--

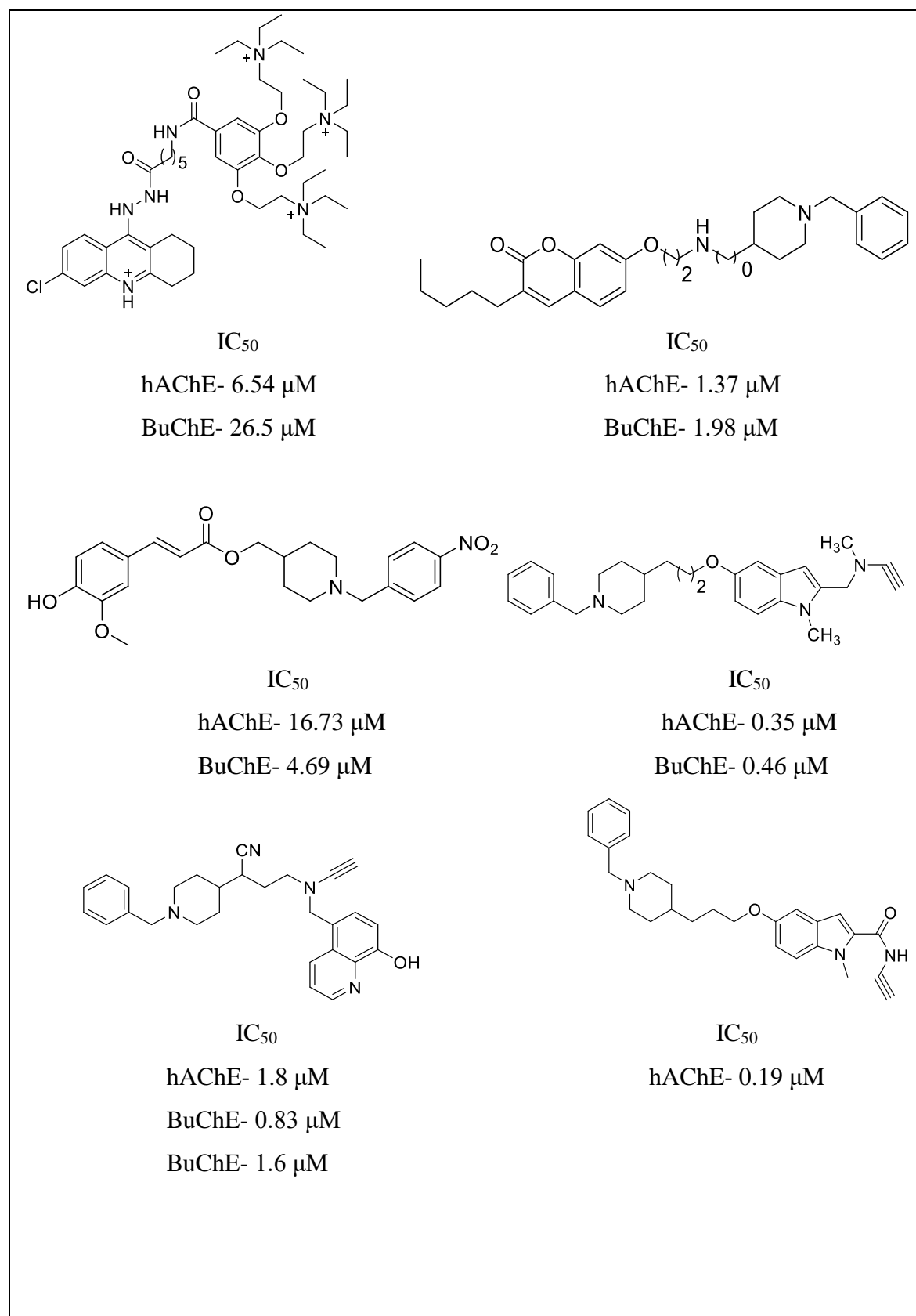
2.2.4 Acetylcholinesterase inhibitors

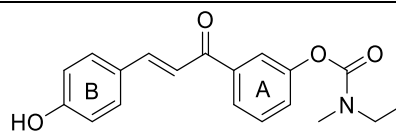
The cholinergic hypothesis in AD focused on the loss of cholinergic neurons. It reduced acetyltransferase (ChAT) activity, primarily in the nucleus basalis of Meynert, a vital source of cholinergic input to the neocortex [67]. This degeneration is associated with cognitive decline, impacting memory, attention, and learning-related brain regions such as the hippocampus and frontal cortex [68]. Issues encompass impaired choline uptake, compromised acetylcholine release, receptor imbalances, disrupted neurotrophin support, and axonal transport deficits [69]. Reduced ChAT and increased AChE activity result in acetylcholine depletion, impairing cognitive function. Treatment primarily relies on acetylcholinesterase inhibitors (AChEIs) to restore acetylcholine levels. Some approved AChEIs include tacrine, donepezil, rivastigmine, galantamine, etc., of which tacrine has been withdrawn [70-72].

2.3 Dual inhibitors

Given the intricate nature of AD and the multitude of factors contributing to its progression, addressing a single causative aspect is unlikely to yield a complete cure or effectively slow down the disease's advancement [73]. Therefore, recent reports involve the development of molecules capable of targeting two distinct factors concurrently. This innovative strategy offers the potential to diminish required dosage concentrations, enhancing the likelihood of effective treatment and disease progression attenuation. Moreover, it could result in cost savings and alleviate the financial burden on patients [74-76]. Examples of such dual inhibitors are given in **figure 8**.

A. Dual inhibitors targeting AChE and BuChE [77,78]



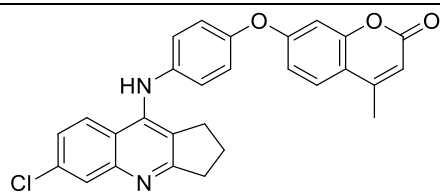


IC₅₀

hAChE- 0.87 μM

BuChE- 0.36 μM

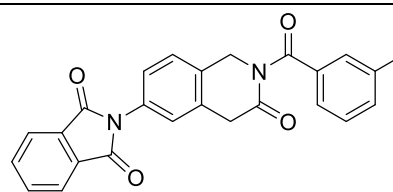
B. Dual inhibitors targeting AChE and BACE 1



IC₅₀ [79]

hAChE- 16.17 μM

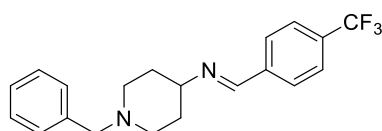
hBACE 1- 11.07 μM



IC₅₀ [79]

hAChE- 25.48 μM

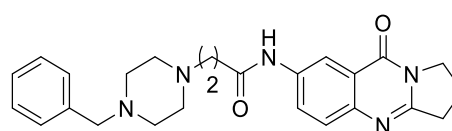
hBACE 1- 4.45 μM



IC₅₀ [80]

hAChE- 0.11 μM

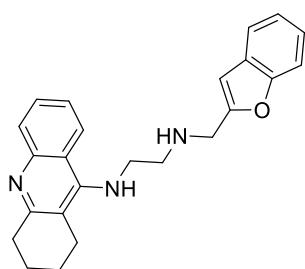
hBACE 1- 0.22 μM



IC₅₀ [80]

hAChE- 0.00329 μM

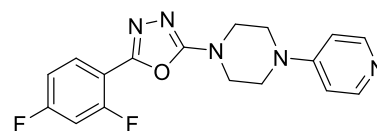
hBACE 1- 0.129 μM



IC₅₀ [81]

hAChE- 0.00086 μM

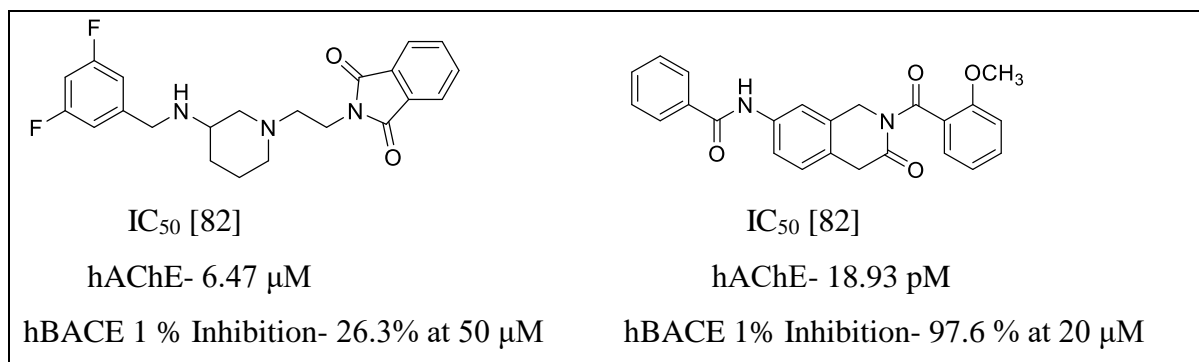
hBACE 1- 1.35 μM



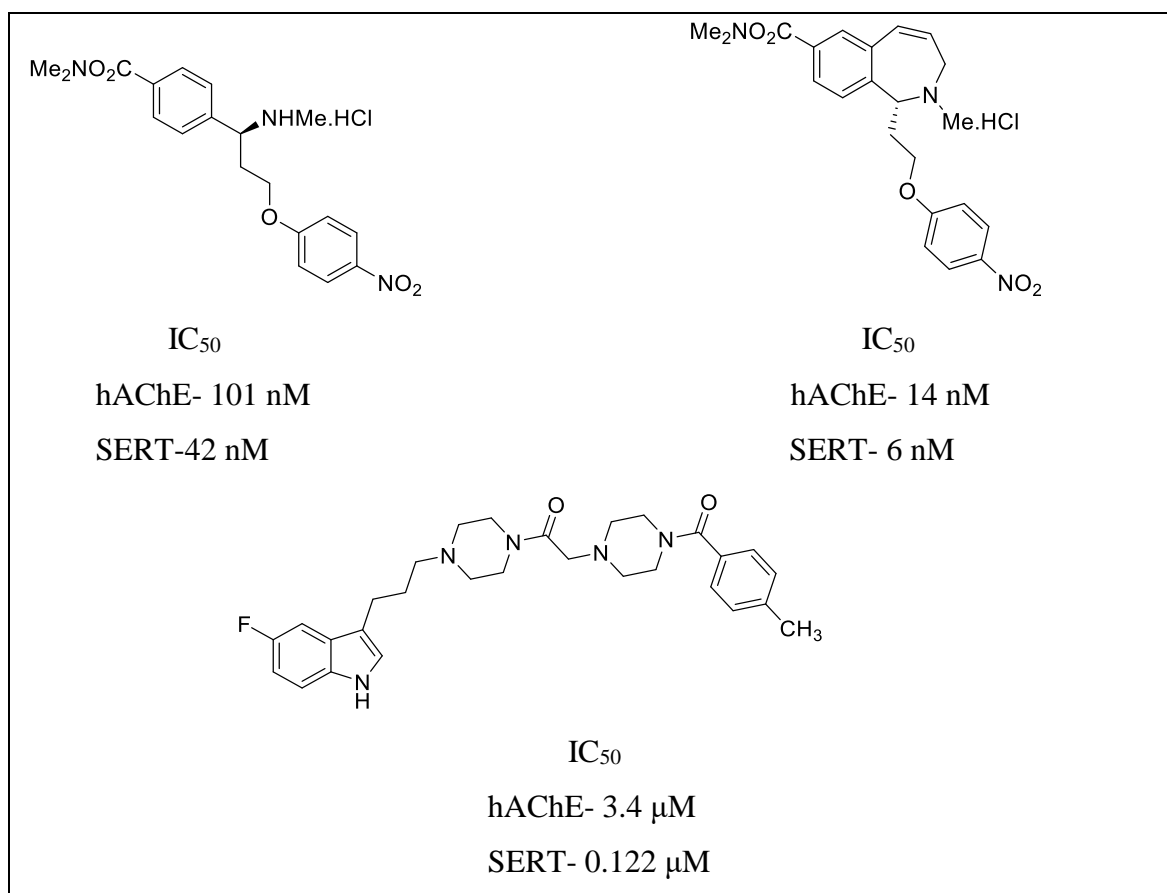
IC₅₀ [81]

hAChE- 0.054 μM

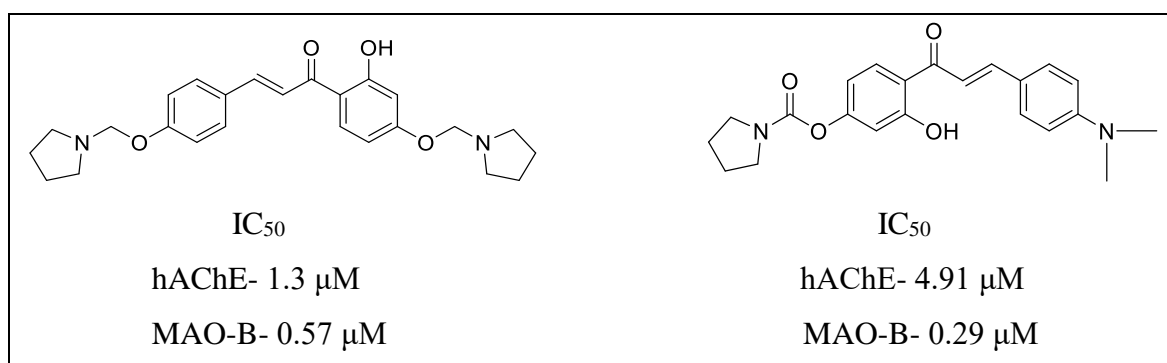
hBACE 1- 0.098 μM

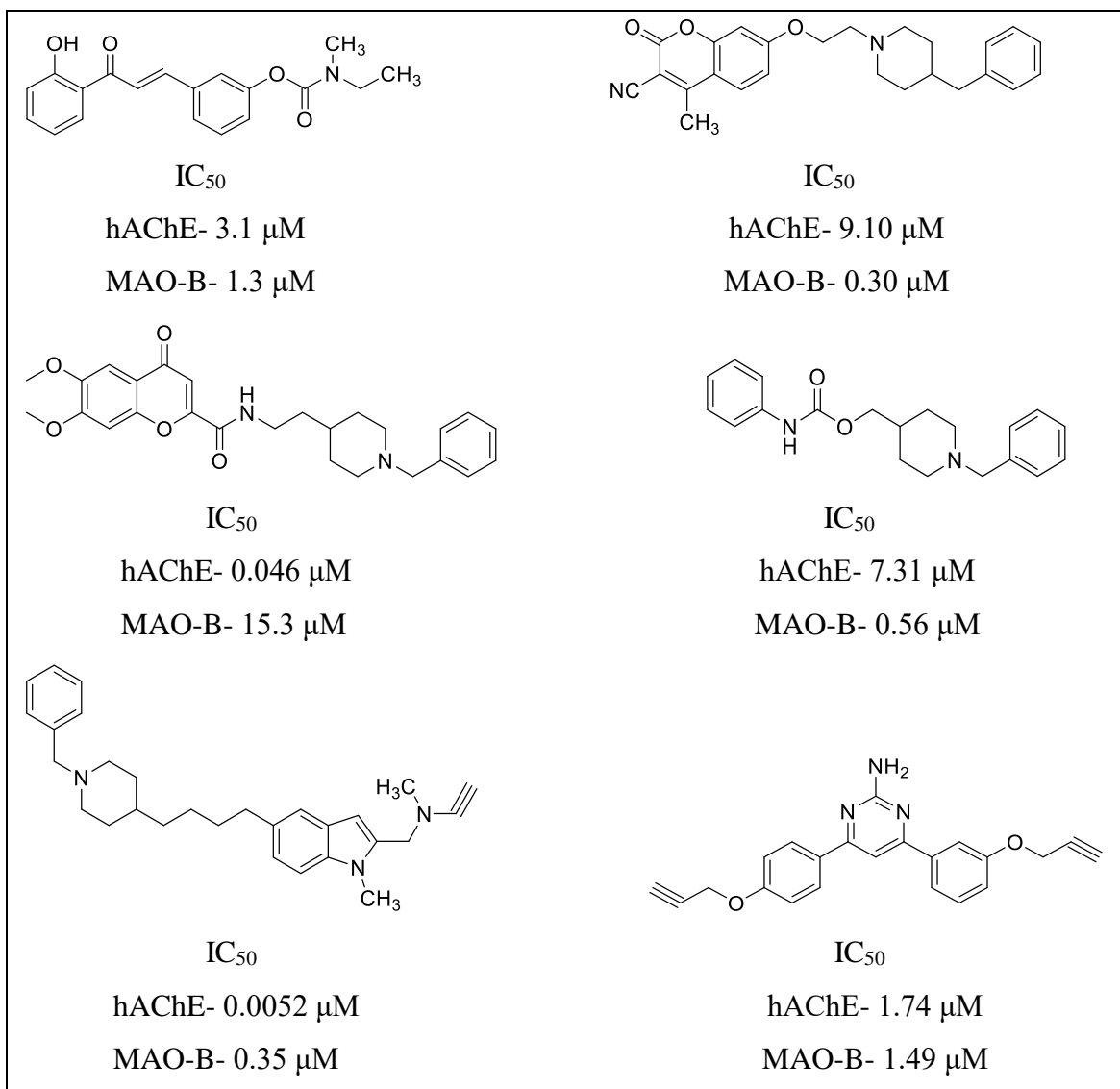


C. Dual inhibitors targeting AChE and Serotonin Transporter [83]

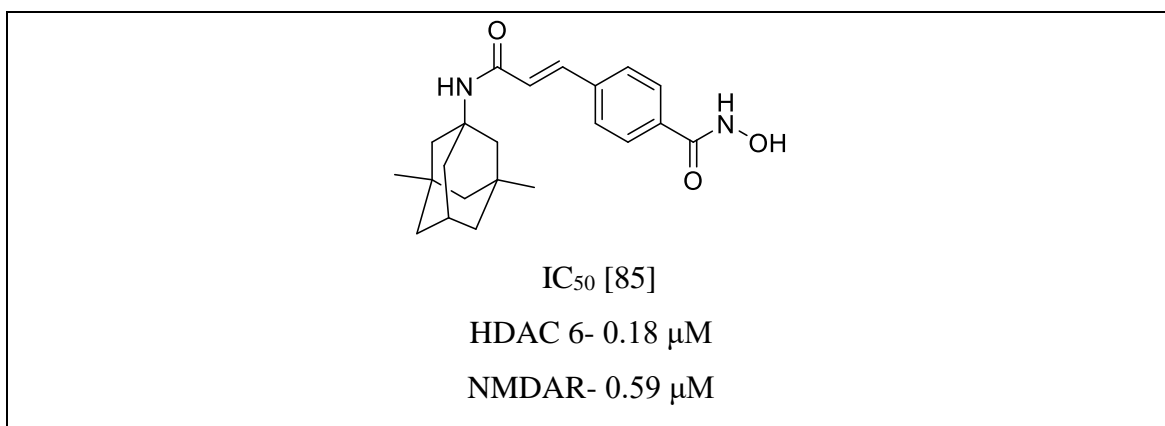


D. Dual inhibitors targeting AChE and MAO-B [84]

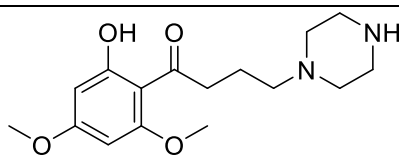




E. Dual inhibitors targeting HDAC and NMDAR



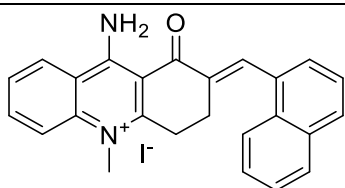
F. Dual inhibitor targeting AChE and IL-6

IC₅₀ [86]

hAChE- 0.73 μM

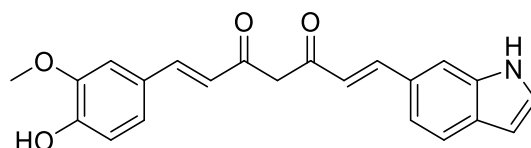
IL-6- 0.38 μM

G. Dual inhibitors targeting Aβ and Tau [87]



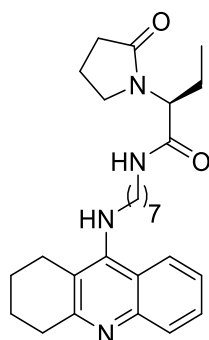
Aβ aggregation - 86.7 %

Tau aggregation - 101.8 %



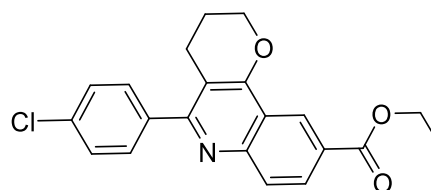
Aβ aggregation - 0.42%

Tau aggregation - 0.44 %



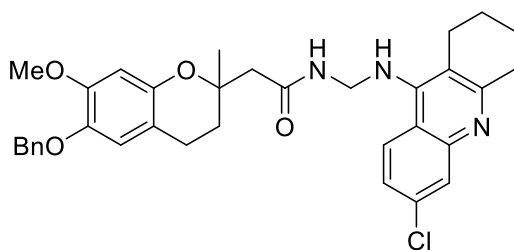
Aβ aggregation - 12.6 %

Tau aggregation - 14.9 %



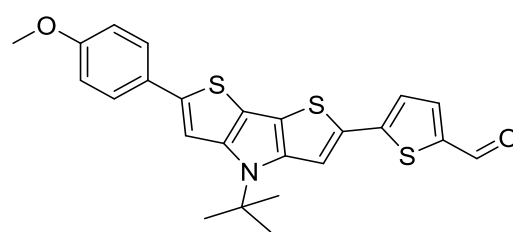
Aβ aggregation - 41.8 %

Tau aggregation - 27.9 %



Aβ aggregation - 41.8 %

Tau aggregation - 55.2 %



Aβ aggregation - 0.38 %

Tau aggregation - 0.29 %

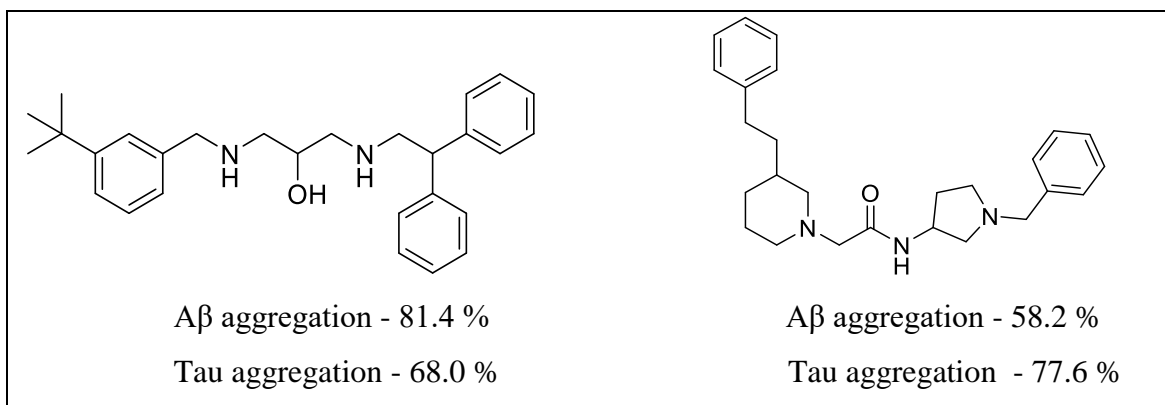
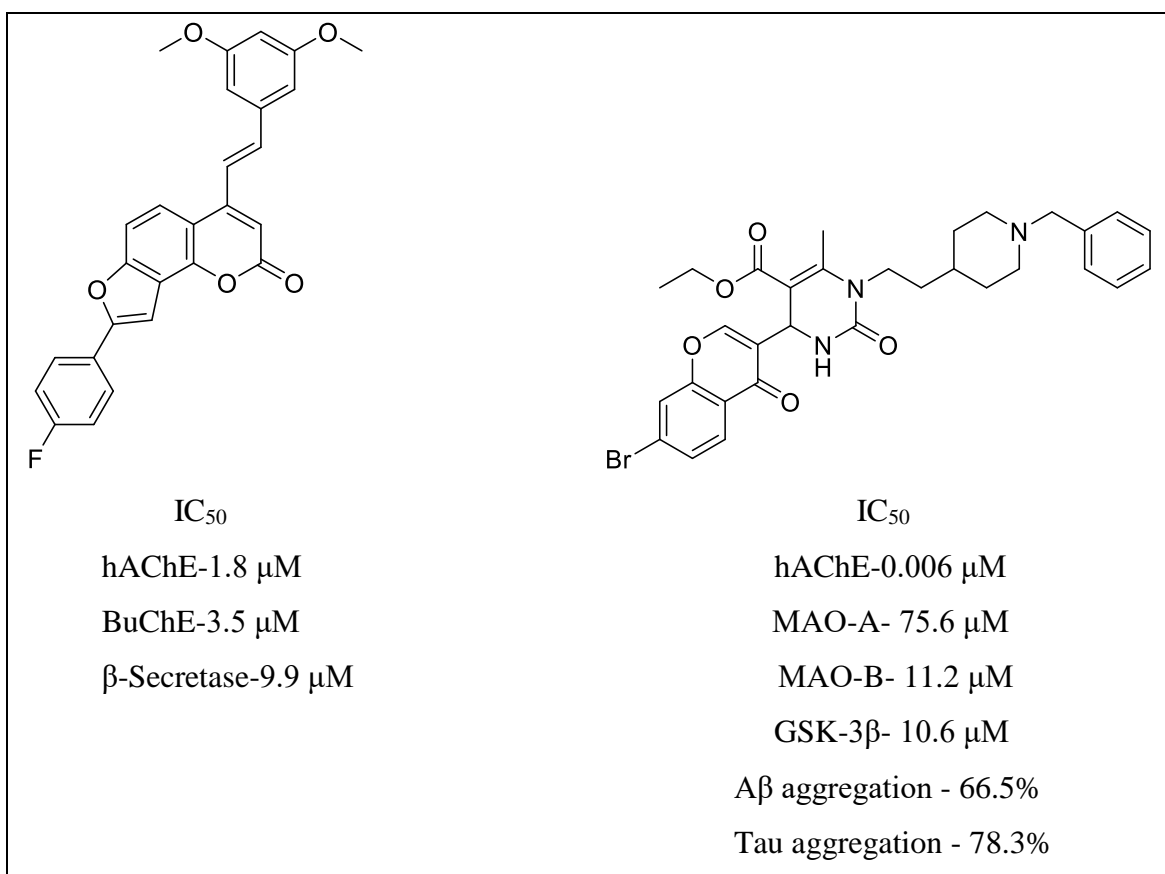
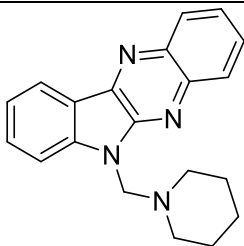


Figure 8. Structures of some of the representative dual inhibitors

2.4 Multi-Target-Directed Ligands

Similar to dual inhibitors, multi-target-directed ligands (MTDLs), often termed "dirty drugs," offer promise for AD treatment [88]. These compounds combine pharmacophore moieties from different bioactive compounds, enhancing therapeutic safety and efficacy compared to single-target drugs [89]. MTDLs offer a comprehensive approach to addressing the intricate network of factors contributing to AD pathogenesis (**figure 9**) [90].



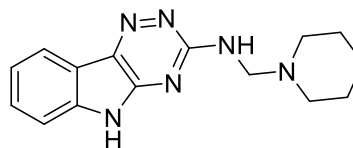


IC₅₀

hAChE- 5.80 μM

BuChE- 0.96 μM

Aβ aggregation - 51.24%

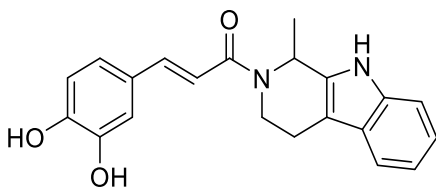


IC₅₀

hAChE- 0.67 μM

BuChE- 0.84 μM

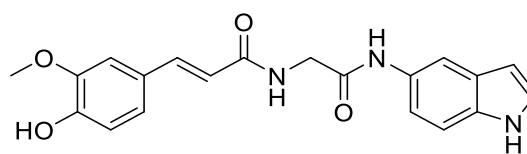
Aβ aggregation - 63.6 %



IC₅₀

BuChE- 1.32 μM

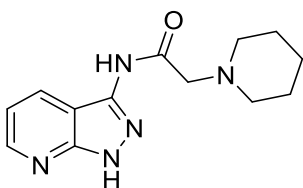
Aβ aggregation - 72.51%



IC₅₀

hAChE- 5.74 μM

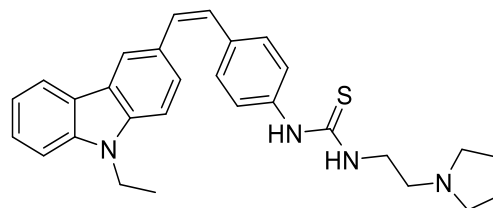
BuChE- 14.05 μM



IC₅₀

hAChE- 4.8 nM

BuChE- 10.58 nM

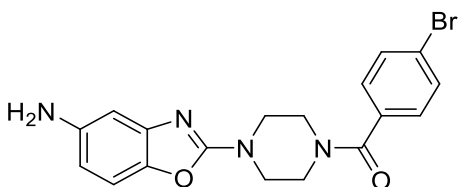


IC₅₀

hAChE- 2.64 μM

BuChE- 1.2 μM

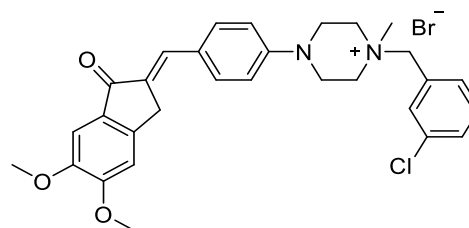
Aβ aggregation - 51.29%



IC₅₀

hAChE- 0.052 μM

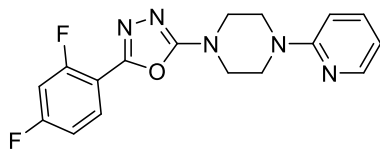
BuChE- 1.08 μM



IC₅₀

hAChE- 0.32 μM

BuChE- 0.43 μM

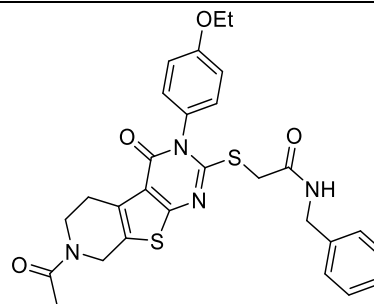


IC₅₀

hAChE- 0.054 μM

BuChE- 0.78 μM

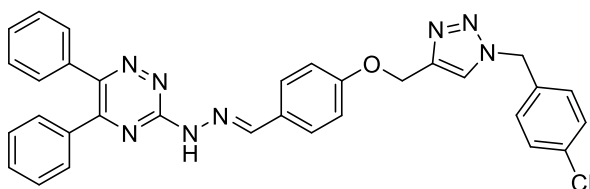
BACE 1- 0.098 μM



IC₅₀

hAChE- 9.0 μM

Aβ Aggregation - 48.8 %



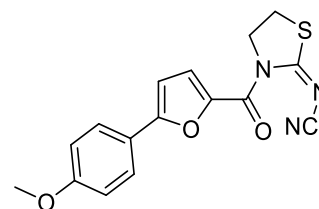
IC₅₀

BACE 1- 8.55 μM

hAChE- 1.56 μM

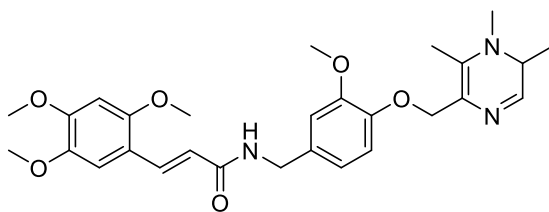
BuChE- 60.31 μM

Aβ aggregation - 43.2 %



IC₅₀

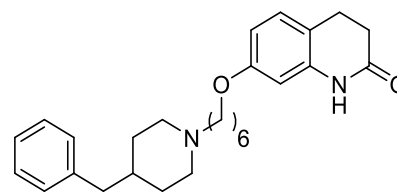
Anti-PDE4B activity- 2.8 μM



IC₅₀

Potent neuroprotectors

SH-SY5Y cells against Aβ-induced toxicity - 3.55 μM



IC₅₀

hAChE- 0.56 μM

BuChE- 2.3 μM

MAO-A- 0.3 μM

MAO-B- 0.0014 μM

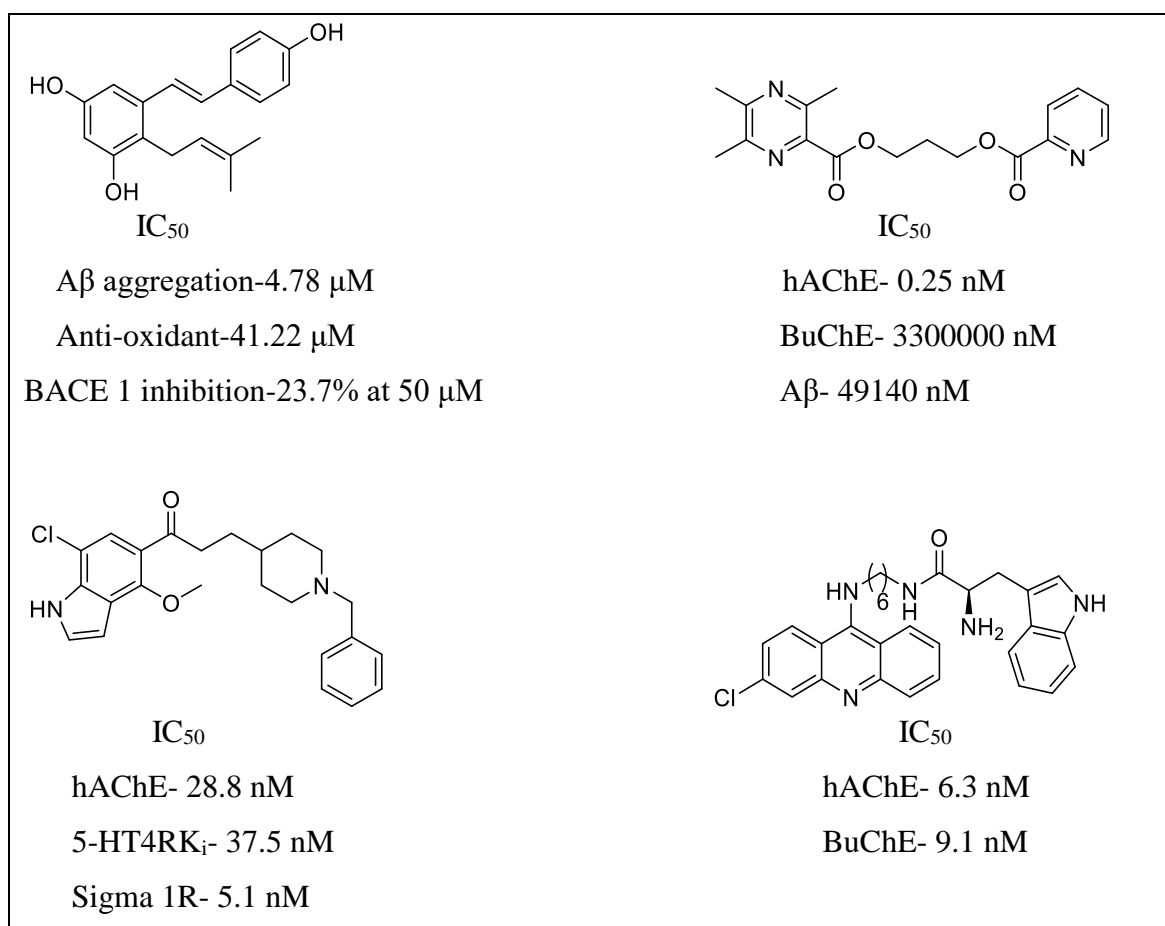


Figure 9. Structures of some of the representative multi-target-directed ligands [83,91].

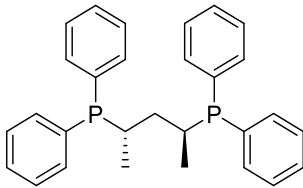
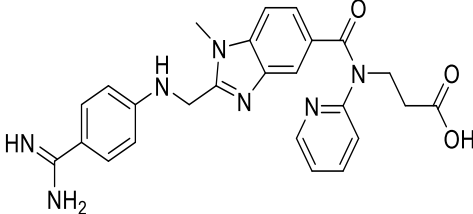
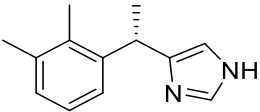
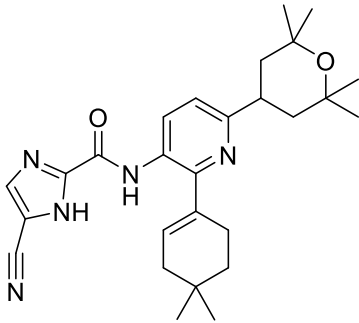
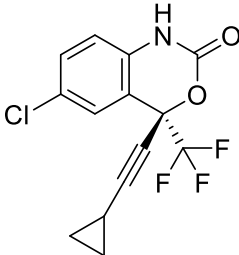
3. Candidates under clinical investigation for AD

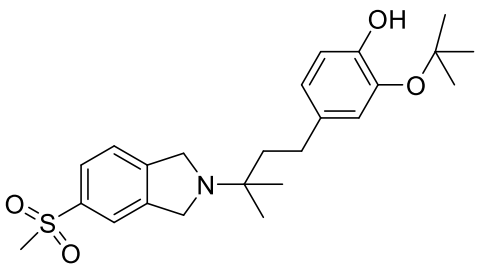
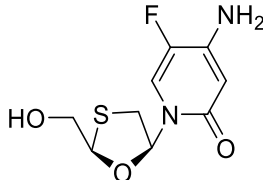
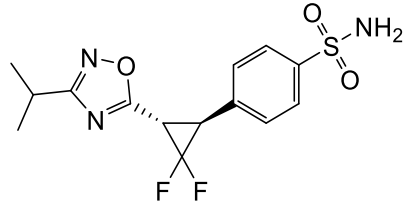
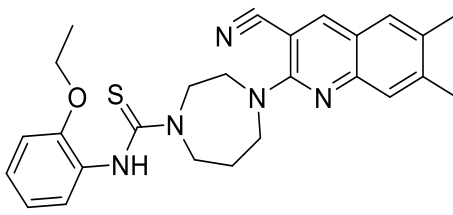
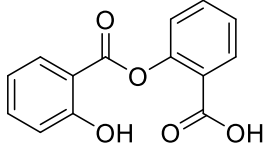
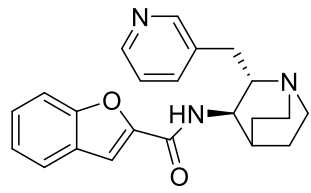
Despite recent clinical trial failures, several promising candidates are in the AD drug development pipeline. **Table 6** collates the available information (updated as of May 2024) on various developmental candidates in clinical trials, phase-wise and by category. The list is in addition to the candidates mentioned in the above sections (<https://clinicaltrials.gov/>).

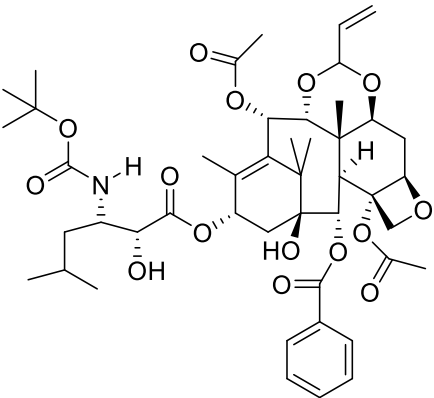
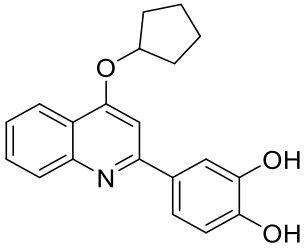
Table 6: Drugs under clinical trials for AD treatment

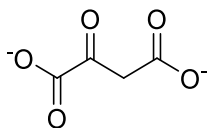
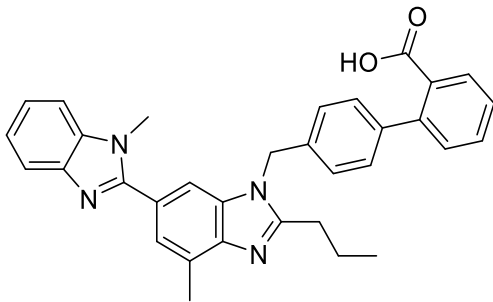
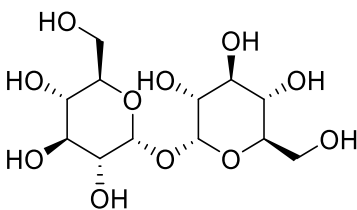
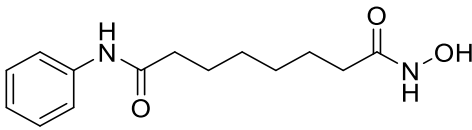
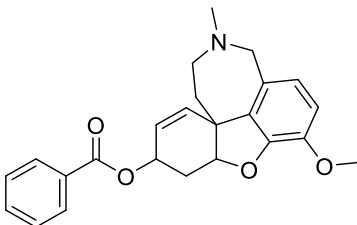
Drug Name	Structure	Mode of Action	Class
Phase I			
Disease-modifying Biologicals			
Mode of Action			
MK-2214		Anti-tau monoclonal antibody	Tau
SHR-1707		Prevent Aβ plaque and activate microglia to phagocytize various forms of Aβ	Amyloid

NIO752	Antisense oligonucleotide to tau, decreasing the abundance of tau aggregates at neuromuscular junction	Tau
IBC-Ab002	Humanized IgG1 antibody inhibits an immune checkpoint protein (PD-L1), stimulating the immune system	Inflammation /immunity
ALN-APP	Small interfering RNA targeting the amyloid precursor protein mRNA	Amyloid
CpG1018	Immune adjuvant made up of short, unmethylated cytosine-phosphate-guanine oligodeoxynucleotides, stimulate clearance of amyloid pathology	Inflammation /immunity
AL003	Monoclonal antibody (MAb) targeting SIGLEC-3 (CD33), reactivates microglia and immune cells in the brain, improves microglial clearance of toxic proteins	Inflammation
AAV-hTERT	Extending telomeres may benefit AD, reduce A β -induced neurotoxicity, and effects on multiple cellular pathways	Epigenetic
Lu AF87908	MAb to reduce Tau	Tau
LY3372993	MAb to reduce amyloid (N3pG-AB)	Amyloid
AAVrh.10hAPOE2	MAb targeting SIGLEC-3 (CD33), reactivates microglia and immune cells in the brain, improves microglial clearance of toxic proteins	Epigenetic
XPro1595	TNF inhibitor, reduces neuroinflammation	Inflammation
GSK933776	MAb against N-terminus of A β	Amyloid
ALZ-101	Vaccine against soluble A β oligomers	Amyloid
VT301	Regulatory T-cells (Tregs)	Inflammation
CAD106	CAD106 combines multiple copies of A β 1-6 peptide derived from the N-terminal B cell epitope of A β , coupled to a Q β virus-like particle. In animals, CAD106 induced A β -antibody titers without activating A β -reactive T cells	Amyloid
KHK6640	MAb that consists of Anti-A β -peptide	Amyloid
NPT088	An Ig-fusion General Amyloid Interaction Motif (GAIM) based dimer	Amyloid

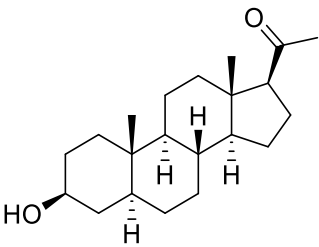
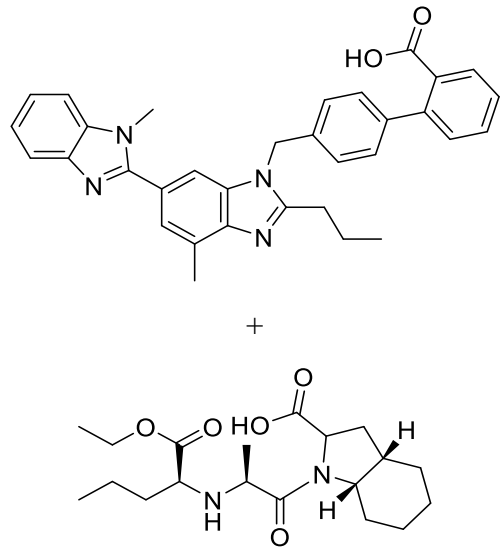
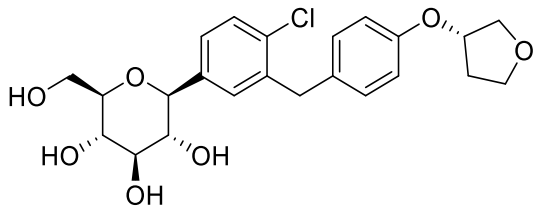
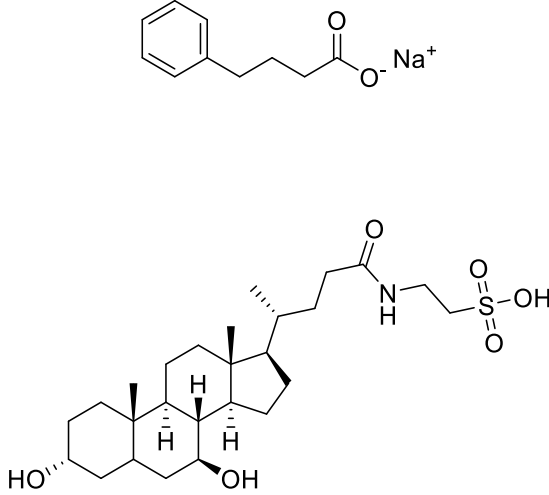
Disease-Modifying Drugs			
BDPP (2S,4S)-(-)-2,4-Bis(diphenylphosphino)pentane		Prevents A β and tau aggregation	Proteostasis/proteinopathies
BEY2153	A β and tau aggregation inhibitor, inhibits neuronal death		Proteostasis/proteinopathies
Dabigatran		Direct thrombin inhibitor, reduce neurovascular damage	Vasculature
Dexmedetomidine		Selective α 2-adrenergic receptor agonist, neuroprotection	Circadian rhythm
Edicotinib		CSF-1R antagonist, attenuates microglial proliferation and neurodegeneration	Inflammation
Efavirenz		NNRTI, promotes cholesterol removal, enhances amyloid reduction	Epigenetics

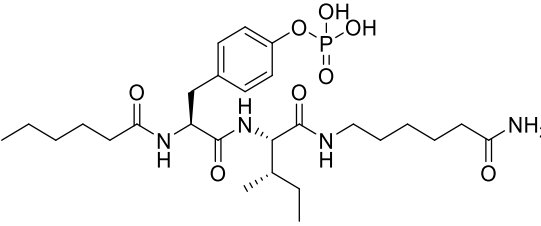
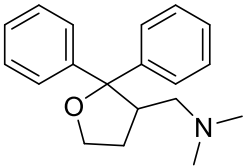
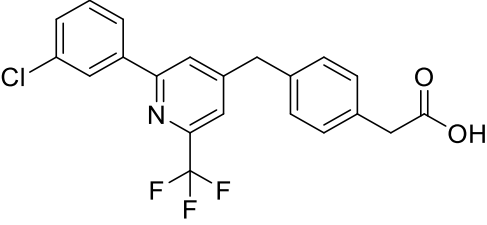
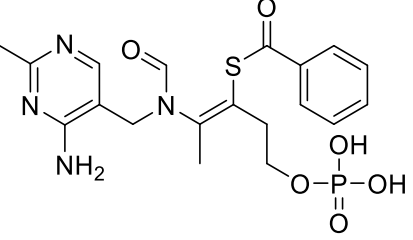
Elayta		Sigma-2 receptor Antagonist, competes with oligomeric A β binding at synapse	Synaptic plasticity/ neuroprotection
Emtricitabine		NRTI, reduces neuroinflammation	Inflammation
MK-4334		positive allosteric modulators of $\alpha 7$ nAChR	Growth factors and hormones
NNI-362 4-(3-cyano-6,7-dimethylquinolin-2-yl)-N-(2-ethoxyphenyl)-1,4-diazepane-1-carbothioamide		Enhance neurogenesis, activates progenitor cells	Neurogenesis
REM0046127	Regulates calcium dyshomeostasis, Tau and A β reduction		Synaptic plasticity/ neuroprotection
Salsalate		NSAID to reduce inflammation	Inflammation
TC-5619 N-((2S,3R)-2-(pyridin-3-ylmethyl)quinuclidinylidene)quinoline-3-carboxamide		Partial agonist at the $\alpha 7$ subtype of the neural nicotinic acetylcholine receptors	Cognition enhancement

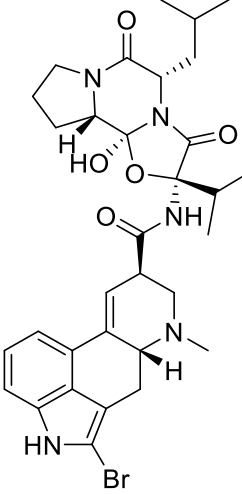
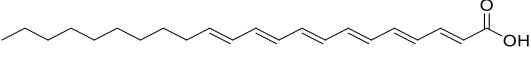
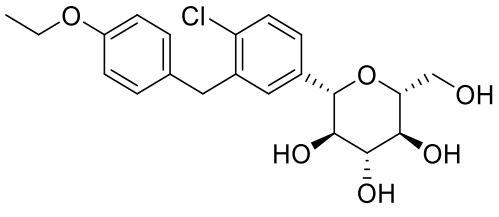
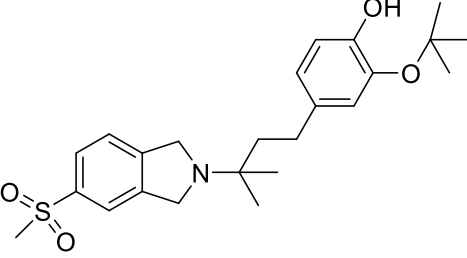
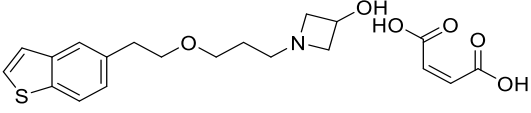
n-3-yl)benzofuran-2-carboxamide			
<p>TPI-287 (1S,4S,7S,7aR,7a1S,10aS,11aR,13aS,13bR)-1-(benzoyloxy)-4-(((2R,3S)-3-(tert-butoxycarbonyl)amino)-2-hydroxy-5-methylhexanoyl)oxy)-2-hydroxy-5,7a1,14,14-tetramethyl-9-vinyl-1,3,4,7,7a,7a1,10a,11,11a,13b-decahydro-2H-8,10,12-trioxa-2,6-methanocyclobuta[b]cyclodeca[de]naphthalene-7,13a(13H)-diyl diacetate</p>		Stabilization of microtubule	Tau
<p>CMS121 4-(4-(cyclopentyloxy)quinolin-2-yl)benzene-1,2-diol</p>		<p>Fatty Acid Synthase inhibitor It protects against excess lipid peroxidation and inflammation and alleviates cognition</p>	Inflammation

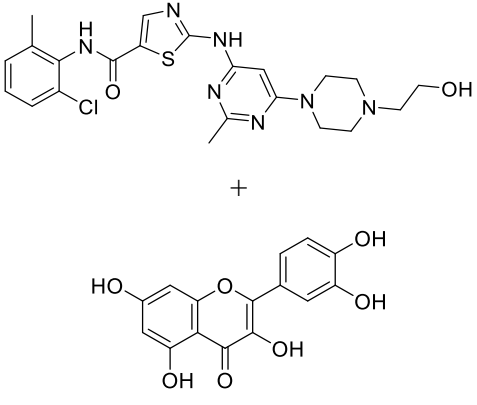
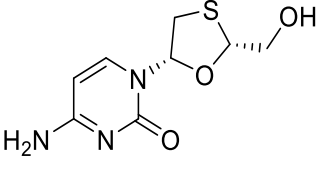
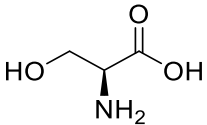
Oxaloacetate		Improves mitochondrial function	Bioenergetics
Telmisartan		Angiotensin II receptor blocker	Vasculature
Trehalose		Induces autophagy and promotes clearance of aggregated proteins	Cell death
Vorinostat		Histone deacetylase (HDAC) inhibitor, enhanced synaptic plasticity	Epigenetics
Symptom-Reducing Small Molecules:			
MK-1942	Improves mitochondrial structure and function		Neurotransmitter receptors
MK-8189	Phosphodiesterase 10A inhibitor		Behavioural changes
Memogain		AChE/BuChE MTDL	Neurotransmitter receptors

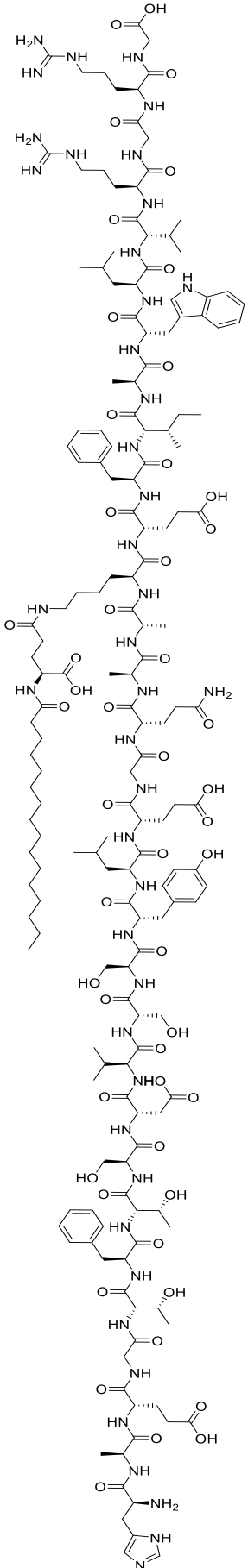
Phase II		
Disease-modifying Biologicals:		
AL002	MAB targeting TREM2 receptors to promote microglial clearance of A β	Inflammation
ACI-35	Active immunotherapy targeting Tau	Tau
ABvac40	Active immunotherapy to remove A β	Amyloid
AADvac1	This is an active vaccine designed to elicit an immune response against pathologically modified forms of tau protein	Tau
BCG vaccine	Vaccination against tuberculosis infection, immunomodulator	Inflammation
Bryostatin 1	Protein Kinase C inhibitor, facilitates synaptogenesis	Synaptic plasticity/ neuroprotection
Daratumumab	MAB targeting CD38, regulates microglial activity	Inflammation / immunity
Etanercept	Inhibits the function of a pro-inflammatory cytokine called tumor necrosis factor alpha (TNF- α)	Inflammation
Crenezumab	MAB targeting soluble A β oligomers	Amyloid
Gosuranemab	MAB targeting truncated form of Tau	Tau
Gantenerumab	Human IgG1 Ab against A β fibrils	Amyloid
Lecanemab	MAB directed at protofibrils	Amyloid
Pepinemab	MAB directed at semaphorin 4D to reduce inflammation	Inflammation
GV1001	hTERT peptide vaccine, mimics extra-telomeric functions to inhibit neurotoxicity, apoptosis, and reactive oxygen species	Epigenetic
GB301	Regulatory T cells, Reduce neuroinflammation	Inflammation / immunity
IVIG	Polyclonal antibody, remove amyloid	Amyloid
JNJ-63733657	MAB targeting soluble Tau	Tau
IONIS MAPTRx	Antisense oligonucleotide targeting tau expression, MAPT RNA inhibitor	Tau
R07126209	Anti-A β MAB with enhanced BBB penetration	Amyloid
Semorinemab	MAB to remove extracellular Tau	Tau

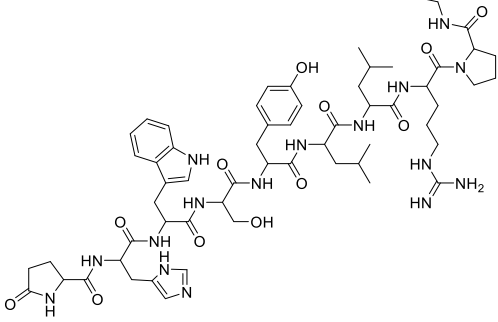
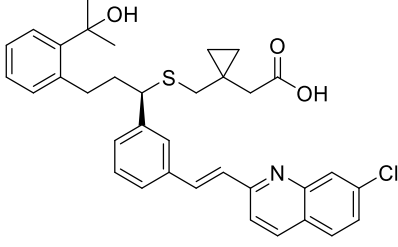
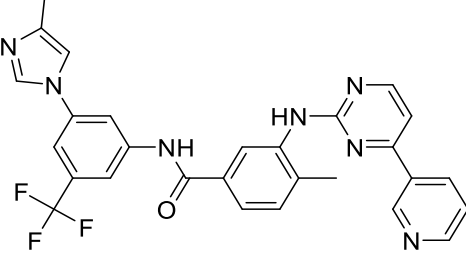
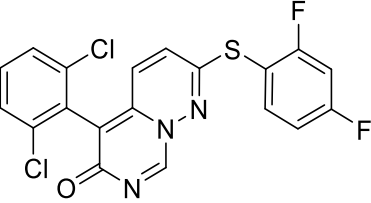
Tilavonemab	MAb to remove Tau and prevent propagation	Tau	
Zagotenemab	MAB to remove Tau and reduce tau propagation	Tau	
Disease-modifying Drugs:			
Allopregnanolone		GABA-A receptor modulator, promote neurogenesis and reduce inflammation	Growth factors/hormones
Telmisartan + Perindopril		Telmisartan: Angiotensin II receptor blocker Perindopril : Angiotensin Converting Enzyme inhibitor	Vasculature
Empagliflozin		SGLT2 inhibitor, improve glycemic control, enhance neuronal function	Metabolism and bioenergetics
Sodium phenylbutyrate + Tauroursodeoxycholic acid		Reduce cell death associated with mitochondrial dysfunction, modulate neuroinflammation	Cell death

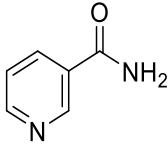
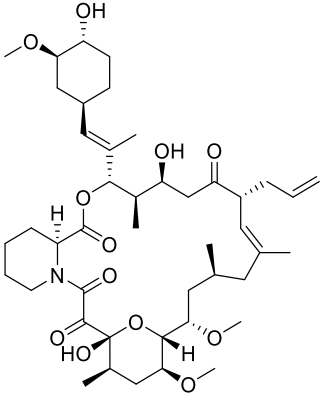
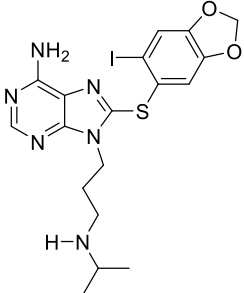
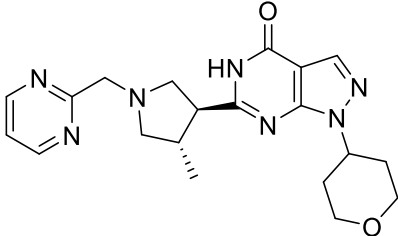
<p>Fosgonimeton</p>		<p>Activates signalling via the hepatocyte growth factor system to regenerate neurons and enhance synaptic plasticity</p>	<p>Synaptic plasticity/ neuroprotection</p>
<p>AR1001</p>	<p>PDE-5 inhibitor It improves synaptic plasticity</p>		<p>Synaptic plasticity/ neuroprotection</p>
<p>Blarcamesine</p>		<p>Sigma-1 receptor agonist, M2 antagonist, ameliorate oxidative stress, protein misfolding, mitochondrial dysfunction and inflammation</p>	<p>Synaptic plasticity/ neuroprotection</p>
<p>Zatolmilast</p>		<p>PDE-4 inhibitor, prolongs cAMP activity and improves neuronal plasticity</p>	<p>Synaptic plasticity/ neuroprotection</p>
<p>Benfotiamine</p>		<p>Synthetic thiamine to improve neuronal function</p>	<p>Metabolism and Bioenergetics</p>

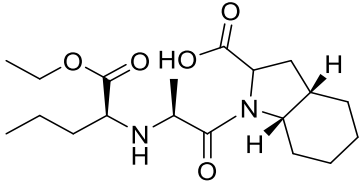
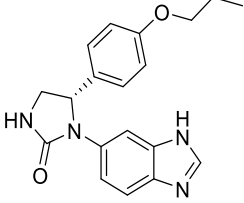
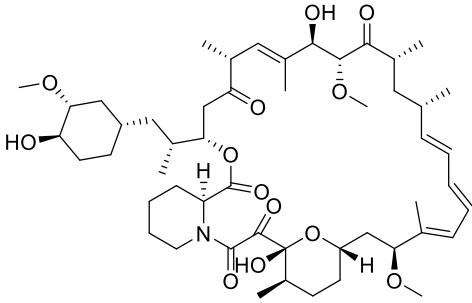
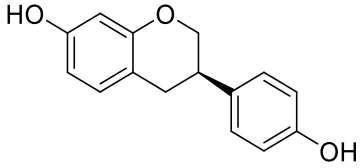
Bromocriptine	 <p>The structure shows a complex molecule with a piperidine ring, a pyrrolidine ring, and a brominated indole ring system.</p>	Dopamine agonist with anti-A β effects	Neurotransmitter receptors
DHA (Docosahexanoic acid)	 <p>The structure is a long-chain polyunsaturated fatty acid with 22 carbon atoms and six double bonds.</p>	Omega 3 fatty acid, improve synaptic function, antioxidant	Oxidative stress
Dapagliflozin	 <p>The structure features a central benzene ring with a chlorine atom and an ethoxy group, connected to a pyranose ring with multiple hydroxyl groups.</p>	SGLT2 inhibitor, to improve insulin sensitivity and CNS glucose metabolism	Metabolism and bioenergetics
Elayta	 <p>The structure consists of a benzimidazole ring system with a sulfonamide group and a side chain containing a phenol and a tert-butyl ether group.</p>	Sigma-2 receptor antagonist, competes with oligomeric A β binding, protect against A β -induced synaptic toxicity	Synaptic plasticity/ neuroprotection
Edonerpic acid	 <p>The structure includes a thiophene ring, a piperazine ring, and a carboxylic acid group.</p>	Neurotrophic agent, activates sigma receptors to preserve synaptic	Synaptic plasticity/ neuroprotection

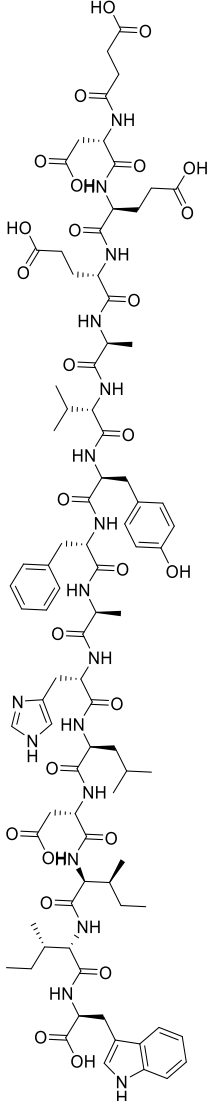
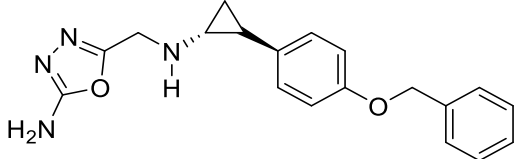
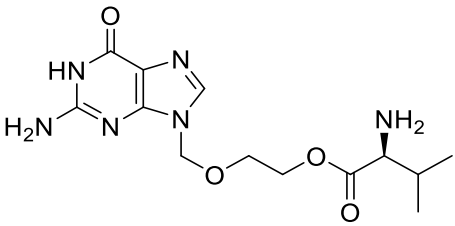
		plasticity, protect against A β toxicity	
Dasatinib + Quercetin	 <p>The image shows the chemical structures of Dasatinib and Quercetin. Dasatinib is a tyrosine kinase inhibitor with a complex structure including a thiazole ring, a pyridine ring, and a piperazine ring with a hydroxyethyl group. Quercetin is a flavonoid with a central chromone ring and multiple hydroxyl groups.</p>	<p>Dasatinib: Tyrosine kinase inhibitor</p> <p>Quercetin: flavonoid, senolytic therapy approach to reduce senescent cells and tau aggregation</p>	Inflammation / immunity
Lamivudine	 <p>The image shows the chemical structure of Lamivudine, a nucleoside reverse transcriptase inhibitor. It features a pyrimidine ring with an amino group and a carbonyl group, attached to a ribose sugar ring.</p>	Nucleoside reverse transcriptase inhibitor, reduces genetic rearrangements	Epigenetic
L-serine	 <p>The image shows the chemical structure of L-serine, a dietary amino acid. It consists of a central carbon atom bonded to a hydroxyl group, an amino group, a carboxyl group, and a hydroxymethyl group.</p>	Dietary amino acid, reduce brain inflammation and preserve nerve cells	Inflammation

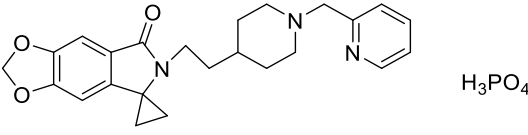
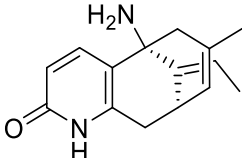
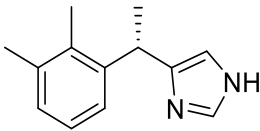
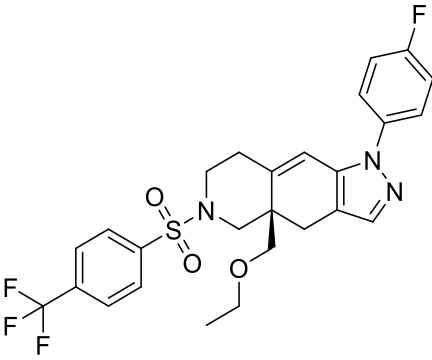
<p>Liraglutide</p>		<p>Glucagon-like peptide 1 receptor agonist, improve CNS glucose metabolism</p>	<p>Metabolism and bioenergetics</p>
--------------------	--	---	-------------------------------------

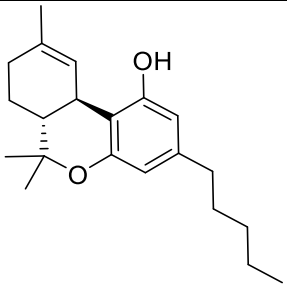
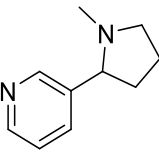
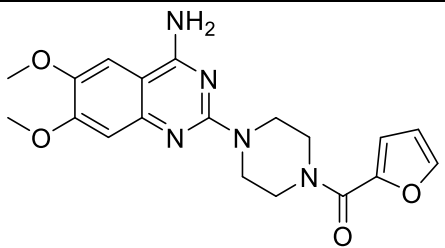
<p>Lupron</p>		<p>GnRH receptor agonist, reduce effects of elevated GnRH and gonadotropins on the brain</p>	<p>Growth factors and hormones</p>
<p>Montelukast</p>		<p>Cysteinyl leukotriene type 1 (cysLT-1) receptor antagonist, effects on inflammatory processes, neuronal injury, blood-brain-barrier integrity, and Aβ protein accumulation</p>	<p>Inflammation</p>
<p>Nilotinib</p>		<p>Tyrosine kinase inhibitor, autophagy enhancer, promotes clearance of Aβ and Tau</p>	<p>Proteostasis/proteinopathies</p>
<p>Neflamapimod</p>		<p>p38 MAPK-α inhibitor, enhance endolysosomal function to reduce synaptic dysfunction</p>	<p>Synaptic plasticity/neuroprotection</p>

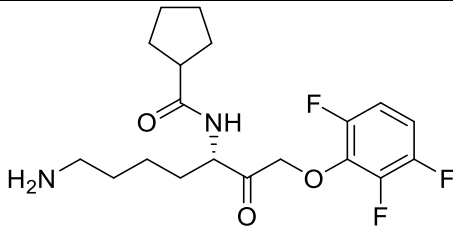
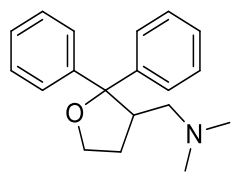
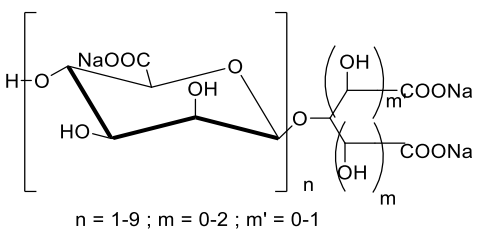
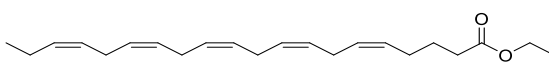
Nicotinamide		HDAC inhibitor, reduce tau-induced microtubule depolymerization and tau phosphorylation	Tau
Tacrolimus		Calcineurin inhibitor, prevent Aβ- induced dendritic spine loss and synaptic dysfunction	Synaptic plasticity/ neuroprotecti on
PU-AD 8-((6- iodobenzo[d][1,3]d ioxol-5-yl)thio)-9- (3- (isopropylamino)pr opyl)-9H-purin-6- amine		Heat shock protein 90 inhibitor, prevent aggregation and hyperphosphorylat ion of Tau	Tau
PF-04447943 6-((3S,4S)-4- methyl-1- (pyrimidin-2- ylmethyl)pyrrolidin -3-yl)-1- (tetrahydro-2H- pyran-4-yl)-1,5- dihydro-4H- pyrazolo[3,4- d]pyrimidin-4-one		selective phosphodiesterase 9 (PDE9) inhibitor	Cognition Enhancement

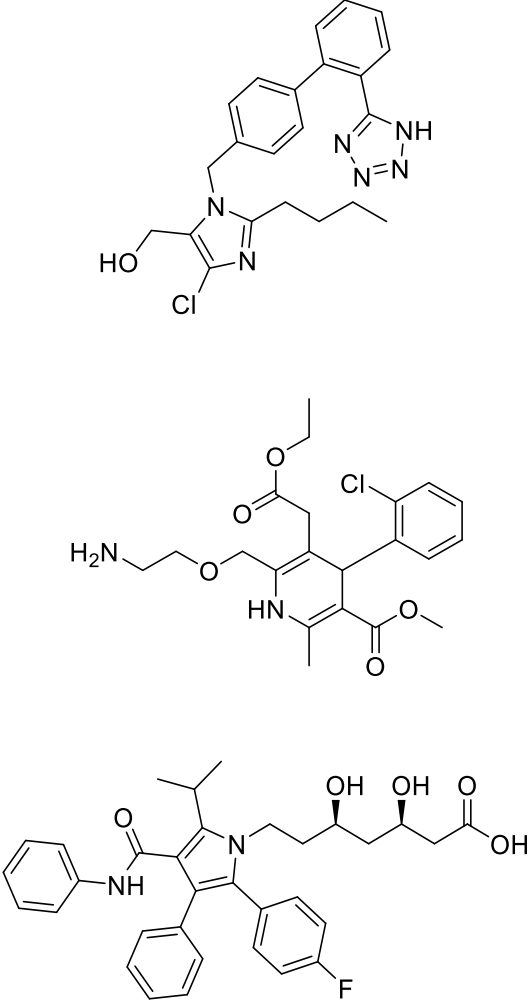
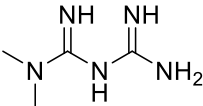
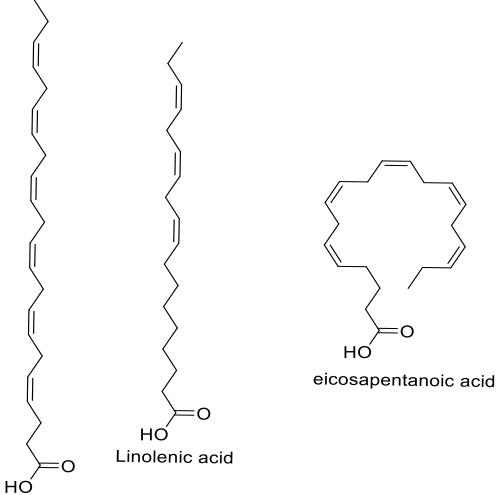
Perindopril		Angiotensin Converting Enzyme inhibitor	vasculature
PQ912 (S)-1-(1H- benzo[d]imidazol- 6-yl)-5-(4- propoxyphenyl)imi- dazolidin-2-one		Glutamyl cyclase (QC) enzyme inhibitor to reduce pyroglutamate A β (pGlu-A β) production	Amyloid
Rapamycin		mTOR inhibitor, ameliorate metabolic and vascular effects of aging	Proteostasis/ proteinopathi- es
S-Equol		Agonist of non- hormonal estrogen receptor B located on mitochondria to potentiate mitochondrial function	Metabolism and bioenergetics

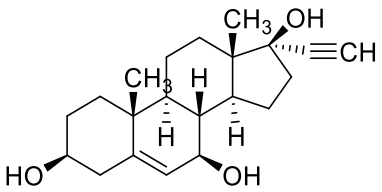
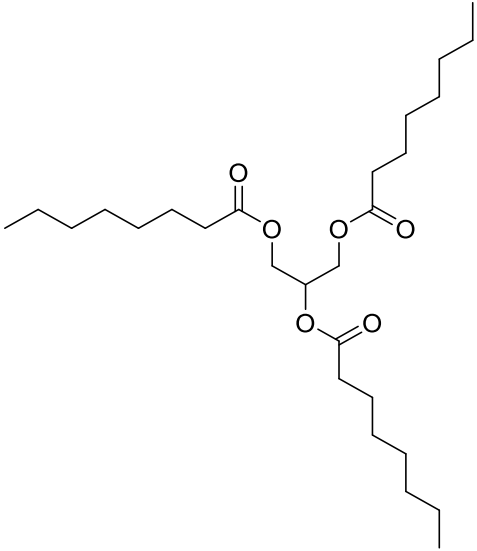
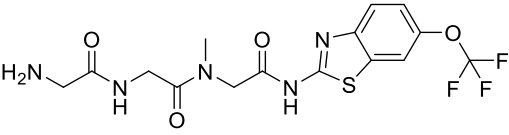
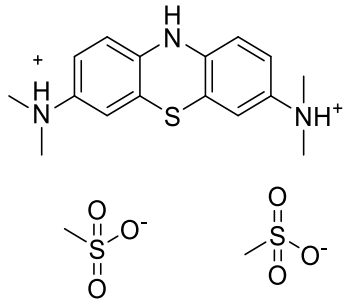
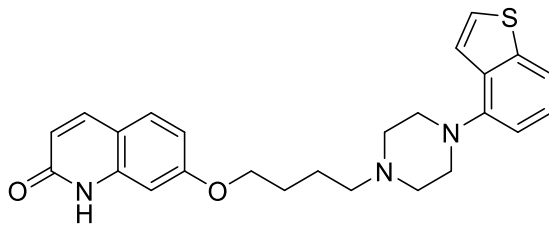
Sovateltide		Endothelin B receptor agonist, augments activity of neuronal progenitor cells	Neurogenesis
Vafidemstat		HDAC demethylase inhibitor and MAO-B inhibitor, neuroprotective	Synaptic plasticity/ neuroprotection
Valacyclovir		Antiviral against HSV-1 and -2 infection, prevent Aβ aggregation and plaque deposition	Infection/ immunity

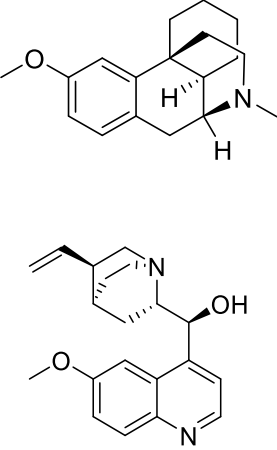
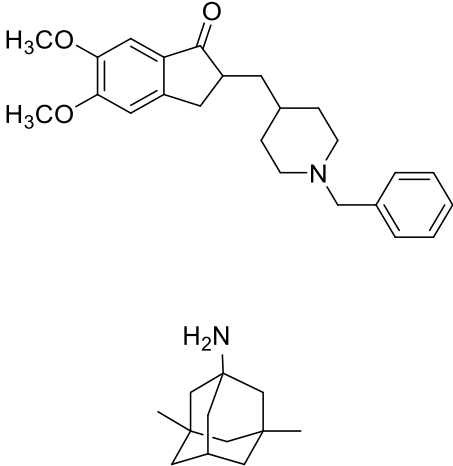
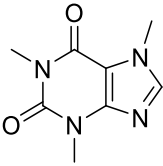
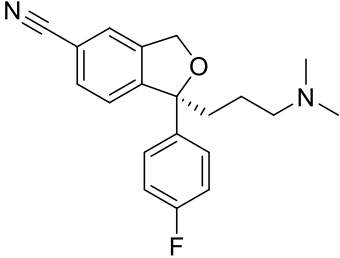
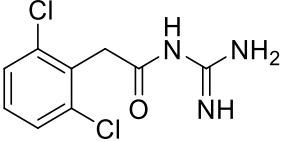
Symptom-Reducing Small Molecules:			
AD-35 phosphenoperoxoic acid compound with 6'-(2-(1- (pyridin-2- ylmethyl)piperidin- 4- yl)ethyl)spiro[cyclo propane-1,5'- [1,3]dioxolo[4,5- f]isoindol]-7'(6H)- one		Acetylcholinesterase inhibitor	Neurotransmitter receptors
Huperzine A		NMDA receptor antagonist and AChE inhibitor (MTDL)	Neurotransmitter receptors
Dexmedetomidine		Sublingual Dexmedetomidine, selective α_2 - adrenergic receptor agonist	Neurotransmitter receptors
CORT108297 (R)-4a- (ethoxymethyl)-1- (4-fluorophenyl)-6- ((4- (trifluoromethyl)ph enyl)sulfonyl)- 4,4a,5,6,7,8- hexahydro-1H- pyrazolo[3,4- g]isoquinoline		Selective glucocorticoid receptor antagonist, reduce neuroendocrine stress responses	Hormone (Cognition Enhancement)

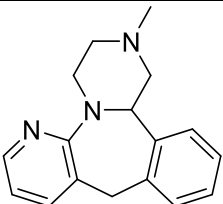
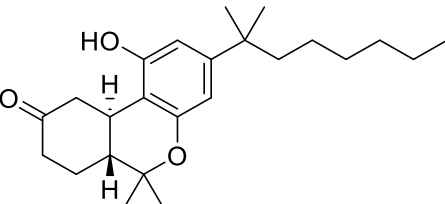
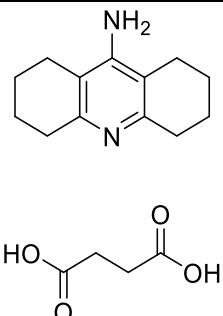
Dronabinol		CB1 and CB2 Endocannabinoid receptor partial agonist	Neurotransmitter receptors
Nicotine		Nicotinic acetylcholine receptor agonist Enhances cognition	Neurotransmitter receptors
Prazosin		α -1 adrenoreceptor antagonist	Neurotransmitter receptors
SAGE-718	First-in-class, oxysterol-based positive allosteric modulator (PAM) of N-methyl-D-aspartate (NMDA) receptors		Neurotransmitter receptors
Phase III			
Disease-modifying Biologicals:			
Donanemab	MAB specific for pyroglutamate form of A β		Amyloid
Gantenerumab	MAB directed at A β plaques and oligomers		A β
Lecanemab	MAB directed at A β protofibrils		A β
UB311	Vaccine that stimulates a T-helper type 2 regulatory immune response over a T-helper type 1 pro-inflammatory response, and to avoid cross-reactivity with similar endogenous antigens, i.e., autoimmune responses		Amyloid

Disease-modifying Drugs:			
Atuzaginstat		It reduces neuroinflammation and hippocampal degeneration	Inflammation / Infection due to <i>P.gingivalis</i>
Blarcamesine		Sigma-1 receptor agonist, M2 autoreceptor antagonist. It ameliorates oxidative stress, protein misfolding, mitochondrial dysfunction, and inflammation	Synaptic plasticity
GV-971 sodium (2S,3S,4S,5S,6R)-6-((1-carboxylato-2,4-dihydroxyhexan-3-yl)oxy)-3,4,5-trihydroxytetrahydro-2H-pyran-2-carboxylate oxo-13-methanolate	 $n = 1-9 ; m = 0-2 ; m' = 0-1$	Algae-derived acidic oligosaccharides, changes microbiome to reduce peripheral and central inflammation.	Inflammation
Icosapent ethyl		Purified form of the omega-3 fatty acid EPA. It improves synaptic function and reduces inflammation	Oxidative stress

<p>Losartan + Amlodipine + Atorvastatin</p>	 <p>The image displays three chemical structures. The top structure is Losartan, featuring a tetrazole ring connected to a biphenyl system, which is further linked to a dihydroisoxazole ring containing a hydroxymethyl group and a chlorine atom. The middle structure is Amlodipine, showing a dihydropyridine ring with a methyl group, a methoxycarbonyl group, and a side chain containing a chlorine atom and a propyl ester group. The bottom structure is Atorvastatin, consisting of a pyrazole ring with a phenylamide group, an isopropyl group, and a side chain with two hydroxyl groups and a terminal carboxylic acid group.</p>	<p>Losartan: Angiotensin II receptor blocker Amlodipine: Calcium Channel Blocker Atorvastatin: Anti- hyperlipidemic (HMG-CoA reductase inhibitor)</p>	<p>Vasculature</p>
<p>Metformin</p>	 <p>The image shows the chemical structure of Metformin, which is a 1,3,5-triazin-2(1H)-thione derivative with a methyl group on the nitrogen at position 4.</p>	<p>Insulin sensitizer to improve CNS glucose metabolism</p>	<p>Metabolism and bioenergetics</p>
<p>Omega-3 fatty acids</p>	 <p>The image shows three chemical structures of omega-3 fatty acids. On the left is a long-chain polyunsaturated fatty acid with three double bonds. In the middle is Linolenic acid, a 18-carbon chain with three double bonds and a carboxylic acid group. On the right is eicosapentanoic acid, a 20-carbon chain with five double bonds and a carboxylic acid group.</p>	<p>Antioxidant</p>	<p>Oxidative stress</p>

<p>NE3107</p>		<p>MAPK-1/3 inhibitor. It reduces pro-inflammatory NFκB activation</p>	<p>Inflammation</p>
<p>Tricaprilin</p>		<p>Caprylic triglyceride. It induces ketosis and improves mitochondrial and neuronal function</p>	<p>Metabolism and bioenergetics</p>
<p>Troriluzole</p>		<p>Glutamate modulator; prodrug of riluzole. It improves synaptic function</p>	<p>Synaptic plasticity / neuroprotection</p>
<p>Leuco-methylthioninium (LMTX) mesylate</p>		<p>Tau protein aggregation inhibitor</p>	<p>Tau</p>
<p>Symptom-Reducing Small Molecules</p>			
<p>Brexpiprazole</p>		<p>Atypical antipsychotic, D2 receptor partial agonist</p>	<p>Neurotransmitter receptors</p>

<p>Dextromethorphan + Quinidine</p>	 <p>The image shows two chemical structures. The top structure is Dextromethorphan, a morphine derivative with a methoxy group at the 3-position and a methyl group on the nitrogen. The bottom structure is Quinidine, a quinoline alkaloid with a vinyl group and a hydroxyl group on the quinoline ring system.</p>	<p>Signal receptor agonist, NMDA receptor antagonist</p>	<p>Neurotransmitter receptors</p>
<p>Donepezil + Memantine</p>	 <p>The image shows two chemical structures. The top structure is Donepezil, a carbamate cholinesterase inhibitor with two methoxy groups on the benzene ring and a benzylpiperazine side chain. The bottom structure is Memantine, a non-competitive NMDA receptor antagonist with a bicyclic tropane-like core and a primary amine group.</p>	<p>Donepezil: binds to AChE and reversibly inactivates it Memantine: blocks current flow through NMDA receptor channels</p>	<p>Cognition enhancement</p>
<p>Caffeine</p>	 <p>The image shows the chemical structure of Caffeine, a purine alkaloid with methyl groups on the nitrogen atoms.</p>	<p>Pleiotropic Effect on CNS</p>	<p>Metabolism and bioenergetic, Cognition Enhancement</p>
<p>Escitalopram</p>	 <p>The image shows the chemical structure of Escitalopram, a selective serotonin reuptake inhibitor (SSRI) with a cyano group, a fluorine atom, and a dimethylaminoethyl side chain.</p>	<p>Selective Serotonin reuptake inhibitor</p>	<p>Neurotransmitter receptors</p>
<p>Guanfacine</p>	 <p>The image shows the chemical structure of Guanfacine, an alpha-2 adrenergic agonist with a dichlorophenyl ring and a guanidino group.</p>	<p>α-2 adrenergic agonist</p>	<p>Cognition enhancement</p>

Mirtazapine		α -1 antagonist	Neurotransmitter receptors
Nabilone		Synthetic cannabinoid, CB1 and CB2 receptor agonist. It suppresses neuronal excitability and neurotransmitter release	Neurotransmitter receptors
Octahydroaminoacridine succinate		AChE inhibitor	Cognition Enhancement

4. Why Dual Inhibitors?

Dual inhibitors are characterized by their bifunctional profile, enabling simultaneous action on two distinct biological targets. They serve as potent tools in addressing multiple disease states. Over the years, MTDLs have become synonymous with dual ligands, triple blockers, heterodimers, etc. The selection of these targets depends on data from previous literature and various clinical sources [92]

The design of dual inhibitors is grounded in the idea that they can expedite disease resolution by concurrently acting on multiple targets that govern the progression of a specific ailment. These inhibitors may also exhibit the ability to bind to and suppress diseases beyond their original therapeutic intent [93]. Given the activation of numerous protein complexes due to the regulation of upstream proteins, targeting these complexes can block entire signaling pathways. The development of dual inhibitors is a laborious and time-intensive process, guided by various considerations related to the nature and physiology of the target [94].

4.1 Advantages of dual inhibitors:

- Dual inhibitors exhibit potency even at low doses, resulting in reduced dosing frequency and enhanced patient adherence attributed to the fact that many diseases stem from multiple causes.
- The disease symptoms can be effectively reversed with minimal drug dosage, by simultaneously blocking two of these causes.
- Crucially, dual inhibitors address a significant issue associated with single-target inhibiting agents, namely, drug resistance.
- In the context of multifactorial diseases, the inhibition of a single target may allow the disease to persist and thrive through alternative pathways. This challenge impedes the permanent alleviation of the disease.
- However, the simultaneous targeting of two distinct pathways involved in the disease creates a synergistic effect, reducing the likelihood of drug resistance.
- Additionally, the binary action of a single molecule on two disease-related targets ensures superior efficacy in treatment. This approach not only offers cost-effectiveness but also enables the management of symptoms associated with multiple diseases swiftly and efficiently at the cost of a single drug [95].

4.2 Limitations and challenges faced by dual inhibitors:

4.2.1 Limitations

- Dual inhibitors operate on two disease targets concurrently, potentially resulting in increased drug affinity for one target and decreased affinity for the other.
- In many instances, drugs designed for dual targeting tend to exhibit lower affinity interactions compared to single-target drugs, given that small molecules are less likely to bind equally strongly to multiple targets. Therefore, careful design of the agent is crucial to improve binding to both targets, a process achieved by identifying and utilizing the shared chemical space between the two targets [96].
- Another drawback associated with the utilization of these agents is that their dual action frequently leads to toxicity.
- Agents with the potential to inhibit two proteins simultaneously can induce unpredictable reactions, as the blockade of a protein implicated in a specific disease may disrupt multiple other pathways in which the same protein plays a significant role.

- Additionally, the integration of two distinct pharmacophores employed to construct dual inhibitors may create a synergism of adverse reactions.
- These adverse effects may also manifest if the drug binds to targets other than those explicitly intended. These reactions are often a combination of different effects and have an unknown origin. Therefore, careful consideration of protein interlinking is essential when designing such entities [97].
- An additional drawback associated with dual inhibitors is the potential for dosing errors. Given that a single molecule acts on multiple targets involved in the disease, the dosage profile and tolerance of these agents are likely to differ from mono-targeted drugs used for the same disease.
- Consequently, calculating the correct dose and implementing vigilant monitoring of drug intake become crucial. To ensure the safety and efficacy of these agents, they must undergo meticulously designed experiments for dose determination [98].

In addition to this, various factors, including the location and nature of the target, the ligand's binding to the target, the interaction between the ligand and the target, the ligand's quality, dosage scheme, storage conditions, and ultimately cost-effectiveness, must be meticulously assessed in the development of these agents. Utilizing network analysis based on the nature of diseases and known resistance mechanisms is crucial for improving target selection. In summary, extensive research, both in terms of study and experimentation, is imperative to mitigate harmful side reactions related to drug use [99].

4.2.2 Challenges

- A significant challenge concerning drug targets is the variability of proteins and their regulation across different species, races, genders, ages, environments, daily dietary habits, and exercise routines.
- The internal interactive dynamics of a drug with the body cannot be precisely regulated. Additionally, there are numerous proteins that remain unknown, and it's possible that the identified proteins are linked to undiscovered pathways. Consequently, it is not always feasible to control the precise manner in which a designed drug functions [100].
- Pharmacokinetics plays a crucial role in determining the temporal trajectory of a drug within the body. Understanding the Absorption, Distribution, Metabolism, and

Excretion (ADME) profile of a drug is essential for comprehending the behavior of the drug compound in the body and establishing an appropriate dosage regimen.

- Obtaining pharmacokinetic data for such drugs is challenging, primarily because the two distinct components comprising these agents have independent absorption, distribution, metabolism, and excretion profiles [101].
- Predicting the duration in which the drug undergoes all four phases is consequently challenging.
- Similarly, grasping the pharmacodynamics data associated with the drug is complex due to its independent action on two receptors and its varying affinity for the same [102] (**figure 10**).

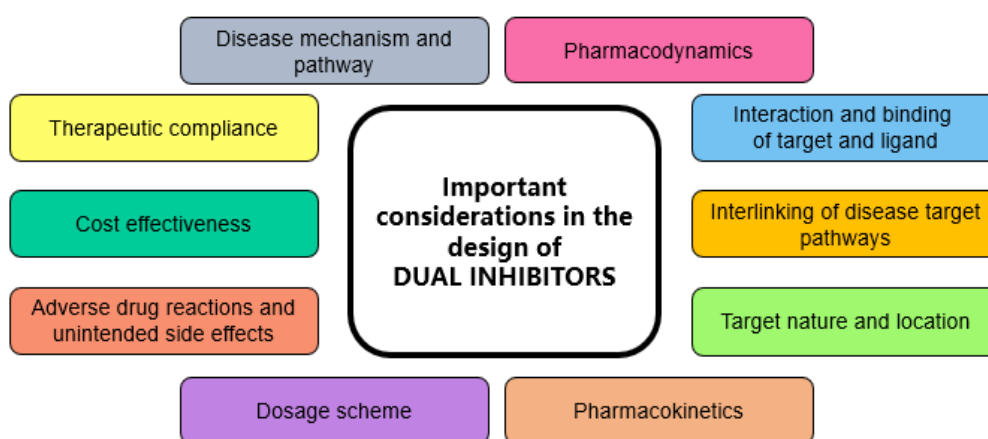


Figure 10. Important considerations in the design of dual inhibitors

5. Literature review on dual inhibitors targeting AChE and BACE 1

The growing recognition of Alzheimer's disease's complex nature has ushered in a new approach to drug design. This involves exploring compounds that can interact with multiple targets associated with Alzheimer's, potentially leading to improved outcomes and reduced side effects. The emerging concept of multi-target directed ligands (MTDLs)/dual inhibitors has become a focal point in medicinal chemistry research. Various strategies have been employed to target multiple aspects of Alzheimer's, including AChE, BACE 1, GSK-3 β , monoamine oxidase, metal ions, and A β aggregation. One prevalent strategy involves combining two or more molecular scaffolds, each with known properties or targets, into a unified molecular entity [103].

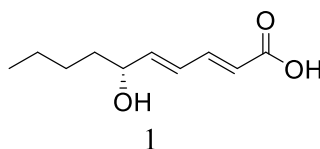
This review encompasses both synthetic and natural compounds that have been identified, since 2003, as dual inhibitors targeting both AChE and BACE 1.

5.1 AChE and BACE 1 dual-target inhibitors from natural sources:

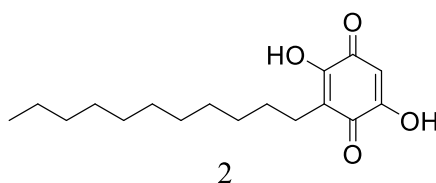
Plants, marine organisms, and even fruits are commonly regarded as reliable reservoirs of pharmacologically significant compounds. The meticulous investigation of their biological properties, especially those of unfamiliar compounds, can unveil notable activities against a range of specific biological targets.

In this section, compounds obtained from natural sources, which exhibited interesting inhibitory activities against AChE and BACE 1, are discussed [104].

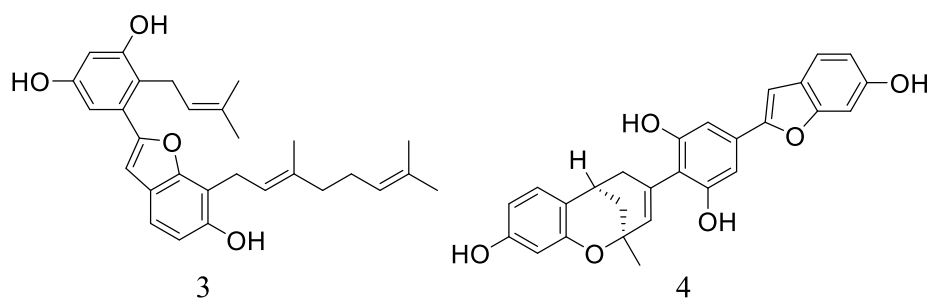
Nguyen *et al.*, in 2015 provided the initial instance wherein they extracted multiple compounds from *Lycopodiella cernua* L., a traditional Chinese herb from the Lycopodiaceae family with medicinal applications. They subsequently assessed the inhibitory activities of these compounds against both AChE and BACE 1. In this investigation, a novel hydroxy unsaturated fatty acid **1** (AChE: IC_{50} 0.22 ± 0.03 μ M; BACE 1: IC_{50} 6.91 ± 0.44 μ M), were identified. These compounds exhibited intriguing inhibitory properties against both AChE and BACE 1 enzymes [105].



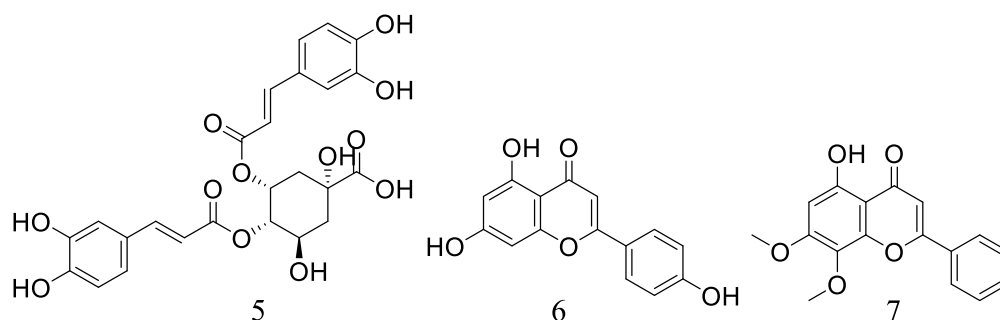
Nuthakki *et al.*, in 2019 investigated the therapeutic potential of plants in Alzheimer's disease (AD) and reported the discovery of embelin, a 3-undecyl-1,4-benzoquinone, extracted from *Embelia ribes* (found in fruits). They also highlighted its capability to inhibit AChE and recombinant human BACE 1. The authors demonstrated that compound **2** exhibited significant inhibition of both tested AChE: IC_{50} of 2.50 ± 0.082 μ M, and for BACE 1: IC_{50} of 2.11 ± 0.33 μ M [106].



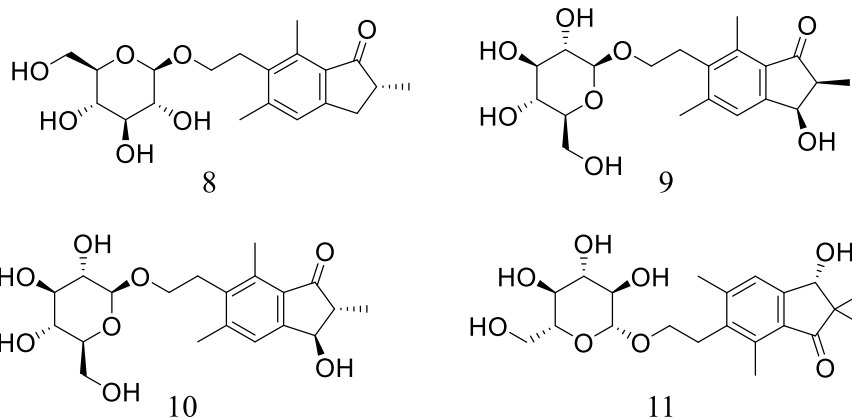
In a separate study, Paudel and colleagues in 2019 isolated five arylbenzofurans from the root bark of *Morus alba*. These compounds exhibited noteworthy inhibitory activities against AChE and demonstrated even greater effectiveness against BACE 1. Compound **3** and **4** exhibited lower inhibitory activity for AChE (IC_{50} 4.61 ± 0.08 μ M and $IC_{50} > 200$ μ M, respectively) compared to berberine. However, compounds **3** and **4** demonstrated improved inhibitory activity for BACE 1 (IC_{50} 0.73 ± 0.03 μ M and IC_{50} 1.04 ± 0.78 respectively) when compared to quercetin [107].



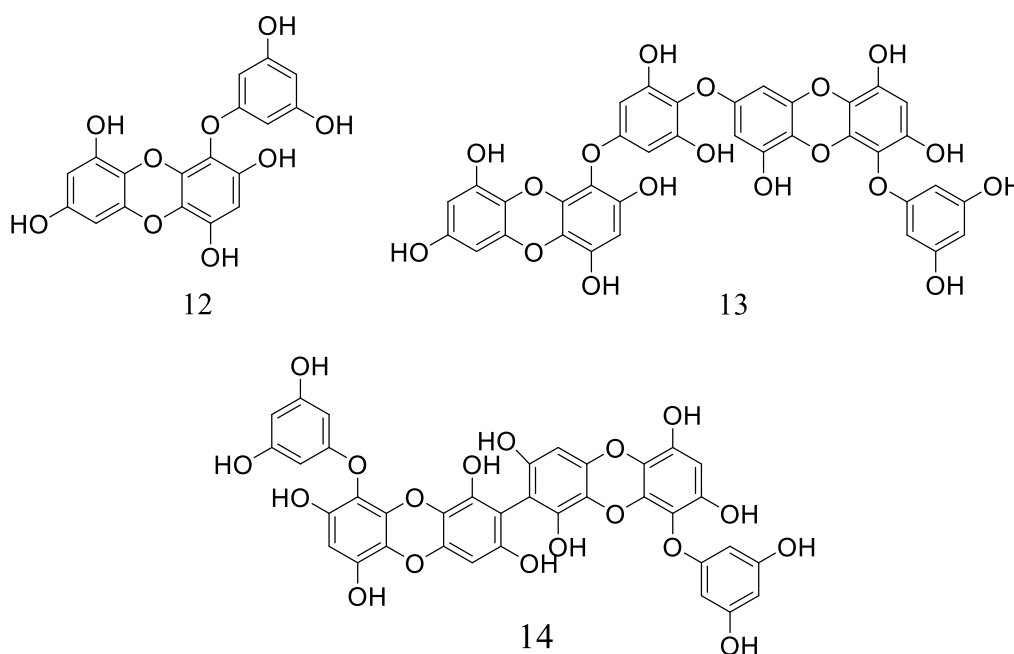
Panche *et al.*, in 2019 examined the inhibitory potentials of specific compounds obtained from medicinal herbs, *Andrographis paniculata* and *Spilanthes paniculata*. Among the compounds isolated, 3,4-di-O-caffeoylquinic acid **5**, apigenin **6**, and 7-o-methylwogonin **7** were chosen as the most favorable candidates for their potential inhibitory effects against both AChE and BACE 1. Compound **5** demonstrated an IC_{50} of 2.14 ± 0.04 μ M for the AChE inhibitory assay and 3.31 ± 0.12 μ M for BACE 1. Similarly, compounds **6** and **7** exhibited noteworthy inhibitory properties against AChE (IC_{50} 3.42 ± 0.02 μ M and 2.46 ± 0.03 μ M, respectively) and BACE 1 (IC_{50} 3.79 ± 0.26 μ M and 2.91 ± 0.04 μ M, respectively) [108].



Jannat *et al.*, in 2019 obtained pterisin derivatives from *Pteridium aquilinum* and investigated their efficacy in relation to AChE and BACE 1. The most potent compounds included (2R)-pteriside B **8**, (2S,3R)-pteriside C **9**, (2R,3R)-pteriside C **10**, and (3S)-pteriside D **11**, exhibiting IC_{50} values of 2.55 ± 0.23 μ M, 9.17 ± 0.82 μ M, 3.77 ± 0.38 μ M, and 27.4 ± 1.2 μ M, respectively, against AChE. For BACE 1, the corresponding IC_{50} values were 18.0 ± 2.8 μ M, 28.9 ± 2.2 μ M, 9.74 ± 1.9 μ M, and 10.7 ± 1.5 μ M, respectively. Remarkably, compounds **8**, **10**, and **11** exhibited greater activities in BACE 1 inhibition compared to quercetin (IC_{50} 18.8 ± 1.0 μ M), although they were less potent than berberine (IC_{50} 0.39 ± 0.01 μ M, used as a positive control in the AChE inhibitory test) [109].

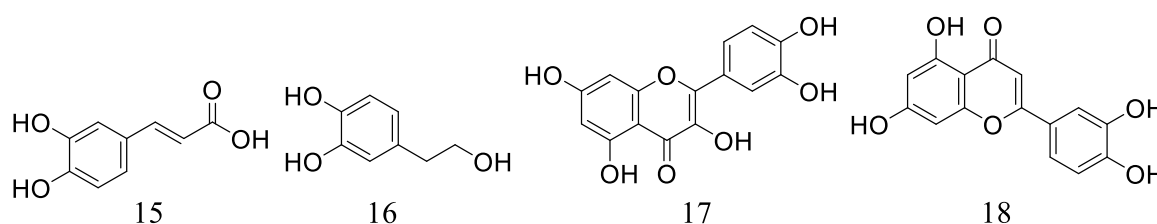


Marine organisms represent an abundant reservoir of bioactive molecules, with phenolic compounds being among them. In an investigation conducted by Lee *et al.*, three phlorotannins, members of the polyphenolic family and classified as tannins, were extracted from *Ecklonia cava*, a brown alga in 2019. These compounds were then evaluated for their inhibitory potential against AChE and BACE 1. In terms of inhibiting AChE, eckol **12** (IC_{50} 10.03 ± 0.94 μ M), dieckol **13** (IC_{50} 5.69 ± 0.42 μ M), and 8,8'-bieckol **14** (IC_{50} 4.59 ± 0.32 μ M) exhibited lower activity than the positive control, galantamine (IC_{50} 0.99 ± 0.07 μ M). However, it is noteworthy that all three compounds, **12** (IC_{50} 7.67 ± 0.71 μ M), **13** (IC_{50} 2.34 ± 0.10 μ M), and **14** (IC_{50} 1.62 ± 0.14 μ M), demonstrated higher inhibitory activity against BACE 1 compared to the standard resveratrol (IC_{50} 14.89 ± 0.54 μ M) [110].

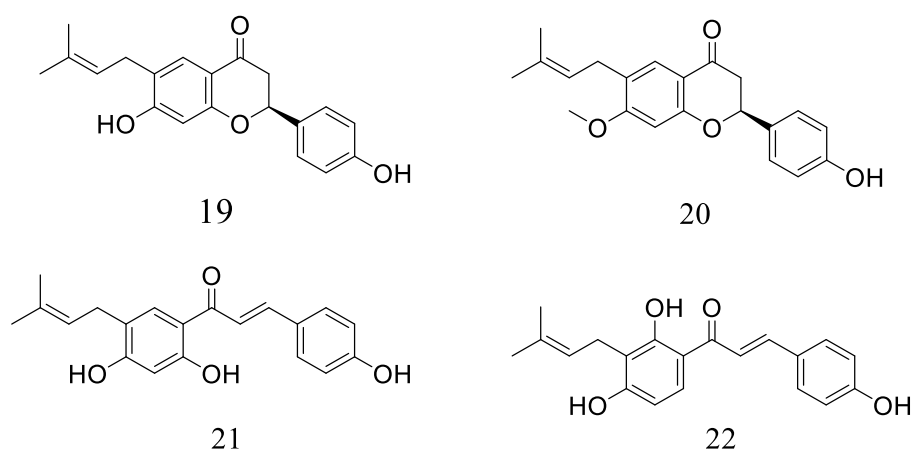


Omar *et al.*, in 2018 assessed the inhibitory potential of a variety of phenolic compounds, including both non-flavonoids and flavonoids, that were isolated from *Olea europaea* L., against AChE and BACE 1. Compounds **15**, **16**, and **18** demonstrated mild inhibition against

AChE. However, the results were notably encouraging in terms of their BACE 1 inhibitory potential, especially for caffeic acid **15** (IC_{50} $16.67 \pm 0.03 \mu\text{M}$) and hydroxytyrosol **16** (IC_{50} $0.035 \pm 0.04 \mu\text{M}$), surpassing the effectiveness of the positive control, epigallocatechin gallate (IC_{50} $96.26 \pm 0.04 \mu\text{M}$). Among the identified flavonoids, quercetin **17** (IC_{50} : $55.44 \pm 0.03 \mu\text{M}$) and luteolin **18** (IC_{50} not detectable) were found to be less potent than galantamine for AChE (IC_{50} : $0.59 \pm 0.004 \mu\text{M}$). However, both compounds **17** and **18** demonstrated superior effectiveness against BACE 1 compared to epigallocatechin gallate (IC_{50} of $0.55 \pm 0.24 \mu\text{M}$ and $0.52 \pm 0.28 \mu\text{M}$, respectively) [111].



In 2018, Xu *et al.* isolated natural flavonoids from the dried mature fruits of *Psoralea Fructus*, a medicinal plant, and proceeded to assess their inhibitory effects on both AChE and BACE 1. At a concentration of $100 \mu\text{M}$, Bavachin **19** demonstrated approximately 34% inhibition of AChE and 14% inhibition of BACE 1. Bavachinin **20** exhibited 80% inhibition of AChE and 20% inhibition of BACE 1 at the same concentration, while bavachalcone **21** inhibited about 46% of AChE and 68% of BACE 1. Finally, Isobavachalcone **22** showed approximately 83% inhibition of AChE and 34% inhibition of BACE 1 [112].



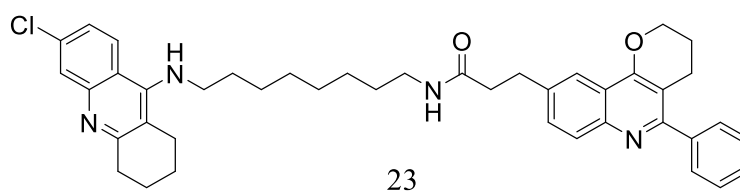
5.2 Synthetic AChE and BACE 1 dual inhibitors

The extensive investigation into the multifaceted nature of Alzheimer's disease has led to the identification of various potential drug targets. Despite ongoing research to validate new targets for treating AD, the connection between specific targets and the disease remains incompletely understood. Nonetheless, the widely acknowledged significance of AChE and

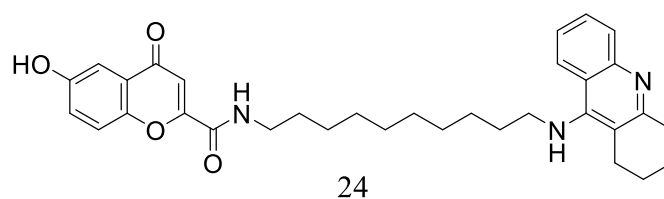
BACE 1 in AD has prompted the scientific community to recognize their paramount importance. Consequently, numerous compounds have been synthesized, employing diverse strategies and molecular templates, with the aim of serving as dual inhibitors for both AChE and BACE 1 [113,114].

In this section, synthetic compounds that target both enzymes, covering the period from 2003 to 2022 are discussed with their inhibitory activity against both targets.

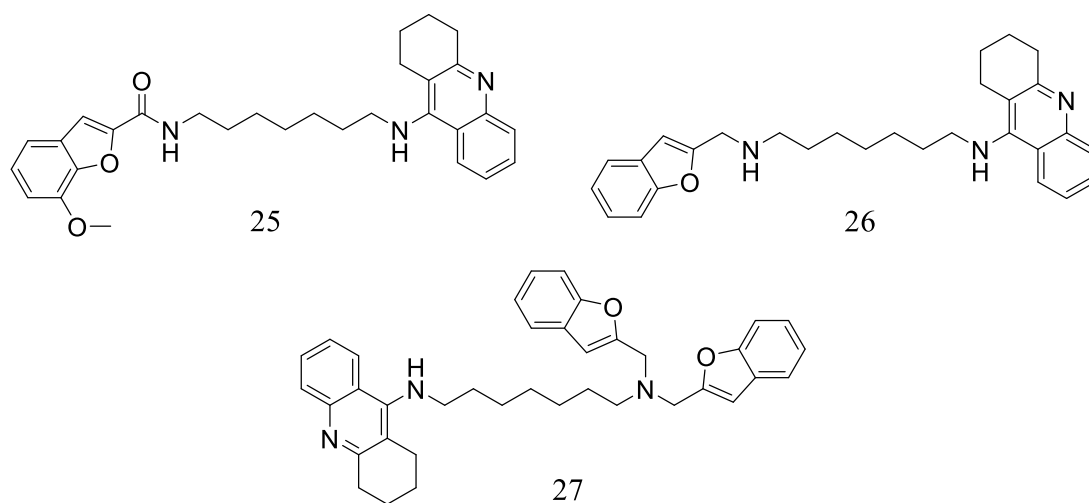
Camps *et al.*, in 2009 synthesized hybrids of pyrano[3,2-c] quinoline-6-chlorotacrine (compound **23**) to assess their anti-Alzheimer activities targeting AChE and β -amyloid through BACE 1 inhibition. These hybrid compounds combine the 6-chlorotacrine and pyrano[3,2-c] quinoline moieties. Compound **23** preserves the strong and selective inhibition of human AChE observed in the parent 6-chlorotacrine. Moreover, it displays notable in vitro inhibitory activity against both AChE (IC_{50} 14.0 ± 1.2 nM) and BACE 1 (% inhibition 77.8 ± 6.4 at a concentration of $2.5 \mu\text{M}$). Additionally, it demonstrates the ability to penetrate the central nervous system, establishing it as a promising lead compound for the development of anti-Alzheimer's drugs [115].



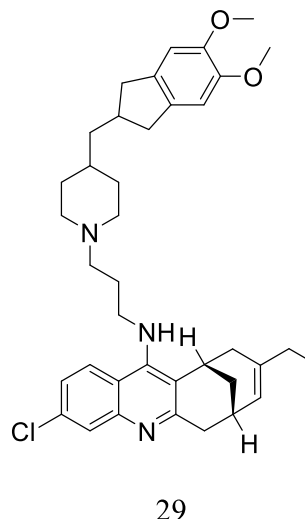
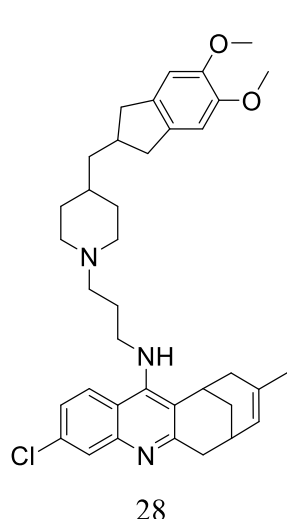
In 2012, Bachiller *et al.*, synthesized novel hybrids (compound **24**) combining tacrine and 4H-chromen-4-one, designed as multi-functional agents with two distinct moieties targeting various Alzheimer's disease-related factors. The choice of the tacrine fragment was based on its established inhibitory effects on cholinesterases, while the flavonoid scaffold derived from 4H-chromen-4-one was selected for its scavenging and BACE 1 inhibitory properties. Among the examined hybrids, compound **24** demonstrates robust dual inhibition against human BACE 1 (IC_{50} $2.80 \pm 0.01 \mu\text{M}$) and AChE (IC_{50} 8.0 ± 0.2 nM), along with favorable antioxidant properties and the ability to penetrate the central nervous system [116].



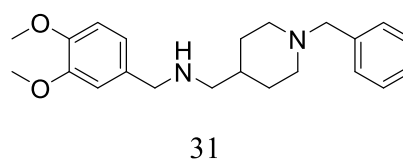
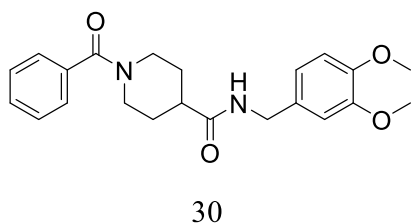
Zha *et al.*, in 2016 synthesized tacrine-benzofuran hybrids, specifically **25**, **26**, and **27**, with the intention of serving as multi-target agents against the selected targets AChE and BACE 1. The design of these compounds incorporated the properties of the benzofuran moiety to address amyloid aggregation and AChE/BACE 1 inhibition. Additionally, the inclusion of a tacrine analogue was anticipated to enhance inhibitory properties against AChE. Compounds **25**, **26**, and **27** exhibited a particularly noteworthy profile, serving as subnanomolar selective inhibitors of human acetylcholinesterase (hAChE) with IC_{50} values of 44.2 ± 3.3 nM, 0.86 ± 0.05 nM, and 117 ± 8 nM, respectively. Additionally, they displayed favorable hBACE 1 activity with IC_{50} values of 0.43 ± 0.22 μ M, 1.35 ± 0.13 μ M, and 0.62 ± 0.18 μ M, respectively [117].



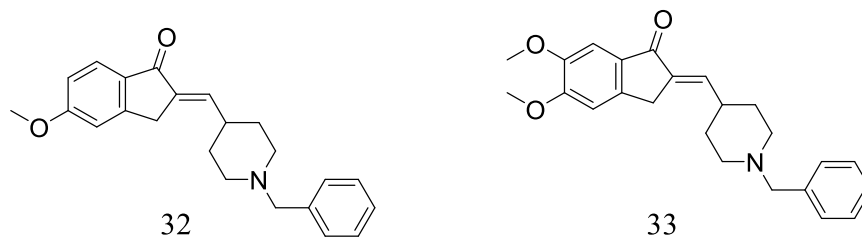
In 2010, Gómez *et al.*, synthesized and assessed huprine-donepezil hybrids **28** and **29** for their potential as inhibitors of AChE and BACE 1. They employed a hybridization strategy, incorporating the donepezil-related fragment- 5,6-dimethoxy-2-[(4-piperidiny)-methyl]indane to enhance the binding with these enzymes. The most effective inhibitors of AChE and BACE 1, namely, heterodimers **28** and **29**, surpass the parent huprines in potency and exhibit comparable effectiveness to donepezil. Specifically, compounds **28** and **29** showed an IC_{50} value of 2.61 ± 0.2 nM and 3.85 ± 0.2 nM for AChE. For BACE 1, it displayed a % inhibition of 30.8 ± 4.1 and 14.9 ± 3.9 at 10 μ M concentration under the same assay conditions [118].



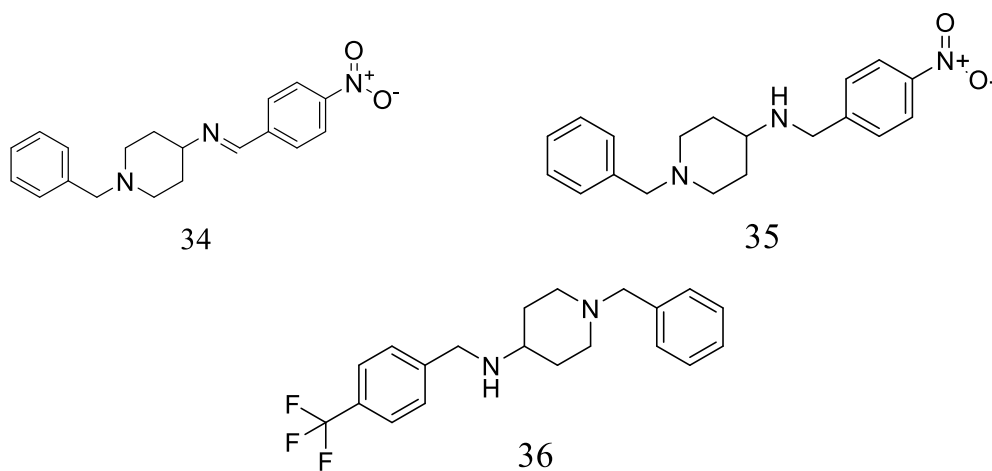
In 2018, Gabr and Abdel-Raziq designed novel analogues of donepezil with the aim of serving as dual inhibitors of AChE and BACE 1. These analogues incorporated a donepezil fragment attached to various linkers, allowing for an exploration of the influence of the linker on inhibitory activity against both AChE and BACE 1. *In vitro* assays demonstrated the dual mode of action exhibited by compounds **30** and **31** against hAChE and BACE 1. Notably, both compounds **30** and **31** exhibited potent inhibition of hAChE, with IC_{50} values of 4.11 ± 0.12 nM and 145 ± 1.42 nM, respectively, as well as BACE 1 inhibition with IC_{50} values of 18.3 ± 0.17 nM and 243 ± 1.13 nM, respectively. These values were compared to donepezil, which displayed IC_{50} values of 6.21 nM and 194 nM against hAChE and BACE 1, respectively [119].



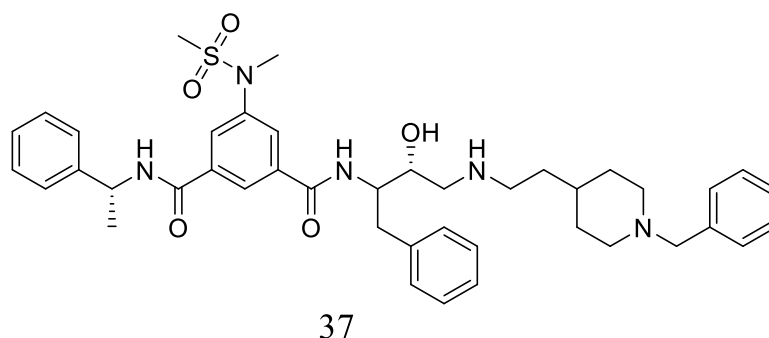
In 2016, Constanzo *et al.*, designed the donepezil analogues **32** and **33**, incorporating indanone and piperidine moieties, which are key pharmacophoric fragments of donepezil. Notably, these analogues feature a double bond linked to the indanone nucleus, a deliberate inclusion. It has been reported that the presence of this type of unsaturation can enhance BACE 1 inhibitory ability due to increased structural rigidity. However, compounds **32** and **33** exhibited superior dual activity with lower IC_{50} values against both AChE (0.342 ± 0.029 μ M and 0.043 ± 0.007 μ M) and BACE 1 enzyme (% inhibition 59 and 13 at a concentration of 1.0 μ M), respectively [120].



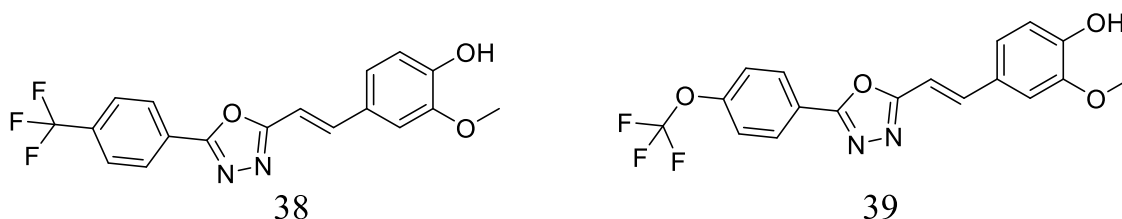
In 2019, Sharma *et al.*, adopted a similar strategy for developing dual inhibitors of AChE and BACE 1, utilizing N-benzylpiperidine analogues of donepezil, specifically compounds **34**, **35** and **36**. The rationale behind the design of these derivatives was based on the observation that the N-benzylpiperidine core present in donepezil can interact with the catalytic active site of AChE, and modifications on the indanone core were expected to enhance BACE 1 inhibitory potential. Structural analogues distinguished by the imine or amine linkage, respectively, were synthesized and assessed for their potential against these enzymes. The *in vitro* assay results indicated a well-balanced inhibitory potential against both AChE and BACE 1 in the sub-micromolar range for compounds **34** (AChE: $IC_{50} = 0.90 \mu\text{M}$; BACE 1: $IC_{50} = 0.73 \mu\text{M}$), **35** (AChE: $IC_{50} = 0.72 \mu\text{M}$; BACE 1: $IC_{50} = 0.43 \mu\text{M}$), and **36** (AChE: $IC_{50} = 0.11 \mu\text{M}$; BACE 1: $IC_{50} = 0.22 \mu\text{M}$) [121].



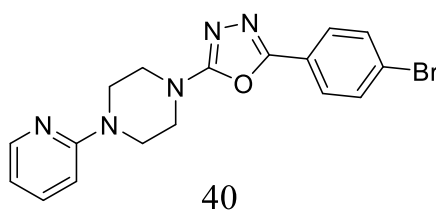
In 2009, Zhu *et al.*, synthesized a novel class of dual inhibitors for AChE and BACE 1 by combining isophthalamide and N-benzylpiperidine fragments. The design of derivative **37** was guided by the pharmacophoric structures of isophthalamide and the N-benzylpiperidine moiety extracted from donepezil. These structural elements are crucial for establishing specific interactions with AChE. Compound **37** displayed robust dual potency in enzyme inhibitory assays, with an IC_{50} of $0.567 \mu\text{M}$ for BACE 1 and $1.83 \mu\text{M}$ for AChE. Furthermore, it demonstrated significant inhibitory effects on $A\beta$ production in APP-transfected HEK293 cells, with an IC_{50} of 98.7 nM , and showed mild protective effects against hydrogen peroxide-induced PC12 cell injury [122].



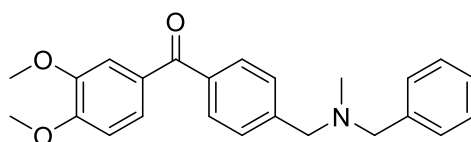
In 2020, Tripathi *et al.*, utilized a molecular hybridization approach to synthesize and evaluate the biological activity of 1,3,4-oxadiazole hybrids **38** and **39**, which are based on ferulic acid. These hybrids were designed as multi-functional therapeutics for Alzheimer's disease, and their inhibitory capacity against AChE and BACE 1 was investigated. Compound **38** emerged as the most potent AChE inhibitor, exhibiting an IC_{50} of 0.068 μM . Additionally, it demonstrated equipotent inhibition of BChE and BACE 1, with IC_{50} values of 0.218 μM and 0.255 μM , respectively. On the other hand, Compound **39** displayed the most substantial inhibition of BChE and BACE 1, with IC_{50} values of 0.163 μM and 0.211 μM , respectively [123].



In 2019, Tripathi *et al.* delved into oxadiazole heterocycles and developed molecular hybrids of 1,3,4-oxadiazole and 2-pyridylpiperazine, specifically compound **40**. They assessed the inhibitory activity of these compounds against AChE and BACE 1. The design of these compounds was inspired by a fragment of verubecestat, a potent inhibitor of BACE 1, which contains a 2-pyridyl ring crucial for binding to the BACE 1 enzyme. Specifically, compound **40** was identified as the most promising lead, exhibiting inhibition of acetylcholinesterase (hAChE) with IC_{50} values of 0.074 μM and beta-secretase-1 (hBACE 1) with IC_{50} values of 0.098 μM [124].

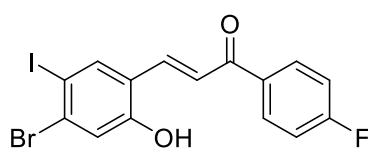


In 2014, Belluti *et al.*, endeavored to create multi-potent agents against AChE and BACE 1, synthesizing benzophenone derivatives **41**. These compounds were designed to engage with both targets, incorporating two pharmacophoric moieties: benzophenone and N,N'-benzylmethylamine, known for their modulation of AChE. The resulting compound **41** exhibited a notable shift in its biological profile, demonstrating a significant increase in both BACE 1 (% inhibition 20 at a concentration of 5.0 μM) and AChE inhibition with an IC_{50} of $0.46 \pm 0.04 \mu\text{M}$ [125].

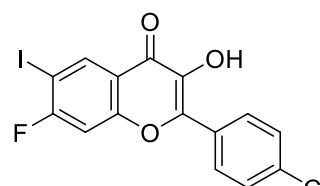


41

In 2018, Mphahlele *et al.*, synthesized new families of iodochalcones **42** and their iodoflavonol analogues **43** to investigate their inhibitory effects on AChE and BACE 1. The study involved the development of various iodochalcones and their corresponding iodoflavonol derivatives with distinct substitution patterns were evaluated against both enzymes. The chalcone derivative **42** displayed moderate inhibition of AChE activity (IC_{50} of $10.98 \pm 0.03 \mu\text{M}$) compared to donepezil. Notably, it exhibited an enhanced inhibitory effect and selectivity against BChE. Specifically, compound **42** showed potential as a dual inhibitor, with IC_{50} values of $5.73 \pm 0.05 \mu\text{M}$ for BChE and $4.70 \pm 0.06 \mu\text{M}$ for BACE 1 activities. The flavonol derivative **43** seems to demonstrate higher selectivity against AChE activity (IC_{50} of $3.45 \pm 0.07 \mu\text{M}$) and displays significantly reduced inhibitory effects on BChE (IC_{50} of $37.51 \pm 0.08 \mu\text{M}$) and moderate effects on BACE 1 activity (IC_{50} of $19.69 \pm 0.05 \mu\text{M}$) [126].

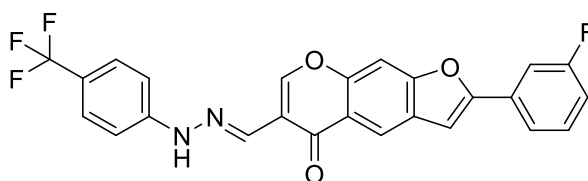


42



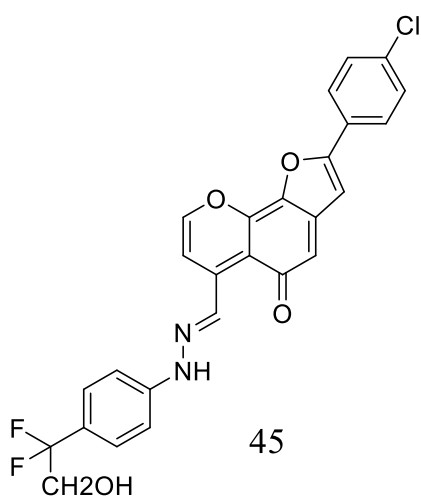
43

In 2019, Mphahlele *et al.*, assessed the inhibitory potential of compound **44**, derived from chromone-6-carbaldehyde, on AChE and BACE 1. These compounds were designed based on evidence suggesting that benzo[b]furan-based compounds and chromone moieties exhibit anti-Alzheimer's disease properties, with potential applications in various neurodegenerative diseases. Particularly, compound **44** exhibits the potential to act as dual inhibitors for both AChE (IC_{50} of $10.98 \pm 0.03 \mu\text{M}$) and BACE 1 activities (IC_{50} of $4.70 \pm 0.06 \mu\text{M}$) [127].

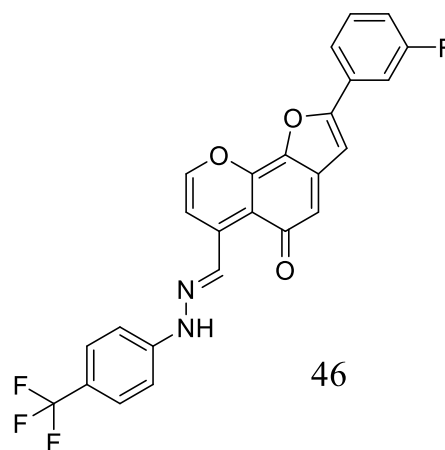


44

In 2019, Mphahlele et al. reported the synthesis of 4-oxo-4H-furo[2,3-h]chromene derivatives **45** and **46**, incorporating the furan ring into their structure. Specifically, compounds **45** and **46** demonstrate the potential to function as dual inhibitors for both AChE (IC_{50} of 5.4 ± 0.02 and 10.4 ± 0.02 μ M) and BACE 1 activities (IC_{50} of 13.6 ± 0.02 and 15.8 ± 0.01 μ M) [128].

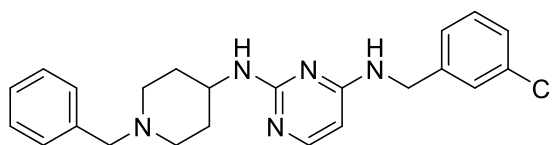


45



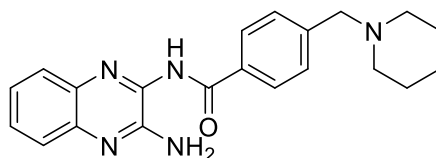
46

In 2012, Mohamed *et al.*, developed compound **47** based on the template of a 2,4-disubstituted pyrimidine ring, recognized for its effectiveness as an inhibitor of AChE, BACE 1, and A β -aggregation. The design involved the combination of pharmacophoric fragments, specifically pyrimidine-2,4-diamine and benzylpiperidine, to create hybrid compounds targeting AChE and BACE 1. Following *in vitro* screening, compound **47** was identified as the lead candidate, displaying a dual inhibitory profile against AChE (AChE IC_{50} = 9.9 μ M) and BACE 1 (34% inhibition at 10 μ M). Moreover, it exhibited favorable cell viability, with neuroblastoma cell viability at 40 μ M reaching 81.0% respectively [129].



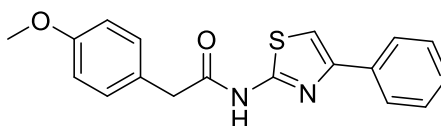
47

In 2011, Huang *et al.*, devised a series of innovative quinoxaline-based hybrids, labeled as compound **48**, employing a linkage approach that integrated quinazoline and the *N*-benzyl pyrrolidine fragment of donepezil, known for its AChE inhibitory properties. Precisely, compound **48** demonstrates the potential to act as a dual inhibitor for both AChE (IC_{50} of $0.483 \pm 0.005 \mu\text{M}$) and BACE 1 activities ($46.64 \pm 2.55\%$ inhibition at $10 \mu\text{M}$) [130].



48

In 2016, Sun and colleagues developed a series of thiazole-acetamide hybrid compound **49** to investigate the AChE inhibitory potential of thiazoles and acetamides. Thiazoles are noteworthy heterocyclic molecules known for their anti-cholinesterase activity. Compound **49** exhibited significant dual potency in enzyme inhibitory assays, with an IC_{50} of $9.24 \mu\text{M}$ for BACE 1 and $3.14 \mu\text{M}$ for AChE [131,132].



49

CHAPTER 2. OBJECTIVE OF THE WORK

2.1. Objective of the present work

The amyloid hypothesis is the most accepted mechanism for AD etiology, making BACE 1 a suitable target for AD drug development. Clinically, AChE inhibitors are used to give symptomatic relief. AChE is also considered a valid target because the peripheral anionic site at the entrance of the AChE active site is involved in aggregation, and inhibition of AChE increases acetylcholine availability at the synapse. Considering the failures of drugs acting on single targets, current investigations focus on developing dual inhibitors that act on two targets or multi-target directed ligands. Among reported dual inhibitors, none have made it to the clinics due to the lack of desired pharmacokinetic and brain permeability profiles. Considering the importance of BACE 1 and AChE, synthesizing dual inhibitors of both these enzymes becomes a valid strategy. This thesis work is based on this particular strategy with the following aim:

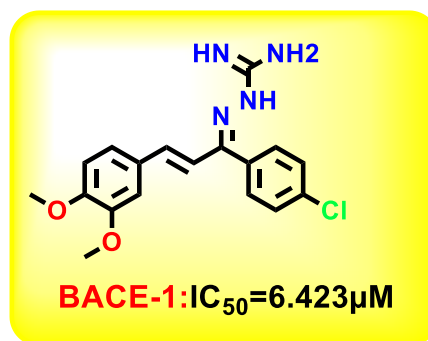
To design, synthesize, and evaluate the dual inhibitors of β -secretase and acetylcholinesterase for the possible treatment of Alzheimer's disease.

To achieve this aim, the following steps were planned:

- i To design novel dual inhibitors of BACE 1 and AChE by *in silico* methods
- ii To synthesize *in-silico* designed compounds by different synthetic approaches followed by purification and characterization
- iii To screen synthesized compounds for *in-vitro* BACE 1 and AChE inhibitory potential
- iv To deduce the structure-activity relationship

2.2. Rationale of the work

The previous work from our laboratory became the starting point for designing the dual inhibitors. A novel class of allylidene hydrazine carboximidamide derivatives was reported as potent BACE 1 inhibitors, having aminoguanidine substitution on allyl linker with two aromatic groups on either side. The most potent compound had IC_{50} of 6.423 μ M against BACE 1. It was reported that two aromatic rings separated by three carbon linker are needed to occupy the S1 and S3 cavity of BACE 1, while guanidine functionality binds with catalytic aspartate dyad [133].



Recently, our collaborators at CSIR-Indian Institute of Integrative Medicine (IIIM), Jammu, have reported that the compounds based on N-benzyl triazole scaffold exhibit dual inhibition of AChE and BACE-1 [134]. Donepezil also has a benzyl substitution and has two aromatic rings separated by a linker. Considering these similarities, it was inferred that incorporating an additional ring in our BACE 1 inhibitor could impart AChE inhibitor property.

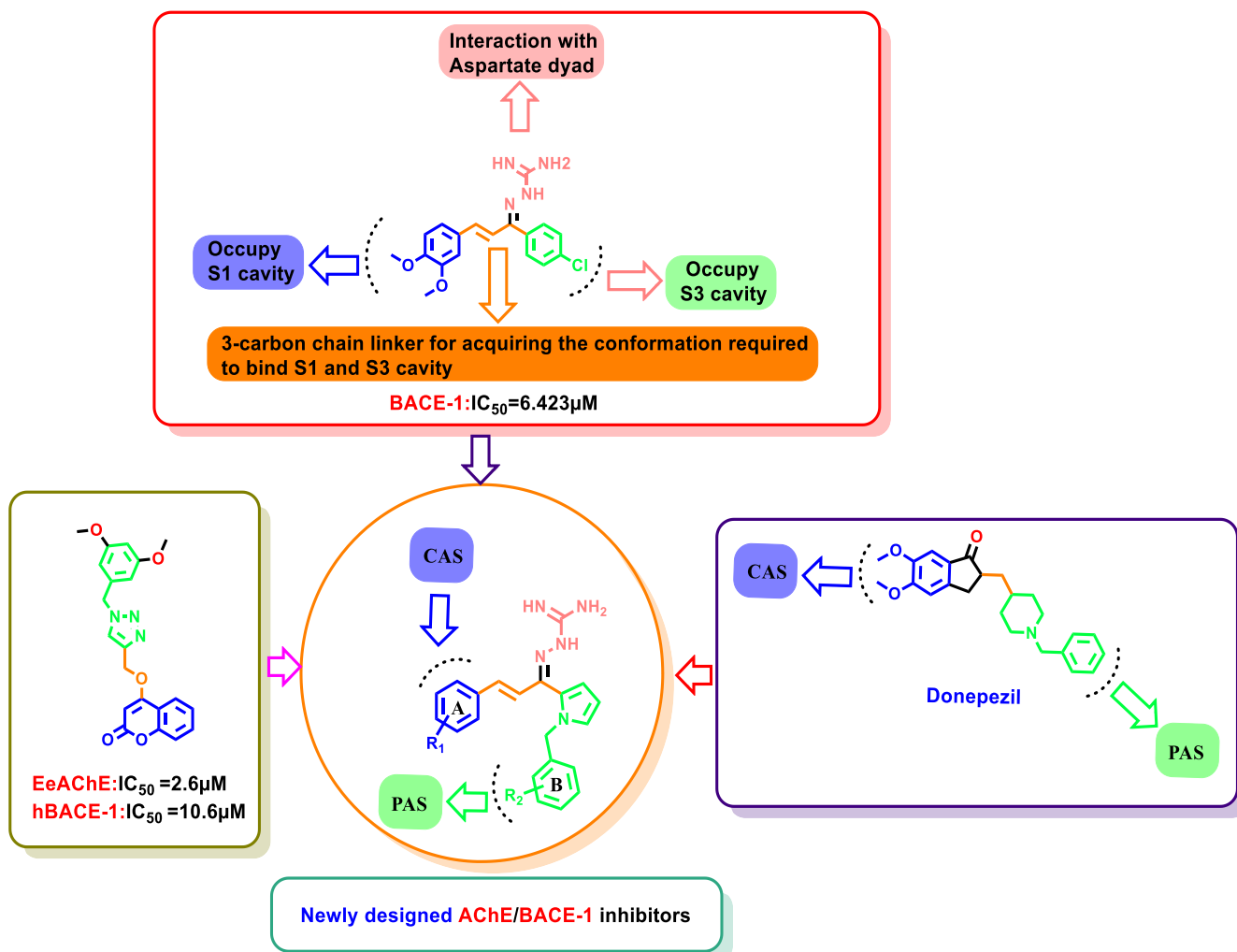


Figure 11. Design strategy using molecular hybridization approach.

It was hypothesized that the replacement of one of the two aromatic rings of allylidene hydrazine carboximidamide (BACE 1 inhibitor) with an *N*-containing hetero-aromatic ring system could help the structure to interact with the catalytic sites of AChE. Two nitrogen heterocycles, namely, pyrrole and indole, were considered. Pyrrole, a 5-membered heterocycle, is expected to mimic the phenyl ring, and indole, a bicyclic system, is expected to add bulk. Thus, the effect of shrinking the phenyl ring and extending the structure by a bicyclic ring can be studied.

N-benzyl pyrrole was considered on one side of the 3-carbon linker, having guanidine substitution, in the first set of compounds. It was hypothesized that –the NH group of guanidine could form a hydrogen bond with ASP 32 and ASP 228 (key amino acid of BACE 1), and rings A and B could occupy the S1 and S3 cavities of BACE 1. Also, *N*-benzyl pyrrole could occupy PAS, and the other aromatic ring could bind to CAS of AChE. For the design strategy, three series were considered since there are two rings, A and B, on the sides of the linker. In the first, the ring A was substituted, and B was not. In the second, ring B was substituted, and ring A was unsubstituted. In the third series, both rings were substituted. This way, the effect of substitution on AChE and BACE 1 inhibition could be studied, and SAR could be drawn.

In the second set, *N*-benzyl indole was considered on one side of the 3-carbon linker, having guanidine substitution. As in the previous set, it was hypothesized that –the NH group of guanidine could form a hydrogen bond with ASP 32 and ASP 228 (key amino acid of BACE 1), and rings A and B could occupy the S1, S3 cavities of BACE 1. Similarly, *N*-benzyl indole could occupy PAS, and the other aromatic ring could bind to CAS of AChE. As in the first set, three series were considered in this case also based on ring A and/or ring B substitution.

CHAPTER 3. MATERIALS AND METHODS

3. Materials and Methods

3.1 *In-silico* Studies

3.1.1. Requirements for AChE and BACE 1 inhibitor

The analysis of AChE X-ray crystal structure (PDB ID: **4EY7**) revealed the presence of two binding sub-sites, namely PAS (peripheral anionic site) and CAS (catalytic active site), that play a role in the binding of acetylcholine. The PAS is distinctly separated from the choline-binding pocket, which is situated in the active site. At the same time, the CAS is thought to be similar to the catalytic sub-sites seen in other serine hydrolases. The active site of AChE is a long and narrow gorge-like structure that spans about 20 Angstroms in length. This pocket extends halfway into the enzyme and gradually widens as it approaches the base. The gorge pocket contains only a few acidic amino acid residues, which include Asp285, Glu273, and Asp72 hydrogen bonded to Tyr334 and Glu199, respectively. For a compound to be considered an effective inhibitor of AChE, the inhibitor must engage with both the CAS amino acids - Trp86, Tyr337, Trp439, and Tyr341 - as well as the PAS amino acids - Trp286, Phe297, Phe295, Phe338, Tyr124, and Tyr72.

Insights into the key functional groups required to inhibit beta-secretase activity can be gleaned from the X-ray crystal structure of beta-secretase (PDB ID: **6UWP**), which suggests that these groups must possess a basic nature. The presence of an H-bond donor group is essential for forming H-bonding interactions with the catalytic residues Asp-228 and Asp-32. Additionally, significant hydrophobic pockets (S1, S3, S2') exist that are critical sites for beta-secretase inhibition and require hydrophobic groups to occupy these areas. The side chains of Tyr71, Phe108, Trp115, Ile118, and Leu30 collectively shape the S1 hydrophobic cleft. Similarly, the S3 cavity is primarily hydrophobic and is formed by the side chains of Trp115 and Ile110, along with the main chains of Gln12, Gly11, Gly230, Thr231, Thr232, and Ser35. Additionally, S2' consists of the amino acid residues Ile126, Trp76, Val69, Arg128, and Tyr198.

3.1.2. Docking Protocol

X-ray crystal structure of the AChE and BACE 1 complex (PDB ID: **4EY7 & 6UWP**) protein was downloaded from the RCSB protein data bank and further adapted for Glide docking calculations. For Glide (Schrödinger-2019-1) calculations, AChE and BACE 1 complex was imported to Maestro (Schrödinger-2019-1), the co-crystallized ligands were identified and removed from the structure, and non-bridge water molecules were also removed from the complex. Hydrogen atoms were added to the structure, and partial atomic

charges were assigned according to the force field. Protein was minimized until the average root mean square deviation (RMSD) of the non-hydrogen atoms reached 0.3Å by applying the OPLS3e force field to remove the steric hindrance using the protein preparation wizard of Maestro. A grid file was generated using prepared protein as an input file for docking simulation. The grid of active sites was procreated at the centroid of -17.27, 29.10, and 66.61 on the x, y, and z-axis, respectively, using Maestro. Grid box dimension was set to 10, 10, and 10 Å along the x, y, and z directions, respectively. The preparation of ligands was executed using the "Lig-Prep" module of Schrodinger Suite 2019. Compounds were imported into the software's workspace, and energy was minimized using two algorithms, steepest descent, and conjugate gradient, of the Impact module having default options (Friesner, 2004). Poses with an RMSD of less than 0.5Å and a maximum atomic displacement of less than 1.3Å were removed as redundant to increase diversity in the retained ligand/compound poses. The application of Lig-Prep is to construct a particular, low-energy, 3D structure with accurate chirality for each successfully processed input structure. Lig-Prep can also produce several structures from each input structure with numerous ionization states, tautomers, stereochemistries, and ring conformations. Chemaxon Marvin Sketch was used to draw compounds' structures and energy minimization using the OPLS3e Force Field of Lig-Prep of Maestro (<http://www.chemaxon.com>).

The ionization states in a given pH range of 7 ± 2 for AChE and 4.5 ± 2 for BACE 1 were produced by adding or deleting protons from the ligand using the EPIK 4.7010 module. The potential of non-polar parts of ligands was softened by scaling Vander Waals radii of ligand atoms by 0.8 Å with a partial charge cut-off of 0.15. During docking simulation, glide first places the Centre of ligand at various grid positions of a 1 Å grid. Then, rotating ligands in all the Euler angles generate various possible conformations that pass through a filter series composed of initial rough positioning followed by the scoring phase. The docking simulation was performed by allowing flexible torsions in ligands using extra precision (XP) mode.

After completing each docking step, around 50 poses per compound were generated. The best-docked structure/pose was selected based on the Glide score (G-score) function, Glide Energy, and the number of residual matches (hydrogen bonds, hydrophobic interactions) with the original drug complex.

3.1.3. Validation of Docking Protocol

Glide-XP docking was validated using co-crystallized ligands (PDB ID: **4EY7** & **6UWP**) extracted from the protein, corrected, and re-docked to the same protein. The re-docked conformer was then compared with the original by superimposition and visualization. The RMSD (Root mean square deviation) was calculated, which provides the deviation between the re-docked conformer and the co-crystallized ligand. The validated protocols were considered for docking simulations. The proposed ligands were docked into the active site to find the interaction energy between the target and the ligand. The interaction energy in the form of a score has been used to assess the binding affinity.

3.1.4. *In-silico* Determination of Drug-like Properties

Drug-likeness features were calculated using Schrodinger Maestro's Qik-Prop module 2022–1. The properties of drug-likeness in the molecule were determined by predicting many descriptors, such as molecular weight of the compound (Mol_Wt.), Hydrogen bond donor in a molecule (Donor HB), Hydrogen bond acceptor within a molecule (Acceptor HB), total solvent accessible surface area (SASA) in square angstroms using a probe with a 1.4 Å radius, predicted brain/blood partition coefficient (QplogBB), and Predicted octanol/water (Qplog_{o/w}).

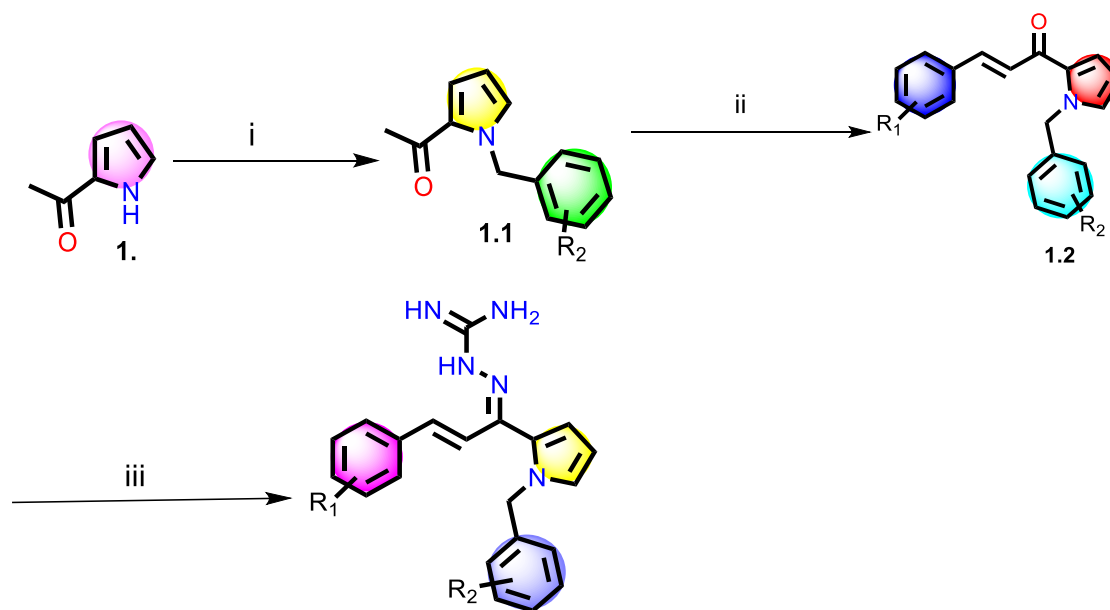
3.2 Synthetic Methodology

3.2.1 Materials

The chemicals employed in synthetic procedures were procured from Spectrochem Pvt. Ltd, Mumbai, SD Fine Chem Limited, Mumbai, and Sigma Aldrich, Mumbai. Solvents of analytical grade, without further purification, were used. Analytical TLC involved plates pre-coated with silica gel 60 F₂₅₄ (0.25 mm thick) were used. Melting points were determined using open capillary tubes on a Precision Buchi B530 apparatus from Flawil, Switzerland. The progress of the reactions was monitored by Thin Layer Chromatography (TLC) analysis (Silica gel G₆₀ F₂₅₄, Merck). ¹H and ¹³C NMR spectra were recorded on a Bruker Avance II 400 spectrometer using *DMSO-d₆* as the solvent and tetramethylsilane (TMS) as an internal standard (chemical shifts indicated in δ). HRMS-ESI+ mode analysis was performed on Agilent Technologies 6545, Version-Q-TOF B.06.01(B6172 SP1).

3.2.2 Synthesis of Pyrrol-2-yl-phenyl allylidene hydrazine carboximidamide analogues

A total of **81** Pyrrol-2-yl-phenyl allylidene hydrazine carboximidamide (**Series-I, II, and III**) analogues were synthesized using the following scheme.



Series	R ₁	R ₂	Compounds
I	-EDG or -EWG	-H	1a-1z, 1aa-1ak
II	-H	-EDG or -EWG	2a-2y
III	-EDG or -EWG	-EDG or -EWG	3a-3s

Scheme 1. Reagents and conditions: (i) Substituted benzyl bromide, KOH, DMF, ultra-sonication, 25°C, 1 h (ii) Substituted benzaldehyde, NaOH, EtOH, ultra-sonication, 25°C, 30min (iii) Aminoguanidine-HCl, conc. HCl, EtOH, ultra-sonication, 25°C, 2.0 h.

3.2.2.1 General procedure for the synthesis of 1-(1-benzyl-1H-pyrrol-2-yl)ethan-1-one (1.1)

A 100 mL round-bottom flask was used to hold 10 mL of DMF, to which 25.6 mmol of KOH was added. The mixture was for ultrasonication for 15 minutes at room temperature. Subsequently, 8.5 mmol of 2-acetylpyrrole was added to the mixture, and stirring continued. After 30 minutes, a solution of benzyl bromide or substituted benzyl bromide (8.5 mmol) in 5 mL DMF was slowly added dropwise to the reaction mixture for over 5 minutes. The reaction was then continued for 1h. Next, the reaction mixture was transferred to ice-cold water and stirred for 5 minutes, forming a white residue. The precipitate was filtered and re-precipitated from ethanol to obtain 1-(1-benzyl-1H-pyrrol-2-yl)ethan-1-one (**1.1**).

3.2.2.2 General procedure for the Synthesis of (*E*)-1-(1-benzyl-1*H*-pyrrol-2-yl)-3-phenylprop-2-en-1-one (1.2)

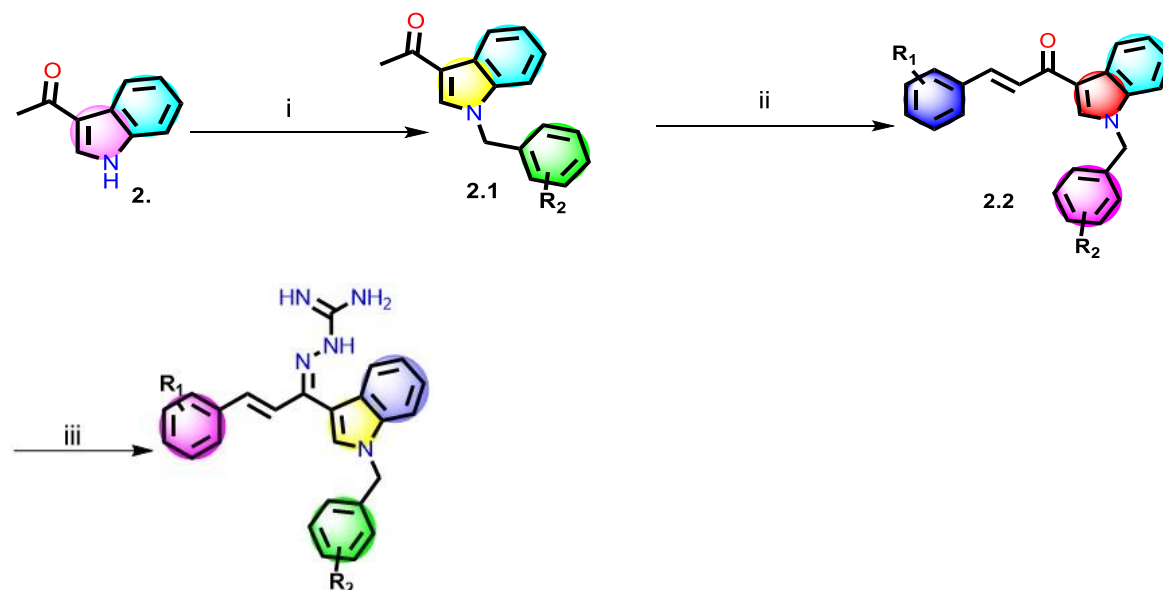
An equimolar mixture of benzaldehyde or substituted benzaldehyde (1mmol) and compound 1.1 (1mmol) were dissolved in 15 ml ethanol. Then, 10ml NaOH solution (6g in 10ml H₂O) was added dropwise to the reaction mixture with continuous stirring. The reaction temperature was maintained between 20-25° C using a cold water ultrasonic bath. The progress of the reaction was monitored by TLC (ethyl acetate/hexane). After vigorous stirring for 20-25min, the reaction mixture was removed from the ultrasonic water bath. It was then neutralized by acidified cold water to precipitate the solid product. On filtering off, the crude product was dried in air and recrystallized using ethanol.

3.2.2.3 General procedure for the synthesis of (*E*)-2-((*E*)-1-(1-benzyl-1*H*-pyrrol-2-yl)-3-phenylallylidene)hydrazine-1-carboximidamide (1a-1z, 1aa-1ak, 2a-2y, 3a-3s)

To the equimolar mixture of compound 1.2 (1mmol) and aminoguanidine hydrochloride (0.11g, 1mmol), 0.5 ml HCl and 10 ml EtOH were added and set in the ultrasonic water bath for 2.0 hrs. The reaction was monitored by TLC for completion. Solvent system used for TLC was dichloromethane and methanol in different ratios (5-40% methanol/dichloromethane). The solvent was evaporated under reduced pressure. After completion, the mixture was poured into water (10 ml) and extracted with DCM (3 x 10 ml). The combined extract was concentrated, and the residue was subjected to column chromatography (silica gel, 3-22% MeOH: DCM solvent system) to afford the desired purified product.

3.2.3 Synthesis of indol-3-yl-phenyl allylidene hydrazine carboximidamide analogues

A total of **79** indol-3-yl-phenyl allylidene hydrazine carboximidamide (**Series-IV, V, and VI**) analogues were synthesized using the following scheme.



Series	R ₁	R ₂	Compounds
IV	-EDG or -EWG	-H	4a-4z, 4aa-4af
V	-H	-EDG or -EWG	5a-5x
VI	-EDG or -EWG	-EDG or -EWG	6a-6u

Scheme 2. Reagents and conditions: (i) Substituted benzyl bromide, KOH, DMF, ultra-sonication, 25°C, 1 h (ii) Substituted benzaldehyde, NaOH, EtOH, ultra-sonication, 25°C, 30 min (iii) Aminoguanidine-HCl, conc. HCl, EtOH, ultra-sonication, 25°C, 2.0 h.

3.2.3.1 General procedure for the synthesis of 1-(1-benzyl-1H-indol-3-yl)ethan-1-one (2.1)

A round-bottom flask, with a volume of 100 mL, was utilized to contain 10 mL of DMF and 25.6 mmol of KOH. After being subjected to ultrasonication for 15 min at room temperature, the mixture was supplemented with 8.5 mmol of 3-acetylindole, and stirring was sustained. Following a period of 30 min, a solution of substituted benzyl bromide (8.5 mmol) in 5 mL DMF was gradually drip-fed into the reaction mixture for 5 min. The reaction was then continued for 1hr. The ensuing mixture was then moved to ice-cold water and agitated for 5 min, which led to the emergence of a white residue. After filtration, the residue was retrieved and re-precipitated from ethanol to acquire 1-(1-benzyl-1H-indol-3-yl)ethan-1-one.

3.2.3.2 General procedure for the Synthesis of (*E*)-1-(1-benzyl-1*H*-indol-3-yl)-3-phenylprop-2-en-1-one (2.2)

A solution of an equimolar combination of substituted benzaldehyde (1 mmol) and compound 2.1 (1 mmol) was prepared in 15 mL of ethanol. Subsequently, the reaction mixture was subjected to continuous stirring while a 10 mL solution of NaOH (6 g in 10 mL H₂O) was gradually dripped in. The reaction temperature was held within the 20-25°C range, utilizing a cold water ultrasonic bath. TLC was utilized to monitor the course of the reaction (ethyl acetate/hexane). Following intense stirring for 20-25 minutes, the reaction mixture was removed from the ultrasonic water bath. The solid product was then precipitated by acidified cold water to neutralize the mixture. The crude product was filtered, dried in the air, and then subjected to recrystallization using ethanol.

3.2.3.3 General procedure for the synthesis of (*Z*)-2-((*E*)-1-(1-benzyl-1*H*-indol-3-yl)-3-phenylallylidene)hydrazine-1-carboximidamide (4a-4z, 4aa-4af, 5a-5x, 6a-6u)

A mixture comprising compound 2.2 (1 mmol) and aminoguanidine hydrochloride (0.11 g, 1 mmol) in equimolar amounts was combined with 0.5 mL of HCl and 10 mL of EtOH. The resulting mixture was placed in an ultrasonic water bath for 2.0 hours. The reaction was monitored by TLC for completion. Solvent system used for TLC was dichloromethane and methanol in different ratios (5-40% methanol/dichloromethane). The solvent was evaporated under reduced pressure. After completion, the mixture was poured into water (10 ml) and extracted with DCM (3 x 10 ml). The combined extract was concentrated, and the residue was subjected to column chromatography (silica gel, 3-22% MeOH: DCM solvent system) to afford the desired purified product.

3.3 *In vitro* evaluation

3.3.1. *In-vitro* BACE 1 Inhibition

The BACE 1 fluorescence resonance energy transfer (FRET) assay kit, obtained from Sigma-Aldrich (Product No. CS0010, Saint Louis), was used following the manufacturer's protocol. Molecular biology grade DMSO from Sigma was used for biological assays. A stock solution of the substrate (500 µM) was prepared using DMSO, and aliquots were stored at -20°C. Test compounds were dissolved in DMSO to create a 10 mM stock solution, and desired concentrations were achieved through further dilutions with fluorescent assay buffer (FAB, 50 mM sodium acetate buffer, pH 4.5) provided in the kit. Before starting the assay, a BACE 1 enzyme solution (0.3 unit/µL) and a 50 µM substrate solution were prepared by

dilution with FAB. The fluorometer was configured in the well plate reader mode with excitation set at 320 nm and emission at 405 nm. For the assay, 10 μ L of the test compound, 20 μ L of the substrate, and 68 μ L of FAB were added to each well of a 96-well black polystyrene microplate. Two microliters of BACE 1 were then added, and fluorescence was immediately measured after enzyme addition. Following the initial reading ("time zero"), the plate was covered and incubated for 2 hours at 37°C. After the incubation period, fluorescence intensities were measured again. The difference between the fluorescence readings at "time zero" and after 2 hours provided Δ fluorescence, which was used for subsequent calculations. Each concentration was assayed in triplicate. The background signal was determined in control wells containing all reagents except BACE 1 and was subsequently subtracted. Fluorescence intensities of assay solutions without inhibitors were also measured. The percentage of inhibition due to the presence of the test compound was calculated by the following expression: $100 - (IF_i/IF_o \times 100)$, where IF_i and IF_o are the respective fluorescence intensities obtained in the presence and the absence of inhibitor. The compounds' percentage inhibition of the enzyme is reported as mean \pm SD (an average of three experiments). BACE 1 inhibitor IV (Calbiochem IV; CAS no. 797035-11-1) (IC_{50} = 18 nM; Literature value. 15 nM) was used as a reference compound.

3.3.2. *In-vitro* AChE Inhibition

The inhibitory effect of compounds on EeAChE was assessed using a modified Ellman assay [135]. *Electrophorus electricus* acetylcholinesterase (EeAChE, EC 3.1.1.7, from electric eel, Type V-S, 827 U/mg solid; 1,256 U/mg of protein), acetylthiocholine iodide (ATChI), 5,5-dithiobis-(2-nitrobenzoic acid) (DTNB, Ellman reagent), donepezil was purchased from Sigma-Aldrich. Molecular biology grade DMSO from Sigma was used for biological assays. Each compound was accurately weighed and dissolved in molecular biology grade DMSO to create a 10 mM stock solution. AChE was dissolved in 0.1 M phosphate buffer (pH 7.2) to prepare enzyme stock solution at 1 mg/mL concentration, which was then further diluted with PBS to yield working solutions with enzyme activity of 2.5 units/mL. Working solutions of DTNB and ATChI were also prepared in PBS at concentrations of 0.3 mM, 10 mM, and 10 mM, respectively. Test compound concentrations ranging from 1 to 100 μ M were prepared from the stock solutions by dilution with PBS. In the experimental procedure, 20 μ L of enzyme solution (AChE), 20 μ L of test compound solution (inhibitor), and 140 μ L of 0.3 mM DTNB solution were added to each well of a 96-well plate. Control wells contained the same components as the test wells, with the addition of the proportion of

DMSO present in the test compound solution to account for any interference from DMSO. The assay solutions, with and without inhibitor, were pre-incubated at 25°C for 20 minutes before adding 20 µL of 10 mM ATChI solution. The reaction was monitored by measuring absorbance at 412 nm at 1-minute intervals for 10 minutes using a 96-well microplate reader, as the absorbance is directly proportional to enzymatic activity. Each experiment was performed in triplicate, and donepezil was used as the reference standard. Blank solutions containing all components, except the enzyme solution, were prepared alongside the test solutions to account for nonenzymatic substrate hydrolysis. Percent inhibition values were calculated from the slopes of absorbance readings over different time intervals for both control and test compounds. IC₅₀ values were determined graphically from the observed percentage inhibition values at different inhibitor concentrations using GraphPad Prism 6 software and are reported as mean ± SD (an average of three experiments).

3.3.3. Statistical Analysis

The experimental results were provided as mean standard deviation (± SD.) GraphPad Prism 8.0 was used to analyze the data.

3.4. Molecular Dynamics Simulation

To confirm the binding strength and pattern of the compounds in AChE and BACE 1 complex using Desmond, a molecular dynamics simulation run of 100ns was conducted. The clear-cut water environment was created by soaking the ligand-protein complex in the TIP3P water molecules encompassed by the orthorhombic water box. The prepared complex system was neutralized by adding the necessary counter ions, and the isosmotic salt environment was maintained by adding 0.15 M NaCl. The system's energy minimization was achieved by using a combined gradient algorithm with maximal 2000 interactions with convergence criteria of 1 kcal/mol/Å. A simulation run of 100ns with periodic boundary conditions under an isothermal-isobaric ensemble (NPT) was performed after energy minimization, and the system temperature and pressure were set respectively at 310 K and 1.013 bar.

CHAPTER 4. RESULTS AND DISCUSSION

4.1 *In-silico* Studies

4.1.1 Validation of Docking Protocol

Glide-XP docking has been validated using co-crystallized ligands (PDB ID: 4EY7 & 6UWP) extracted from the protein, corrected, and re-docked to the same protein. The re-docked conformer is then compared with the original by superimposition and visualization. The RMSD (Root mean square deviation) is calculated, which provides the deviation between the re-docked conformer and the co-crystallized ligand. The RMSD for 4EY7 (Donepezil) and 6UWP (QKA) was 0.14 Å and 0.08 Å respectively. The calculated binding free energy of Donepezil and QKA were found to be -16.88 and -12.24 Kcal/mole, respectively. The validated protocols were considered for docking simulations. The proposed ligands were docked into the active site to find the interaction energy between the target and the ligand. The interaction energy in the form of a score has been used to assess the binding affinity.

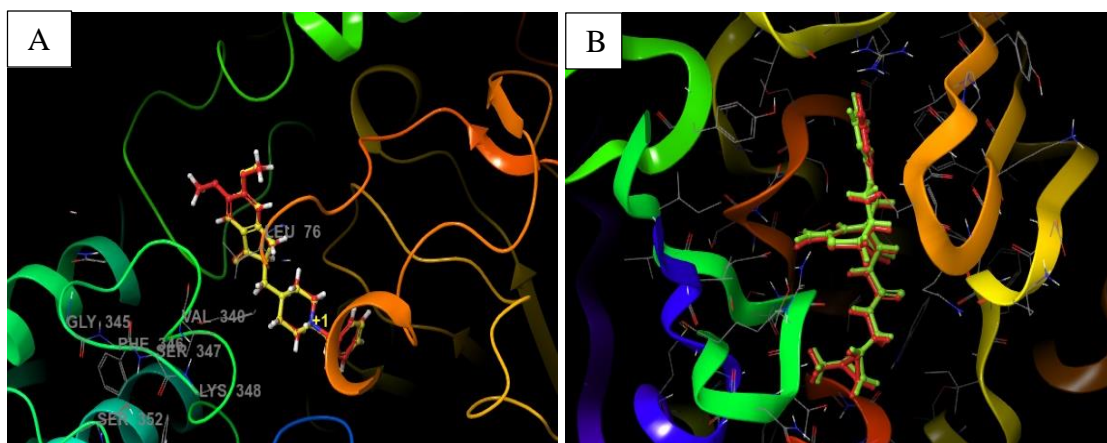


Figure 12. Docking validation of 4EY7 and 6UWP (A) Redocked pose of Donepezil (red) in 4EY7 (AChE) superimposed on the co-crystallized ligand (yellow) (RMSD: 0.14 Å, Glide score: -14.56 Kcal/mol); (B) Redocked pose of QKA (red) in 6UWP (BACE 1) superimposed on the co-crystallized ligand (green) (RMSD: 0.08Å, Glide score: -9.64 Kcal/mol).

4.1.2 Molecular docking of Pyrrol-2-yl-phenyl allylidene hydrazine carboximidamide analogues

Molecular docking studies were conducted to gain insights into the interaction and binding free energy between the compounds and the AChE and BACE 1 pocket residues. Compounds **1a-1ak** having ring A substituted, **2a-2y** having ring B substituted, and **3a-3s** with both rings substituted, were docked into the crystal structure of Human AChE and BACE 1 (PDB ID: 4EY7 and 6UWP). **Figure 13** shows that all the docked compounds **1a-1ak**, **2a-2y**, and **3a-3s** overlapped within the BACE1 (PDB: 6UWP) and AChE (PDB: 4EY7) active sites.

The derivatives showed promising results in the docking simulations, exhibiting interactions similar to those observed in the co-crystallized ligands and favorable binding energies (as presented in Tables 10 and 11). These docking results, in conjunction with the *in vitro* enzymatic inhibition data, further support the potential of these derivatives as effective inhibitors (Tables 7-9).

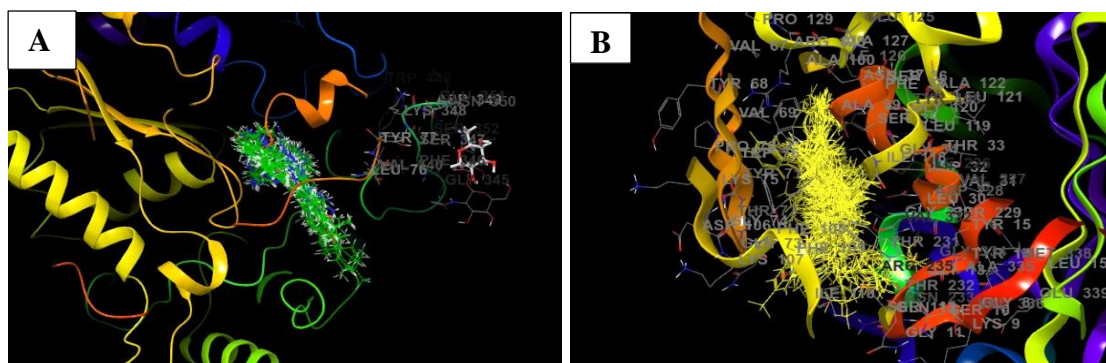
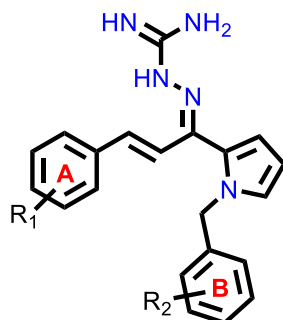


Figure 13. (A) and (B) show overlapping of all of the docked compounds within the active site of 4EY7 and 6UWP, respectively.

Table 7. *In silico* docking results of **Series-I** derivatives



Compound Code	R ₁	R ₂	Mol. Wt.	Glide Score AChE (4EY7) (kcal/mol)	Glide Score BACE 1 (6UWP) (kcal/mol)
1a	-H	-H	343.43	-10.51	-7.33
1b	4-Cl	-H	377.88	-10.29	-5.61
1c	4-F	-H	361.17	-9.97	-5.89
1d	3-phenylacetaldehyde	-H	357.46	-10.56	-7.52
1e	3-phenyl propionaldehyde	-H	371.49	-9.40	-7.26
1f	5-methoxy indole	-H	412.50	-11.56	-9.78
1g	furan-2-yl	-H	333.40	-10.27	-7.50
1h	pyridin-2-yl	-H	344.42	-12.26	-8.03

1i	2-Cl	-H	377.88	-12.57	-9.65
1j	4-NO ₂	-H	388.43	-11.47	-9.35
1k	2,4-di-Cl	-H	411.10	-10.10	-8.22
1l	3-benzyloxy	-H	449.22	-11.08	-8.05
1m	2-NO ₂	-H	388.43	-11.99	-6.21
1n	3-NO ₂	-H	388.43	-11.01	-8.32
1o	biphenyl-4-yl	-H	419.21	-10.04	-6.27
1p	3,4-di-Cl	-H	412.32	-13.17	-8.38
1q	3-F	-H	361.42	-12.54	-7.92
1r	4-CN	-H	368.44	-10.83	-7.44
1s	3-CN	-H	368.44	-10.02	-8.94
1t	2,5-di-F	-H	379.41	-12.97	-7.54
1u	2,4-di-F	-H	379.41	-10.29	-7.61
1v	2-F	-H	361.42	-9.87	-8.54
1w	4-CH ₃	-H	357.46	-11.10	-6.22
1x	4-OCH ₃	-H	373.46	-11.04	-8.30
1y	4-CF ₃	-H	411.43	-10.22	-9.13
1z	3,4-di-F	-H	379.41	-11.73	-7.89
1aa	3-phenoxy	-H	435.53	-9.47	-2.79
1ab	4-tertbutyl	-H	399.54	-10.08	-7.05
1ac	3,4-di-OCH ₃	-H	403.49	-10.99	-8.21
1ad	4-isopropyl	-H	385.52	-13.01	-9.67
1ae	3-OCH ₃	-H	373.46	-12.04	-9.27
1af	2,6-difluoro,4-bromo	-H	458.31	-10.99	-9.26
1ag	4-benzyloxy	-H	449.56	-8.96	-6.95
1ah	4-Dimethylamino	-H	386.50	-10.74	-8.57
1ai	3-Br	-H	422.23	-12.09	-10.90
1aj	4-Br	-H	422.33	-9.88	-5.94
1ak	2,5-di-OCH ₃	-H	403.49	-10.15	-8.31
Donepezil			-	-14.56	-
β-Secretase Inhibitor IV			-	-	-7.65

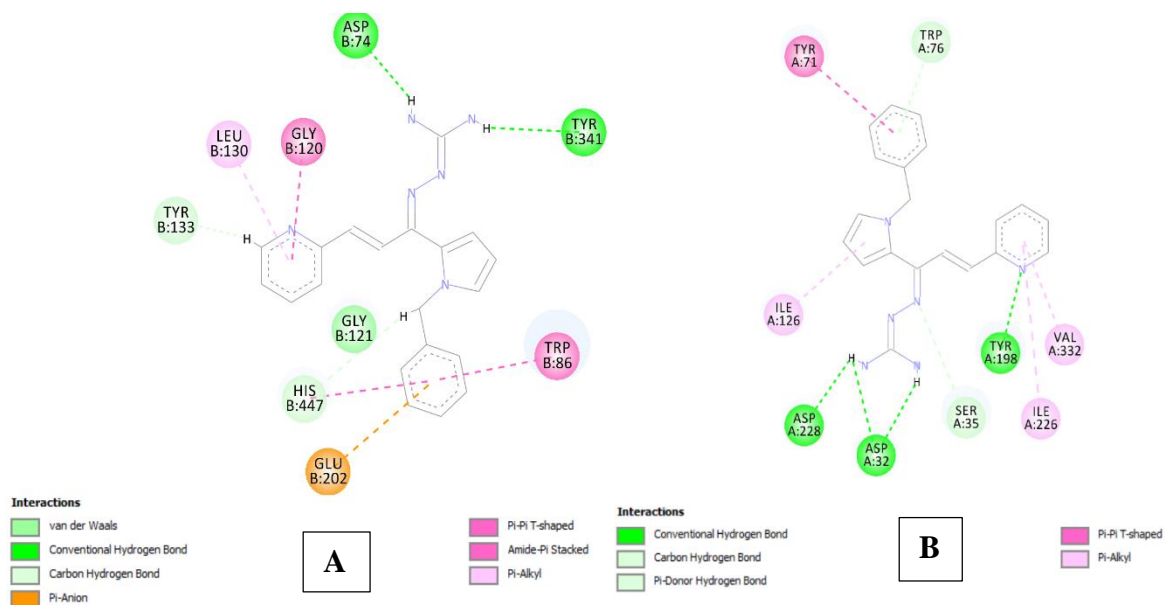
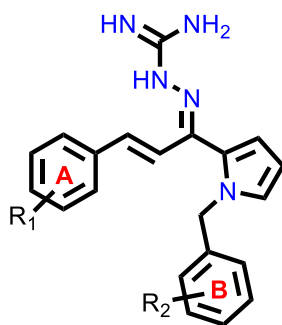


Figure 14. (A) 2D interaction plot of compound **1h** in AChE (Glide score-12.26 kcal/mol); (B) 2D interaction plot of compound **1h** in BACE 1 (Glide score-8.03 kcal/mol)

The analysis of series 1 compounds in the active site of both the enzymes (**Figure 14**), as exemplified by compound **1h**, revealed the occupancy of substrate-binding cavities and interactions with active site amino acids. It was seen that along with the occupancy of the S1 cavity by ring A, ring B was accommodated in the S3 pocket of BACE 1. Its guanidinium moiety formed strong hydrogen bonding interactions with the key aspartate dyads Asp228 and Asp 32. In the case of AChE, ring A was seen to accommodate in the CAS pocket with enhanced π - π stacked interactions with Leu130, Gly120, Tyr133, and ring B occupied PAS with π - π stacking with Glu202, Trp86, His447. Similar results were observed for series 2 compounds, as indicated by compound **2o**, and are shown in **Figure 15**.

Table 8. *In silico* docking results of **Series-II** derivatives

Compound Code	R ₁	R ₂	Mol. Wt.	Glide Score AChE (4EY7) (kcal/mol)	Glide Score BACE 1 (6UWP) (kcal/mol)
2a	-H	3,5-di-OCH ₃	403.49	-8.55	-9.62
2b	-H	4-Cl	377.88	-7.73	-4.65
2c	-H	4-Br	422.33	-8.68	-6.79
2d	-H	4-OCF ₃	427.43	-11.32	-9.12
2e	-H	biphenyl-4-yl	419.53	-11.47	-9.87
2f	-H	4-CF ₃	411.43	-10.21	-9.68
2g	-H	4-F	361.42	-10.49	-9.81
2h	-H	2-CN	368.44	-11.24	-9.64
2i	-H	4-OCHF ₂	409.44	-11.31	-8.58
2j	-H	2,5-di-F	379.41	-11.07	-9.53
2k	-H	4-bromo,2-fluoro	440.32	-10.82	-7.35
2l	-H	2,5-di-Cl	412.32	-10.91	-7.88
2m	-H	4-CH ₃	357.46	-14.63	-3.74
2n	-H	2-F	361.42	-10.03	-9.23
2o	-H	4-F-2-CF ₃	429.42	-12.59	-7.94
2p	-H	3,5-bis-CF ₃	479.43	-10.97	-6.74
2q	-H	4-butyl	399.54	-6.29	-3.61
2r	-H	2,4-di-F	379.41	-12.54	-7.69
2s	-H	4-NO ₂	388.43	-10.10	-6.22
2t	-H	3-Br	422.33	-10.04	-7.30
2u	-H	4-CN	368.44	-9.22	-8.13

2v	-H	3-CN	368.44	-10.73	-6.89
2w	-H	5-F,2-CH ₃	375.45	-8.47	-2.79
2x	-H	4-tertbutyl	399.54	-9.08	-6.05
2y	-H	4-isopropyl	385.52	-10.34	-8.35
Donepezil			-	-14.56	-
β -Secretase Inhibitor IV			-	-	-7.65

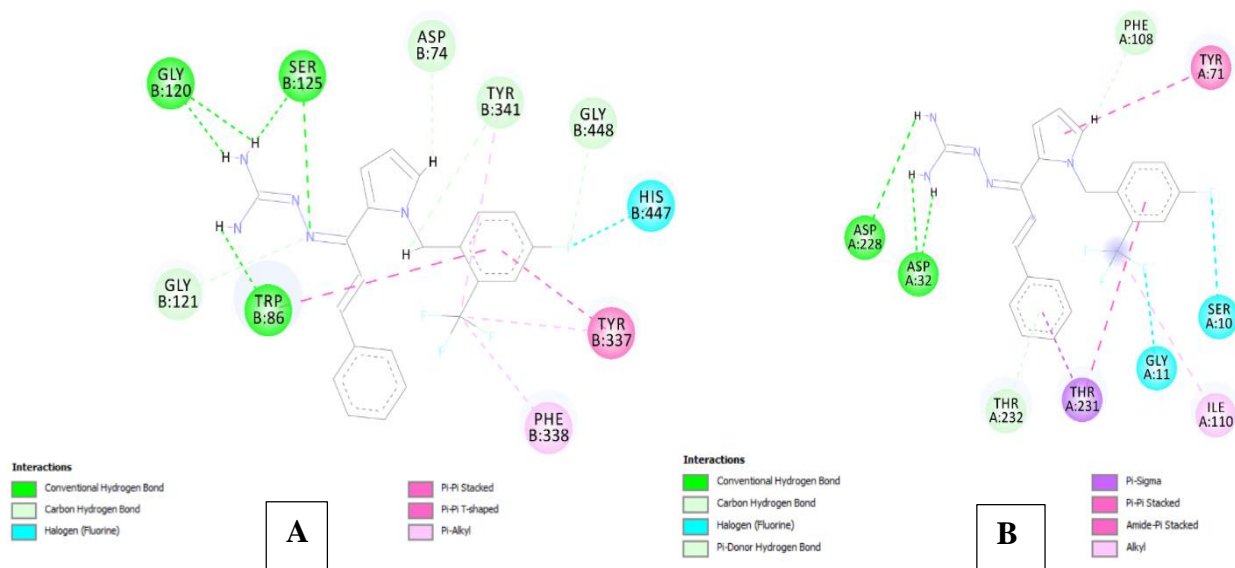
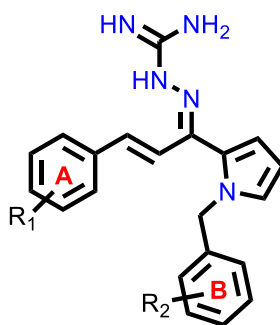


Figure 15. (A) 2D interaction plot of compound **2o** in 4EY7 (Glide score-12.59 kcal/mol); (B) 2D interaction plot of compound **2o** in 6UWP (Glide score-7.94 kcal/mol)

Table 9. *In silico* docking results of **Series-III** derivatives



Compound Code	R ₁	R ₂	Mol. Wt.	Glide Score AChE (4EY7) (kcal/mol)	Glide Score BACE 1 (6UWP) (kcal/mol)
3a	4-Cl	4-Br	456.77	-12.75	-9.77

3b	4-F	4-Br	440.32	-11.64	-10.67
3c	4-CF ₃	4-Br	490.33	-10.24	-3.82
3d	4-CH ₃	4-Br	436.36	-12.40	-9.80
3e	4-CF ₃	4-butyl	467.54	-5.02	-7.94
3f	4-tertbutyl	4-OCF ₃	483.54	-10.97	-6.74
3g	4-CF ₃	4-CF ₃	479.43	-6.29	-3.61
3h	2,3-di-OCH ₃	4-CH ₃	417.51	-8.55	-9.62
3i	3,4-di-OCH ₃	4-F,2-CF ₃	489.47	-7.73	-4.65
3j	2,3-di-OCH ₃	4-OCF ₃	487.48	-8.68	-6.79
3k	4-tertbutyl	2,4-di-F	435.52	-11.32	-9.12
3l	3,4-di-OCH ₃	3,5-di-OCH ₃	463.54	-11.47	-9.87
3m	3,4-di-F	4-tertbutyl	435.52	-10.21	-9.68
3n	4-tertbutyl	biphenyl-4-yl	475.64	-10.49	-9.81
3o	4-tertbutyl	4-CF ₃	505.67	-11.24	-9.64
3p	4-isopropyl	3,6-di-F	421.50	-8.55	-9.62
3q	4-tertbutyl	4-Br	478.44	-7.73	-4.65
3r	3,4-di-OCH ₃	4-tertbutyl	459.59	-9.93	-7.35
3s	4-tertbutyl	4-tertbutyl	455.65	-12.73	-9.35
Donepezil			-	-14.56	-
β-Secretase Inhibitor IV			-	-	-7.65

Compound **3l**, having substituted rings A and B, showed moderate BACE 1 inhibition and displayed hydrogen bonding interactions with aspartate dyad Asp228, Asp 32. It was seen ring A occupies the S1 cavity (Tyr71, Lys107), and the S3 cavity is occupied by ring B (Arg235, Thr72). In the case of AChE, **3l** was seen to accommodate the CAS pocket with enhanced π - π stacked interactions with Trp286, hydrogen bonded with Phe295, Tyr341 and occupies PAS by π - π stacking with Phe297, Trp86 as shown in **Figure 16**.

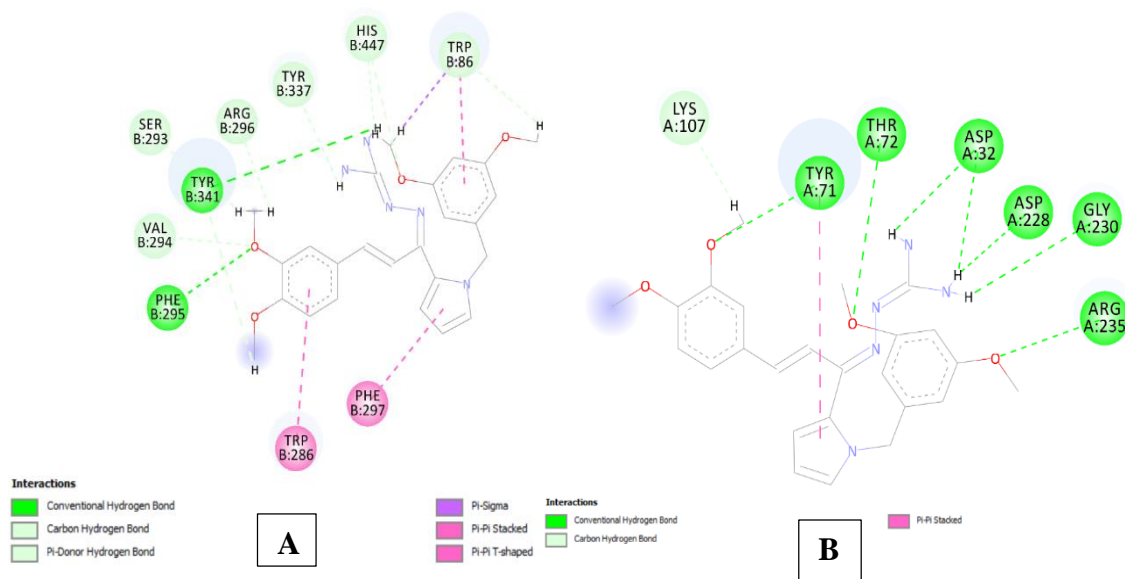


Figure 16. (A) 2D interaction plot of compound **31** in 4EY7 (Glide score-11.47 kcal/mol); (B) 2D interaction plot of compound **31** in 6UWP (Glide score-9.87 kcal/mol).

Table 10. Interactions of the representative compounds in the active site of BACE 1 (6UWP)

Compounds	Glide score (kcal/mol)	Hydrogen Bonds Interacting residues and bonding distance	Hydrophobic Interactions
1j	-9.35	Asp32 (1.85Å), Asp228 (2.49 Å), Thr231 (2.44 Å), Asn233 (2.48 Å), Ser325 (1.59 Å)	Tyr71 (π - π stacked, 3.42 Å), Gln73 (π - π stacked, 2.54 Å), Thr231 (π - π stacked, 1.79 Å), Thr232 (π - π stacked, 2.34 Å)
1k	-8.22	Asp228 (1.80Å)	Asp228 (salt bridge, 2.79Å)
1h	-8.03	Asp32 (2.43Å and 1.89Å), Asp228 (2.14 Å), Tyr198 (1.65 Å), Ser35 (1.45Å)	Tyr71 (π - π stacked, 4.02Å), Trp76 (π - π stacked, 2.80Å), Ile126 (π - π stacked, 5.49 Å), Ile226 (π - π stacked, 3.25 Å), Val332 (π - π stacked, 2.58 Å)
2i	-8.58	Asp32 (1.99Å and 1.89Å), Asp228 (1.94 Å), Phe108 (1.65 Å), Ser10 (2.64 Å), Thr232 (1.32 Å), Gly230 (1.24 Å), Gly13 (1.84 Å)	Tyr71 (π - π stacked, 2.22 Å), Gln12 (halogen bond, 1.59 Å), Ser229 (halogen bond, 2.34 Å), Thr231 (halogen bond, 1.57 Å)

2o	-7.94	Asp32 (1.96Å and 1.75Å), Asp228 (2.31 Å), Thr232 (1.35 Å), Phe108 (1.88 Å)	Thr231 (π - π stacked, 1.54 Å), Gly11 (π - π stacked, 2.11 Å), Ser10 (π - π stacked, 2.55 Å), Ile110 (π - π stacked, 2.36 Å)
2q	-8.64	Asp32 (2.40Å), Asp228 (2.11 and 1.75 Å)	Tyr71 (π - π stacked, 5.28 Å), Arg128 (π -cation, 3.26 Å), Asp228 (salt bridge, 2.71Å)
2r	-7.69	Asp32 (2.16 and 1.88Å), Asp228 (1.71Å)	Tyr71 (π - π stacked, 3.99 Å)
2s	-6.22	Asp32 (1.74 and 1.90Å)	Asp228 (salt bridge, 4.99 Å), Asp32 (salt bridge, 2.76Å)
2t	-7.34	Ile126 (2.15Å), Asn37 (1.89Å), Trp76 (2.54Å)	Gln73 (halogen bond, 3.25Å), Tyr71 (π - π stacked, 3.35 Å)
2u	-8.13	Trp76 (2.71Å), Asn37 (1.88Å)	-
3l	-9.87	Asp32 (1.57 and 2.50Å), Asp228 (2.25Å), Gly230 (1.34 Å), Arg235 (1.25 Å), Thr72 (1.58 Å), Thr71 (2.31 Å), Lys107 (1.75 Å),	Tyr71 (π - π stacked, 2.34 Å)
3s	-9.35	Asp32 (1.77 and 2.12Å)	Asp228 (salt bridge, 4.81Å), Asp32 (salt bridge, 2.93Å)

Table 11. Interactions of the representative compounds in the active site of AChE (4EY7)

Compounds	Glide score (kcal/mol)	Hydrogen Bonds Interacting residues and bonding distance	Hydrophobic Interactions
1j	-11.47	His447 (1.64 and 2.12Å), Asp74 (1.85Å), Gly121 (1.75Å), Ser125 (1.35Å), Val73 (1.38Å), Asn87 (2.15Å), Pro88 (1.68Å),	Tyr124 (π - π stacked, 4.27 Å), His447 (π - π stacked, 4.21 Å), Tyr337 (π - π stacked, 3.85 Å), Trp86 (π - π stacked, 2.75 Å)

1k	-10.12	His447 (2.38Å)	Trp86 (π -cation, 3.12 Å), Phe338 (π - π stacked, 5.47 Å), His447 (π - π stacked, 5.01 Å), Tyr341 (π - π stacked, 3.98 Å),
1h	-12.26	Asp74 (2.22Å), Tyr341 (1.74Å), His447 (2.14Å), Gly121 (1.22Å), Tyr133 (2.35Å),	Gly120 (π - π stacked, 3.68Å), Leu130 (π - π stacked, 3.97 Å), Glu202 (π - π stacked, 2.82 Å), Trp86 (π - π stacked, 1.89 Å), His447 (π - π stacked, 2.48 Å)
2i	-11.31	Ser203 (2.80Å), His447 (2.14 and 2.12Å), Gly121 (1.36Å), Phe338 (1.59Å)	Tyr124 (π - π stacked, 3.65 Å), Ser125 (π - π stacked, 2.31Å), Trp86 (π - π stacked, 3.43 Å), Tyr337 (π - π stacked, 1.45 Å), Tyr337 (halogen bond, 1.45 Å), Phe338 (π - π stacked, 1.35 Å)
2o	-12.59	Ser125 (2.15 and 2.12Å), Gly120 (1.36 and 2.36Å), Trp86 (1.37Å), Gly121 (2.68Å), Asp74 (1.39Å), Tyr341 (3.49Å), Gly448 (1.29Å)	Trp86 (π - π stacked, 3.42 Å), Tyr341 (π - π stacked, 2.37 Å), Tyr337 (π - π stacked, 1.39 Å), Phe338 (π - π stacked, 2.49 Å), Gly448 (π - π stacked, 2.31 Å), His447 (halogen bond, 2.24Å),
2q	-6.29	Glu202 (2.07Å)	Phe338 (π - π stacked, 4.37 Å), Tyr124 (π - π stacked, 5.41 Å)
2r	-12.54	-	Trp86 (π - π stacked, 5.00 and 5.23 Å), Phe338 (π - π stacked, 3.97Å), Tyr341 (π - π stacked, 4.93 Å), Trp286 (π - π stacked, 4.21 Å)
2s	-10.15	Glu202 (1.91 and 2.08Å), Phe295 (2.21Å)	Tyr124 (π - π stacked, 5.40 Å), Tyr337 (π - π stacked, 3.90Å), Glu202 (salt bridge, 3.02Å)
2t	-10.04	His447 (2.08Å)	Phe338 (π - π stacked, 4.87 Å), Tyr124 (π - π stacked, 5.47Å),

			Tyr72 (halogen bond, 3.39 Å), Asp74 (halogen bond, 2.84Å)
2u	-9.99	Glu202 (2.20Å)	Tyr124 (π - π stacked, 5.43 and 5.45Å), Tyr341 (π - π stacked, 3.85Å),
3l	-11.47	Tyr341 (2.04Å), Phe295 (2.25Å), Val294 (1.65Å), Ser293 (2.38Å), Arg296 (1.28Å), Tyr337 (1.49Å), His447 (2.04 and 1.77Å), Trp86 and 1.54Å)	Trp86 (π - π stacked, 3.23 and 2.31Å), Trp286 (π - π stacked, 4.46Å), Phe297 (π - π stacked, 1.83Å)
3s	-12.73	Asp74 (2.03Å)	Tyr337 (π - π stacked, 5.48Å), Asp74 (salt bridge, 2.95Å)

4.1.3. Theoretical prediction of the drug-likeness and ADMET properties of series I, II, and III compounds

The net desired pharmacological activities of drugs/ drug candidates depend on their in-vitro potential and the pharmacokinetic fate (i.e., ADME). Generally, drug discovery and development is a complicated and lengthy process that deals with huge financial and time investments. Due to the unintended side/adverse effects and lack of site delivery, numerous drug candidates fail during the drug discovery program. Drug candidates' fate can be predicted using numerous *in-silico* molecular and/or data modeling methods to reduce the attrition rate during the discovery process. These approaches offer an option to reduce the overall attrition rate during the drug discovery process.

The drug-like characteristics of target compounds were evaluated using Schrödinger QikProp software, which indicated that the properties are comparable to that of donepezil (Tables 12-14). It includes molecular weight of the molecule [mol MW (130-725)], estimated number of hydrogen bonds that the solute would donate to water molecules in an aqueous solution [Donor HB (0–6.0)], estimated number of hydrogen bonds that would be accepted by the solute from water molecules in an aqueous solution [Acceptor HB (2.0–20.0)] as well as the other important factors like total solvent accessible surface area [SASA (300–1000)], predicted brain/blood partition coefficient [QPlogBB (-3.0 to 1.2)], predicted octanol/water partition coefficient [QPlogPo/w (-2.0 to 6.5)], predicted qualitative human oral absorption [% Human oral

absorption (0 to 100% scale)] and predicted IC₅₀ value for blockage of HERG K⁺ channels [QplogHERG (concern below -5)]. The results indicated that all the compounds from series I, II, and III possess "drug-like" properties.

Table 12. *In-silico* Predicted Drug-likeness and ADME characteristics of **series-1** as determined by QikProp

Compound Code	Mol_Wt.^a	Donor HB^b	Acceptor HB^c	SASA^d	Qplog BB^e	Qplog o/w^f	% Human oral absorption^g	Qplog HERG^h
1a	343.430	4.000	3.500	630.010	-1.087	4.117	100.000	-6.430
1b	377.875	4.000	3.500	646.608	-0.934	4.559	100.000	-6.214
1c	361.421	4.000	3.500	630.741	-0.977	4.295	100.000	-6.149
1d	357.457	4.000	3.500	668.000	-1.128	4.510	100.000	-6.675
1e	371.484	4.000	3.000	701.294	-1.060	5.056	100.000	-6.929
1f	412.493	5.000	4.250	703.622	-1.470	4.360	100.000	-6.536
1g	333.392	4.000	4.000	605.697	-1.100	3.524	100.000	-6.176
1h	344.418	4.000	4.500	620.429	-1.215	3.557	100.000	-6.197
1i	377.875	4.000	3.500	642.624	-0.938	4.539	100.000	-6.172
1j	388.428	4.000	4.500	659.177	-2.115	3.417	82.950	-6.192
1k	412.321	4.000	3.500	667.126	-0.792	5.029	96.031	-6.114
1l	449.554	4.000	4.250	811.092	-1.471	6.052	100.000	-8.227
1m	388.428	4.000	4.500	644.328	-1.895	3.493	86.104	-5.967
1n	388.428	4.000	4.500	668.991	-2.178	3.441	82.853	-6.389
1o	419.528	4.000	3.500	752.204	-1.288	5.679	100.000	-7.707
1p	412.321	4.000	3.500	665.310	-0.903	4.942	100.000	-6.016
1q	361.421	4.000	3.500	629.172	-0.964	4.318	100.000	-6.079
1r	368.440	4.000	5.000	657.560	-1.880	3.388	87.066	-6.337
1s	368.440	4.000	5.000	667.442	-1.923	3.426	87.288	-6.536
1t	379.411	4.000	3.500	633.479	-0.859	4.513	100.000	-5.925
1u	379.411	4.000	3.500	638.710	-0.901	4.491	100.000	-6.061
1v	361.421	4.000	3.500	624.836	-0.968	4.282	100.000	-6.041
1w	357.457	4.000	3.500	652.693	-1.116	4.362	100.000	-6.167

1x	373.457	4.000	4.250	660.750	-1.182	4.209	100.000	-6.227
1y	411.429	4.000	3.500	668.679	-0.876	4.997	100.000	-6.130
1z	379.411	4.000	3.500	638.004	-0.975	4.474	100.000	-5.915
1aa	435.527	4.000	4.000	764.137	-1.331	5.706	100.000	-7.804
1ab	399.538	4.000	3.500	719.893	-1.215	5.302	100.000	-6.196
1ac	403.483	4.000	5.000	710.042	-1.304	4.370	100.000	-6.402
1ad	385.511	4.000	3.500	708.922	-1.233	5.025	95.748	-6.365
1ae	373.457	4.000	4.250	660.516	-1.279	4.166	100.000	-6.143
1af	458.307	4.000	3.500	670.742	-0.779	5.025	96.075	-6.091
1ag	449.554	4.000	4.250	805.833	-1.472	6.019	100.000	-8.121
1ah	386.499	4.000	4.500	699.430	-1.240	4.544	100.000	-6.313
1ai	422.326	4.000	3.500	649.620	-1.017	4.589	100.000	-6.107
1aj	422.326	4.000	3.500	658.707	-0.928	4.676	100.000	-6.396
1ak	403.483	4.000	5.000	705.052	-1.274	4.404	100.000	-6.258
Donepezil	379.49	-	5.5	707.05	0.057	4.293	100.000	-6.588

a. Mol_Wt.-Molecular weight of the compound, **b.** Donor HB- Hydrogen bond donor in a molecule, **c.** Acceptor HB-Hydrogen bond acceptor with in a molecule, **d.** SASA- Total solvent accessible surface area (SASA) in square angstroms using a probe with a 1.4 Å radius, **e.** QplogBB-Predicted brain/blood partition coefficient, **f.** Qplogo/w-Predicted octanol/water partition coefficient, **g.** % Human oral absorption-Predicted human oral absorption on 0 to 100% scale, **h.** QplogHERG-Predicted IC₅₀ value for blockage of HERG K⁺ channels.

Table 13. *In-silico* Predicted Drug-likeness and ADME characteristics of **series-II** as determined by QikProp

Compound Code	Mol_Wt.^a	Donor HB^b	Acceptor HB^c	SASA^d	Qplog BB^e	Qplog o/w^f	% Human oral absorption^g	Qplog HERG^h
2a	403.483	4.000	5.000	684.161	-1.133	4.415	100.000	-5.996
2b	377.875	4.000	3.500	639.135	-0.903	4.513	100.000	-6.132
2c	422.326	4.000	3.500	651.121	-0.875	4.647	100.000	-6.334
2d	427.428	4.000	3.500	671.090	-0.791	5.153	100.000	-6.285

2e	419.528	4.000	3.500	724.230	-1.079	5.637	100.000	-7.301
2f	411.429	4.000	3.500	654.948	-0.760	4.933	100.000	-6.085
2g	361.421	4.000	3.500	630.291	-0.984	4.283	100.000	-6.151
2h	368.440	4.000	5.000	629.020	-1.435	3.520	94.248	-6.015
2i	409.438	4.000	3.500	657.333	-0.831	4.961	100.000	-6.122
2j	379.411	4.000	3.500	629.178	-0.997	4.358	100.000	-5.887
2k	440.317	4.000	3.500	648.608	-0.848	4.700	100.000	-6.137
2l	412.321	4.000	3.500	648.197	-0.899	4.721	100.000	-6.014
2m	357.457	4.000	3.500	644.886	-1.036	4.373	100.000	-6.116
2n	361.421	4.000	3.500	624.077	-1.098	4.152	100.000	-6.064
2o	429.419	4.000	3.500	690.374	-1.029	5.032	93.997	-6.629
2p	479.427	4.000	3.500	843.008	-1.012	6.642	100.000	-8.194
2q	399.538	4.000	3.500	795.211	-1.684	5.607	96.498	-7.389
2r	379.411	4.000	3.500	628.502	-0.906	4.423	100.000	-5.867
2s	388.428	4.000	4.500	655.038	-1.936	3.511	86.516	-6.225
2t	422.326	4.000	3.500	633.645	-0.883	4.549	100.000	-5.969
2u	368.440	4.000	5.000	651.492	-1.780	3.413	88.634	-6.268
2v	368.440	4.000	5.000	645.573	-1.687	3.456	90.085	-6.172
2w	375.448	4.000	3.500	622.419	-1.246	4.038	100.000	-5.426
2x	399.538	4.000	3.500	679.572	-0.935	5.252	100.000	-5.725
2y	385.511	4.000	3.500	680.828	-0.999	5.035	100.000	-6.052
Donepezil	379.49	-	5.5	707.05	0.057	4.293	100.000	-6.588

a. Mol_Wt.-Molecular weight of the compound, **b.** Donor HB- Hydrogen bond donor in a molecule, **c.** Acceptor HB-Hydrogen bond acceptor with in a molecule, **d.** SASA- Total solvent accessible surface area (SASA) in square angstroms using a probe with a 1.4 Å radius, **e.** QplogBB-Predicted brain/blood partition coefficient, **f.** Qplogo/w-Predicted octanol/water partition coefficient, **g.** % Human oral absorption-Predicted human oral absorption on 0 to 100% scale, **h.** QplogHERG-Predicted IC₅₀ value for blockage of HERG K⁺ channels.

Table 14. *In-silico* Predicted Drug-likeness and ADME characteristics of **series-III** as determined by QikProp

Compoun d	Mol_Wt. ^a	Donor HB ^b	Acceptor HB ^c	SASA ^d	Qplog BB ^e	Qplog o/w ^f	% Human oral	Qplog HERG ^h
--------------	----------------------	--------------------------	-----------------------------	-------------------	--------------------------	---------------------------	-----------------	----------------------------

Code							absorption g	
3a	456.772	4.000	3.500	673.254	-0.722	5.129	100.000	-6.222
3b	440.317	4.000	3.500	657.876	-0.762	4.881	100.000	-6.156
3c	490.325	4.000	3.500	691.961	-0.655	5.527	100.000	-6.116
3d	436.353	4.000	3.500	675.060	-0.912	4.889	100.000	-6.100
3e	467.536	4.000	3.500	737.972	-1.427	5.678	94.319	-5.945
3f	483.535	4.000	3.500	763.803	-0.917	6.333	100.000	-6.138
3g	479.427	4.000	3.500	712.250	-0.506	5.961	100.000	-6.179
3h	417.510	4.000	5.000	722.610	-1.195	4.712	100.000	-6.110
3i	489.472	4.000	5.000	766.335	-1.217	5.301	95.609	-6.465
3j	487.481	4.000	5.000	731.897	-0.928	5.404	100.000	-5.942
3k	435.519	4.000	3.500	730.537	-1.063	5.655	100.000	-5.913
3l	463.535	4.000	6.500	748.316	-1.307	4.603	100.000	-5.683
3m	435.519	4.000	3.500	705.680	-0.788	5.702	100.000	-5.655
3n	475.635	4.000	3.500	832.957	-1.212	6.901	100.000	-7.415
3o	467.536	4.000	3.500	766.147	-1.004	6.224	100.000	-6.145
3p	421.492	4.000	3.500	716.294	-1.049	5.367	100.000	-6.112
3q	478.434	4.000	3.500	742.424	-1.009	5.813	100.000	-6.151
3r	459.590	4.000	5.000	766.015	-1.112	5.553	100.000	-5.853
3s	455.645	4.000	3.500	787.746	-1.034	6.554	100.000	-5.912
Donepezil	379.49	0.0	5.5	707.05	0.057	4.293	100.000	-6.588

a. Mol_Wt.-Molecular weight of the compound, **b.** Donor HB- Hydrogen bond donor in a molecule, **c.** Acceptor HB-Hydrogen bond acceptor with in a molecule, **d.** SASA- Total solvent accessible surface area (SASA) in square angstroms using a probe with a 1.4 Å radius, **e.** QplogBB-Predicted brain/blood partition coefficient, **f.** Qplog_{o/w}-Predicted octanol/water partition coefficient, **g.** % Human oral absorption-Predicted human oral absorption on 0 to 100% scale, **h.** QplogHERG-Predicted IC₅₀ value for blockage of HERG K⁺ channels

4.1.4. Molecular docking of Indol-3-yl-phenyl allylidene hydrazine carboximidamide analogues

The compounds, **4a-4af** having ring A substituted, **5a-5x** having ring B substituted, and **6a-6u** both rings were substituted and docked into the crystal structures of Human AChE and BACE

1 (PDB ID: 4EY7 and 6UWP). **Figure 17** shows that the docked compounds overlapped within the BACE1 (PDB: 6UWP) and AChE (PDB: 4EY7) active sites.

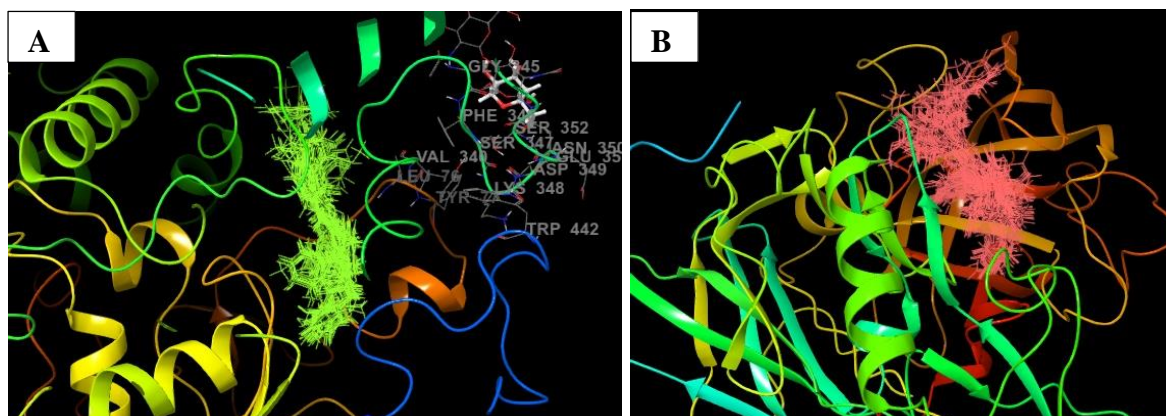
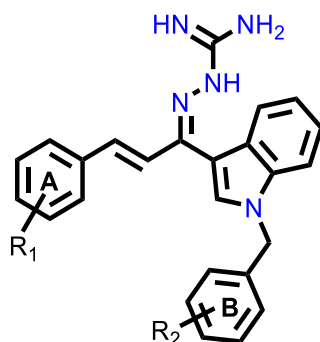


Figure 17. (A) and (B) show overlapping of all of the docked compounds within the active site of 4EY7 and 6UWP, respectively.

The derivatives showed promising results in the docking simulations, exhibiting interactions similar to those observed in the co-crystallized ligands and favorable binding energies (**Tables 15-17**). The analysis of compound **4o** in the active site of both enzymes (**Figure 18**) revealed the occupancy of substrate-binding cavities and interactions with active site amino acids. It was seen that along with the occupancy of the S1 cavity by ring A, ring B was accommodated in the S3 pocket of BACE 1. Its guanidinium moiety formed strong hydrogen bonding interactions with the key aspartate dyads Asp228 and Asp 32. In the case of AChE, ring A was seen to accommodate in the CAS pocket with enhanced π - π stacked interactions with Tyr341, Val294, and Phe295, and ring B occupied PAS by π - π stacking with Trp86.

Table 15. *In silico* docking results of Series-IV (**4a-4z**, **4aa-4af**) derivatives



Compound Code	R ₁	R ₂	Mol. Wt.	Glide Score	Glide Score
				AChE (4EY7)	BACE 1 (6UWP)

				(kcal/mol)	(kcal/mol)
4a	3,4-di-F	-H	429.47	-9.99	-5.21
4b	3-Phenoxy	-H	485.59	-7.01	-6.35
4c	4-tertbutyl	-H	449.60	-7.04	-5.27
4d	3,4-di-OCH ₃	-H	453.55	-8.99	-4.26
4e	4-isopropyl	-H	435.58	-10.87	-8.36
4f	3-OCH ₃	-H	423.52	-12.28	-7.68
4g	3-F	-H	411.48	-8.96	-6.95
4h	4-Benzyloxy	-H	499.62	-10.74	-8.57
4i	4-dimethylamino	-H	436.56	-12.09	-10.90
4j	3-Br	-H	472.39	-9.88	-5.94
4k	4-Br	-H	472.39	-10.15	-3.31
4l	2,5-di-OCH ₃	-H	453.55	-10.56	-7.52
4m	4-CH ₃	-H	407.52	-9.40	-7.26
4n	3-NO ₂	-H	438.49	-11.56	-8.67
4o	4-CN	-H	418.50	-11.08	-10.98
4p	2-F	-H	411.48	-4.26	-6.03
4q	2,4-di-F	-H	429.47	-7.55	-6.34
4r	-H	-H	393.49	-10.73	-7.98
4s	4-OCH ₃	-H	423.52	-10.28	-9.78
4t	2-NO ₂	-H	438.49	-11.27	-6.85
4u	4-CF ₃	-H	461.49	-12.10	-7.25
4v	2-Br,5-Cl	-H	506.83	-11.22	-7.78
4w	3-Benzyloxy	-H	499.62	-12.75	-9.77
4x	4-NO ₂	-H	438.49	-11.64	-10.67
4y	3-CN	-H	418.50	-10.24	-3.82
4z	2,5-di-F	-H	429.47	-12.40	-9.80
4aa	2,3-di-OCH ₃	-H	453.55	-12.41	-5.64
4ab	2,4-di-Cl	-H	462.38	-10.13	-10.02
4ac	4-Cl	-H	427.94	-10.46	-9.81
4ad	3,4-di-Cl	-H	462.38	-10.17	-9.92

4ae	4-F	-H	411.48	-11.91	-10.13
4af	2-CH ₃	-H	407.52	-10.84	-7.36
Donepezil			-	-14.56	-
β-Secretase Inhibitor IV			-	-	-7.65

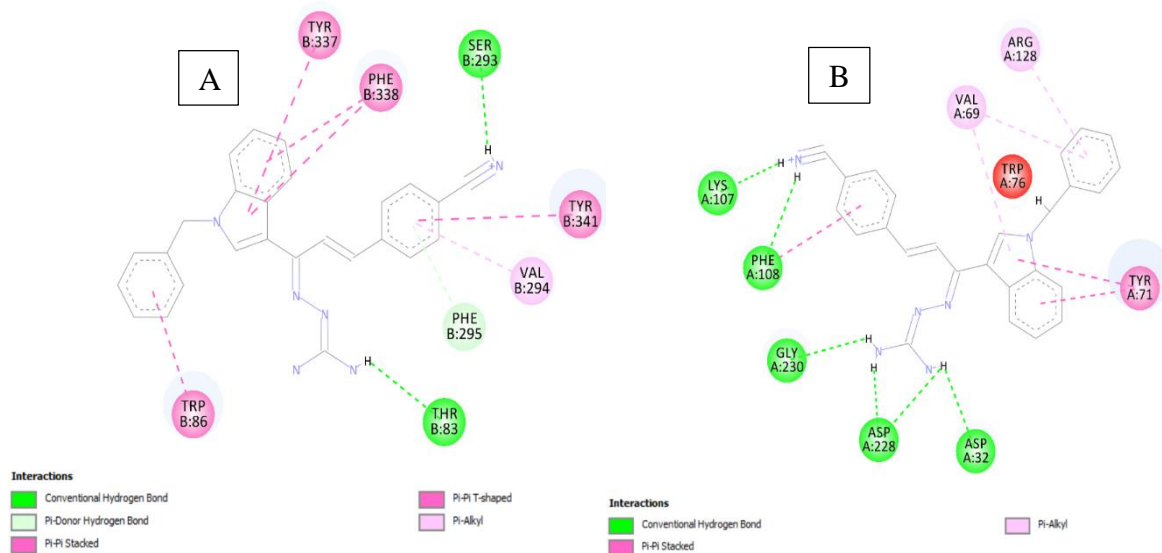
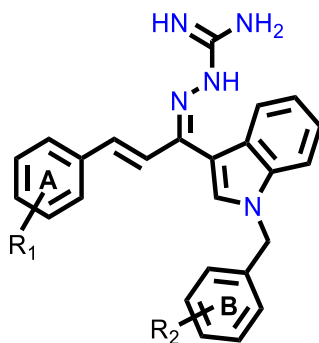


Figure 18. (A) 2D interaction plot of compound **4o** in AChE (Glide score -11.08 kcal/mol); (B) 2D interaction plot of compound **4o** in BACE 1 (Glide score -10.98 kcal/mol)

Table 16. *In silico* docking results of Series-V (**5a-x**) derivatives



Compound Code	R ₁	R ₂	Mol. Wt.	Glide Score AChE (4EY7) (kcal/mol)	Glide Score BACE 1 (6UWP) (kcal/mol)
5a	-H	4-butyl	449.60	-9.98	-7.48
5b	-H	4-OCF ₃	477.49	-8.71	-7.34
5c	-H	2,4-di-F	429.47	-12.89	-9.68
5d	-H	4-tertbutyl	449.60	-12.54	-8.64

5e	-H	4-CF ₃	461.49	-10.54	-9.13
5f	-H	3,5-bis-CF ₃	529.49	-11.05	-7.87
5g	-H	2,5-di-F	429.47	-10.36	-7.54
5h	-H	4-F-2-CF ₃	479.48	-10.69	-8.56
5i	-H	4-CH ₃	407.52	-10.35	-9.04
5j	-H	2-CN	418.50	-11.13	-8.24
5k	-H	4-bromo methylbiphenyl	469.59	-5.02	-7.94
5l	-H	4-Cl	427.94	-10.97	-6.74
5m	-H	3-benzyloxy	499.62	-6.29	-3.61
5n	-H	4-Br	472.39	-12.54	-7.69
5o	-H	3,5-di-OCH ₃	453.55	-10.10	-6.22
5p	-H	4-F	411.48	-10.04	-7.30
5q	-H	2-F	411.48	-9.22	-8.13
5r	-H	4-Br-2-F	490.38	-10.73	-6.89
5s	-H	2,5-di-Cl	462.38	-8.47	-2.79
5t	-H	4-NO ₂	438.49	-9.08	-6.05
5u	-H	3-Br	472.39	-9.99	-5.21
5v	-H	3-CN	418.50	-7.01	-6.35
5w	-H	4-CN	418.50	-7.04	-5.27
5x	-H	4-isopropyl	435.58	-10.37	-8.89
Donepezil			-	-14.56	-
β-Secretase Inhibitor IV			-	-	-7.65

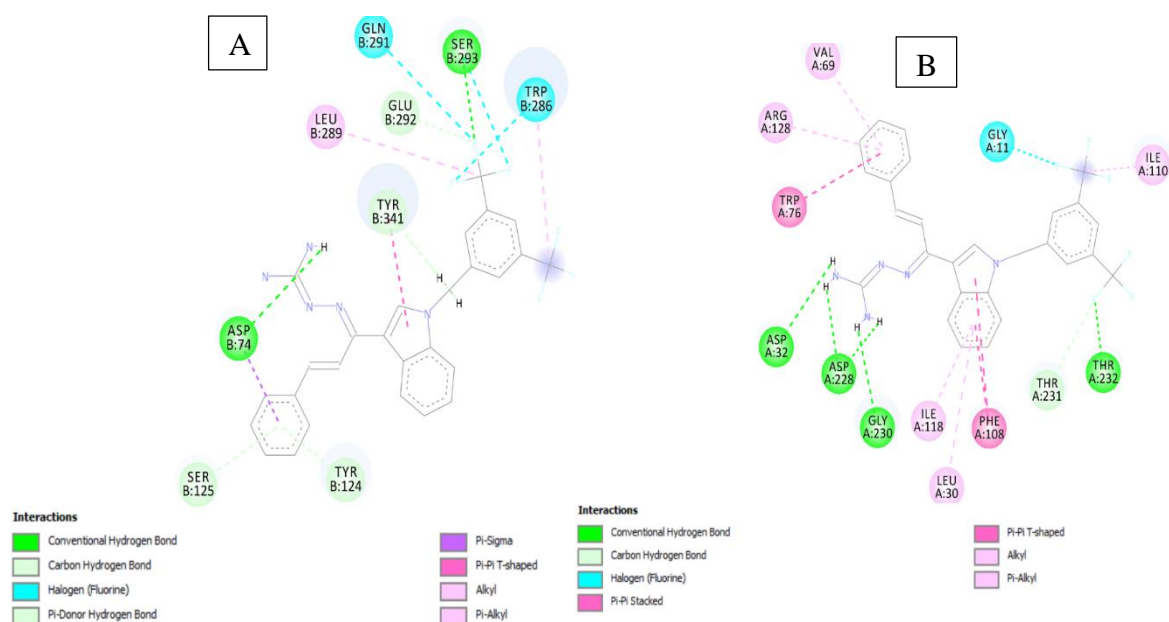
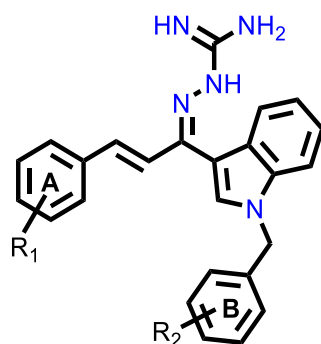


Figure 19. (A) 2D interaction plot of compound **5f** in 4EY7 (Glide score -11.05 kcal/mol); (B) 2D interaction plot of compound **5f** in 6UWP (Glide score -7.87 kcal/mol)

Table 17. *In silico* docking results of **Series-VI (6a-u)** derivatives



Compound Code	R ₁	R ₂	Mol. Wt.	Glide Score AChE (4EY7) (kcal/mol)	Glide Score BACE 1 (6UWP) (kcal/mol)
6a	2,3-di-OCH ₃	4-OCF ₃	537.54	-8.99	-4.26
6b	3-Phenoxy	3-Br	564.49	-10.87	-8.36
6c	4-tertbutyl	2,4-di-F	485.58	-12.28	-7.68
6d	4-CF ₃	4-CF ₃	529.49	-8.96	-6.95
6e	3,4-di-OCH ₃	3,5-di-OCH ₃	513.60	-10.74	-8.57
6f	4-tertbutyl	4-bromomethylbiphenyl	525.70	-12.09	-10.90
6g	3,4-di-F	4-tertbutyl	485.58	-9.88	-5.94

6h	4-benzyloxy	4-CH ₃	513.65	-10.15	-3.31
6i	4-isopropyl	2,5-di-F	471.56	-10.56	-7.52
6j	4-CF ₃	4-F	479.48	-11.56	-8.67
6k	2,4-di-F	2-F	447.47	-10.27	-7.50
6l	4-tertbutyl	4-Br	528.50	-4.26	-6.03
6m	4-tertbutyl	4-F	467.59	-7.55	-6.34
6n	3,4-di-OCH ₃	4-bromomethylbiphenyl	529.64	-10.73	-7.98
6o	4-tertbutyl	4-tertbutyl	505.71	-10.28	-9.78
6p	4-benzyloxy	3-benzyloxy	605.74	-11.27	-6.85
6q	4-CF ₃	4-butyl	517.60	-12.05	-6.89
6r	4-tertbutyl	4-CF ₃	517.60	-11.22	-7.78
6s	3-Phenoxy	4-bromomethylbiphenyl	561.69	-13.67	-11.53
6t	4-benzyloxy	4-butyl	555.73	-12.15	-9.73
6u	2,3-di-OCH ₃	4-butyl	509.65	-10.34	-9.65
Donepezil			-	-14.56	-
β-Secretase Inhibitor IV			-	-	-7.65

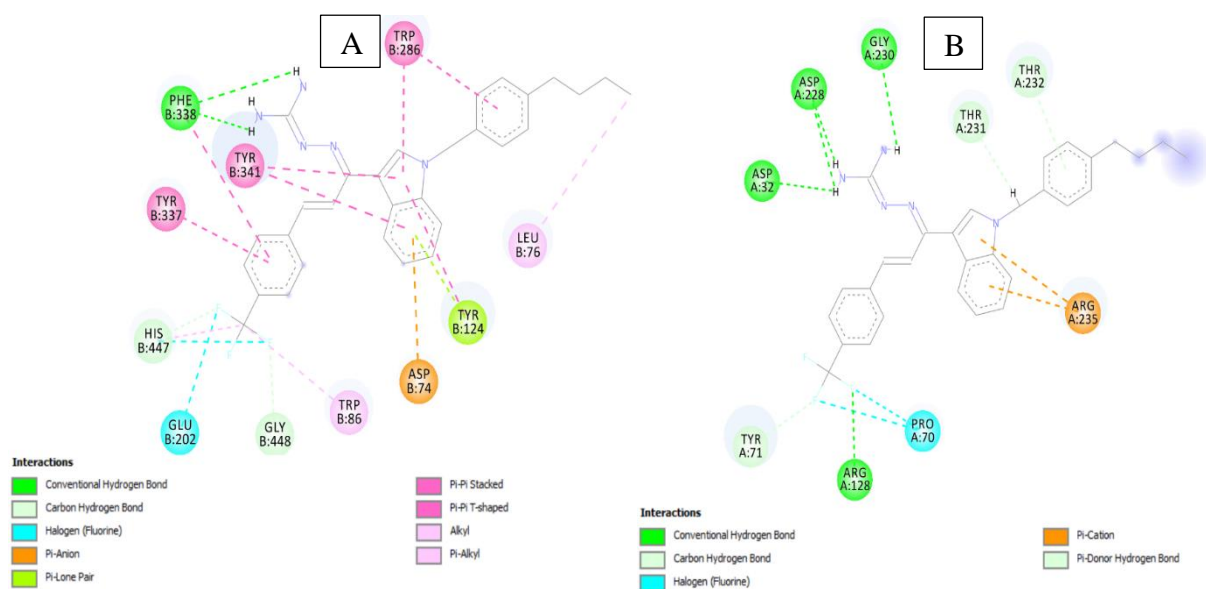


Figure 20. (A) 2D interaction plot of compound **6q** in 4EY7 (Glide score -12.05 kcal/mol); (B) 2D interaction plot of compound **6q** in BACE 1 (Glide score -6.89 kcal/mol).

Compound **6q**, having substituted rings A and B, showed moderate BACE 1 inhibition and displayed hydrogen bonding interactions with aspartate dyads Asp228, Asp 32, and Gly230. It was seen that ring A occupies the S1 cavity, and ring B is oriented towards the S3 cavity, but there are few interactions. In the case of AChE, **6q** was seen to accommodate the CAS pocket with enhanced π - π stacked interactions with Trp86, Gly448, Glu202, His447, hydrogen bonded with Phe338 and occupy PAS with π - π stacked with Tyr124, Trp286, Asp74, Leu76 were also observed and are shown in **figure 20**. The interactions of representative compounds with BACE 1 and AChE and their GLIDE score are given in **Tables 18** and **19**, respectively.

Table 18. Interactions of the representative compounds in the active site of BACE 1 (6UWP)

Compounds	Glide score (kcal/mol)	Hydrogen Bonds Interacting residues and bonding distance	Hydrophobic Interactions
4a	-7.58	Asp32 (2.37 and 1.60Å)	Asp228 (salt bridge, 4.58Å), Asp32 (salt bridge, 3.12Å)
4d	-4.78	Asp32 (2.14 Å), Asp228 (1.76 and 1.28 Å), Phe108 (1.40Å), Gln73 (2.24 and 2.73 Å), Lys107 (2.58 Å)	Tyr71 (π - π stacked, 3.35, 2.23 and 1.27 Å), Arg128 (π - π stacked, 2.86 Å), Val69 (π - π stacked, 1.72 Å)
4e	-8.58	Asp32 (1.61 and 2.34Å)	Asp32 (salt bridge, 2.62Å)
4g	-7.08	Asp32 (2.18 and 1.95Å)	Asp32 (salt bridge, 2.89Å), Asp228 (salt bridge, 4.90Å)
4i	-10.94	Asp32 (2.11Å), Asp228 (1.86 Å)	Asp228 (salt bridge, 2.85Å)

4j	-6.35	Asp32 (1.96 and 1.67Å), Asp228 (2.73 and 1.78 Å), Trp76 (1.95 Å)	Arg235 (π - π stacked, 3.25 and 2.54 Å), Asp228 (salt bridge, 2.77Å), Tyr71 (π - π stacked, 4.12 and 249 Å), Val69 (π -alkyl, 1.79 Å), Asp32 (π - π stacked, 3.21 Å)
4l	-8.40	Asp32 (1.74 and 1.90Å)	Asp32 (salt bridge, 3.00Å), Asp228 (salt bridge, 4.75Å)
4o	-10.98	Asp32 (1.58 and 1.39 Å), Asp228 (2.21 and 1.46 Å), Gly230 (2.98 Å), Tyr71 (2.62 Å), Lys107 (1.65 Å)	Tyr71 (π - π stacked, 3.26 and 2.85 Å), Ile126 (π - π stacked, 3.70 Å)
4q	-7.38	Asp32 (2.09Å), Asp228 (1.88Å)	Asp32 (salt bridge, 2.87Å)
4t	-8.37	Asp32 (1.84 and 1.97Å), Asp228 (2.16Å), Gly230 (1.99Å), Arg235 (2.29Å)	Asp228 (salt bridge, 4.90Å), Asp32 (salt bridge, 2.87Å), Tyr71 (π - π stacked, 3.96 and 4.37 Å), Trp76 (π - π stacked, 5.10 Å)
4ac	-7.94	Asp32 (2.75Å), Asp228 (1.25Å), Gly230 (1.48Å), Gly34 (1.57Å), Tyr71 (2.21Å), Ser36 (1.50Å),	Tyr71 (π - π stacked, 1.94, 3.28 and 2.97 Å), Lys107 (π - π alkyl, 4.07 Å), Val69 (π - π stacked,

			1.52 Å), Arg128 (π - π stacked, 2.43 Å)
5f	-7.87	Asp32 (1.19Å), Asp228 (1.27 and 1.64Å), Gly230 (2.72Å), Thr231 (1.38Å)	Trp76 (π - π stacked, 1.69 Å), Arg128 (π - π stacked, 2.28 Å), Val69 (π - π stacked, 3.21 Å), Gly11 (halogen bond, 1.56 Å), Ile110 (π - π stacked, 2.19 Å), Phe108 (π - π stacked, 1.32 Å), Leu30 (π - π stacked, 3.21 Å), Ile118 (π - π stacked, 1.82 Å), Tyr71 (π - π stacked, 3.35 Å)
5o	-8.87	Asp32 (2.31Å), Asp228 (1.65 and 2.10Å), Asn37 (2.42 and 1.82Å), Gly34 (1.47Å)	Arg235 (π - π stacked, 2.61 Å), Arg128 (π - π stacked, 1.47 Å), Val69 (π - π stacked, 2.43 Å)
6e	-6.24	Asp32 (2.72 and 2.00Å), Asp228 (2.41Å)	Asp228 (salt bridge, 4.77Å), Asp32 (salt bridge, 2.77Å), Arg128 (π -cation, 5.08 Å)

6q	-6.89	Asp32 (2.59Å), Asp228 (1.75 and 1.94Å), Tyr71 (1.68Å), Thr231 (3.36Å), Gly230 (2.72Å)	Pro70 (halogen bond, 1.71 and 1.42 Å), Arg235 (π - π stacked, 3.19 and 1.36 Å), Thr232 (π - π stacked, 1.53 Å)
-----------	-------	--	---

Table 19. Interactions of the representative compounds in the active site of AChE (4EY7)

Compounds	Glide score (kcal/mol)	Hydrogen Bonds Interacting residues and bonding distance	Hydrophobic Interactions
4a	-9.99	-	Trp286 (π - π stacked, 5.06 and 4.83 Å), Tyr341 (π - π stacked, 3.64 and 4.37 Å), Trp86 (π - π stacked, 5.28 Å), Asp74 (salt bridge, 4.97Å)
4d	-10.31	Tyr124 (2.64Å), Thr83 (1.32Å), Asn87 (1.29 and 1.94Å), Tyr72 (2.28Å)	Trp286 (π - π stacked, 2.88 Å), Tyr124 (π - π stacked, 1.53 Å), Trp86 (π - π stacked, 2.23 Å), His447 (π - π stacked, 1.93 Å), Glu202 (π - π anion, 3.64 Å), Try337 (π - π stacked, 2.86 and 1.46 Å), Phe338 (π - π stacked, 2.67 Å)
4e	-11.36	Tyr124 (1.98Å), Thr83 (2.15Å), Asn87 (1.59Å)	Asp74 (salt bridge, 3.66Å), Trp286 (π - π stacked, 4.29 Å), Try337 (π - π stacked, 3.86 Å)
4g	-10.83	Tyr72 (2.28Å), Trp86 (2.22Å)	Trp86 (π - π stacked, 3.81 Å), Tyr337 (π - π stacked, 4.15Å), Tyr341 (π - π stacked, 4.69 Å), Trp72 (π - π stacked, 5.32 Å)

4i	-12.09	Tyr124 (1.92Å), Tyr72 (2.59Å)	Trp86 (π - π stacked, 3.97 Å), Tyr337 (π - π stacked, 3.86 Å), Trp286 (π - π stacked, 4.30 Å)
4j	-10.85	Ser125 (2.53Å), Tyr124 (2.15Å), Asn87 (1.38Å), Gly120 (1.75 and 2.18Å),	Tyr341 (π - π stacked, 4.14 and 2.36 Å), Trp86 (π - π stacked, 3.84, 2.73 and 1.21 Å), Gly126 (π - π stacked, 3.93 Å), Val294 (π - π stacked, 1.82 Å)
4l	-10.56	Phe295 (2.41Å)	Asp74 (salt bridge, 4.11Å), Trp286 (π - π stacked, 4.03 Å), Tyr337 (π - π stacked, 5.06 Å), Trp86 (π - π stacked, 4.38 and 3.62 Å)
4o	-11.08	Ser293 (2.32Å), Thr83 (2.34Å), Phe295 (2.17Å)	Trp86 (π - π stacked, 3.82 Å), Tyr337 (π - π stacked, 4.09Å), Phe338 (π - π stacked, 3.90 and 2.81Å), Tyr341 (π - π stacked, 2.47Å), Val294 (π - π stacked, 1.38Å)
4q	-10.89	-	Trp286 (π - π stacked, 4.36 Å), Tyr337 (π - π stacked, 4.99Å), Asp74 (salt bridge, 4.09Å), Trp86 (π - π stacked, 4.35 and 3.54Å)
4t	-11.44	Asp74 (2.15Å), Asn87 (2.31Å), Ser125 (2.19Å), Tyr124 (1.95Å)	Trp86 (π - π stacked, 4.00 Å), Tyr337 (π - π stacked, 3.66Å), Asp74 (salt bridge, 4.54Å)
4ac	-10.96	Tyr124 (2.28Å), Asn87 (2.26Å)	Trp286 (π - π stacked, 4.09Å), Tyr337 (π - π stacked, 4.18 and 2.49Å), Trp86 (π - π stacked, 3.83Å), Phe338 (π - π stacked, 1.67 Å), Tyr341 (π - π stacked,

			1.38Å), Val294 (π - π stacked, 2.28Å), Ser293 (halogen bond, 1.37Å)
5f	-11.05	Asp74 (1.65Å), Ser293 (1.71Å), Tyr341 (2.42Å), Glu292 (1.33Å)	Tyr124 (π - π stacked, 2.43 Å), Tyr341 (π - π stacked, 1.83Å), Trp286 (π - π stacked, 1.94Å), Leu289 (π - π stacked, 3.63Å), Trp86 (halogen bond, 2.59Å), Ser293 (halogen bond, 1.80Å), Gln291 (halogen bond, 2.83Å),
5o	-10.37	Phe295 (2.55Å), Arg296 (1.31Å), Ser293 (2.78Å), Asp74 (1.33Å), Gly82 (1.98Å)	Trp86 (π - π stacked, 2.07 and 1.19Å), Tyr341 (π - π stacked, 2.43 and 1.24Å), Tyr337 (π - π stacked, 3.87Å), Trp286 (π - π stacked, 1.63Å), Tyr124 (π - π stacked, 2.49Å)
6e	-11.74	Tyr72 (1.82Å)	Tyr341 (π - π stacked, 3.95Å), Trp86 (π - π stacked, 4.07 and 4.20Å), Trp286 (π - π stacked, 3.70Å)
6q	-12.05	Phe338 (1.83Å), His447 (2.35Å), Gly448 (1.56Å)	Trp286 (π - π stacked, 4.92 and 4.72Å), Tyr337 (π - π stacked, 4.59Å), Tyr341 (π - π stacked, 3.47 and 4.24Å), His447 (halogen bond, 3.14Å), Asp74 (π -anion, 2.34Å), Phe338 (π - π stacked, 2.30Å), Tyr124 (π - π stacked, 2.28Å)

4.1.5. Theoretical prediction of the drug-likeness and ADME properties of series IV, V, and VI compounds

The drug-like characteristics of the compounds are given in **Tables 20-22**. The results indicated that all the compounds from series IV, V, and VI possess "drug-like" properties.

Table 20. *In-silico* Predicted Drug-likeness and ADME characteristics of **series-IV** as determined by QikProp

Compound d Code	Mol_Wt.^a	Donor HB^b	Acceptor HB^c	SASA^d	Qplog BB^e	Qplog o/w^f	% Human oral absorption g	Qplog HERG^h
4a	429.471	4.000	3.500	764.608	-1.370	5.534	94.431	-7.524
4b	485.587	4.000	4.000	883.523	-1.828	6.714	100.000	-8.990
4c	449.597	4.000	3.500	847.714	-1.702	6.340	100.000	-7.652
4d	453.543	4.000	5.000	821.100	-1.754	5.329	93.262	-7.534
4e	435.571	4.000	3.500	833.299	-1.713	6.057	100.000	-7.744
4f	423.516	4.000	4.250	785.654	-1.667	5.220	92.544	-7.671
4g	411.481	4.000	3.500	756.823	-1.466	5.324	93.150	-7.649
4h	499.614	4.000	4.250	927.400	-1.950	7.083	100.000	-9.304
4i	436.558	4.000	4.500	827.517	-1.746	5.564	94.146	-7.780
4j	472.386	4.000	3.500	775.778	-1.409	5.655	95.161	-7.684
4k	472.386	4.000	3.500	776.328	-1.416	5.650	95.064	-7.693
4l	453.543	4.000	5.000	825.580	-1.765	5.365	93.438	-7.568
4m	407.517	4.000	3.500	778.636	-1.592	5.405	93.783	-7.648
4n	438.488	4.000	4.500	785.931	-2.780	4.422	84.290	-7.673
4o	418.500	4.000	5.000	785.877	-2.492	4.413	88.719	-7.828
4p	411.481	4.000	3.500	754.475	-1.481	5.285	92.930	-7.666
4q	429.471	4.000	3.500	762.646	-1.376	5.514	94.281	-7.528
4r	393.490	4.000	3.500	745.505	-1.559	5.076	91.766	-7.750
4s	423.516	4.000	4.250	784.598	-1.658	5.220	92.632	-7.661
4t	438.488	4.000	4.500	773.165	-2.498	4.516	88.191	-7.559
4u	461.489	4.000	3.500	800.090	-1.338	6.075	100.000	-7.727
4v	506.831	4.000	3.500	790.697	-1.246	6.080	84.980	-7.500
4w	499.614	4.000	4.250	920.929	-1.935	7.036	100.000	-9.194
4x	438.488	4.000	4.500	785.735	-2.765	4.439	84.540	-7.668
4y	418.500	4.000	5.000	784.536	-2.502	4.384	88.390	-7.815
4z	429.471	4.000	3.500	763.473	-1.378	5.520	94.304	-7.535

4aa	453.543	4.000	5.000	813.320	-1.680	5.378	94.196	-7.465
4ab	462.380	4.000	3.500	788.760	-1.269	6.016	100.000	-7.520
4ac	427.935	4.000	3.500	771.333	-1.423	5.573	94.616	-7.670
4ad	462.380	4.000	3.500	791.622	-1.300	6.008	100.000	-7.568
4ae	411.481	4.000	3.500	756.622	-1.464	5.320	93.169	-7.648
4af	407.517	4.000	3.500	771.757	-1.557	5.401	94.004	-7.646
Donepezil	379.49	-	5.5	707.05	0.057	4.293	100.000	-6.588

a. Mol_Wt.-Molecular weight of the compound, **b.** Donor HB- Hydrogen bond donor in a molecule, **c.** Acceptor HB-Hydrogen bond acceptor with in a molecule, **d.** SASA- Total solvent accessible surface area (SASA) in square angstroms using a probe with a 1.4 Å radius, **e.** Qplog BB-Predicted brain/blood partition coefficient, **f.** Qplog_{o/w}-Predicted octanol/water partition coefficient, **g.** % Human oral absorption-Predicted human oral absorption on 0 to 100% scale, **h.** Qplog HERG-Predicted IC₅₀ value for blockage of HERG K⁺ channels

Table 21. *In-silico* Predicted Drug-likeness and ADME characteristics of **Series-V** as determined by QikProp

Compound d Code	Mol_Wt.^a	Donor HB^b	Acceptor HB^c	SASA^d	Qplog BB^e	Qplog o/w^f	% Human oral absorption g	Qplog HERG^h
5a	449.597	4.000	3.500	875.232	-1.892	6.512	100.000	-8.023
5b	477.488	4.000	3.500	808.453	-1.395	6.215	100.000	-7.748
5c	429.471	4.000	3.500	743.599	-1.364	5.364	93.467	-7.295
5d	449.597	4.000	3.500	847.238	-1.707	6.311	100.000	-7.661
5e	461.489	4.000	3.500	795.142	-1.318	6.048	100.000	-7.641
5f	529.487	4.000	3.500	831.014	-1.071	6.960	89.907	-7.335
5g	429.471	4.000	3.500	767.702	-1.418	5.495	94.194	-7.670
5h	479.479	4.000	3.500	782.347	-1.216	6.082	100.000	-7.367
5i	407.517	4.000	3.500	777.199	-1.597	5.382	93.557	-7.631
5j	418.500	4.000	5.000	756.374	-2.051	4.486	94.123	-7.514
5k	469.588	4.000	3.500	866.381	-1.750	6.684	100.000	-8.836
5l	427.935	4.000	3.500	769.953	-1.415	5.568	94.649	-7.650
5m	499.614	4.000	4.250	920.872	-1.937	7.030	100.000	-9.193

5n	472.386	4.000	3.500	773.702	-1.405	5.636	95.047	-7.655
5o	453.543	4.000	5.000	764.559	-1.587	5.116	92.024	-6.735
5p	411.481	4.000	3.500	753.221	-1.456	5.302	93.039	-7.604
5q	411.481	4.000	3.500	760.689	-1.528	5.267	92.852	-7.840
5r	490.377	4.000	3.500	789.845	-1.375	5.837	96.183	-7.752
5s	462.380	4.000	3.500	782.344	-1.274	5.965	100.000	-7.550
5t	438.488	4.000	4.500	785.934	-2.776	4.428	84.374	-7.677
5u	472.386	4.000	3.500	773.233	-1.404	5.641	95.040	-7.649
5v	418.500	4.000	5.000	776.167	-2.445	4.373	88.522	-7.670
5w	418.500	4.000	5.000	782.864	-2.491	4.378	88.425	-7.797
5x	435.571	4.000	3.500	832.992	-1.717	6.056	100.000	-7.744
Donepezil	379.49	-	5.5	707.05	0.057	4.293	100.000	-6.588

a. Mol_Wt.-Molecular weight of the compound, **b.** Donor HB- Hydrogen bond donor in a molecule, **c.** Acceptor HB-Hydrogen bond acceptor with in a molecule, **d.** SASA- Total solvent accessible surface area (SASA) in square angstroms using a probe with a 1.4 Å radius, **e.** Qplog BB-Predicted brain/blood partition coefficient, **f.** Qplog_{o/w}-Predicted octanol/water partition coefficient, **g.** % Human oral absorption-Predicted human oral absorption on 0 to 100% scale, **h.** Qplog HERG-Predicted IC₅₀ value for blockage of HERG K⁺ channels

Table 22. *In-silico* Predicted Drug-likeness and ADME characteristics of **Series-VI** as determined by QikProp

Compoun d Code	Mol_Wt.^a	Donor HB^b	Acceptor HB^c	SASA^d	Qplog BB^e	Qplog o/w^f	% Human oral absorption g	Qplog HERG^h
6a	537.540	4.000	5.000	872.918	-1.510	6.493	87.652	-7.428
6b	564.483	4.000	4.000	809.931	-1.482	6.668	88.036	-7.442
6c	485.578	4.000	3.500	846.815	-1.512	6.634	100.000	-7.232
6d	529.487	4.000	3.500	848.283	-1.099	7.056	90.350	-7.564
6e	513.595	4.000	6.500	837.026	-1.790	5.309	80.089	-6.542
6f	525.695	4.000	3.500	966.807	-1.901	7.944	95.412	-8.673
6g	485.578	4.000	3.500	863.344	-1.514	6.775	100.000	-7.374
6h	513.641	4.000	4.250	960.120	-2.017	7.367	91.953	-9.166

6i	471.552	4.000	3.500	842.502	-1.605	6.372	100.000	-7.476
6j	479.479	4.000	3.500	806.767	-1.223	6.301	100.000	-7.557
6k	447.462	4.000	3.500	774.246	-1.328	5.694	95.370	-7.556
6l	528.493	4.000	3.500	875.719	-1.550	6.900	89.426	-7.540
6m	467.588	4.000	3.500	855.900	-1.594	6.559	100.000	-7.513
6n	529.640	4.000	5.000	942.841	-1.947	6.927	89.643	-8.593
6o	505.705	4.000	3.500	937.978	-1.815	7.527	93.226	-7.389
6p	605.738	4.000	5.000	930.395	-1.931	7.959	95.503	-8.438
6q	517.596	4.000	3.500	928.561	-1.666	7.504	93.048	-7.936
6r	517.596	4.000	3.500	897.770	-1.476	7.310	91.792	-7.533
6s	561.685	4.000	4.000	928.041	-1.909	7.858	93.739	-8.905
6t	555.721	4.000	4.250	1048.56	-2.350	8.407	100.000	-9.311
6u	509.650	4.000	5.000	948.928	-2.143	6.769	87.674	-7.679
Donepezil	379.49	-	5.5	707.05	0.057	4.293	100.000	-6.588

a. Mol_Wt.-Molecular weight of the compound, **b.** Donor HB- Hydrogen bond donor in a molecule, **c.** Acceptor HB-Hydrogen bond acceptor with in a molecule, **d.** SASA- Total solvent accessible surface area (SASA) in square angstroms using a probe with a 1.4 Å radius, **e.** Qplog BB-Predicted brain/blood partition coefficient, **f.** Qplogo/w-Predicted octanol/water partition coefficient, **g.** % Human oral absorption-Predicted human oral absorption on 0 to 100% scale, **h.** Qplog HERG-Predicted IC₅₀ value for blockage of HERG K⁺ channels

4.2 Synthesis and characterization of designed compounds

4.2.1 Pyrrol-2-yl-phenyl allylidene hydrazine carboximidamide analogues

A total of 81 analogues were synthesized as per the procedure given in section 3.2. The characterization data is given below:

4.2.1.1 (*E*)-2-((*E*)-1-(1-benzyl-1*H*-pyrrol-2-yl)-3-phenylallylidene)hydrazine-1-carboximidamide (**1a**)

Yield 89 %, brown solid; mp: 211–213 °C; ¹H NMR (400 MHz, DMSO-*d*₆) δ 10.88 (s, 1H), 8.07 – 7.44 (m, 3H), 7.43 – 7.16 (m, 6H), 7.14 – 7.00 (m, 2H), 6.90 (d, J = 7.4 Hz, 3H), 6.73 (d, J = 2.2 Hz, 1H), 6.20 – 6.16 (m, 1H), 5.58 (s, 2H), 2.20 (s, 2H); ¹³C NMR (100 MHz, DMSO-*d*₆) δ 170.31, 159.63, 159.18, 156.12, 148.85, 147.57, 139.96, 129.23, 129.00, 128.93, 128.85, 128.71, 127.34, 126.72, 126.34, 116.21, 108.54, 52.60, 21.22, 18.55, 16.91.; HRMS-ESI⁺ calculated for C₂₁H₂₂N₅ [M+H]⁺ 344.1875, found: 344.1874.

4.2.1.2 (Z)-2-((E)-1-(1-benzyl-1H-pyrrol-2-yl)-3-(4-chlorophenyl)allylidene)hydrazine-1-carboximidamide (1b)

Yield 79 %, yellow solid; mp: 208–220 °C; ¹H NMR (400 MHz, DMSO-*d*₆) δ 10.90 (s, 1H), 7.92 – 7.47 (m, 3H), 7.43 (s, 1H), 7.29 (t, J = 7.4 Hz, 3H), 7.21 (t, J = 7.3 Hz, 1H), 7.17 – 7.01 (m, 2H), 6.89 (d, J = 7.2 Hz, 3H), 6.73 (dd, J = 3.8, 1.6 Hz, 1H), 6.18 (dd, J = 3.7, 2.7 Hz, 1H), 5.57 (s, 2H), 2.20 (s, 2H).; ¹³C NMR (100 MHz, DMSO-*d*₆) δ 170.48, 159.34, 156.25, 147.90, 140.32, 129.18, 129.09, 128.94, 128.84, 128.75, 127.48, 127.41, 127.35, 127.12, 126.76, 126.45, 115.98, 108.36, 52.89, 21.34, 16.84.; HRMS-ESI+ calculated for C₂₁H₂₁ClN₅ [M+H]⁺ 378.1485, found: 378.1478.

4.2.1.3 (Z)-2-((E)-1-(1-benzyl-1H-pyrrol-2-yl)-3-(4-fluorophenyl)allylidene)hydrazine-1-carboximidamide (1c)

Yield 88 %, yellow solid; mp: 180–208 °C; ¹H NMR (400 MHz, DMSO-*d*₆) δ 10.86 (s, 1H), 7.42 (s, 3H), 7.25 (dt, J = 30.6, 7.2 Hz, 5H), 7.11 (s, 2H), 6.89 (d, J = 7.3 Hz, 3H), 6.73 (d, J = 2.2 Hz, 1H), 6.22 – 6.14 (m, 1H), 5.58 (s, 2H), 2.20 (s, 2H).; ¹³C NMR (100 MHz, DMSO-*d*₆) δ 170.20, 159.59, 159.15, 156.12, 147.49, 139.99, 129.25, 128.99, 128.93, 128.81, 128.67, 127.52, 127.35, 127.09, 127.00, 126.34, 116.02, 108.37, 52.60, 21.22, 16.97.; HRMS-ESI+ calculated for C₂₁H₂₁FN₅ [M+H]⁺ 362.1781, found: 362.1778.

4.2.1.4 (Z)-2-((E)-1-(1-benzyl-1H-pyrrol-2-yl)-4-phenylbut-2-en-1-ylidene)hydrazine-1-carboximidamide (1d)

Yield 76 %, yellow solid; mp: 201–225 °C; ¹H NMR (400 MHz, DMSO-*d*₆) δ 10.98 (s, 1H), 7.86 – 7.53 (m, 3H), 7.46 – 7.26 (m, 5H), 7.20 (dd, J = 15.5, 8.1 Hz, 2H), 7.15 – 7.02 (m, 2H), 6.89 (d, J = 7.2 Hz, 2H), 6.73 (dd, J = 3.8, 1.7 Hz, 1H), 6.21 – 6.15 (m, 1H), 5.57 (d, J = 7.3 Hz, 2H), 3.43 (s, 2H), 2.21 (s, 2H).

4.2.1.5 (Z)-2-((E)-1-(1-benzyl-1H-pyrrol-2-yl)-5-phenylpent-2-en-1-ylidene)hydrazine-1-carboximidamide (1e)

Yield 73 %, yellow solid; mp: 200–218 °C; ¹H NMR (400 MHz, DMSO-*d*₆) δ 11.09 (s, 1H), 7.71 (dd, J = 95.5, 22.9 Hz, 3H), 7.38 (d, J = 7.4 Hz, 1H), 7.36 – 7.15 (m, 6H), 7.14 – 6.97 (m, 2H), 6.90 (d, J = 7.4 Hz, 2H), 6.73 (d, J = 2.2 Hz, 1H), 6.25 – 6.08 (m, 1H), 5.58 (s, 2H), 3.81 – 3.53 (m, 1H), 2.77 – 2.57 (m, 1H), 2.21 (s, 4H).; ¹³C NMR (100 MHz, DMSO-*d*₆) δ 156.10, 151.33, 147.52, 142.32, 141.56, 140.64, 140.00, 136.73, 129.24, 129.02, 128.94, 128.81, 128.77, 128.71, 128.59, 127.35, 126.35, 116.01, 108.37, 52.60, 34.73, 30.98, 16.93.

4.2.1.6 (Z)-2-((E)-1-(1-benzyl-1H-pyrrol-2-yl)-3-(5-methoxy-1H-indol-3-yl)allylidene)hydrazine-1-carboximidamide (1f)

Yield 88 %, light yellow solid; mp: 211–213 °C; ¹H NMR (400 MHz, DMSO-*d*₆) δ 10.96 (s, 1H), 8.10 – 7.45 (m, 3H), 7.34 (s, 1H), 7.25 (dt, J = 31.0, 7.2 Hz, 4H), 7.16 – 6.97 (m, 2H), 6.96 – 6.58 (m, 4H), 6.18 (dd, J = 3.8, 2.7 Hz, 1H), 5.58 (s, 2H), 5.18 – 4.25 (m, 1H), 3.37 (s, 3H), 2.21 (s, 2H).; ¹³C NMR (100 MHz, DMSO-*d*₆) δ 170.20, 159.59, 159.15, 156.12, 147.49, 139.99, 129.25, 128.99, 128.93, 128.81, 128.67, 127.52, 127.35, 127.09, 127.00, 126.34, 116.02, 108.37, 52.60, 21.22, 16.97.

4.2.1.7 (Z)-2-((E)-1-(1-benzyl-1H-pyrrol-2-yl)-3-(furan-2-yl)allylidene)hydrazine-1-carboximidamide (1g)

Yield 92 %, yellow solid; mp: 203–209 °C; ¹H NMR (400 MHz, DMSO-*d*₆) δ 10.96 (s, 1H), 8.04 – 7.42 (m, 3H), 7.36 (d, J = 14.5 Hz, 1H), 7.25 (dt, J = 31.0, 7.2 Hz, 4H), 7.15 – 6.96 (m, 2H), 6.91 (t, J = 12.8 Hz, 2H), 6.73 (dd, J = 3.8, 1.7 Hz, 1H), 6.18 (dd, J = 3.7, 2.7 Hz, 1H), 5.58 (s, 2H), 2.21 (s, 2H).; ¹³C NMR (100 MHz, DMSO-*d*₆) δ 170.20, 159.59, 159.15, 156.12, 147.49, 139.99, 129.25, 128.99, 128.93, 128.81, 128.67, 127.52, 127.35, 127.09, 127.00, 126.34, 116.02, 108.37, 52.60, 21.22, 16.97.

4.2.1.8 (Z)-2-((E)-1-(1-benzyl-1H-pyrrol-2-yl)-3-(pyridin-2-yl)allylidene)hydrazine-1-carboximidamide (1h)

Yield 93 %, yellow solid; mp: 190–205 °C; ¹H NMR (400 MHz, DMSO-*d*₆) δ 10.95 (s, 1H), 7.55 (s, 3H), 7.25 (dt, J = 30.9, 7.2 Hz, 5H), 7.16 – 7.00 (m, 2H), 6.90 (d, J = 7.2 Hz, 3H), 6.73 (dd, J = 3.9, 1.7 Hz, 1H), 6.18 (dd, J = 3.8, 2.7 Hz, 1H), 5.58 (s, 2H), 2.21 (s, 2H).

4.2.1.9 (E)-2-((E)-1-(1-benzyl-1H-pyrrol-2-yl)-3-(2-chlorophenyl)allylidene)hydrazine-1-carboximidamide (1i)

Yield 85 %, yellow solid; mp: 203–215 °C; ¹H NMR (400 MHz, DMSO-*d*₆) δ 8.23 – 8.12 (m, 1H), 7.96 – 7.67 (m, 3H), 7.62 (dd, J = 4.1, 1.5 Hz, 1H), 7.54 (ddd, J = 6.9, 4.4, 2.1 Hz, 1H), 7.50 – 7.36 (m, 4H), 7.27 (dt, J = 30.5, 7.2 Hz, 4H), 7.11 (d, J = 7.1 Hz, 2H), 7.02 – 6.78 (m, 1H), 6.33 (dd, J = 4.1, 2.5 Hz, 1H), 5.69 (s, 2H).; LCMS/MS-ESI+ calculated for C₂₁H₂₀ClN₅ [M+H] 377.87, found: 377.96.

4.2.1.10 (E)-2-((E)-1-(1-benzyl-1H-pyrrol-2-yl)-3-(4-nitrophenyl)allylidene)hydrazine-1-carboximidamide (1j)

Yield 83 %, yellow solid; mp: 213–218 °C; ¹H NMR (400 MHz, DMSO-*d*₆) δ 10.89 (s, 1H), 7.93 – 7.54 (m, 3H), 7.53 – 7.35 (m, 2H), 7.34 – 7.08 (m, 6H), 6.89 (d, J = 7.3 Hz, 2H), 6.73 (s, 1H), 6.18 (s, 1H), 5.58 (s, 2H), 2.20 (s, 2H).; ¹³C NMR (100 MHz, DMSO-*d*₆) δ 170.10,

159.36, 156.26, 147.61, 140.31, 130.74, 129.84, 129.44, 129.25, 129.11, 129.01, 128.85, 127.54, 127.42, 127.12, 126.44, 116.02, 108.37, 52.89, 21.34, 16.83.; HRMS-ESI+ calculated for C₂₁H₂₁N₆O₂ [M+H]⁺ 388.1849, found: 388.1838.

4.2.1.11 (E)-2-((E)-1-(1-benzyl-1H-pyrrol-2-yl)-3-(2,4-dichlorophenyl)allylidene)hydrazine-1-carboximidamide (1k)

Yield 79 %, yellow solid; mp: 201–226 °C; ¹H NMR (400 MHz, DMSO-*d*₆) δ 8.20 (d, J = 8.6 Hz, 1H), 7.89 – 7.71 (m, 3H), 7.67 – 7.61 (m, 1H), 7.59 – 7.39 (m, 3H), 7.34 – 7.16 (m, 5H), 7.09 (t, J = 10.0 Hz, 2H), 6.90 (d, J = 6.1 Hz, 1H), 6.33 (dd, J = 4.0, 2.5 Hz, 1H), 5.68 (s, 2H).; LCMS/MS-ESI+ calculated for C₂₁H₂₀Cl₂N₅ [M+H]⁺ 412.10, found: 412.08.

4.2.1.12 (Z)-2-((E)-1-(1-benzyl-1H-pyrrol-2-yl)-3-(3-(benzyloxy)phenyl)allylidene)hydrazine-1-carboximidamide (1l)

Yield 79 %, yellow solid; mp: 206–215 °C; ¹H NMR (400 MHz, DMSO-*d*₆) δ 10.94 (s, 1H), 8.24 – 7.58 (m, 3H), 7.58 – 7.32 (m, 3H), 7.32 – 7.15 (m, 6H), 7.10 (dd, J = 9.9, 7.5 Hz, 2H), 7.02 – 6.80 (m, 4H), 6.74 (d, J = 1.7 Hz, 1H), 6.73 (d, J = 1.8 Hz, 1H), 6.18 (dd, J = 3.8, 2.7 Hz, 2H), 5.58 (s, 2H), 2.21 (s, 2H).; ¹³C NMR (100 MHz, DMSO-*d*₆) δ 170.12, 159.57, 159.08, 156.26, 147.56, 139.90, 132.23, 130.93, 129.27, 128.99, 128.94, 128.85, 127.42, 127.10, 126.34, 116.04, 109.46, 108.76, 52.59, 20.95, 16.81.; HRMS-ESI+ calculated for C₂₈H₂₈N₅O [M+H]⁺ 450.2294, found: 450.2291.

4.2.1.13 (Z)-2-((E)-1-(1-benzyl-1H-pyrrol-2-yl)-3-(2-nitrophenyl)allylidene)hydrazine-1-carboximidamide (1m)

Yield 93 %, yellow solid; mp: 225–230 °C; ¹H NMR (400 MHz, DMSO-*d*₆) δ 7.66 (d, J = 89.1 Hz, 3H), 7.39 (s, 2H), 7.35 – 7.18 (m, 5H), 7.14 – 7.00 (m, 2H), 6.90 (d, J = 7.3 Hz, 2H), 6.72 (s, 1H), 6.16 (d, J = 16.3 Hz, 1H), 5.56 (d, J = 12.3 Hz, 2H), 2.20 (s, 2H).; ¹³C NMR (100 MHz, DMSO-*d*₆) δ 170.11, 159.65, 159.18, 156.17, 138.85, 129.51, 129.31, 129.04, 129.00, 128.90, 128.81, 128.73, 128.67, 128.25, 127.65, 116.36, 108.36, 51.91, 34.30, 21.34, 16.75.; HRMS-ESI+ calculated for C₂₁H₂₁N₆O₂ [M+H]⁺ 389.1726, found: 389.1730.

4.2.1.14 (Z)-2-((E)-1-(1-benzyl-1H-pyrrol-2-yl)-3-(3-nitrophenyl)allylidene)hydrazine-1-carboximidamide (1n)

Yield 92 %, brown solid; mp: 170–195 °C; ¹H NMR (400 MHz, DMSO-*d*₆) δ 10.06 (s, 1H), 7.73 – 7.57 (m, 3H), 7.46 (s, 2H), 7.33 – 7.15 (m, 5H), 7.10 (t, J = 10.3 Hz, 1H), 7.04 – 6.96 (m, 1H), 6.89 (d, J = 7.4 Hz, 1H), 6.67 (dd, J = 43.1, 9.1 Hz, 1H), 6.38 – 6.15 (m, 1H), 5.69 – 5.46 (m, 2H), 2.20 (s, 1H), 1.89 (s, 1H).; ¹³C NMR (100 MHz, DMSO-*d*₆) δ 179.14, 170.11, 161.03, 159.34, 156.57, 147.91, 142.71, 142.33, 135.40, 129.30, 129.16, 124.34, 121.93,

115.98, 108.36, 104.53, 99.04, 55.29, 52.58, 20.95, 16.88.; HRMS-ESI+ calculated for $C_{21}H_{21}N_6O_2$ $[M+H]^+$ 389.1726, found: 389.1724.

4.2.1.15 (Z)-2-((E)-3-([1,1'-biphenyl]-4-yl)-1-(1-benzyl-1H-pyrrol-2-yl)allylidene)hydrazine-1-carboximidamide (1o)

Yield 89 %, creamish yellow solid; mp: 203–209 °C; 1H NMR (400 MHz, DMSO-*d*6) δ 10.94 (s, 1H), 7.65 (dd, $J = 41.3, 35.9$ Hz, 3H), 7.53 – 7.38 (m, 2H), 7.23 (ddd, $J = 31.1, 19.3, 12.0$ Hz, 6H), 7.14 – 6.96 (m, 2H), 6.90 (d, $J = 7.4$ Hz, 3H), 6.72 (d, $J = 2.2$ Hz, 2H), 6.29 – 6.11 (m, 2H), 5.57 (s, 2H), 2.21 (s, 2H).; ^{13}C NMR (100 MHz, DMSO-*d*6) δ 156.12, 147.52, 140.02, 130.69, 130.62, 130.55, 129.25, 129.04, 128.95, 128.75, 127.51, 127.36, 127.12, 126.78, 126.36, 124.48, 124.17, 123.99, 123.86, 119.68, 119.24, 119.06, 118.75, 116.02, 108.38, 52.61, 16.92.; HRMS-ESI+ calculated for $C_{27}H_{26}N_5$ $[M+H]^+$ 420.2188, found: 420.2195

4.2.1.16 (Z)-2-((E)-1-(1-benzyl-1H-pyrrol-2-yl)-3-(3,4-dichlorophenyl)allylidene)hydrazine-1-carboximidamide (1p)

Yield 76 %, yellow solid; mp: 206–211 °C; 1H NMR (400 MHz, DMSO-*d*6) δ 10.96 (s, 1H), 7.53 (d, $J = 18.9$ Hz, 3H), 7.29 (t, $J = 7.4$ Hz, 3H), 7.21 (t, $J = 7.3$ Hz, 1H), 7.17 – 7.00 (m, 2H), 6.90 (d, $J = 7.2$ Hz, 3H), 6.73 (dd, $J = 3.8, 1.7$ Hz, 1H), 6.18 (dd, $J = 3.8, 2.7$ Hz, 1H), 5.58 (s, 2H), 2.21 (s, 2H).; ^{13}C NMR (100 MHz, DMSO-*d*6) δ 170.22, 159.59, 159.14, 156.03, 147.50, 141.66, 135.86, 129.54, 129.45, 129.38, 129.18, 128.90, 128.82, 128.65, 128.46, 128.38, 127.46, 108.37, 51.93, 21.06, 16.76.; HRMS-ESI+ calculated for $C_{21}H_{20}Cl_2N_5$ $[M+H]^+$ 412.1096, found: 412.1098

4.2.1.17 (Z)-2-((E)-1-(1-benzyl-1H-pyrrol-2-yl)-3-(3-fluorophenyl)allylidene)hydrazine-1-carboximidamide (1q)

Yield 73 %, yellow solid; mp: 170–185 °C; 1H NMR (400 MHz, DMSO-*d*6) δ 11.01 (s, 1H), 7.90 – 7.51 (m, 3H), 7.49 – 7.37 (m, 1H), 7.24 (ddd, $J = 24.4, 16.0, 8.5$ Hz, 5H), 7.14 – 7.00 (m, 2H), 6.91 (t, $J = 9.9$ Hz, 2H), 6.71 (t, $J = 11.0$ Hz, 1H), 6.18 (dd, $J = 9.0, 6.1$ Hz, 1H), 5.58 (s, 2H), 2.21 (s, 2H).; ^{13}C NMR (100 MHz, DMSO-*d*6) δ 178.66, 170.75, 170.16, 158.99, 141.22, 138.72, 135.29, 134.61, 133.39, 131.51, 130.58, 129.29, 128.97, 127.94, 126.99, 125.98, 124.37, 121.49, 109.35, 50.92, 21.33.; HRMS-ESI+ calculated for $C_{21}H_{21}FN_5$ $[M+H]^+$ 362.1781, found: 362.1764

4.2.1.18 (Z)-2-((E)-1-(1-benzyl-1H-pyrrol-2-yl)-3-(4-cyanophenyl)allylidene)hydrazine-1-carboximidamide (1r)

Yield 86 %, yellow solid; mp: 206–215 °C; 1H NMR (400 MHz, DMSO-*d*6) δ 11.00 (s, 1H), 7.63 (s, 3H), 7.34 (s, 1H), 7.25 (dt, $J = 31.1, 7.2$ Hz, 4H), 7.15 – 6.99 (m, 2H), 6.90 (d, $J = 7.1$ Hz, 3H), 6.73 (dd, $J = 3.9, 1.8$ Hz, 1H), 6.18 (dd, $J = 3.8, 2.7$ Hz, 1H), 5.58 (s, 2H), 2.21 (s,

2H).; ^{13}C NMR (100 MHz, DMSO-*d*₆) δ 156.16, 155.74, 147.67, 146.09, 141.58, 137.45, 135.73, 129.53, 129.40, 129.23, 129.14, 129.10, 128.62, 127.44, 117.39, 117.14, 116.27, 109.67, 108.77, 60.18, 46.64, 17.06.; HRMS-ESI+ calculated for C₂₂H₂₁N₆ [M+H]⁺ 369.1828, found: 369.1818

4.2.1.19 (Z)-2-((E)-1-(1-benzyl-1H-pyrrol-2-yl)-3-(3-cyanophenyl)allylidene)hydrazine-1-carboximidamide (1s)

Yield 89 %, light brown solid; mp: 195–216 °C; ^1H NMR (400 MHz, DMSO-*d*₆) δ 11.07 (s, 1H), 8.27 – 7.72 (m, 3H), 7.46 (ddd, J = 32.9, 17.2, 11.0 Hz, 3H), 7.34 – 7.01 (m, 5H), 6.91 (t, J = 9.5 Hz, 2H), 6.76 – 6.68 (m, 1H), 6.20 – 6.13 (m, 1H), 5.57 (d, J = 9.7 Hz, 2H), 2.22 (s, 1H), 1.91 (s, 1H).; ^{13}C NMR (100 MHz, DMSO-*d*₆) δ 171.10, 158.78, 155.81, 153.66, 151.83, 150.15, 130.37, 130.09, 129.38, 129.21, 128.87, 128.40, 128.33, 127.51, 119.24, 116.55, 113.92, 108.51, 98.17, 98.06, 50.92, 20.96.; HRMS-ESI+ calculated for C₂₂H₂₁N₆ [M+H]⁺ 369.1828, found: 369.1860

4.2.1.20 (Z)-2-((E)-1-(1-benzyl-1H-pyrrol-2-yl)-3-(2,5-difluorophenyl)allylidene)hydrazine-1-carboximidamide (1t)

Yield 91 %, yellow solid; mp: 230–232 °C; ^1H NMR (400 MHz, DMSO-*d*₆) δ 11.08 (s, 1H), 7.81 (dd, J = 123.2, 66.1 Hz, 3H), 7.36 (s, 2H), 7.32 – 7.05 (m, 5H), 6.90 (d, J = 6.8 Hz, 2H), 6.72 (s, 1H), 6.39 – 6.08 (m, 1H), 5.74 – 5.26 (m, 2H), 2.22 (s, 1H), 1.90 (s, 1H).; ^{13}C NMR (100 MHz, DMSO-*d*₆) δ 170.31, 159.63, 159.18, 156.12, 148.85, 147.57, 139.96, 129.23, 129.00, 128.93, 128.85, 128.71, 127.34, 126.72, 126.34, 116.21, 108.54, 52.60, 21.22, 18.55, 16.91.; HRMS-ESI+ calculated for C₂₁H₂₀F₂N₅ [M+H]⁺ 380.1687, found: 380.1664

4.2.1.21 (Z)-2-((E)-1-(1-benzyl-1H-pyrrol-2-yl)-3-(2,4-difluorophenyl)allylidene)hydrazine-1-carboximidamide (1u)

Yield 93 %, yellow solid; mp: 264–266 °C; ^1H NMR (400 MHz, DMSO-*d*₆) δ 10.13 (s, 1H), 9.58 (s, 1H), 7.71 (d, J = 24.1 Hz, 3H), 7.52 (d, J = 50.3 Hz, 2H), 7.43 – 7.07 (m, 5H), 6.90 (s, 1H), 6.72 (s, 1H), 6.32 (dd, J = 58.5, 46.9 Hz, 1H), 5.83 – 5.35 (m, 2H), 2.22 (s, 1H), 1.90 (s, 1H).; ^{13}C NMR (100 MHz, DMSO-*d*₆) δ 169.83, 159.12, 155.81, 147.53, 141.58, 139.54, 132.63, 131.40, 129.96, 129.30, 129.19, 129.16, 129.09, 129.06, 127.06, 116.36, 110.03, 109.02, 50.56, 21.04, 16.77.; HRMS-ESI+ calculated for C₂₁H₂₀F₂N₅ [M+H]⁺ 380.1687, found: 380.1659

4.2.1.22 (E)-2-((E)-1-(1-benzyl-1H-pyrrol-2-yl)-3-(2-fluorophenyl)allylidene)hydrazine-1-carboximidamide (1v)

Yield 84 %, yellow solid; mp: 252–264 °C; ^1H NMR (400 MHz, DMSO-*d*₆) δ 10.15 (s, 1H), 9.60 (s, 1H), 7.87 – 7.68 (m, 3H), 7.49 (ddd, J = 30.5, 22.0, 6.7 Hz, 2H), 7.35 – 7.08 (m, 6H),

6.91 (t, $J = 9.4$ Hz, 2H), 6.72 (s, 1H), 5.80 – 5.29 (m, 2H), 2.23 (d, $J = 14.1$ Hz, 1H), 1.90 (s, 1H).; ^{13}C NMR (100 MHz, DMSO- d_6) δ 160.88, 158.45, 156.22, 147.67, 129.64, 129.56, 129.25, 129.02, 128.64, 128.36, 128.32, 127.47, 126.86, 126.72, 125.11, 125.08, 115.96, 115.68, 108.38, 46.99, 16.81.; HRMS-ESI+ calculated for $\text{C}_{21}\text{H}_{21}\text{FN}_5$ $[\text{M}+\text{H}]^+$ 362.1781, found: 362.1796.

4.2.1.23 (Z)-2-((E)-1-(1-benzyl-1H-pyrrol-2-yl)-3-(p-tolyl)allylidene)hydrazine-1-carboximidamide (1w)

Yield 81 %, yellow solid; mp: 228– 230 °C; ^1H NMR (400 MHz, DMSO- d_6) δ 11.09 (s, 1H), 7.67 (dd, $J = 23.1, 9.5$ Hz, 3H), 7.51 (dd, $J = 40.7, 25.1$ Hz, 2H), 7.37 – 7.04 (m, 6H), 7.00 – 6.82 (m, 2H), 6.79 – 6.61 (m, 1H), 6.19 (d, $J = 14.0$ Hz, 1H), 5.75 – 5.36 (m, 2H), 3.47 (s, 3H), 2.22 (s, 1H), 1.91 (s, 1H).; ^{13}C NMR (100 MHz, DMSO- d_6) δ 170.25, 159.19, 156.17, 147.46, 140.00, 129.92, 129.24, 129.00, 128.93, 128.82, 128.75, 128.65, 127.51, 127.34, 127.11, 126.77, 126.35, 116.00, 108.36, 52.61, 21.23, 16.99.; HRMS-ESI+ calculated for $\text{C}_{22}\text{H}_{24}\text{N}_5$ $[\text{M}+\text{H}]^+$ 358.2032, found: 358.2008.

4.2.1.24 (E)-2-((E)-1-(1-benzyl-1H-pyrrol-2-yl)-3-(4-methoxyphenyl)allylidene)hydrazine-1-carboximidamide (1x)

Yield 89 %, yellow solid; mp: 198–200 °C; ^1H NMR (400 MHz, DMSO- d_6) δ 11.08 (s, 1H), 8.12 – 7.62 (m, 3H), 7.46 (dd, $J = 41.7, 25.9$ Hz, 1H), 7.36 – 7.01 (m, 6H), 7.00 – 6.60 (m, 4H), 6.18 (s, 1H), 5.59 (s, 2H), 3.82 – 3.44 (m, 3H), 2.23 (s, 1H), 1.92 (s, 1H).; ^{13}C NMR (100 MHz, DMSO- d_6) δ 156.23, 138.16, 136.92, 130.25, 129.11, 129.06, 129.01, 128.83, 127.97, 127.69, 127.49, 126.71, 122.84, 121.03, 115.00, 114.62, 111.65, 55.70, 50.11, 49.05, 25.46, 18.55.; HRMS-ESI+ calculated for $\text{C}_{22}\text{H}_{24}\text{N}_5\text{O}$ $[\text{M}+\text{H}]^+$ 374.1981, found: 374.1955.

4.2.1.25 (Z)-2-((E)-1-(1-benzyl-1H-pyrrol-2-yl)-3-(4-(trifluoromethyl)phenyl)allylidene)hydrazine-1-carboximidamide (1y)

Yield 84 %, yellow solid; mp: 210–212 °C; ^1H NMR (400 MHz, DMSO- d_6) δ 10.12 (s, 1H), 9.57 (s, 1H), 8.89 (d, $J = 14.5$ Hz, 1H), 7.94 – 7.72 (m, 3H), 7.66 – 7.52 (m, 3H), 7.48 (d, $J = 11.6$ Hz, 1H), 7.39 – 7.20 (m, 3H), 7.13 (dd, $J = 25.7, 6.0$ Hz, 2H), 6.96 – 6.79 (m, 1H), 5.96 – 5.29 (m, 2H), 2.26 – 2.20 (m, 1H), 1.89 (s, 1H).; ^{13}C NMR (100 MHz, DMSO- d_6) δ 156.23, 138.16, 136.92, 130.25, 129.11, 129.06, 129.01, 128.83, 127.97, 127.69, 127.49, 126.71, 122.84, 121.03, 115.00, 114.62, 111.65, 55.70, 50.11, 49.05, 25.46, 18.55.; HRMS-ESI+ calculated for $\text{C}_{22}\text{H}_{21}\text{F}_3\text{N}_5$ $[\text{M}+\text{H}]^+$ 412.1749, found: 412.1720.

4.2.1.26 (Z)-2-((E)-1-(1-benzyl-1H-pyrrol-2-yl)-3-(3,4-difluorophenyl)allylidene)hydrazine-1-carboximidamide (1z)

Yield 93 %, brown solid; mp: 268–270 °C; ¹H NMR (400 MHz, DMSO-*d*₆) δ 11.05 (s, 1H), 7.91 – 7.54 (m, 3H), 7.52 – 7.35 (m, 1H), 7.33 – 7.15 (m, 4H), 7.14 – 6.98 (m, 2H), 6.96 – 6.86 (m, 2H), 6.72 (dd, *J* = 3.8, 1.7 Hz, 1H), 6.45 – 6.14 (m, 1H), 5.68 – 5.43 (m, 2H), 2.21 (s, 2H), 1.96 – 1.83 (m, 1H); ¹³C NMR (100 MHz, DMSO-*d*₆) δ 170.48, 159.34, 156.25, 147.90, 140.32, 129.18, 129.09, 128.94, 128.84, 128.75, 127.48, 127.41, 127.35, 127.12, 126.76, 126.45, 115.98, 108.36, 52.89, 21.34, 16.84.; HRMS-ESI⁺ calculated for C₂₁H₂₀F₂N₅ [M+H]⁺ 380.1687, found: 380.1681.

4.2.1.27 (Z)-2-((E)-1-(1-benzyl-1H-pyrrol-2-yl)-3-(3-phenoxyphenyl)allylidene)hydrazine-1-carboximidamide (1aa)

Yield 87 %, white solid; mp: 280–282 °C; ¹H NMR (400 MHz, DMSO-*d*₆) δ 11.04 (s, 1H), 8.20 – 7.67 (m, 3H), 7.66 – 7.34 (m, 4H), 7.33 – 6.99 (m, 8H), 6.95 – 6.81 (m, 3H), 6.78 – 6.60 (m, 1H), 6.41 – 6.10 (m, 1H), 5.56 (d, *J* = 18.3 Hz, 2H), 2.21 (s, 2H); ¹³C NMR (100 MHz, DMSO-*d*₆) δ 156.12, 147.52, 140.02, 130.69, 130.62, 130.55, 129.25, 129.04, 128.95, 128.75, 127.51, 127.36, 127.12, 126.78, 126.36, 124.48, 124.17, 123.99, 123.86, 119.68, 119.24, 119.06, 118.75, 116.02, 108.38, 52.61, 16.92.; HRMS-ESI⁺ calculated for C₂₇H₂₆N₅O [M+H]⁺ 436.2137, found: 436.2132.

4.2.1.28 (Z)-2-((E)-1-(1-benzyl-1H-pyrrol-2-yl)-3-(4-(tert-butyl)phenyl)allylidene)hydrazine-1-carboximidamide (1ab)

Yield 81 %, yellow solid; mp: 224–226 °C; ¹H NMR (400 MHz, DMSO-*d*₆) δ 10.96 (s, 1H), 7.72 (ddd, *J* = 17.8, 17.0, 8.4 Hz, 2H), 7.61 – 7.50 (m, 1H), 7.47 (d, *J* = 6.6 Hz, 1H), 7.43 – 7.37 (m, 1H), 7.32 – 7.21 (m, 3H), 7.17 – 6.82 (m, 4H), 6.77 – 6.59 (m, 1H), 6.50 – 6.28 (m, 1H), 6.24 – 6.10 (m, 1H), 5.74 – 5.38 (m, 2H), 2.21 (s, 2H), 1.53 – 0.95 (m, 9H); ¹³C NMR (100 MHz, DMSO-*d*₆) δ 156.05, 153.12, 147.61, 140.31, 129.26, 129.01, 128.94, 128.87, 128.77, 128.47, 127.50, 127.35, 127.27, 127.12, 126.77, 126.36, 126.14, 125.98, 118.62, 116.03, 108.37, 52.60, 34.88, 31.40, 16.82.; HRMS-ESI⁺ calculated for C₂₅H₃₀N₅ [M+H]⁺ 400.2501, found: 400.2497.

4.2.1.29 (E)-2-((E)-1-(1-benzyl-1H-pyrrol-2-yl)-3-(3,4-dimethoxyphenyl)allylidene)hydrazine-1-carboximidamide (1ac)

Yield 80 %, yellow solid; mp: 231–233 °C; ¹H NMR (400 MHz, DMSO-*d*₆) δ 10.94 (s, 1H), 7.56 (ddd, *J* = 27.5, 21.8, 15.5 Hz, 3H), 7.39 – 7.19 (m, 4H), 7.15 – 7.07 (m, 1H), 6.95 – 6.84 (m, 2H), 6.73 (dd, *J* = 3.9, 1.7 Hz, 1H), 6.24 – 6.10 (m, 1H), 5.55 (d, *J* = 20.2 Hz, 2H), 3.93 – 3.65 (m, 1H), 3.51 – 3.26 (m, 6H), 2.21 (s, 2H), 1.91 (d, *J* = 7.9 Hz, 1H); ¹³C NMR (100 MHz,

DMSO-*d*₆) δ 170.17, 159.10, 156.07, 147.56, 140.02, 139.70, 129.28, 129.01, 128.95, 128.88, 128.84, 127.52, 127.37, 127.13, 126.82, 126.37, 116.05, 108.38, 56.48, 56.00, 52.60, 21.21, 16.89.; HRMS-ESI+ calculated for C₂₃H₂₆N₅O₂ [M+H]⁺ 404.2087, found: 404.2073.

4.2.1.30 (*E*)-2-((*E*)-1-(1-benzyl-1*H*-pyrrol-2-yl)-3-(4-isopropylphenyl)allylidene)hydrazine-1-carboximidamide (1ad)

Yield 76 %, yellow solid; mp: 248–250 °C; ¹H NMR (400 MHz, DMSO-*d*₆) δ 11.10 (s, 1H), 8.00 – 7.74 (m, 2H), 7.68 (dd, *J* = 21.6, 6.4 Hz, 1H), 7.63 – 7.45 (m, 1H), 7.35 (dd, *J* = 26.1, 18.0 Hz, 1H), 7.29 – 7.20 (m, 4H), 7.19 – 7.09 (m, 2H), 6.98 (dd, *J* = 23.1, 7.1 Hz, 1H), 6.78 (ddd, *J* = 25.7, 21.4, 14.6 Hz, 2H), 6.51 – 6.26 (m, 1H), 6.25 – 6.14 (m, 1H), 5.74 – 5.40 (m, 2H), 3.07 – 2.69 (m, 1H), 2.22 (s, 2H), 1.36 – 0.89 (m, 6H).; ¹³C NMR (100 MHz, DMSO-*d*₆) δ 156.25, 147.61, 140.29, 129.21, 129.10, 129.04, 128.93, 128.86, 128.83, 128.77, 127.84, 127.57, 127.49, 127.35, 127.30, 127.13, 126.77, 126.35, 115.97, 108.76, 52.61, 33.45, 23.75, 16.83.; HRMS-ESI+ calculated for C₂₄H₂₈N₅ [M+H]⁺ 386.2345, found: 386.234.

4.2.1.31 (*E*)-2-((*E*)-1-(1-benzyl-1*H*-pyrrol-2-yl)-3-(3-methoxyphenyl)allylidene)hydrazine-1-carboximidamide (1ae)

Yield 77 %, yellow solid; mp: 229–231 °C; ¹H NMR (400 MHz, DMSO-*d*₆) δ 10.02 (d, *J* = 60.2 Hz, 1H), 7.72 (d, *J* = 15.5 Hz, 2H), 7.63 – 7.52 (m, 1H), 7.38 (m, 1H), 7.25 (ddd, *J* = 13.2, 9.5, 7.4 Hz, 3H), 7.18 (d, *J* = 7.7 Hz, 1H), 7.15 – 7.07 (m, 1H), 7.05 – 6.93 (m, 2H), 6.91 – 6.87 (m, 1H), 6.78 – 6.66 (m, 1H), 6.42 – 6.33 (m, 1H), 6.19 (ddd, *J* = 6.5, 5.1, 2.8 Hz, 1H), 5.61 – 5.42 (m, 2H), 3.91 – 3.60 (m, 3H), 2.21 (s, 1H), 1.88 (d, *J* = 12.5 Hz, 1H).; ¹³C NMR (100 MHz, DMSO-*d*₆) δ 170.12, 159.34, 155.88, 147.90, 139.93, 129.25, 129.01, 128.94, 128.88, 128.77, 127.51, 127.36, 127.30, 127.11, 126.78, 126.35, 116.02, 108.37, 55.66, 52.59, 21.34, 17.20.; HRMS-ESI+ calculated for C₂₂H₂₄N₅O [M+H]⁺ 374.1981, found: 374.1978.

4.2.1.32 (*Z*)-2-((*E*)-1-(1-benzyl-1*H*-pyrrol-2-yl)-3-(4-bromo-2,6-difluorophenyl)allylidene)hydrazine-1-carboximidamide (1af)

Yield 73 %, yellow solid; mp: 247–249 °C; ¹H NMR (400 MHz, DMSO-*d*₆) δ 11.03 (s, 1H), 10.25 – 9.99 (m, 1H), 7.88 – 7.58 (m, 3H), 7.54 – 7.25 (m, 3H), 7.23 – 7.17 (m, 1H), 7.08 (d, *J* = 16.2 Hz, 1H), 6.97 – 6.82 (m, 2H), 6.79 – 6.66 (m, 1H), 6.36 – 6.10 (m, 1H), 5.72 – 5.52 (m, 2H), 2.21 (s, 2H), 1.90 (s, 1H).; ¹³C NMR (100 MHz, DMSO-*d*₆) δ 170.20, 159.59, 159.15, 156.12, 147.49, 139.99, 129.25, 128.99, 128.93, 128.81, 128.67, 127.52, 127.35, 127.09, 127.00, 126.34, 116.02, 108.37, 52.60, 21.22, 16.97.; HRMS-ESI+ calculated for C₂₁H₁₉BrF₂N₅ [M+H]⁺ 458.0792, found: 458.0798.

4.2.1.33 (Z)-2-((E)-1-(1-benzyl-1H-pyrrol-2-yl)-3-(4-(benzyloxy)phenyl)allylidene)hydrazine-1-carboximidamide (1ag)

Yield 91 %, yellow solid; mp: 258–260 °C; ¹H NMR (400 MHz, DMSO-*d*₆) δ 11.00 (s, 1H), 7.78 (ddd, *J* = 71.7, 63.0, 57.8 Hz, 3H), 7.62 – 7.33 (m, 4H), 7.24 (ddd, *J* = 26.2, 16.9, 9.5 Hz, 5H), 7.16 – 6.97 (m, 3H), 6.96 – 6.82 (m, 3H), 6.72 (d, *J* = 2.2 Hz, 2H), 6.46 – 6.09 (m, 2H), 5.58 (s, 2H), 2.21 (s, 2H).; ¹³C NMR (100 MHz, DMSO-*d*₆) δ 170.49, 159.53, 159.09, 156.10, 147.48, 140.02, 129.19, 129.08, 128.94, 128.88, 128.75, 128.36, 128.14, 127.48, 127.35, 126.78, 126.35, 115.93, 115.93, 108.36, 108.36, 69.53, 52.58, 52.58, 21.35, 21.21, 17.20, 16.86.; HRMS-ESI+ calculated for C₂₈H₂₈N₅O [M+H]⁺ 450.2294, found: 450.2287.

4.2.1.34 (Z)-2-((E)-1-(1-benzyl-1H-pyrrol-2-yl)-3-(4-(dimethylamino)phenyl)allylidene)hydrazine-1-carboximidamide (1ah)

Yield 93 %, yellow solid; mp: 208–210 °C; ¹H NMR (400 MHz, DMSO-*d*₆) δ 10.88 (d, *J* = 18.3 Hz, 1H), 7.86 – 7.60 (m, 2H), 7.57 – 7.40 (m, 2H), 7.38 – 7.27 (m, 3H), 7.26 – 7.18 (m, 2H), 7.10 (d, *J* = 7.9 Hz, 2H), 6.90 (d, *J* = 7.2 Hz, 1H), 6.73 (dd, *J* = 5.0, 3.2 Hz, 2H), 6.22 (ddd, *J* = 33.6, 3.8, 2.6 Hz, 1H), 5.62 (dd, *J* = 44.6, 8.0 Hz, 2H), 3.19 – 2.64 (m, 6H), 2.19 (d, *J* = 13.2 Hz, 2H), 1.94 (dd, *J* = 24.7, 11.2 Hz, 1H).; ¹³C NMR (100 MHz, DMSO-*d*₆) δ 179.38, 156.02, 147.58, 142.19, 140.01, 131.96, 130.64, 129.28, 128.99, 128.94, 128.81, 127.46, 127.36, 127.12, 126.35, 120.23, 116.06, 112.28, 109.03, 108.38, 52.60, 51.93, 16.85.; HRMS-ESI+ calculated for C₂₃H₂₇N₆ [M+H]⁺ 387.2297, found: 387.2295.

4.2.1.35 (Z)-2-((E)-1-(1-benzyl-1H-pyrrol-2-yl)-3-(3-bromophenyl)allylidene)hydrazine-1-carboximidamide (1ai)

Yield 84 %, yellow solid; mp: 226–228 °C; ¹H NMR (400 MHz, DMSO-*d*₆) δ 10.98 (s, 1H), 8.05 – 7.55 (m, 3H), 7.43 (dddd, *J* = 23.0, 15.1, 9.5, 4.8 Hz, 2H), 7.33 – 7.18 (m, 4H), 7.16 – 6.98 (m, 2H), 6.95 – 6.82 (m, 2H), 6.73 (dd, *J* = 3.9, 1.8 Hz, 1H), 6.19 (ddd, *J* = 10.0, 3.9, 2.6 Hz, 1H), 5.74 – 5.48 (m, 2H), 2.21 (s, 2H), 1.99 – 1.87 (m, 1H).; ¹³C NMR (100 MHz, DMSO-*d*₆) δ 170.10, 159.36, 156.26, 147.61, 140.31, 130.74, 129.84, 129.44, 129.25, 129.11, 129.01, 128.85, 127.54, 127.42, 127.12, 126.44, 116.02, 108.37, 52.89, 21.34, 16.83.; HRMS-ESI+ calculated for C₂₁H₂₁BrN₅ [M+H]⁺ 422.0980, found: 422.0973.

4.2.1.36 (Z)-2-((E)-1-(1-benzyl-1H-pyrrol-2-yl)-3-(4-bromophenyl)allylidene)hydrazine-1-carboximidamide (1aj)

Yield 91 %, yellow solid; mp: 231–233 °C; ¹H NMR (400 MHz, DMSO-*d*₆) δ 10.94 (s, 1H), 7.87 – 7.55 (m, 3H), 7.54 – 7.33 (m, 2H), 7.25 (qd, *J* = 7.2, 3.3 Hz, 4H), 7.10 (dt, *J* = 7.7, 3.9 Hz, 2H), 6.89 (d, *J* = 7.1 Hz, 2H), 6.73 (dd, *J* = 3.9, 1.8 Hz, 1H), 6.18 (dd, *J* = 3.8, 2.7 Hz, 1H), 5.57 (s, 2H), 2.21 (s, 2H), 1.99 – 1.85 (m, 1H).; ¹³C NMR (100 MHz, DMSO-*d*₆) δ 170.12,

159.57, 159.08, 156.26, 147.56, 139.90, 132.23, 130.93, 129.27, 128.99, 128.94, 128.85, 127.42, 127.10, 126.34, 116.04, 109.46, 108.76, 52.59, 20.95, 16.81.; HRMS-ESI+ calculated for $C_{21}H_{21}BrN_5$ $[M+H]^+$ 422.0980, found: 422.0973.

4.2.1.37 (Z)-2-((E)-1-(1-benzyl-1H-pyrrol-2-yl)-3-(2,5-dimethoxyphenyl)allylidene)hydrazine-1-carboximidamide (1ak)

Yield 89 %, yellow solid; mp: 242–244 °C; 1H NMR (400 MHz, DMSO-*d*6) δ 10.10 (d, J = 37.2 Hz, 1H), 9.56 (s, 1H), 7.69 – 7.49 (m, 3H), 7.23 (ddd, J = 20.9, 16.3, 10.1 Hz, 4H), 7.11 (d, J = 9.0 Hz, 1H), 7.00 (d, J = 8.3 Hz, 1H), 6.91 (dd, J = 18.6, 6.0 Hz, 2H), 6.82 – 6.67 (m, 1H), 6.41 – 6.13 (m, 1H), 5.55 (t, J = 50.2 Hz, 2H), 3.86 – 3.60 (m, 6H), 2.21 (s, 1H), 1.90 (s, 2H).; ^{13}C NMR (100 MHz, DMSO-*d*6) δ 170.52, 159.36, 156.27, 156.12, 153.75, 147.55, 140.00, 139.74, 129.28, 128.95, 128.87, 127.54, 127.37, 127.10, 126.79, 126.33, 116.05, 113.39, 108.40, 56.36, 52.60, 21.33, 16.82.; HRMS-ESI+ calculated for $C_{23}H_{26}N_5O_2$ $[M+H]^+$ 404.2087, found: 404.2085.

4.2.1.38 (E)-2-((E)-1-(1-(3,5-dimethoxybenzyl)-1H-pyrrol-2-yl)-3-phenylallylidene)hydrazine-1-carboximidamide (2a)

Yield 89 %, yellow solid; mp: 182–184°C; 1H NMR (400 MHz, DMSO-*d*6) δ 11.11 – 10.89 (m, 1H), 10.09 (s, 1H), 9.53 (s, 1H), 7.98 – 7.69 (m, 3H), 7.47 (dddd, J = 30.0, 18.8, 15.6, 6.1 Hz, 6H), 7.05 (ddd, J = 25.3, 21.4, 12.4 Hz, 1H), 6.90 – 6.72 (m, 1H), 6.68 – 6.14 (m, 1H), 5.74 – 5.26 (m, 2H), 3.40 (s, 6H), 2.26 – 2.15 (m, 1H), 1.90 (s, 1H).; ^{13}C NMR (100 MHz, DMSO-*d*6) δ 178.78, 170.14, 159.14, 156.12, 147.23, 139.45, 131.82, 131.78, 131.74, 129.53, 129.34, 129.30, 129.19, 129.01, 128.84, 128.62, 115.99, 109.37, 108.37, 52.07, 51.55, 21.03, 17.04.; HRMS-ESI+ calculated for $C_{23}H_{25}N_5O_2$ $[M+H]^+$ 404.2087, found: 404.2065.

4.2.1.39 (Z)-2-((E)-1-(1-(4-chlorobenzyl)-1H-pyrrol-2-yl)-3-phenylallylidene)hydrazine-1-carboximidamide (2b)

Yield 84 %, yellow solid; mp: 204–206°C; 1H NMR (400 MHz, DMSO-*d*6) δ 10.13 (d, J = 22.6 Hz, 1H), 9.57 (s, 1H), 8.86 (s, 1H), 7.80 – 7.57 (m, 3H), 7.45 – 7.31 (m, 3H), 7.17 – 6.98 (m, 3H), 6.93 – 6.70 (m, 1H), 6.30 (ddd, J = 56.3, 16.8, 8.3 Hz, 1H), 5.82 – 5.12 (m, 2H), 4.71 (s, 2H), 2.22 (d, J = 11.8 Hz, 1H), 1.89 (s, 1H).; ^{13}C NMR (100 MHz, DMSO-*d*6) δ 170.11, 159.65, 159.18, 156.17, 138.85, 129.51, 129.31, 129.04, 129.00, 128.90, 128.81, 128.73, 128.67, 128.25, 127.65, 116.36, 108.36, 51.91, 34.30, 21.34, 16.75.; HRMS-ESI+ calculated for $C_{21}H_{21}ClN_5$ $[M+H]^+$ 378.1485, found: 378.1481.

4.2.1.40 (Z)-2-((E)-1-(1-(4-bromobenzyl)-1H-pyrrol-2-yl)-3-phenylallylidene)hydrazine-1-carboximidamide (2c)

Yield 80 %, yellow solid; mp: 213–215 °C; ¹H NMR (400 MHz, DMSO-*d*₆) δ 11.22 – 10.83 (m, 1H), 10.06 (d, J = 33.5 Hz, 1H), 9.53 (s, 1H), 7.90 – 7.68 (m, 2H), 7.57 (d, J = 15.7 Hz, 1H), 7.52 – 7.31 (m, 2H), 7.27 – 7.01 (m, 1H), 6.82 – 6.63 (m, 1H), 6.45 – 6.27 (m, 1H), 6.24 – 6.12 (m, 1H), 6.10 – 5.96 (m, 1H), 5.48 (dd, J = 59.1, 34.5 Hz, 2H), 3.67 (d, J = 5.7 Hz, 3H), 2.26 – 2.18 (m, 1H), 1.92 – 1.87 (m, 1H).; ¹³C NMR (100 MHz, DMSO-*d*₆) δ 179.14, 170.11, 161.03, 159.34, 156.57, 147.91, 142.71, 142.33, 135.40, 129.30, 129.16, 124.34, 121.93, 115.98, 108.36, 104.53, 99.04, 55.29, 52.58, 20.95, 16.88.; HRMS-ESI+ calculated for C₂₁H₂₁BrN₅ [M+H]⁺ 422.0980, found: 422.0933.

4.2.1.41 (E)-2-((E)-3-phenyl-1-(1-(4-(trifluoromethoxy)benzyl)-1H-pyrrol-2-yl)allylidene)hydrazine-1-carboximidamide (2d)

Yield 92 %, yellow solid; mp: 217–219 °C; ¹H NMR (400 MHz, DMSO-*d*₆) δ 10.17 (s, 1H), 7.80 (s, 3H), 7.58 (dd, J = 16.2, 7.8 Hz, 5H), 7.41 (t, J = 7.5 Hz, 2H), 7.33 – 7.28 (m, 1H), 7.12 (s, 1H), 6.97 (d, J = 8.0 Hz, 1H), 6.73 (d, J = 2.3 Hz, 1H), 6.19 – 6.15 (m, 1H), 5.65 (d, J = 41.1 Hz, 2H), 1.89 (s, 2H).; ¹³C NMR (100 MHz, DMSO-*d*₆) δ 170.40, 159.55, 159.10, 156.08, 155.57, 155.54, 148.93, 147.68, 140.06, 139.19, 129.36, 128.91, 127.86, 127.21, 127.00, 126.97, 116.19, 108.51, 52.32, 21.03, 18.64, 16.76.; HRMS-ESI+ calculated for C₂₂H₂₀F₃KN₅O [M+K]⁺ 466.1257, found: 466.1251.

4.2.1.42 (Z)-2-((E)-1-(1-([1,1'-biphenyl]-4-ylmethyl)-1H-pyrrol-2-yl)-3-phenylallylidene)hydrazine-1-carboximidamide (2e)

Yield 94 %, yellow solid; mp: 208–210 °C; ¹H NMR (400 MHz, DMSO-*d*₆) δ 11.06 (s, 1H), 7.82 (s, 3H), 7.80 – 7.51 (m, 4H), 7.46 – 6.91 (m, 10H), 6.70 (d, J = 39.3 Hz, 1H), 6.41 (t, J = 12.8 Hz, 1H), 6.21 (d, J = 15.4 Hz, 1H), 5.74 – 5.38 (m, 2H), 2.93 (s, 1H), 2.23 (s, 1H).; ¹³C NMR (100 MHz, DMSO-*d*₆) δ 159.09, 156.14, 147.65, 141.60, 139.48, 139.11, 137.63, 135.86, 130.07, 129.22, 128.89, 128.69, 128.62, 128.26, 127.81, 127.43, 127.03, 126.27, 124.32, 121.56, 121.48, 121.30, 116.29, 108.60, 51.61, 21.04, 17.06.; HRMS-ESI+ calculated for C₂₇H₂₆N₅ [M+H]⁺ 420.2188, found: 420.2171.

4.2.1.43 (Z)-2-((E)-3-phenyl-1-(1-(4-(trifluoromethyl)benzyl)-1H-pyrrol-2-yl)allylidene)hydrazine-1-carboximidamide (2f)

Yield 87 %, yellow solid; mp: 224–226 °C; ¹H NMR (400 MHz, DMSO-*d*₆) δ 10.97 (s, 1H), 7.72 (s, 3H), 7.68 – 7.60 (m, 2H), 7.54 (dd, J = 17.6, 8.9 Hz, 1H), 7.50 – 7.29 (m, 3H), 7.25 – 7.05 (m, 3H), 6.83 (dd, J = 40.4, 8.9 Hz, 1H), 6.49 – 6.32 (m, 1H), 6.29 – 6.17 (m, 1H), 5.81 – 5.51 (m, 2H), 2.22 (s, 2H).; ¹³C NMR (100 MHz, DMSO-*d*₆) δ 169.82, 158.52, 155.81, 147.52,

144.89, 141.19, 137.58, 135.55, 129.44, 129.29, 128.87, 128.61, 128.04, 127.44, 127.01, 125.88, 125.62, 115.99, 108.68, 52.31, 21.04, 16.76.; HRMS-ESI+ calculated for C₂₂H₂₁F₃N₅ [M+H]⁺ 412.1749, found: 412.1748.

4.2.1.44 (Z)-2-((E)-1-(1-(4-fluorobenzyl)-1H-pyrrol-2-yl)-3-phenylallylidene)hydrazine-1-carboximidamide (2g)

Yield 81 %, yellow solid; mp: 216–218 °C; ¹H NMR (400 MHz, DMSO-*d*₆) δ 10.92 (d, J = 71.4 Hz, 1H), 10.14 (s, 1H), 9.56 (s, 1H), 8.02 – 7.64 (m, 4H), 7.54 – 7.22 (m, 3H), 7.18 – 6.88 (m, 4H), 6.77 – 6.54 (m, 1H), 6.46 – 5.90 (m, 1H), 5.76 – 5.04 (m, 2H), 2.22 (t, J = 7.7 Hz, 1H), 1.90 (s, 1H).; ¹³C NMR (100 MHz, DMSO-*d*₆) δ 170.22, 159.59, 159.14, 156.03, 147.50, 141.66, 135.86, 129.54, 129.45, 129.38, 129.18, 128.90, 128.82, 128.65, 128.46, 128.38, 127.46, 108.37, 51.93, 21.06, 16.76.; HRMS-ESI+ calculated for C₂₁H₂₁FN₅ [M+H]⁺ 362.1781, found: 362.1778.

4.2.1.45 (Z)-2-((E)-1-(1-(2-cyanobenzyl)-1H-pyrrol-2-yl)-3-phenylallylidene)hydrazine-1-carboximidamide (2h)

Yield 89 %, yellow solid; mp: 228–230 °C; ¹H NMR (400 MHz, DMSO-*d*₆) δ 10.95 (d, J = 41.6 Hz, 1H), 8.08 – 7.68 (m, 3H), 7.61 – 7.47 (m, 2H), 7.44 – 7.23 (m, 4H), 7.21 – 7.05 (m, 3H), 6.95 – 6.65 (m, 1H), 6.41 (dt, J = 20.0, 13.7 Hz, 1H), 6.28 – 6.16 (m, 1H), 5.76 – 5.46 (m, 2H), 2.26 – 1.87 (m, 2H).; ¹³C NMR (100 MHz, DMSO-*d*₆) δ 156.16, 155.74, 147.67, 146.09, 141.58, 137.45, 135.73, 129.53, 129.40, 129.23, 129.14, 129.10, 128.62, 127.44, 117.39, 117.14, 116.27, 109.67, 108.77, 60.18, 46.64, 17.06.; HRMS-ESI+ calculated for C₂₂H₂₁N₆ [M+H]⁺ 369.1828, found: 369.1825.

4.2.1.46 (E)-2-((E)-1-(1-(4-(difluoromethoxy)benzyl)-1H-pyrrol-2-yl)-3-phenylallylidene)hydrazine-1-carboximidamide (2i)

Yield 93 %, yellow solid; mp: 242–244 °C; ¹H NMR (400 MHz, DMSO-*d*₆) δ 10.19 – 9.33 (m, 1H), 7.71 (dd, J = 55.7, 33.1 Hz, 4H), 7.40 (d, J = 15.0 Hz, 4H), 7.22 – 6.84 (m, 7H), 6.29 (dt, J = 45.8, 24.1 Hz, 1H), 5.48 (ddd, J = 204.2, 150.0, 95.9 Hz, 2H), 1.91 (d, J = 10.8 Hz, 2H).; ¹³C NMR (100 MHz, DMSO-*d*₆) δ 171.10, 158.78, 155.81, 153.66, 151.83, 150.15, 130.37, 130.09, 129.38, 129.21, 128.87, 128.40, 128.33, 127.51, 119.24, 116.55, 113.92, 108.51, 98.17, 98.06, 50.92, 20.96.; HRMS-ESI+ calculated for C₂₂H₂₂ F₂N₅O [M+H]⁺ 410.1792, found: 410.1788.

4.2.1.47 (E)-2-((E)-1-(1-(2,5-difluorobenzyl)-1H-pyrrol-2-yl)-3-phenylallylidene)hydrazine-1-carboximidamide (2j)

Yield 76 %, yellow solid; mp: 231–233 °C; ¹H NMR (400 MHz, DMSO-*d*₆) δ 8.00 (s, 1H), 7.83 – 7.69 (m, 3H), 7.63 (dd, J = 4.1, 1.5 Hz, 1H), 7.57 – 7.51 (m, 3H), 7.46 (dd, J = 9.4, 5.6

Hz, 1H), 7.42 (dd, $J = 5.8, 4.7$ Hz, 2H), 7.37 (dd, $J = 7.6, 5.5$ Hz, 1H), 7.28 (dd, $J = 6.5, 3.2$ Hz, 1H), 6.36 (qd, $J = 8.5, 4.0$ Hz, 2H), 5.88 (d, $J = 6.9$ Hz, 2H), 2.06 – 1.81 (m, 2H).; ^{13}C NMR (100 MHz, DMSO-*d*₆) δ 178.66, 170.75, 170.16, 158.99, 141.22, 138.72, 135.29, 134.61, 133.39, 131.51, 130.58, 129.29, 128.97, 127.94, 126.99, 125.98, 124.37, 121.49, 109.35, 50.92, 21.33.; HRMS-ESI+ calculated for C₂₁H₂₀F₂N₅ [M+H]⁺ 380.1687, found: 380.1686.

4.2.1.48 (Z)-2-((E)-1-(1-(4-bromo-2-fluorobenzyl)-1H-pyrrol-2-yl)-3-phenylallylidene)hydrazine-1-carboximidamide (2k)

Yield 72 %, yellow solid; mp: 228–230 °C; ^1H NMR (400 MHz, DMSO-*d*₆) δ 7.86 (s, 1H), 7.77 (dd, $J = 28.5, 10.7$ Hz, 4H), 7.64 (d, $J = 2.5$ Hz, 1H), 7.54 (dd, $J = 18.7, 9.6$ Hz, 3H), 7.41 (s, 4H), 7.21 (dd, $J = 72.6, 22.5$ Hz, 2H), 6.59 (t, $J = 8.1$ Hz, 1H), 6.38 (d, $J = 23.8$ Hz, 1H), 5.65 (d, $J = 25.3$ Hz, 2H).; ^{13}C NMR (100 MHz, DMSO-*d*₆) δ 178.80, 160.88, 158.52, 141.52, 135.24, 133.27, 131.24, 130.55, 129.81, 129.29, 129.01, 128.14, 126.56, 126.41, 124.14, 121.68, 120.82, 119.06, 118.76, 109.65, 46.32.; HRMS-ESI+ calculated for C₂₁H₂₀BrFN₅ [M+H]⁺ 442.0866, found: 442.0862.

4.2.1.49 (E)-2-((E)-1-(1-(2,5-dichlorobenzyl)-1H-pyrrol-2-yl)-3-phenylallylidene)hydrazine-1-carboximidamide (2l)

Yield 73 %, yellow solid; mp: 234–236 °C; ^1H NMR (400 MHz, DMSO-*d*₆) δ 7.76 (ddd, $J = 16.2, 5.8, 2.4$ Hz, 3H), 7.63 – 7.21 (m, 8H), 7.18 – 7.07 (m, 1H), 7.05 – 6.60 (m, 1H), 6.54 – 6.13 (m, 2H), 5.64 (dd, $J = 40.3, 25.1$ Hz, 2H), 2.24 (s, 1H), 1.99 – 1.86 (m, 1H).; ^{13}C NMR (100 MHz, DMSO-*d*₆) δ 169.83, 159.12, 155.81, 147.53, 141.58, 139.54, 132.63, 131.40, 129.96, 129.30, 129.19, 129.16, 129.09, 129.06, 127.06, 116.36, 110.03, 109.02, 50.56, 21.04, 16.77.; HRMS-ESI+ calculated for C₂₁H₂₀Cl₂N₅ [M+H]⁺ 412.1096, found: 412.1093.

4.2.1.50 (E)-2-((E)-1-(1-(4-methylbenzyl)-1H-pyrrol-2-yl)-3-phenylallylidene)hydrazine-1-carboximidamide (2m)

Yield 86 %, yellow solid; mp: 226–228 °C; ^1H NMR (400 MHz, DMSO-*d*₆) δ 11.06 (s, 1H), 8.16 – 7.65 (m, 3H), 7.63 – 7.19 (m, 3H), 7.18 – 6.94 (m, 4H), 6.94 – 6.77 (m, 2H), 6.71 (d, $J = 2.1$ Hz, 1H), 6.38 (ddd, $J = 29.2, 23.4, 18.3$ Hz, 1H), 6.24 – 6.04 (m, 1H), 5.63 – 5.37 (m, 2H), 2.23 (s, 2H), 2.22 – 2.13 (m, 3H).; ^{13}C NMR (100 MHz, DMSO-*d*₆) δ 156.15, 147.48, 136.88, 136.43, 129.71, 129.49, 129.37, 129.30, 129.17, 129.10, 128.97, 128.65, 127.49, 127.24, 126.78, 126.37, 115.98, 109.30, 108.28, 52.42, 21.10, 16.97.; HRMS-ESI+ calculated for C₂₂H₂₄N₅ [M+H]⁺ 358.2032, found: 358.2030.

4.2.1.51 (*E*)-2-((*E*)-1-(1-(2-fluorobenzyl)-1*H*-pyrrol-2-yl)-3-phenylallylidene)hydrazine-1-carboximidamide (2n)

Yield 93 %, yellow solid; mp: 262–264 °C; ¹H NMR (400 MHz, DMSO-*d*₆) δ 11.03 (s, 1H), 8.18 – 7.65 (m, 3H), 7.60 – 7.32 (m, 3H), 7.28 – 6.89 (m, 6H), 6.74 (d, *J* = 2.3 Hz, 1H), 6.60 – 6.43 (m, 1H), 6.41 – 6.09 (m, 1H), 5.60 (d, *J* = 26.2 Hz, 2H), 2.22 (s, 2H).; ¹³C NMR (100 MHz, DMSO-*d*₆) δ 160.88, 158.45, 156.22, 147.67, 129.64, 129.56, 129.25, 129.02, 128.64, 128.36, 128.32, 127.47, 126.86, 126.72, 125.11, 125.08, 115.96, 115.68, 108.38, 46.99, 16.81.; HRMS-ESI+ calculated for C₂₁H₂₁FN₅ [M+H]⁺ 362.1781, found: 362.1778.

4.2.1.52 (*E*)-2-((*E*)-1-(1-(4-fluoro-2-(trifluoromethyl)benzyl)-1*H*-pyrrol-2-yl)-3-phenylallylidene)hydrazine-1-carboximidamide (2o)

Yield 89 %, yellow solid; mp: 252–254 °C; ¹H NMR (400 MHz, DMSO-*d*₆) δ 11.06 (d, *J* = 38.4 Hz, 1H), 8.15 – 7.72 (m, 2H), 7.72 – 7.52 (m, 3H), 7.51 – 7.23 (m, 4H), 7.23 – 6.89 (m, 2H), 6.86 – 6.68 (m, 1H), 6.55 – 6.22 (m, 2H), 5.86 – 5.63 (m, 2H), 2.23 (s, 2H).; ¹³C NMR (100 MHz, DMSO-*d*₆) δ 162.14, 159.73, 156.16, 147.91, 141.91, 135.79, 135.76, 134.96, 130.19, 129.64, 129.57, 129.49, 129.28, 129.19, 128.66, 127.75, 127.43, 120.29, 116.17, 109.07, 49.12, 17.08.; HRMS-ESI+ calculated for C₂₂H₂₀F₄N₅ [M+H]⁺ 430.1655, found: 430.1654.

4.2.1.53 (*E*)-2-((*E*)-1-(1-(3,5-bis(trifluoromethyl)benzyl)-1*H*-pyrrol-2-yl)-3-phenylallylidene)hydrazine-1-carboximidamide (2p)

Yield 93 %, white solid; mp: 209–211 °C; ¹H NMR (400 MHz, DMSO-*d*₆) δ 10.87 (s, 1H), 8.10 – 7.86 (m, 2H), 7.66 (d, *J* = 30.6 Hz, 2H), 7.61 – 7.37 (m, 5H), 7.34 – 6.98 (m, 2H), 6.81 (d, *J* = 2.2 Hz, 1H), 6.29 (d, *J* = 39.7 Hz, 1H), 5.81 (s, 2H), 2.16 (s, 2H), 1.90 (s, 1H).; ¹³C NMR (100 MHz, DMSO-*d*₆) δ 170.17, 159.09, 156.11, 147.56, 143.68, 131.24, 130.87, 130.55, 130.22, 129.62, 128.52, 127.73, 127.37, 125.02, 122.31, 121.24, 121.21, 119.63, 117.06, 108.94, 51.96, 21.19, 16.71.; HRMS-ESI+ calculated for C₂₃H₂₀F₆N₅ [M+H]⁺ 480.1623, found: 480.1620.

4.2.1.54 (*E*)-2-((*E*)-1-(1-(4-butylbenzyl)-1*H*-pyrrol-2-yl)-3-phenylallylidene)hydrazine-1-carboximidamide (2q)

Yield 83 %, white solid; mp: 214–216 °C; ¹H NMR (400 MHz, DMSO-*d*₆) δ 11.10 (s, 1H), 8.07 – 7.72 (m, 2H), 7.70 – 7.21 (m, 4H), 7.19 – 6.97 (m, 4H), 6.94 – 6.61 (m, 3H), 6.44 – 6.08 (m, 1H), 5.63 – 5.31 (m, 2H), 2.85 (s, 1H), 2.23 (s, 2H), 1.65 – 1.12 (m, 5H), 1.01 – 0.66 (m, 4H).; ¹³C NMR (100 MHz, DMSO-*d*₆) δ 156.16, 147.48, 141.41, 137.12, 133.52, 129.25, 129.09, 129.02, 128.96, 128.81, 128.73, 128.69, 128.61, 127.44, 127.21, 126.85, 126.37,

115.88, 108.30, 52.40, 34.89, 33.53, 22.21, 16.98, 14.21.; HRMS-ESI+ calculated for $C_{25}H_{30}N_5$ [M+H]⁺ 400.2501, found: 400.2502.

4.2.1.55 (*E*)-2-((*E*)-1-(1-(2,4-difluorobenzyl)-1*H*-pyrrol-2-yl)-3-phenylallylidene)hydrazine-1-carboximidamide (2r)

Yield 91 %, yellow solid; mp: 198–200 °C; ¹H NMR (400 MHz, DMSO-*d*₆) δ 11.05 (s, 1H), 7.72 (ddd, *J* = 49.6, 28.7, 21.8 Hz, 3H), 7.44 (ddd, *J* = 30.6, 19.8, 6.8 Hz, 2H), 7.29 – 7.15 (m, 2H), 7.13 – 6.82 (m, 3H), 6.73 (d, *J* = 2.2 Hz, 1H), 6.67 – 6.56 (m, 1H), 6.46 – 6.10 (m, 2H), 5.70 – 5.44 (m, 2H), 2.21 (d, *J* = 16.6 Hz, 2H).; ¹³C NMR (100 MHz, DMSO-*d*₆) δ 156.27, 147.92, 129.69, 129.37, 129.18, 128.90, 128.78, 128.64, 127.44, 127.39, 123.18, 123.15, 123.03, 123.00, 116.36, 112.21, 112.03, 108.37, 104.24, 46.34, 16.83.; HRMS-ESI+ calculated for $C_{21}H_{20}F_2N_5$ [M+H]⁺ 380.1687, found: 380.1690.

4.2.1.56 (*E*)-2-((*E*)-1-(1-(4-nitrobenzyl)-1*H*-pyrrol-2-yl)-3-phenylallylidene)hydrazine-1-carboximidamide (2s)

Yield 82 %, yellow solid; mp: 212-214 °C; ¹H NMR (400 MHz, DMSO-*d*₆) δ 7.95 (d, *J* = 7.2 Hz, 1H), 7.80 (d, *J* = 6.8 Hz, 1H), 7.73 (dd, *J* = 5.7, 3.3 Hz, 1H), 7.67 (dd, *J* = 5.6, 3.4 Hz, 1H), 7.52 (dd, *J* = 16.3, 8.2 Hz, 4H), 7.43 – 7.38 (m, 4H), 7.32 (d, *J* = 4.5 Hz, 1H), 6.38 (t, *J* = 19.6 Hz, 1H), 5.89 (dd, *J* = 19.2, 16.2 Hz, 2H), 4.28 (q, *J* = 7.1 Hz, 2H), 1.90 (m, 1H), 1.28 (s, 1H).; ¹³C NMR (100 MHz, DMSO-*d*₆) δ 170.22, 167.38, 159.07, 155.97, 132.14, 131.97, 129.83, 129.72, 129.36, 129.16, 129.11, 129.03, 128.49, 128.37, 127.25, 127.07, 126.87, 113.51, 61.53, 20.96, 14.41.; HRMS-ESI+ calculated for $C_{21}H_{20}N_6O_2$ [M]⁺ 388.1802, found: 388.1803.

4.2.1.57 (*E*)-2-((*E*)-1-(1-(3-bromobenzyl)-1*H*-pyrrol-2-yl)-3-phenylallylidene)hydrazine-1-carboximidamide (2t)

Yield 89 %, yellow solid; mp: 228-230 °C; ¹H NMR (400 MHz, DMSO-*d*₆) δ 7.77 (ddd, *J* = 15.7, 7.3, 2.0 Hz, 2H), 7.54 (dd, *J* = 19.4, 10.6 Hz, 1H), 7.47 – 7.31 (m, 5H), 7.30 – 7.18 (m, 2H), 7.18 – 7.04 (m, 1H), 6.99 (dd, *J* = 17.4, 6.6 Hz, 1H), 6.92 – 6.74 (m, 1H), 6.51 – 6.32 (m, 1H), 6.27 – 6.18 (m, 1H), 5.66 – 5.43 (m, 2H), 4.98 (d, *J* = 10.1 Hz, 1H), 2.21 (s, 1H), 2.03 – 1.88 (m, 1H).; ¹³C NMR (100 MHz, DMSO-*d*₆) δ 156.26, 146.22, 142.58, 135.75, 131.13, 130.90, 130.32, 129.98, 129.37, 129.24, 128.64, 127.51, 127.33, 125.81, 125.47, 122.19, 119.50, 116.36, 108.45, 50.92, 16.85.; HRMS-ESI+ calculated for $C_{21}H_{21}BrN_5$ [M+H]⁺ 422.0980, found: 422.0974.

4.2.1.58 (*Z*)-2-((*E*)-1-(1-(4-cyanobenzyl)-1*H*-pyrrol-2-yl)-3-phenylallylidene)hydrazine-1-carboximidamide (2u)

Yield 79 %, yellow solid; mp: 223-225 °C; ¹H NMR (400 MHz, DMSO-*d*₆) δ 7.82 (ddd, *J* = 14.1, 10.4, 6.9 Hz, 3H), 7.74 – 7.61 (m, 2H), 7.55 – 7.47 (m, 1H), 7.44 – 7.38 (m, 1H), 7.34

(dd, $J = 15.5, 3.7$ Hz, 2H), 7.29 – 7.23 (m, 1H), 7.18 (d, $J = 5.6$ Hz, 1H), 7.11 (d, $J = 21.5$ Hz, 1H), 7.03 (dd, $J = 15.9, 5.2$ Hz, 1H), 6.97 – 6.88 (m, 1H), 6.43 – 6.19 (m, 1H), 5.97 – 5.43 (m, 2H), 4.83 – 4.09 (m, 1H), 2.27 – 2.07 (m, 1H), 2.02 – 1.81 (m, 1H).; ^{13}C NMR (100 MHz, DMSO-*d*6) δ 170.13, 159.33, 156.27, 130.03, 129.91, 129.75, 129.60, 129.33, 129.17, 128.99, 128.57, 127.53, 127.08, 126.55, 108.37, 61.25, 51.53, 25.16, 21.34, 18.54, 16.83, 14.43.; HRMS-ESI+ calculated for $\text{C}_{22}\text{H}_{24}\text{N}_7$ $[\text{M}+\text{NH}_4]^+$ 386.2093, found: 386.2130.

4.2.1.59 (*E*)-2-((*E*)-1-(1-(3-cyanobenzyl)-1*H*-pyrrol-2-yl)-3-phenylallylidene)hydrazine-1-carboximidamide (2v)

Yield 83 %, yellow solid; mp: 217-219°C; ^1H NMR (400 MHz, DMSO-*d*6) δ 8.25 – 7.69 (m, 4H), 7.68 – 7.41 (m, 3H), 7.40 – 7.24 (m, 4H), 7.24 – 7.11 (m, 2H), 7.11 – 6.61 (m, 2H), 5.62 – 5.33 (m, 2H), 4.00 – 3.75 (m, 1H), 3.24 – 3.02 (m, 1H), 1.98 – 1.90 (m, 1H).; ^{13}C NMR (100 MHz, DMSO-*d*6) δ 156.23, 138.16, 136.92, 130.25, 129.11, 129.06, 129.01, 128.83, 127.97, 127.69, 127.49, 126.71, 122.84, 121.03, 115.00, 114.62, 111.65, 55.70, 50.11, 49.05, 25.46, 18.55.; HRMS-ESI+ calculated for $\text{C}_{22}\text{H}_{21}\text{N}_6$ $[\text{M}+\text{H}]^+$ 369.1835, found: 369.1838.

4.2.1.60 (*E*)-2-((*E*)-1-(1-(5-fluoro-2-methylbenzyl)-1*H*-pyrrol-2-yl)-3-phenylallylidene)hydrazine-1-carboximidamide (2w)

Yield 86 %, yellow solid; mp: 216-218°C; ^1H NMR (400 MHz, DMSO-*d*6) δ 11.24 – 10.98 (m, 1H), 10.25 – 10.05 (m, 1H), 9.58 (s, 1H), 8.91 (s, 1H), 7.73 – 7.66 (m, 2H), 7.23 (d, $J = 11.9$ Hz, 8H), 7.04 – 6.94 (m, 1H), 5.69 – 5.25 (m, 2H), 3.15 (s, 1H), 2.24 – 2.20 (m, 1H), 1.96 (d, $J = 6.1$ Hz, 3H).; ^{13}C NMR (100 MHz, DMSO-*d*6) δ 170.16, 159.68, 159.22, 156.50, 156.26, 155.06, 147.43, 141.15, 129.28, 129.01, 115.88, 113.75, 112.06, 111.83, 108.70, 50.99, 49.01, 25.13, 21.23, 18.67, 18.09, 17.04.; HRMS-ESI+ calculated for $\text{C}_{22}\text{H}_{23}\text{FN}_5$ $[\text{M}+\text{H}]^+$ 376.1954, found: 376.1955.

4.2.1.61 (*E*)-2-((*E*)-1-(1-(4-(tert-butyl)benzyl)-1*H*-pyrrol-2-yl)-3-phenylallylidene)hydrazine-1-carboximidamide (2x)

Yield 88 %, yellow solid; mp: 220-222°C; ^1H NMR (400 MHz, DMSO-*d*6) δ 9.56 (s, 1H), 8.90 (d, $J = 18.4$ Hz, 1H), 7.72 (dd, $J = 10.1, 6.4$ Hz, 1H), 7.64 (d, $J = 15.8$ Hz, 1H), 7.53 (d, $J = 9.9$ Hz, 1H), 7.37 (t, $J = 10.6$ Hz, 1H), 7.29 (dd, $J = 9.7, 4.9$ Hz, 2H), 7.21 (dd, $J = 10.5, 5.0$ Hz, 1H), 7.12 – 7.06 (m, 1H), 7.02 – 6.85 (m, 2H), 6.85 – 6.69 (m, 1H), 6.53 – 6.01 (m, 1H), 5.66 – 5.19 (m, 2H), 2.24 (s, 1H), 1.98 – 1.90 (m, 2H), 1.32 – 1.28 (m, 1H), 1.25 – 1.22 (m, 6H), 1.17 – 1.04 (m, 3H).; ^{13}C NMR (100 MHz, DMSO-*d*6) δ 170.13, 159.64, 159.19, 156.22, 149.78, 147.59, 136.97, 129.11, 129.03, 126.62, 126.18, 125.70, 115.88, 108.35, 56.47, 52.19, 34.62, 31.57, 31.49, 31.44, 25.13, 21.22, 19.03, 18.64, 17.08.; HRMS-ESI+ calculated for $\text{C}_{25}\text{H}_{30}\text{N}_5$ $[\text{M}+\text{H}]^+$ 400.2501, found: 400.2506.

4.2.1.62 (E)-2-((E)-1-(1-(4-isopropylbenzyl)-1H-pyrrol-2-yl)-3-phenylallylidene)hydrazine-1-carboximidamide (2y)

Yield 92 %, yellow solid; mp: 239-241°C; ¹H NMR (400 MHz, DMSO-*d*₆) δ 11.06 (s, 1H), 7.80 (d, J = 8.5 Hz, 1H), 7.70 (ddd, J = 23.4, 5.9, 3.0 Hz, 1H), 7.55 (dd, J = 21.1, 11.8 Hz, 1H), 7.46 – 7.30 (m, 2H), 7.26 – 7.13 (m, 3H), 7.12 – 6.99 (m, 2H), 6.93 (d, J = 6.5 Hz, 1H), 6.90 – 6.79 (m, 2H), 6.71 (dd, J = 3.8, 1.7 Hz, 1H), 6.20 – 6.12 (m, 1H), 5.52 (s, 2H), 2.82 (dt, J = 13.8, 6.9 Hz, 1H), 2.23 (s, 2H), 1.20 – 1.04 (m, 6H).; ¹³C NMR (100 MHz, DMSO-*d*₆) δ 159.61, 159.57, 156.17, 156.14, 147.60, 147.54, 147.50, 137.34, 129.33, 129.13, 129.01, 128.64, 127.51, 126.85, 126.77, 126.60, 126.45, 115.92, 108.34, 52.29, 33.49, 24.32, 24.17, 17.00.; HRMS-ESI+ calculated for C₂₄H₂₈N₅ [M+H]⁺ 386.2358, found: 386.2361.

4.2.1.63 (E)-2-((E)-1-(1-(4-bromobenzyl)-1H-pyrrol-2-yl)-3-(4-chlorophenyl)allylidene)hydrazine-1-carboximidamide (3a)

Yield 90 %, yellow solid; mp: 231-233°C; ¹H NMR (400 MHz, DMSO-*d*₆) δ 10.15 (s, 1H), 9.58 (s, 1H), 7.98 – 7.73 (m, 3H), 7.71 – 7.52 (m, 3H), 7.51 – 7.31 (m, 3H), 7.08 (dd, J = 35.7, 12.3 Hz, 1H), 6.94 – 6.59 (m, 2H), 6.55 – 6.05 (m, 1H), 5.96 – 5.32 (m, 2H), 2.21 (s, 1H), 1.90 (s, 1H).; ¹³C NMR (100 MHz, DMSO-*d*₆) δ 170.31, 159.63, 159.18, 156.12, 148.85, 147.57, 139.96, 129.23, 129.00, 128.93, 128.85, 128.71, 127.34, 126.72, 126.34, 116.21, 108.54, 52.60, 21.22, 18.55, 16.91.

4.2.1.64 (E)-2-((E)-1-(1-(4-bromobenzyl)-1H-pyrrol-2-yl)-3-(4-fluorophenyl)allylidene)hydrazine-1-carboximidamide (3b)

Yield 93 %, yellow solid; mp: 242-244°C; ¹H NMR (400 MHz, DMSO-*d*₆) δ 11.05 (s, 1H), 8.04 – 7.66 (m, 3H), 7.65 – 7.54 (m, 1H), 7.53 – 7.26 (m, 5H), 7.15 – 7.09 (m, 1H), 6.84 (d, J = 8.4 Hz, 2H), 6.76 – 6.67 (m, 1H), 6.21 – 6.14 (m, 1H), 5.58 (d, J = 13.2 Hz, 2H), 2.22 (s, 1H), 1.91 (d, J = 5.1 Hz, 1H).

4.2.1.65 (Z)-2-((E)-1-(1-(4-bromobenzyl)-1H-pyrrol-2-yl)-3-(4-(trifluoromethyl)phenyl)allylidene)hydrazine-1-carboximidamide (3c)

Yield 76 %, yellow solid; mp: 223-235°C; ¹H NMR (400 MHz, DMSO-*d*₆) δ 11.07 (s, 1H), 8.15 – 7.76 (m, 3H), 7.74 – 7.55 (m, 3H), 7.54 – 7.40 (m, 3H), 7.15 – 7.06 (m, 1H), 6.89 – 6.71 (m, 3H), 6.22 – 6.13 (m, 1H), 5.57 (s, 2H), 2.22 (s, 2H).

4.2.1.66 (Z)-2-((E)-1-(1-(4-bromobenzyl)-1H-pyrrol-2-yl)-3-(p-tolyl)allylidene)hydrazine-1-carboximidamide (3d)

Yield 76 %, yellow solid; mp: 221-223°C; ¹H NMR (400 MHz, DMSO-*d*₆) δ 10.14 (s, 1H), 9.59 (s, 1H), 8.02 – 7.69 (m, 3H), 7.67 – 7.35 (m, 5H), 7.32 – 7.01 (m, 3H), 6.88 (ddd, J = 24.7,

12.2, 6.3 Hz, 1H), 6.47 – 6.10 (m, 1H), 5.69 – 4.56 (m, 2H), 3.45 (s, 3H), 2.36 – 2.25 (m, 1H), 1.90 (s, 1H).

4.2.1.67 (E)-2-((E)-1-(1-(4-butylbenzyl)-1H-pyrrol-2-yl)-3-(4-(trifluoromethyl)phenyl)allylidene)hydrazine-1-carboximidamide (3e)

Yield 89 %, yellow solid; mp: 236-238°C; ¹H NMR (400 MHz, DMSO-*d*₆) δ 11.18 – 10.98 (m, 1H), 10.11 (d, *J* = 24.0 Hz, 1H), 9.56 (s, 1H), 7.69 (dd, *J* = 14.6, 7.1 Hz, 4H), 7.54 (dd, *J* = 13.7, 5.7 Hz, 1H), 7.21 (s, 1H), 7.08 (dd, *J* = 7.9, 5.4 Hz, 2H), 6.95 – 6.82 (m, 1H), 6.80 – 6.65 (m, 1H), 6.21 – 6.11 (m, 1H), 5.66 – 5.34 (m, 2H), 3.16 (s, 1H), 2.21 (s, 1H), 1.98 – 1.89 (m, 6H), 1.46 – 1.27 (m, 1H), 0.89 – 0.81 (m, 3H).; ¹³C NMR (100 MHz, DMSO-*d*₆) δ 170.15, 159.63, 159.19, 156.45, 156.19, 155.08, 147.47, 141.40, 137.15, 130.57, 129.11, 128.99, 128.82, 127.25, 126.38, 115.90, 108.28, 62.57, 52.36, 49.02, 25.12, 22.19, 21.21, 18.62, 17.02, 14.21.; HRMS-ESI+ calculated for C₂₆H₂₉F₃N₅ [M+H]⁺ 468.2375, found: 468.2371.

4.2.1.68 (Z)-2-((E)-3-(4-(tert-butyl)phenyl)-1-(1-(4-(trifluoromethoxy)benzyl)-1H-pyrrol-2-yl)allylidene)hydrazine-1-carboximidamide (3f)

Yield 92 %, yellow solid; mp: 241-243°C; ¹H NMR (400 MHz, DMSO-*d*₆) δ 10.14 (d, *J* = 17.4 Hz, 1H), 9.58 (s, 1H), 8.88 (s, 2H), 7.63 (s, 1H), 7.58 – 7.29 (m, 6H), 7.09 (s, 6H), 4.71 (s, 2H), 3.44 (s, 5H), 2.03 – 1.77 (m, 4H).; ¹³C NMR (100 MHz, DMSO-*d*₆) δ 172.85, 170.96, 170.91, 170.87, 170.84, 170.79, 170.70, 170.60, 159.58, 159.42, 159.29, 159.25, 158.96, 158.71, 156.56, 156.20, 155.75, 155.43, 149.19, 147.36, 25.15, 21.62, 21.20, 18.72, 18.55, 15.25.; HRMS-ESI+ calculated for C₂₆H₂₉F₃N₅O [M+H]⁺ 484.2324, found: 484.2317.

4.2.1.69 (Z)-2-((E)-1-(1-(4-(trifluoromethoxy)benzyl)-1H-pyrrol-2-yl)-3-(4-(trifluoromethyl)phenyl)allylidene)hydrazine-1-carboximidamide (3g)

Yield 89 %, yellow solid; mp: 240-242°C; ¹H NMR (400 MHz, DMSO-*d*₆) δ 11.01 (d, *J* = 22.1 Hz, 1H), 8.86 (s, 1H), 8.19 – 7.93 (m, 1H), 7.91 – 7.81 (m, 1H), 7.66 (d, *J* = 7.8 Hz, 3H), 7.54 (d, *J* = 8.6 Hz, 1H), 7.19 (d, *J* = 26.6 Hz, 1H), 7.07 (d, *J* = 7.8 Hz, 2H), 6.98 – 6.59 (m, 1H), 6.41 – 5.98 (m, 1H), 5.92 – 5.34 (m, 2H), 4.64 (d, *J* = 37.5 Hz, 1H), 2.22 (s, 1H), 1.98 – 1.89 (m, 2H).; ¹³C NMR (100 MHz, DMSO-*d*₆) δ 170.13, 159.63, 159.18, 156.43, 156.15, 155.08, 147.59, 144.97, 130.57, 129.42, 128.87, 128.13, 127.24, 127.00, 125.88, 125.84, 116.43, 108.66, 52.31, 25.12, 21.21, 18.60, 16.92.

4.2.1.70 (Z)-2-((E)-3-(2,3-dimethoxyphenyl)-1-(1-(4-methylbenzyl)-1H-pyrrol-2-yl)allylidene)hydrazine-1-carboximidamide (3h)

Yield 92 %, yellow solid; mp: 218-220°C; ¹H NMR (400 MHz, DMSO-*d*₆) δ 11.21 – 10.95 (m, 1H), 10.12 (d, *J* = 20.4 Hz, 1H), 9.57 (s, 1H), 8.90 (s, 2H), 7.76 (s, 1H), 7.73 – 7.52 (m, 2H), 7.43 – 7.01 (m, 9H), 4.94 – 3.98 (m, 6H), 2.31 – 2.09 (m, 1H), 2.02 – 1.81 (m, 3H).; ¹³C

NMR (100 MHz, DMSO-*d*₆) δ 170.13, 159.84, 159.78, 159.66, 159.52, 159.48, 159.26, 159.21, 159.09, 159.04, 158.98, 156.61, 156.51, 156.48, 156.05, 155.06, 154.96, 154.17, 153.53, 153.01, 41.86, 25.13, 21.22, 18.66.; HRMS-ESI+ calculated for C₂₄H₂₈N₅O₂ [M+H]⁺ 418.2243, found: 418.2194.

4.2.1.71 (*E*)-2-((*E*)-3-(3,4-dimethoxyphenyl)-1-(1-(4-fluoro-2-(trifluoromethyl)benzyl)-1*H*-pyrrol-2-yl)allylidene)hydrazine-1-carboximidamide (3i)

Yield 81 %, yellow solid; mp: 252-254 °C; ¹H NMR (400 MHz, DMSO-*d*₆) δ 8.90 (s, 1H), 7.73 (s, 1H), 7.63 – 7.50 (m, 2H), 7.48 – 7.41 (m, 1H), 7.24 (s, 3H), 7.12 (s, 1H), 6.97 – 6.79 (m, 1H), 6.46 (d, *J* = 15.9 Hz, 1H), 6.27 (d, *J* = 22.3 Hz, 1H), 5.92 – 5.34 (m, 2H), 4.15 – 3.45 (m, 6H), 2.24 (s, 1H), 1.98 – 1.90 (m, 2H).; ¹³C NMR (100 MHz, DMSO-*d*₆) δ 170.13, 159.65, 159.21, 156.47, 156.27, 156.20, 155.06, 147.70, 129.67, 129.21, 128.65, 127.65, 120.49, 120.29, 116.06, 111.73, 109.05, 56.49, 55.99, 49.02, 25.12, 21.22, 18.64, 17.21.; HRMS-ESI+ calculated for C₂₄H₂₄F₄N₅O₂ [M+H]⁺ 490.1814, found: 490.1812.

4.2.1.72 (*Z*)-2-((*E*)-3-(2,3-dimethoxyphenyl)-1-(1-(4-(trifluoromethoxy)benzyl)-1*H*-pyrrol-2-yl)allylidene)hydrazine-1-carboximidamide (3j)

Yield 76 %, yellow solid; mp: 269-271 °C; ¹H NMR (400 MHz, DMSO-*d*₆) δ 11.30 – 11.13 (m, 1H), 10.18 (d, *J* = 22.9 Hz, 1H), 9.56 (d, *J* = 11.0 Hz, 1H), 8.88 (s, 2H), 8.31 – 8.26 (m, 1H), 7.69 (d, *J* = 8.2 Hz, 2H), 7.46 (d, *J* = 8.1 Hz, 1H), 7.41 (d, *J* = 8.1 Hz, 2H), 7.20 (d, *J* = 6.0 Hz, 1H), 7.16 (d, *J* = 8.5 Hz, 1H), 5.72 – 5.54 (m, 2H), 4.71 (s, 6H), 2.42 (s, 1H), 1.90 (d, *J* = 6.7 Hz, 2H).; ¹³C NMR (100 MHz, DMSO-*d*₆) δ 170.14, 159.67, 159.21, 156.33, 151.54, 142.91, 137.30, 133.38, 128.70, 128.39, 128.10, 126.03, 125.99, 125.28, 123.74, 123.26, 123.20, 121.60, 114.24, 110.80, 49.30, 31.46, 21.22, 16.66.; HRMS-ESI+ calculated for C₂₄H₂₅F₃N₅O₃ [M+H]⁺ 488.1909, found: 488.1930.

4.2.1.73 (*E*)-2-((*E*)-3-(4-(*tert*-butyl)phenyl)-1-(1-(2,4-difluorobenzyl)-1*H*-pyrrol-2-yl)allylidene)hydrazine-1-carboximidamide (3k)

Yield 75 %, yellow solid; mp: 263-265 °C; ¹H NMR (400 MHz, DMSO-*d*₆) δ 11.07 (s, 1H), 10.16 (s, 1H), 9.58 (s, 1H), 8.92 (s, 2H), 7.68 (s, 3H), 7.54 – 7.48 (m, 1H), 7.26 (s, 7H), 4.62 (s, 2H), 1.99 – 1.79 (m, 9H).; ¹³C NMR (100 MHz, DMSO-*d*₆) δ 159.57, 156.11, 147.53, 139.48, 131.82, 131.77, 131.62, 129.49, 129.30, 129.00, 128.84, 128.61, 128.52, 127.32, 125.97, 120.53, 120.34, 116.31, 108.52, 52.07, 34.99, 34.94, 31.57, 31.40, 16.92.; HRMS-ESI+ calculated for C₂₅H₂₈F₂N₅ [M+H]⁺ 436.2313, found: 436.2311.

4.2.1.74 (E)-2-((E)-1-(1-(3,5-dimethoxybenzyl)-1H-pyrrol-2-yl)-3-(3,4-dimethoxyphenyl)allylidene)hydrazine-1-carboximidamide (3l)

Yield 96 %, yellow solid; mp: 276-278 °C; ¹H NMR (400 MHz, DMSO-*d*₆) δ 11.05 (d, J = 23.1 Hz, 1H), 8.85 (s, 1H), 7.57 (dd, J = 30.1, 16.4 Hz, 2H), 7.38 (s, 1H), 7.11 (dd, J = 2.5, 1.9 Hz, 1H), 6.97 (dd, J = 26.6, 21.3 Hz, 1H), 6.72 (dd, J = 3.9, 1.8 Hz, 1H), 6.36 – 6.31 (m, 1H), 6.19 – 6.14 (m, 1H), 6.04 (d, J = 2.2 Hz, 1H), 5.42 (d, J = 56.1 Hz, 2H), 4.71 (s, 1H), 3.82 – 3.33 (m, 12H), 2.22 (s, 2H), 1.99 – 1.88 (m, 1H).; ¹³C NMR (100 MHz, DMSO-*d*₆) δ 170.14, 161.01, 159.66, 159.61, 159.16, 156.41, 156.22, 156.18, 147.39, 142.48, 129.52, 129.42, 128.93, 116.05, 108.25, 104.63, 104.53, 98.75, 55.94, 55.50, 52.67, 25.13, 21.21, 18.60, 16.92.; HRMS-ESI+ calculated for C₂₅H₂₉N₅O₄ [M+H]⁺ 464.2338, found: 464.2335.

4.2.1.75 (E)-2-((E)-1-(1-(4-(tert-butyl)benzyl)-1H-pyrrol-2-yl)-3-(3,4-difluorophenyl)allylidene)hydrazine-1-carboximidamide (3m)

Yield 92 %, yellow solid; mp: 282-284 °C; ¹H NMR (400 MHz, DMSO-*d*₆) δ 11.10 (d, J = 38.2 Hz, 1H), 10.14 (s, 1H), 9.57 (s, 1H), 8.88 (s, 1H), 7.30 (d, J = 8.4 Hz, 3H), 7.07 (dd, J = 2.4, 1.9 Hz, 1H), 6.85 (d, J = 8.4 Hz, 2H), 6.71 (dd, J = 3.9, 1.8 Hz, 1H), 6.15 (dd, J = 3.8, 2.7 Hz, 1H), 5.52 (s, 2H), 2.24 (s, 1H), 1.96 (d, J = 7.5 Hz, 1H), 1.89 (s, 2H), 1.23 (s, 9H).; ¹³C NMR (100 MHz, DMSO-*d*₆) δ 170.14, 159.74, 159.65, 159.24, 159.19, 156.46, 156.22, 155.07, 149.78, 147.58, 136.97, 129.12, 129.01, 127.03, 126.17, 125.70, 115.89, 108.35, 52.18, 34.62, 31.57, 25.13, 21.22, 18.65, 17.09.; HRMS-ESI+ calculated for C₂₅H₂₈F₂N₅ [M+H]⁺ 436.2348, found: 436.2352.

4.2.1.76 (E)-2-((E)-1-(1-([1,1'-biphenyl]-4-ylmethyl)-1H-pyrrol-2-yl)-3-(4-(tert-butyl)phenyl)allylidene)hydrazine-1-carboximidamide (3n)

Yield 90 %, yellow solid; mp: 290-292 °C; ¹H NMR (400 MHz, DMSO-*d*₆) δ 10.28 – 9.88 (m, 1H), 8.88 (s, 1H), 7.63 (ddd, J = 22.5, 11.9, 5.5 Hz, 3H), 7.54 (d, J = 8.3 Hz, 1H), 7.50 – 7.38 (m, 3H), 7.34 (ddd, J = 11.9, 7.9, 5.1 Hz, 3H), 7.28 – 7.20 (m, 1H), 7.19 – 7.14 (m, 1H), 7.09 (d, J = 8.2 Hz, 1H), 6.99 (ddd, J = 13.5, 13.0, 5.1 Hz, 2H), 6.90 – 6.72 (m, 1H), 6.44 – 6.33 (m, 1H), 6.26 – 6.15 (m, 1H), 5.68 – 5.38 (m, 1H), 3.58 – 3.40 (m, 2H), 2.24 (s, 1H), 2.03 – 1.82 (m, 2H), 1.33 – 1.03 (m, 7H).; ¹³C NMR (100 MHz, DMSO-*d*₆) δ 170.14, 159.64, 159.19, 156.19, 140.15, 139.41, 139.23, 129.34, 129.25, 129.01, 128.52, 128.00, 127.84, 127.46, 127.25, 127.20, 127.10, 127.04, 127.00, 126.11, 125.93, 116.10, 108.44, 52.32, 34.96, 31.56, 31.38, 25.13, 21.22, 18.64, 17.05.; HRMS-ESI+ calculated for C₃₁H₃₄N₅ [M+H]⁺ 476.2883, found: 476.2889.

4.2.1.77 (*E*)-2-((*E*)-3-(4-(*tert*-butyl)phenyl)-1-(1-(4-(trifluoromethyl)benzyl)-1*H*-pyrrol-2-yl)allylidene)hydrazine-1-carboximidamide (3o)

Yield 93 %, yellow solid; mp 271-273 °C; ¹H NMR (400 MHz, DMSO-*d*6) δ 11.00 (s, 1H), 8.94 – 8.68 (m, 1H), 7.67 (d, *J* = 8.4 Hz, 1H), 7.54 – 7.44 (m, 3H), 7.42 – 7.35 (m, 1H), 7.13 (tt, *J* = 16.8, 8.2 Hz, 2H), 6.97 (dt, *J* = 16.4, 6.0 Hz, 1H), 6.91 – 6.79 (m, 2H), 6.74 (dd, *J* = 3.9, 1.7 Hz, 1H), 6.30 – 6.12 (m, 1H), 5.63 – 5.37 (m, 2H), 4.71 (s, 1H), 2.21 (s, 2H), 1.41 – 0.98 (m, 9H).; ¹³C NMR (100 MHz, DMSO-*d*6) δ 159.57, 156.11, 147.53, 139.48, 131.82, 131.77, 131.62, 129.49, 129.30, 129.00, 128.84, 128.70, 128.61, 128.52, 127.32, 125.97, 120.53, 120.34, 116.31, 108.52, 52.07, 34.99, 34.94, 31.57, 31.40, 16.92.; HRMS-ESI+ calculated for C₂₆H₂₉F₃N₅ [M+H]⁺ 468.2401, found: 468.2403.

4.2.1.78 (*Z*)-2-((*E*)-1-(1-(2,5-difluorobenzyl)-1*H*-pyrrol-2-yl)-3-(4-isopropylphenyl)allylidene)hydrazine-1-carboximidamide (3p)

Yield 85 %, yellow solid; mp: 239-241 °C; ¹H NMR (400 MHz, DMSO-*d*6) δ 11.06 (d, *J* = 29.8 Hz, 1H), 8.86 (s, 1H), 7.65 (d, *J* = 8.2 Hz, 1H), 7.55 (d, *J* = 15.6 Hz, 1H), 7.44 – 7.33 (m, 1H), 7.29 – 7.22 (m, 2H), 7.21 – 7.14 (m, 2H), 7.10 (dd, *J* = 8.4, 6.2 Hz, 1H), 6.90 – 6.72 (m, 1H), 6.47 – 6.35 (m, 1H), 6.22 (ddd, *J* = 12.8, 6.4, 3.7 Hz, 1H), 5.69 – 5.45 (m, 1H), 3.44 (d, *J* = 7.0 Hz, 2H), 2.23 (s, 1H), 2.03 – 1.77 (m, 2H), 1.30 – 0.89 (m, 6H).; ¹³C NMR (100 MHz, DMSO-*d*6) δ 159.61, 156.42, 156.24, 155.09, 147.58, 141.52, 129.11, 128.76, 127.36, 127.18, 117.43, 117.34, 117.18, 117.10, 116.23, 116.04, 115.71, 108.75, 46.90, 33.79, 25.13, 24.12, 18.61, 17.01.; HRMS-ESI+ calculated for C₂₄H₂₆F₂N₅ [M+H]⁺ 422.2156, found: 422.2201.

4.2.1.79 (*E*)-2-((*E*)-1-(1-(4-bromobenzyl)-1*H*-pyrrol-2-yl)-3-(4-(*tert*-butyl)phenyl)allylidene)hydrazine-1-carboximidamide (3q)

Yield 81 %, yellow solid; mp: 234-236 °C; ¹H NMR (400 MHz, DMSO-*d*6) δ 11.00 (s, 1H), 8.94 – 8.68 (m, 1H), 7.67 (d, *J* = 8.4 Hz, 1H), 7.54 – 7.44 (m, 3H), 7.42 – 7.35 (m, 1H), 7.13 (tt, *J* = 16.8, 8.2 Hz, 2H), 6.97 (dt, *J* = 16.4, 6.0 Hz, 1H), 6.91 – 6.79 (m, 2H), 6.74 (dd, *J* = 3.9, 1.7 Hz, 1H), 6.30 – 6.12 (m, 1H), 5.63 – 5.37 (m, 2H), 4.71 (s, 1H), 2.21 (s, 2H), 1.41 – 0.98 (m, 9H).; ¹³C NMR (100 MHz, DMSO-*d*6) δ 159.57, 156.11, 147.53, 139.48, 131.82, 131.77, 131.62, 129.49, 129.30, 129.00, 128.84, 128.61, 128.52, 127.32, 125.97, 120.53, 120.34, 116.31, 108.52, 52.07, 34.99, 34.94, 31.57, 31.40, 16.92.; HRMS-ESI+ calculated for C₂₅H₂₉BrN₅ [M+H]⁺ 478.1606, found: 480.1652.

4.2.1.80 (E)-2-((E)-1-(1-(4-(tert-butyl)benzyl)-1H-pyrrol-2-yl)-3-(3,5-dimethoxyphenyl)allylidene)hydrazine-1-carboximidamide (3r)

Yield 86 %, yellow solid; mp: 264-266 °C; ¹H NMR (400 MHz, DMSO-*d*₆) δ 11.21 – 11.01 (m, 1H), 8.91 (s, 2H), 7.67 (s, 1H), 7.31 (d, J = 1.8 Hz, 1H), 7.29 (s, 1H), 7.24 (s, 2H), 7.07 (dd, J = 2.5, 1.9 Hz, 1H), 6.85 (d, J = 8.4 Hz, 2H), 6.70 (dd, J = 3.9, 1.8 Hz, 1H), 6.15 (dd, J = 3.8, 2.7 Hz, 1H), 5.52 (s, 2H), 4.56 (s, 6H), 2.24 (s, 2H), 1.99 – 1.94 (m, 1H), 1.22 (s, 9H).; ¹³C NMR (100 MHz, DMSO-*d*₆) δ 159.73, 159.66, 156.48, 156.25, 156.21, 155.05, 149.80, 149.78, 149.75, 147.56, 136.98, 129.17, 129.11, 129.02, 128.99, 126.18, 125.74, 125.70, 125.65, 115.88, 108.34, 52.18, 34.62, 31.57, 25.13, 18.67, 17.11.; HRMS-ESI+ calculated for C₂₇H₃₄N₅O₂ [M+H]⁺ 460.2708, found: 460.2704.

4.2.1.81 (E)-2-((E)-1-(1-(4-(tert-butyl)benzyl)-1H-pyrrol-2-yl)-3-(4-(tert-butyl)phenyl)allylidene)hydrazine-1-carboximidamide (3s)

Yield 89 %, yellow solid; mp: 260-262 °C; ¹H NMR (400 MHz, DMSO-*d*₆) δ 11.16 (s, 1H), 8.90 (s, 2H), 7.73 (dd, J = 5.8, 3.1 Hz, 1H), 7.31 (s, 2H), 7.29 (s, 2H), 7.07 (dd, J = 2.5, 1.9 Hz, 2H), 6.85 (d, J = 8.4 Hz, 3H), 6.71 (dd, J = 3.9, 1.8 Hz, 1H), 6.15 (dd, J = 3.8, 2.7 Hz, 1H), 5.52 (s, 2H), 2.24 (s, 2H), 1.23 (s, 18H).; ¹³C NMR (100 MHz, DMSO-*d*₆) δ 159.73, 159.65, 159.60, 156.27, 156.24, 156.21, 149.81, 149.77, 147.60, 147.56, 137.01, 136.98, 129.17, 129.11, 129.07, 129.03, 126.23, 126.18, 125.70, 115.95, 115.88, 115.20, 113.70, 108.42, 108.34, 52.18, 34.63, 31.57, 17.10.; HRMS-ESI+ calculated for C₂₉H₃₈N₅ [M+H]⁺ 456.3122, found: 456.3117.

4.2.2 Synthesis and characterization of Indol-3-yl-phenyl allylidene hydrazine carboximidamide analogues

A total of 79 analogues were synthesized as per the procedure given in section 3.2. The characterization data is given below:

4.2.2.1 (Z)-2-((E)-1-(1-benzyl-1H-indol-3-yl)-3-(3,4-difluorophenyl)allylidene)hydrazine-1-carboximidamide (4a)

Yield 89 %, yellow solid; mp: 263-265 °C; ¹H NMR (400 MHz, DMSO-*d*₆) δ 11.12 (s, 1H), 10.10 (s, 1H), 9.55 (s, 1H), 8.33 – 8.02 (m, 2H), 7.64 (s, 4H), 7.49 (d, J = 7.9 Hz, 1H), 7.32 (dd, J = 10.1, 4.3 Hz, 2H), 7.28 – 7.21 (m, 3H), 7.20 – 7.10 (m, 2H), 5.47 (s, 2H), 2.41 (s, 2H), 1.90 (s, 1H).; ¹³C NMR (100 MHz, DMSO-*d*₆) δ 170.15, 159.61, 159.16, 156.42, 156.18, 151.71, 138.07, 137.37, 133.38, 129.08, 127.99, 127.71, 127.50, 127.33, 125.32, 123.63, 123.04, 121.46, 113.96, 110.94, 49.87, 25.19, 21.22, 18.56, 16.58.; HRMS-ESI+ calculated for C₂₅H₂₂F₂N₅ [M+H]⁺ 430.1843, found: 430.1839.

4.2.2.2(Z)-2-((E)-1-(1-benzyl-1H-indol-3-yl)-3-(3-phenoxyphenyl)allylidene)hydrazine-1-carboximidamide (4b)

Yield 92 %, white solid; mp: 253-255 °C; ¹H NMR (400 MHz, DMSO-*d*₆) δ 11.05 (d, J = 49.3 Hz, 1H), 10.10 (s, 1H), 8.36 – 8.07 (m, 2H), 7.70 (ddd, J = 62.8, 26.5, 8.9 Hz, 6H), 7.47 (tdd, J = 16.1, 11.1, 4.7 Hz, 3H), 7.36 – 7.28 (m, 3H), 7.27 – 7.21 (m, 4H), 7.19 (dd, J = 8.0, 1.2 Hz, 1H), 7.17 – 7.10 (m, 2H), 5.47 (s, 2H), 2.42 (s, 2H), 1.90 (s, 1H).; ¹³C NMR (100 MHz, DMSO-*d*₆) δ 170.16, 159.60, 159.16, 156.41, 156.22, 155.15, 151.73, 138.07, 137.37, 133.39, 130.58, 130.27, 129.13, 129.08, 129.00, 127.99, 127.50, 127.44, 125.29, 123.64, 123.40, 123.05, 121.46, 118.38, 113.94, 110.95, 49.87, 25.14, 21.22, 18.58, 16.57.; HRMS-ESI+ calculated for C₃₁H₂₈N₅O [M+H]⁺ 486.2294, found: 486.2287.

4.2.2.3 (Z)-2-((E)-1-(1-benzyl-1H-indol-3-yl)-3-(4-(tert-butyl)phenyl)allylidene)hydrazine-1-carboximidamide (4c)

Yield 85 %, yellow solid; mp: 254-256 °C; ¹H NMR (400 MHz, DMSO-*d*₆) δ 11.12 (s, 1H), 10.11 (s, 1H), 9.56 (s, 1H), 8.33 – 8.02 (m, 2H), 7.96 – 7.54 (m, 6H), 7.51 – 7.45 (m, 1H), 7.37 – 7.29 (m, 2H), 7.28 – 7.19 (m, 3H), 7.18 – 7.11 (m, 1H), 5.52 – 5.45 (m, 2H), 3.42 (s, 9H), 2.41 (s, 2H), 1.90 (s, 1H).; ¹³C NMR (100 MHz, DMSO-*d*₆) δ 170.16, 160.34, 159.59, 159.14, 156.22, 151.71, 138.05, 137.35, 133.37, 129.06, 128.19, 127.98, 127.76, 127.69, 127.49, 125.27, 123.62, 123.03, 121.54, 121.45, 113.92, 110.93, 60.23, 49.86, 31.53, 21.21, 18.59, 16.58, 14.42.; HRMS-ESI+ calculated for C₂₉H₃₁N₅ [M+H]⁺ 450.2649, found: 450.2646.

4.2.2.4(Z)-2-((E)-1-(1-benzyl-1H-indol-3-yl)-3-(3,4-dimethoxyphenyl)allylidene)hydrazine-1-carboximidamide (4d)

Yield 88 %, yellow solid; mp: 238-240 °C; ¹H NMR (400 MHz, DMSO-*d*₆) δ 11.12 (s, 1H), 8.45 – 8.04 (m, 2H), 7.98 – 7.56 (m, 4H), 7.56 – 7.38 (m, 2H), 7.38 – 7.28 (m, 3H), 7.28 – 7.22 (m, 3H), 7.22 – 7.10 (m, 2H), 5.49 (d, J = 17.4 Hz, 2H), 4.06 – 3.28 (m, 6H), 2.42 (s, 2H), 2.00 – 1.87 (m, 1H).; ¹³C NMR (100 MHz, DMSO-*d*₆) δ 170.16, 159.16, 156.23, 155.37, 151.72, 138.07, 137.37, 133.38, 129.28, 129.08, 127.99, 127.73, 127.50, 127.35, 125.36, 125.29, 123.64, 123.04, 121.46, 113.95, 111.79, 110.94, 49.87, 25.19, 21.22, 16.56, 14.80.; HRMS-ESI+ calculated for C₂₇H₂₈N₅O₂ [M+H]⁺ 454.2239, found: 454.2236.

4.2.2.5 (Z)-2-((E)-1-(1-benzyl-1H-indol-3-yl)-3-(4-isopropylphenyl)allylidene)hydrazine-1-carboximidamide (4e)

Yield 91 %, brown solid; mp: 178-180 °C; ¹H NMR (400 MHz, DMSO-*d*₆) δ 11.07 (d, J = 46.9 Hz, 1H), 10.11 (s, 1H), 8.39 – 8.16 (m, 1H), 8.01 – 7.58 (m, 5H), 7.55 – 7.39 (m, 3H), 7.32 (ddd, J = 11.2, 9.9, 4.9 Hz, 3H), 7.28 – 7.23 (m, 2H), 7.15 (dddd, J = 22.7, 17.4, 7.5, 4.6 Hz, 3H), 5.66 – 5.31 (m, 2H), 3.40 (s, 6H), 2.42 (s, 2H), 1.91 (d, J = 6.8 Hz, 1H).; ¹³C NMR (100

MHz, DMSO-*d*6) δ 170.15, 159.60, 159.15, 158.83, 156.40, 156.22, 155.18, 151.70, 138.06, 137.36, 133.37, 129.06, 127.97, 127.68, 127.49, 127.10, 125.28, 123.63, 123.03, 121.45, 113.93, 110.93, 49.87, 25.14, 24.20, 21.22, 18.59, 16.58.; HRMS-ESI+ calculated for C₂₈H₃₀N₅ [M+H]⁺ 436.2501, found: 436.2500.

4.2.2.6 (Z)-2-((E)-1-(1-benzyl-1*H*-indol-3-yl)-3-(3-methoxyphenyl)allylidene)hydrazine-1-carboximidamide (4f)

Yield 85 %, yellow solid; mp: 178-180 °C; ¹H NMR (400 MHz, DMSO-*d*6) δ 11.61 (d, *J* = 78.1 Hz, 1H), 10.08 (t, *J* = 11.1 Hz, 1H), 8.33 – 7.82 (m, 2H), 7.79 – 7.47 (m, 4H), 7.43 – 7.37 (m, 1H), 7.35 – 7.23 (m, 4H), 7.22 – 7.11 (m, 2H), 6.96 (ddd, *J* = 22.2, 17.5, 7.4 Hz, 2H), 6.82 – 6.61 (m, 1H), 5.43 (ddd, *J* = 73.2, 44.1, 32.3 Hz, 2H), 4.00 – 3.53 (m, 3H), 2.38 (d, *J* = 32.1 Hz, 1H), 2.03 – 1.79 (m, 1H).; ¹³C NMR (100 MHz, DMSO-*d*6) δ 170.16, 160.08, 156.20, 140.82, 138.16, 133.36, 131.83, 130.20, 129.12, 129.08, 129.03, 128.09, 128.00, 127.99, 127.73, 127.69, 127.50, 127.45, 122.94, 120.10, 56.00, 55.59, 49.84, 25.18, 21.29, 16.82.; HRMS-ESI+ calculated for C₂₆H₂₆N₅O [M+H]⁺ 424.2137, found: 424.2140.

4.2.2.7 (Z)-2-((E)-1-(1-benzyl-1*H*-indol-3-yl)-3-(3-fluorophenyl)allylidene)hydrazine-1-carboximidamide (4g)

Yield 84 %, white solid; mp: 208-210 °C; ¹H NMR (400 MHz, DMSO-*d*6) δ 11.08 (s, 1H), 8.39 – 7.91 (m, 2H), 7.67 (dd, *J* = 34.7, 26.0 Hz, 4H), 7.56 – 7.36 (m, 3H), 7.36 – 7.29 (m, 2H), 7.29 – 7.23 (m, 3H), 7.16 (ddd, *J* = 24.8, 15.9, 8.7 Hz, 3H), 5.72 – 5.19 (m, 2H), 2.41 (s, 2H), 2.01 – 1.85 (m, 1H).; ¹³C NMR (100 MHz, DMSO-*d*6) δ 170.15, 159.11, 156.36, 156.29, 156.17, 151.74, 138.06, 137.36, 133.37, 129.07, 129.01, 127.98, 127.69, 127.48, 127.37, 125.28, 123.62, 123.04, 121.45, 113.93, 110.94, 49.87, 25.15, 21.22, 16.53.; HRMS-ESI+ calculated for C₂₅H₂₃FN₅ [M+H]⁺ 412.1937, found: 412.1933.

4.2.2.8 (Z)-2-((E)-1-(1-benzyl-1*H*-indol-3-yl)-3-(4-(benzyloxy)phenyl)allylidene)hydrazine-1-carboximidamide (4h)

Yield 93 %, yellow solid; mp: 209-211 °C; ¹H NMR (400 MHz, DMSO-*d*6) δ 11.39 (s, 1H), 8.39 – 7.85 (m, 2H), 7.72 (ddd, *J* = 43.7, 18.2, 8.3 Hz, 3H), 7.53 (d, *J* = 6.9 Hz, 1H), 7.51 – 7.37 (m, 6H), 7.37 – 7.29 (m, 3H), 7.28 – 7.12 (m, 3H), 7.10 – 6.70 (m, 3H), 6.34 (s, 1H), 5.66 – 4.87 (m, 4H), 2.41 (s, 1H), 2.11 – 1.82 (m, 1H).; ¹³C NMR (100 MHz, DMSO-*d*6) δ 158.51, 156.96, 156.18, 151.72, 138.06, 137.46, 137.43, 133.35, 132.32, 130.19, 130.02, 129.11, 129.07, 129.02, 128.92, 128.90, 128.36, 128.31, 128.27, 128.16, 128.12, 127.98, 127.68, 127.48, 125.29, 121.45, 114.60, 113.96, 110.94, 69.72, 49.90, 16.55.; HRMS-ESI+ calculated for C₃₂H₃₀N₅O [M+H]⁺ 500.2450, found: 500.2454.

4.2.2.9 (Z)-2-((E)-1-(1-benzyl-1H-indol-3-yl)-3-(4-**(dimethylamino)phenyl)allylidene)hydrazine-1-carboximidamide (4i)**

Yield 83 %, yellow creamish solid; mp: 204-206 °C; ¹H NMR (400 MHz, DMSO-*d*₆) δ 11.08 (s, 1H), 8.24 (dd, J = 36.9, 16.6 Hz, 2H), 7.72 – 7.55 (m, 3H), 7.50 (t, J = 8.9 Hz, 1H), 7.39 – 7.30 (m, 3H), 7.29 – 7.23 (m, 4H), 7.22 – 7.12 (m, 2H), 7.05 (t, J = 11.6 Hz, 1H), 6.73 (dd, J = 19.9, 10.4 Hz, 1H), 5.47 (s, 2H), 3.50 – 3.24 (m, 6H), 2.85 (s, 1H), 2.42 (s, 2H).; ¹³C NMR (100 MHz, DMSO-*d*₆) δ 156.18, 151.74, 138.05, 137.72, 137.36, 133.38, 129.12, 129.07, 128.10, 127.98, 127.68, 127.49, 126.62, 125.28, 123.63, 123.04, 121.80, 121.46, 113.93, 113.00, 111.27, 110.94, 107.45, 58.99, 49.87, 45.19, 16.54.; HRMS-ESI+ calculated for C₂₇H₂₉N₆ [M+H]⁺ 437.2454, found: 437.2462.

4.2.2.10 (Z)-2-((E)-1-(1-benzyl-1H-indol-3-yl)-3-(3-bromophenyl)allylidene)hydrazine-1-carboximidamide (4j)

Yield 93 %, yellow solid; mp:199-201 °C; ¹H NMR (400 MHz, DMSO-*d*₆) δ 11.13 (s, 1H), 8.35 – 7.83 (m, 3H), 7.83 – 7.54 (m, 4H), 7.54 – 7.36 (m, 2H), 7.36 – 7.29 (m, 2H), 7.28 – 7.22 (m, 3H), 7.22 – 6.88 (m, 3H), 5.63 – 5.34 (m, 2H), 2.42 (s, 2H), 2.00 – 1.88 (m, 1H).; ¹³C NMR (100 MHz, DMSO-*d*₆) δ 170.15, 159.14, 156.21, 151.71, 138.06, 137.36, 133.36, 131.17, 129.07, 127.98, 127.65, 127.49, 127.38, 125.29, 123.63, 123.04, 121.45, 113.95, 110.94, 49.87, 25.15, 21.22, 18.57, 16.56, 14.56.; HRMS-ESI+ calculated for C₂₅H₂₃BrN₅ [M+H]⁺ 472.1137, found: 472.1131.

4.2.2.11 (Z)-2-((E)-1-(1-benzyl-1H-indol-3-yl)-3-(4-bromophenyl)allylidene)hydrazine-1-carboximidamide (4k)

Yield 83 %, white solid; mp:184-187 °C; ¹H NMR (400 MHz, DMSO-*d*₆) δ 11.12 (s, 1H), 8.36 – 7.99 (m, 2H), 7.75 (ddd, J = 39.0, 23.9, 6.0 Hz, 4H), 7.59 – 7.37 (m, 3H), 7.36 – 7.29 (m, 2H), 7.25 (dd, J = 7.2, 3.9 Hz, 3H), 7.22 – 6.88 (m, 3H), 5.49 (d, J = 14.4 Hz, 2H), 2.42 (s, 2H), 2.01 – 1.84 (m, 1H).; ¹³C NMR (100 MHz, DMSO-*d*₆) δ 170.15, 159.13, 156.21, 151.71, 138.06, 137.36, 133.36, 129.07, 127.98, 127.75, 127.66, 127.48, 127.44, 125.29, 123.62, 123.03, 121.45, 113.95, 110.93, 60.19, 49.87, 25.15, 21.22, 18.51, 16.55.; HRMS-ESI+ calculated for C₂₅H₂₃BrN₅ [M+H]⁺ 472.1137, found: 472.1144.

4.2.2.12 (Z)-2-((E)-1-(1-benzyl-1H-indol-3-yl)-3-(2,5-**dimethoxyphenyl)allylidene)hydrazine-1-carboximidamide (4l)**

Yield 87 %, yellow solid; mp: 281-283 °C; ¹H NMR (400 MHz, DMSO-*d*₆) δ 11.11 (s, 1H), 8.32 – 8.02 (m, 2H), 8.01 – 7.60 (m, 4H), 7.58 – 7.37 (m, 2H), 7.36 – 7.28 (m, 2H), 7.28 – 7.23 (m, 3H), 7.23 – 7.06 (m, 2H), 7.06 – 6.77 (m, 1H), 5.49 (d, J = 15.1 Hz, 2H), 3.85 – 3.37 (m, 6H), 2.42 (s, 2H), 2.06 – 1.82 (m, 1H).; ¹³C NMR (100 MHz, DMSO-*d*₆) δ 159.14, 156.21,

151.72, 138.05, 137.36, 133.38, 129.06, 127.98, 127.64, 127.49, 127.27, 125.28, 125.09, 123.63, 123.04, 121.45, 113.93, 113.45, 111.95, 111.80, 110.94, 56.69, 56.43, 49.87, 21.57, 21.22, 16.57.; HRMS-ESI+ calculated for $C_{27}H_{28}N_5O_2$ $[M+H]^+$ 454.2249, found: 454.2254.

4.2.2.13 (Z)-2-((E)-1-(1-benzyl-1H-indol-3-yl)-3-(p-tolyl)allylidene)hydrazine-1-carboximidamide (4m)

Yield 81 %, yellow solid; mp: 285-287 °C; 1H NMR (400 MHz, DMSO-*d*6) δ 11.08 (d, J = 49.5 Hz, 1H), 10.10 (d, J = 7.5 Hz, 1H), 9.55 (s, 1H), 8.92 – 8.68 (m, 1H), 8.36 – 8.13 (m, 1H), 8.01 – 7.78 (m, 2H), 7.71 – 7.63 (m, 2H), 7.59 – 7.46 (m, 2H), 7.43 – 7.28 (m, 4H), 7.27 – 7.21 (m, 2H), 7.20 – 7.07 (m, 3H), 5.60 – 5.28 (m, 2H), 2.43 – 2.28 (m, 2H), 1.98 – 1.89 (m, 1H).; ^{13}C NMR (100 MHz, DMSO-*d*6) δ 170.14, 159.66, 159.16, 156.24, 155.07, 151.76, 138.06, 137.33, 136.97, 133.44, 129.75, 129.06, 128.61, 127.96, 127.71, 127.68, 127.49, 125.28, 121.45, 113.93, 111.69, 49.87, 25.14, 21.22, 18.61, 16.60.; HRMS-ESI+ calculated for $C_{26}H_{26}N_5$ $[M+H]^+$ 408.2182, found: 408.2179.

4.2.2.14 (Z)-2-((E)-1-(1-benzyl-1H-indol-3-yl)-3-(3-nitrophenyl)allylidene)hydrazine-1-carboximidamide (4n)

Yield 89 %, brown solid; mp: 211-214 °C; 1H NMR (400 MHz, DMSO-*d*6) δ 11.09 (s, 1H), 8.36 – 8.17 (m, 2H), 7.71 (t, J = 97.5 Hz, 4H), 7.45 (t, J = 26.0 Hz, 2H), 7.36 – 7.27 (m, 3H), 7.27 – 7.23 (m, 3H), 7.23 – 6.91 (m, 3H), 5.47 (s, 2H), 2.42 (s, 2H).; ^{13}C NMR (100 MHz, DMSO-*d*6) δ 156.19, 151.73, 138.31, 138.06, 137.48, 137.36, 133.47, 133.37, 133.28, 129.07, 128.84, 128.22, 127.98, 127.63, 127.48, 125.28, 123.73, 123.63, 123.04, 122.77, 121.45, 113.94, 110.94, 49.87, 16.54.; HRMS-ESI+ calculated for $C_{25}H_{23}N_6O_2$ $[M+H]^+$ 439.1882, found: 439.1805.

4.2.2.15 (Z)-2-((E)-1-(1-benzyl-1H-indol-3-yl)-3-(4-cyanophenyl)allylidene)hydrazine-1-carboximidamide (4o)

Yield 95 %, yellow solid; mp: 211-214 °C; 1H NMR (400 MHz, DMSO-*d*6) δ 11.08 (d, J = 49.5 Hz, 1H), 10.25 – 10.02 (m, 1H), 9.55 (s, 1H), 8.31 – 7.86 (m, 2H), 7.84 – 7.41 (m, 6H), 7.38 – 7.18 (m, 6H), 7.15 – 6.97 (m, 1H), 5.49 (dt, J = 64.8, 28.7 Hz, 2H), 2.42 (s, 1H), 1.99 – 1.89 (m, 1H).; ^{13}C NMR (100 MHz, DMSO-*d*6) δ 170.14, 159.17, 156.24, 151.69, 138.06, 137.36, 133.38, 129.14, 129.12, 129.07, 129.00, 128.69, 128.30, 127.98, 127.73, 127.67, 127.49, 125.33, 123.64, 123.03, 121.45, 113.94, 110.79, 49.87, 21.23, 16.60.; HRMS-ESI- calculated for $C_{26}H_{21}N_6$ $[M-H]^-$ 417.0698, found: 417.0694.

4.2.2.16 (Z)-2-((E)-1-(1-benzyl-1H-indol-3-yl)-3-(2-fluorophenyl)allylidene)hydrazine-1-carboximidamide (4p)

Yield 79 %, light yellow solid; mp: 207-210 °C; ¹H NMR (400 MHz, DMSO-*d*₆) δ 11.10 (s, 1H), 8.36 – 8.10 (m, 2H), 8.03 – 7.63 (m, 3H), 7.64 – 7.50 (m, 2H), 7.43 (dd, J = 43.9, 7.9 Hz, 2H), 7.36 – 7.29 (m, 2H), 7.28 – 7.23 (m, 3H), 7.21 (dd, J = 7.1, 1.1 Hz, 1H), 7.17 (dd, J = 4.3, 1.4 Hz, 1H), 7.16 – 7.10 (m, 1H), 5.47 (s, 2H), 2.42 (s, 2H), 1.99 – 1.86 (m, 1H).; ¹³C NMR (100 MHz, DMSO-*d*₆) δ 170.15, 159.14, 156.32, 156.22, 151.72, 138.22, 138.05, 137.36, 133.55, 133.36, 129.22, 129.07, 127.98, 127.49, 125.28, 123.76, 123.62, 123.04, 121.52, 121.45, 113.94, 110.94, 49.87, 21.22, 16.56.; HRMS-ESI- calculated for C₂₅H₂₃FN₅ [M+H]⁺ 412.1937, found: 412.1975.

4.2.2.17 (Z)-2-((E)-1-(1-benzyl-1H-indol-3-yl)-3-(2,4-difluorophenyl)allylidene)hydrazine-1-carboximidamide (4q)

Yield 86 %, light brown solid; mp: 237-240 °C; ¹H NMR (400 MHz, DMSO-*d*₆) δ 10.19 – 10.05 (m, 1H), 9.54 (s, 1H), 8.31 – 7.94 (m, 2H), 7.61 (dddd, J = 25.8, 22.1, 20.3, 16.0 Hz, 6H), 7.39 – 7.20 (m, 5H), 7.19 – 6.98 (m, 2H), 6.95 – 6.50 (m, 1H), 5.60 – 5.34 (m, 2H), 2.42 (s, 1H), 1.91 (d, J = 6.8 Hz, 1H).; ¹³C NMR (100 MHz, DMSO-*d*₆) δ 170.11, 159.61, 159.16, 156.24, 138.09, 136.97, 133.43, 131.86, 129.08, 129.04, 129.01, 127.97, 127.82, 127.67, 127.49, 127.46, 125.29, 122.95, 121.22, 111.54, 49.82, 25.12, 21.22, 18.60, 16.59.; HRMS-ESI+ calculated for C₂₅H₂₂F₂N₅ [M+H]⁺ 430.1740, found: 430.1736.

4.2.2.18 (Z)-2-((E)-1-(1-benzyl-1H-indol-3-yl)-3-phenylallylidene)hydrazine-1-carboximidamide (4r)

Yield 89 %, yellow solid; mp: 211-213 °C; ¹H NMR (400 MHz, DMSO-*d*₆) δ 9.06 – 8.51 (m, 1H), δ 8.33 – 7.89 (m, 2H), 7.83 – 7.60 (m, 3H), 7.57 – 7.45 (m, 1H), 7.37 (dd, J = 14.0, 5.9 Hz, 2H), 7.33 – 7.24 (m, 4H), 7.20 (dd, J = 13.7, 6.9 Hz, 1H), 7.17 – 7.05 (m, 2H), 7.02 – 6.70 (m, 1H), 5.45 (ddd, J = 54.7, 32.4, 12.1 Hz, 2H), 4.82 – 4.41 (m, 1H), 3.45 – 3.31 (m, 2H), 2.42 (s, 1H), 2.00 – 1.87 (m, 1H).; ¹³C NMR (100 MHz, DMSO-*d*₆) δ 170.14, 159.61, 159.16, 156.24, 151.69, 138.06, 137.36, 136.98, 133.38, 129.06, 127.98, 127.68, 127.49, 127.41, 125.28, 123.63, 123.03, 121.45, 113.93, 110.93, 49.87, 25.13, 21.22, 18.60, 16.59.; HRMS-ESI+ calculated for C₂₅H₂₄N₅ [M+H]⁺ 394.2032, found: 394.1938.

4.2.2.19 (Z)-2-((E)-1-(1-benzyl-1H-indol-3-yl)-3-(4-methoxyphenyl)allylidene)hydrazine-1-carboximidamide (4s)

Yield 87 %, yellow solid; mp: 211-213 °C; ¹H NMR (400 MHz, DMSO-*d*₆) δ 10.09 (d, J = 24.5 Hz, 1H), 9.56 (s, 1H), 8.30 – 8.01 (m, 1H), 7.99 – 7.87 (m, 1H), 7.82 – 7.58 (m, 5H), 7.56 – 7.37 (m, 3H), 7.33 – 7.13 (m, 5H), 7.09 – 6.92 (m, 1H), 5.63 – 5.31 (m, 2H), 3.80 – 3.64 (m,

3H), 1.95 – 1.87 (m, 2H).; ^{13}C NMR (100 MHz, DMSO-*d*6) δ 170.14, 159.62, 159.18, 156.26, 138.06, 137.35, 136.90, 133.37, 130.27, 129.10, 129.06, 129.01, 127.96, 127.69, 127.49, 125.28, 123.02, 121.45, 114.62, 113.93, 111.70, 55.71, 25.17, 21.22, 18.51, 16.67.; HRMS-ESI+ calculated for $\text{C}_{26}\text{H}_{26}\text{N}_5\text{O}$ [M+H]⁺ 424.2137, found: 424.2030.

4.2.2.20 (Z)-2-((E)-1-(1-benzyl-1H-indol-3-yl)-3-(2-nitrophenyl)allylidene)hydrazine-1-carboximidamide (4t)

Yield 87 %, yellow solid; mp: 203-205 °C; ^1H NMR (400 MHz, DMSO-*d*6) δ 11.08 (d, J = 50.3 Hz, 1H), 10.08 (d, J = 33.9 Hz, 1H), 9.55 (s, 1H), 8.36 – 7.85 (m, 2H), 7.59 (d, J = 43.4 Hz, 5H), 7.52 – 7.39 (m, 2H), 7.36 – 7.29 (m, 2H), 7.28 – 7.22 (m, 2H), 7.22 – 6.99 (m, 2H), 5.47 (s, 2H), 1.96 – 1.89 (m, 2H).; ^{13}C NMR (100 MHz, DMSO-*d*6) δ 170.15, 160.04, 159.17, 156.43, 156.35, 156.24, 155.12, 151.70, 138.05, 137.35, 133.38, 129.06, 127.97, 127.49, 125.28, 123.63, 123.03, 121.45, 113.92, 110.93, 49.87, 25.13, 21.23, 18.61, 16.60.; HRMS-ESI+ calculated for $\text{C}_{25}\text{H}_{22}\text{N}_6\text{O}_2$ [M+H]⁺ 438.1780, found: 438.1776.

4.2.2.21 (Z)-2-((E)-1-(1-benzyl-1H-indol-3-yl)-3-(4-(trifluoromethyl)phenyl)allylidene)hydrazine-1-carboximidamide (4u)

Yield 93 %, yellow solid; mp: 201-203 °C; ^1H NMR (400 MHz, DMSO-*d*6) δ 11.08 (d, J = 51.1 Hz, 1H), 10.10 (d, J = 29.1 Hz, 1H), 9.56 (s, 1H), 8.36 – 7.90 (m, 2H), 7.83 – 7.55 (m, 6H), 7.52 – 7.46 (m, 1H), 7.35 – 7.26 (m, 2H), 7.26 – 7.22 (m, 2H), 7.22 – 7.11 (m, 2H), 5.60 – 5.34 (m, 2H), 1.90 (s, 2H).; ^{13}C NMR (100 MHz, DMSO-*d*6) δ 170.17, 159.60, 159.18, 156.44, 156.26, 155.12, 151.69, 138.05, 137.34, 133.38, 129.06, 128.01, 127.97, 127.71, 127.49, 125.27, 123.62, 123.03, 121.45, 113.91, 110.93, 49.86, 25.13, 21.22, 18.62, 16.62.; HRMS-ESI+ calculated for $\text{C}_{26}\text{H}_{23}\text{F}_3\text{N}_5$ [M+H]⁺ 462.1906, found: 462.1793.

4.2.2.22 (Z)-2-((E)-1-(1-benzyl-1H-indol-3-yl)-3-(2-bromo-5-chlorophenyl)allylidene)hydrazine-1-carboximidamide (4v)

Yield 95 %, yellow solid; mp: 204-206 °C; ^1H NMR (400 MHz, DMSO-*d*6) δ 11.10 (d, J = 50.3 Hz, 1H), 10.15 (s, 1H), 9.57 (s, 1H), 8.29 – 8.21 (m, 1H), 7.79 – 7.64 (m, 7H), 7.48 (d, J = 8.0 Hz, 2H), 7.33 – 7.29 (m, 1H), 7.27 – 7.22 (m, 2H), 7.15 (ddd, J = 14.8, 8.1, 3.9 Hz, 1H), 5.47 (s, 2H), 1.89 (s, 2H).; ^{13}C NMR (100 MHz, DMSO-*d*6) δ 172.46, 170.16, 159.63, 159.20, 156.46, 156.28, 155.11, 151.67, 138.05, 137.33, 133.38, 129.05, 127.97, 127.49, 125.26, 123.61, 123.02, 121.45, 113.90, 110.93, 49.86, 25.13, 21.22, 18.64, 16.64.; HRMS-ESI+ calculated for $\text{C}_{25}\text{H}_{22}\text{BrClN}_5$ [M+H]⁺ 506.0747, found: 508.0592.

4.2.2.23 (Z)-2-((E)-1-(1-benzyl-1H-indol-3-yl)-3-(3-**(benzyloxy)phenyl)allylidene)hydrazine-1-carboximidamide (4w)**

Yield 85 %, brown solid; mp: 179–182 °C; ¹H NMR (400 MHz, DMSO-*d*₆) δ 11.16 (s, 1H), 10.10 (d, J = 31.6 Hz, 1H), 9.43 (d, J = 110.8 Hz, 1H), 8.36 – 8.08 (m, 3H), 7.87 (dd, J = 96.5, 9.5 Hz, 3H), 7.67 (s, 3H), 7.50 (dd, J = 16.5, 6.6 Hz, 2H), 7.38 (d, J = 5.5 Hz, 1H), 7.37 – 7.33 (m, 1H), 7.30 (d, J = 6.5 Hz, 2H), 7.25 (d, J = 6.3 Hz, 4H), 7.20 (d, J = 7.0 Hz, 1H), 7.17 (d, J = 3.2 Hz, 1H), 7.16 – 7.05 (m, 1H), 5.57 – 5.34 (m, 2H), 1.97 – 1.88 (m, 2H).; ¹³C NMR (100 MHz, DMSO-*d*₆) δ 170.16, 159.62, 159.19, 156.44, 156.26, 155.11, 151.70, 138.05, 137.35, 133.38, 129.06, 128.87, 128.82, 128.28, 128.15, 127.97, 127.69, 127.49, 127.40, 125.28, 123.63, 123.03, 121.46, 113.93, 110.93, 56.49, 49.87, 25.13, 21.23, 19.03, 18.62, 16.62.; HRMS-ESI+ calculated for C₃₂H₃₀N₅O [M+H]⁺ 500.2337, found: 500.2335.

4.2.2.24 (Z)-2-((E)-1-(1-benzyl-1H-indol-3-yl)-3-(4-nitrophenyl)allylidene)hydrazine-1-carboximidamide (4x)

Yield 89 %, yellow solid; mp: 164–166 °C; ¹H NMR (400 MHz, DMSO-*d*₆) δ 8.40 – 7.96 (m, 3H), 7.95 – 7.52 (m, 5H), 7.53 – 7.35 (m, 2H), 7.35 – 6.92 (m, 7H), 5.60 – 5.34 (m, 2H), 3.17 (s, 1H), 2.42 (s, 1H), 1.99 – 1.89 (m, 1H).; ¹³C NMR (100 MHz, DMSO-*d*₆) δ 170.15, 159.19, 156.27, 151.68, 138.06, 137.35, 133.37, 129.12, 129.06, 127.97, 127.68, 127.49, 127.34, 125.28, 123.63, 123.03, 121.45, 113.93, 110.93, 49.87, 49.05, 25.13, 21.23, 18.62, 16.62.; HRMS-ESI+ calculated for C₂₅H₂₃N₆O₂ [M+H]⁺ 439.1882, found: 439.1916.

4.2.2.25 (Z)-2-((E)-1-(1-benzyl-1H-indol-3-yl)-3-(3-cyanophenyl)allylidene)hydrazine-1-carboximidamide (4y)

Yield 88 %, yellow solid; mp: 219–221 °C; ¹H NMR (400 MHz, DMSO-*d*₆) δ 11.14 (s, 1H), 8.32 – 8.01 (m, 2H), 8.00 – 7.51 (m, 5H), 7.51 – 7.34 (m, 2H), 7.35 – 7.23 (m, 5H), 7.22 – 6.79 (m, 3H), 5.57 – 5.31 (m, 2H), 3.18 (s, 1H), 2.42 (s, 1H).; ¹³C NMR (100 MHz, DMSO-*d*₆) δ 156.23, 151.71, 138.06, 137.36, 137.04, 133.36, 129.07, 128.75, 127.98, 127.65, 127.49, 127.38, 127.35, 127.26, 125.29, 123.63, 123.04, 121.45, 113.95, 111.72, 110.93, 49.87, 49.06, 25.15, 16.56, 14.65.; HRMS-ESI+ calculated for C₂₆H₂₃N₆ [M+H]⁺ 419.1984, found: 419.1975.

4.2.2.26 (Z)-2-((E)-1-(1-benzyl-1H-indol-3-yl)-3-(2,5-difluorophenyl)allylidene)hydrazine-1-carboximidamide (4z)

Yield 93 %, yellow solid; mp: 207–209 °C; ¹H NMR (400 MHz, DMSO-*d*₆) δ 8.25 – 7.90 (m, 2H), 7.87 – 7.52 (m, 4H), 7.51 – 7.35 (m, 2H), 7.34 – 7.21 (m, 5H), 7.20 – 7.10 (m, 2H), 7.09 – 6.79 (m, 1H), 5.63 – 5.34 (m, 2H), 3.28 – 3.10 (m, 1H), 2.49 (dd, J = 19.3, 17.5 Hz, 1H), 2.03 – 1.84 (m, 1H).; ¹³C NMR (100 MHz, DMSO-*d*₆) δ 156.24, 150.00, 138.06, 137.95, 136.65,

133.46, 131.87, 129.07, 129.04, 128.75, 128.07, 127.97, 127.84, 127.68, 127.31, 126.06, 122.99, 121.25, 120.06, 111.74, 103.35, 50.05, 49.83, 25.07, 18.58.; HRMS-ESI+ calculated for C₂₅H₂₂F₂N₅ [M+H]⁺ 430.1843, found: 430.1815.

4.2.2.27 (Z)-2-((E)-1-(1-benzyl-1H-indol-3-yl)-3-(2,3-dimethoxyphenyl)allylidene)hydrazine-1-carboximidamide (4aa)

Yield 91 %, light yellow solid; mp: 211–213 °C; ¹H NMR (400 MHz, DMSO-*d*₆) δ 11.71 – 10.98 (m, 1H), 8.92 – 7.90 (m, 2H), 7.89 – 7.44 (m, 5H), 7.43 – 7.24 (m, 5H), 7.23 – 7.08 (m, 3H), 7.06 – 6.70 (m, 1H), 5.74 – 5.19 (m, 2H), 3.89 – 3.34 (m, 6H), 2.42 (s, 1H), 2.01 – 1.87 (m, 1H).; ¹³C NMR (100 MHz, DMSO-*d*₆) δ 159.62, 156.25, 153.08, 147.68, 138.15, 138.06, 133.39, 129.68, 129.07, 129.03, 127.98, 127.67, 127.58, 127.49, 127.40, 125.29, 123.04, 121.46, 113.93, 61.23, 60.68, 56.25, 50.03, 49.10, 25.13, 18.61, 16.60.; HRMS-ESI+ calculated for C₂₇H₂₈N₅O₂ [M+H]⁺ 454.2208, found: 454.2204.

4.2.2.28 (Z)-2-((E)-1-(1-benzyl-1H-indol-3-yl)-3-(2,4-dichlorophenyl)allylidene)hydrazine-1-carboximidamide (4ab)

Yield 82 %, yellow solid; mp: 214–216 °C; ¹H NMR (400 MHz, DMSO-*d*₆) δ 11.88 – 11.50 (m, 1H), 8.48 – 7.95 (m, 2H), 7.91 – 7.72 (m, 2H), 7.71 – 7.47 (m, 4H), 7.46 – 7.33 (m, 2H), 7.32 – 7.21 (m, 4H), 7.20 – 6.98 (m, 2H), 5.61 – 5.34 (m, 2H), 2.49 – 2.28 (m, 1H), 2.02 – 1.83 (m, 1H).; ¹³C NMR (100 MHz, DMSO-*d*₆) δ 156.24, 150.02, 138.05, 137.06, 134.90, 134.53, 133.35, 132.91, 130.28, 129.52, 129.05, 128.23, 128.05, 127.74, 127.69, 127.49, 126.40, 123.68, 123.03, 122.41, 49.78, 25.18, 21.35, 18.56, 16.53.; HRMS-ESI+ calculated for C₂₅H₂₂Cl₂N₅ [M+H]⁺ 462.1252, found: 462.1210.

4.2.2.29 (Z)-2-((E)-1-(1-benzyl-1H-indol-3-yl)-3-(4-chlorophenyl)allylidene)hydrazine-1-carboximidamide (4ac)

Yield 86 %, yellow solid; mp: 204–206 °C; ¹H NMR (400 MHz, DMSO-*d*₆) δ 8.39 – 7.97 (m, 2H), 7.95 – 7.69 (m, 3H), 7.68 – 7.54 (m, 2H), 7.54 – 7.45 (m, 2H), 7.45 – 7.38 (m, 1H), 7.37 – 7.33 (m, 1H), 7.33 – 7.27 (m, 2H), 7.27 – 7.14 (m, 3H), 7.14 – 6.51 (m, 2H), 5.63 – 5.31 (m, 2H), 2.50 – 2.33 (m, 1H), 2.00 – 1.90 (m, 1H).; ¹³C NMR (100 MHz, DMSO-*d*₆) δ 159.05, 156.24, 155.23, 150.00, 138.13, 136.99, 135.17, 133.48, 130.53, 130.31, 129.41, 129.06, 128.65, 128.44, 127.97, 127.66, 127.49, 122.90, 121.45, 111.59, 103.55, 62.60, 49.80, 25.18, 18.56.; HRMS-ESI+ calculated for C₂₅H₂₃ClN₅ [M+H]⁺ 428.1597, found: 428.1598.

4.2.2.30 (Z)-2-((E)-1-(1-benzyl-1H-indol-3-yl)-3-(3,4-dichlorophenyl)allylidene)hydrazine-1-carboximidamide (4ad)

Yield 79 %, yellow solid; mp: 230–232 °C; ¹H NMR (400 MHz, DMSO-*d*₆) δ 8.39 – 7.84 (m, 3H), 7.83 – 7.55 (m, 4H), 7.55 – 7.33 (m, 3H), 7.32 – 7.22 (m, 3H), 7.21 – 6.76 (m, 3H), 5.46

(dt, $J = 34.3, 20.3$ Hz, 2H), 3.28 – 3.07 (m, 1H), 2.42 (s, 1H), 2.01 – 1.87 (m, 1H).; ^{13}C NMR (100 MHz, DMSO-*d*₆) δ 159.05, 156.24, 155.23, 150.00, 138.13, 136.99, 135.17, 133.48, 130.53, 130.31, 129.41, 129.06, 128.65, 128.44, 127.97, 127.66, 127.49, 122.90, 121.45, 111.59, 103.55, 62.60, 49.80, 25.18, 18.56.; HRMS-ESI+ calculated for C₂₅H₂₂Cl₂N₅ [M+H]⁺ 462.1252, found: 462.1266.

4.2.2.31 (Z)-2-((E)-1-(1-benzyl-1H-indol-3-yl)-3-(4-fluorophenyl)allylidene)hydrazine-1-carboximidamide (4ae)

Yield 75 %, yellow solid; mp: 216–218 °C; ^1H NMR (400 MHz, DMSO-*d*₆) δ 7.84 – 7.78 (m, 1H), 7.74 – 7.69 (m, 1H), 7.69 – 7.64 (m, 1H), 7.60 (dd, $J = 11.7, 9.4$ Hz, 1H), 7.52 (dd, $J = 15.1, 8.8$ Hz, 1H), 7.48 – 7.42 (m, 1H), 7.41 – 7.35 (m, 3H), 7.33 (dd, $J = 8.1, 2.2$ Hz, 1H), 7.31 – 7.25 (m, 1H), 7.24 – 7.18 (m, 1H), 7.17 – 7.10 (m, 1H), 7.08 – 6.70 (m, 3H), 6.43 – 6.20 (m, 1H), 5.77 – 5.38 (m, 2H), 4.41 – 4.00 (m, 1H), 2.21 (t, $J = 5.0$ Hz, 1H), 1.98 – 1.90 (m, 1H).; ^{13}C NMR (100 MHz, DMSO-*d*₆) δ 170.14, 159.05, 156.27, 129.32, 129.29, 129.17, 129.03, 129.00, 128.94, 128.76, 128.58, 128.48, 128.11, 127.43, 127.35, 127.25, 119.38, 61.24, 51.53, 25.14, 21.34, 18.55, 16.84, 15.47, 14.41.; HRMS-ESI+ calculated for C₂₅H₂₃FN₅ [M+H]⁺ 412.1937, found: 412.1897.

4.2.2.32 (Z)-2-((E)-1-(1-benzyl-1H-indol-3-yl)-3-(o-tolyl)allylidene)hydrazine-1-carboximidamide (4af)

Yield 78 %, yellow solid; mp: 227–229 °C; ^1H NMR (400 MHz, DMSO-*d*₆) δ 10.15 (s, 1H), 8.25 – 7.87 (m, 3H), 7.86 – 7.42 (m, 4H), 7.34 (ddd, $J = 11.9, 7.5, 2.5$ Hz, 4H), 7.29 – 7.19 (m, 4H), 7.19 – 7.07 (m, 3H), 7.01 (t, $J = 12.7$ Hz, 1H), 5.55 (d, $J = 31.9$ Hz, 2H), 2.26 – 1.82 (m, 3H).; ^{13}C NMR (100 MHz, DMSO-*d*₆) δ 159.67, 156.02, 150.56, 138.09, 136.65, 136.43, 134.81, 131.65, 131.05, 129.60, 129.16, 129.08, 128.97, 128.05, 127.72, 127.51, 126.94, 126.14, 125.63, 122.85, 121.06, 120.23, 111.66, 103.82, 49.96, 19.57.; HRMS-ESI+ calculated for C₂₆H₂₆N₅ [M+H]⁺ 408.2152, found: 408.2149.

4.2.2.33 (Z)-2-((E)-1-(1-(4-butylbenzyl)-1H-indol-3-yl)-3-phenylallylidene)hydrazine-1-carboximidamide (5a)

Yield 95 %, yellow solid; mp: 197– 199 °C; ^1H NMR (400 MHz, DMSO-*d*₆) δ 11.18 (d, $J = 47.3$ Hz, 1H), 10.18 (s, 1H), 9.61 (s, 1H), 8.88 (d, $J = 35.8$ Hz, 1H), 8.29 – 7.94 (m, 2H), 7.76 (d, $J = 43.7$ Hz, 3H), 7.55 – 7.43 (m, 2H), 7.16 (ddd, $J = 23.5, 15.4, 7.6$ Hz, 7H), 5.52 – 5.23 (m, 2H), 2.41 (s, 2H), 1.97 – 1.89 (m, 3H), 1.47 (dt, $J = 15.2, 7.5$ Hz, 2H), 1.31 – 1.17 (m, 2H), 0.84 (t, $J = 7.3$ Hz, 2H).; ^{13}C NMR (100 MHz, DMSO-*d*₆) δ 170.13, 159.74, 159.27, 156.54, 156.36, 155.77, 155.00, 151.61, 142.08, 137.32, 135.29, 133.32, 128.92, 127.50, 125.27,

123.62, 122.97, 121.40, 113.85, 110.93, 49.65, 34.88, 33.54, 25.12, 22.18, 21.23, 18.69, 16.69, 14.20.; HRMS-ESI+ calculated for C₂₉H₃₂N₅ [M+H]⁺ 450.2658, found: 450.2658.

4.2.2.34 (Z)-2-((E)-3-phenyl-1-(1-(4-(trifluoromethoxy)benzyl)-1H-indol-3-yl)allylidene)hydrazine-1-carboximidamide (5b)

Yield 94 %, yellow solid; mp: 201–203 °C; ¹H NMR (400 MHz, DMSO-*d*₆) δ 10.15 (d, J = 14.2 Hz, 1H), 9.59 (s, 1H), 8.89 (s, 1H), 8.28 (d, J = 8.9 Hz, 1H), 7.83 (d, J = 14.2 Hz, 1H), 7.69 (s, 2H), 7.53 – 7.47 (m, 2H), 7.37 (d, J = 8.8 Hz, 2H), 7.32 (d, J = 8.3 Hz, 2H), 7.22 – 7.19 (m, 1H), 7.17 (dd, J = 6.1, 1.2 Hz, 1H), 7.14 (d, J = 6.9 Hz, 1H), 5.46 (d, J = 45.6 Hz, 2H), 4.71 (s, 1H), 1.96 (t, J = 4.7 Hz, 2H), 1.89 (s, 1H).; ¹³C NMR (100 MHz, DMSO-*d*₆) δ 170.15, 159.70, 159.23, 156.50, 156.34, 155.06, 151.56, 148.70, 148.04, 137.61, 137.25, 133.30, 129.38, 125.27, 123.69, 123.14, 121.71, 121.55, 114.14, 110.83, 48.99, 25.12, 21.23, 18.67, 16.68, 15.39.; HRMS-ESI+ calculated for C₂₆H₂₃F₃N₅O [M+H]⁺ 478.1855, found: 478.1856.

4.2.2.35 (Z)-2-((E)-1-(1-(2,4-difluorobenzyl)-1H-indol-3-yl)-3-phenylallylidene)hydrazine-1-carboximidamide (5c)

Yield 93 %, yellow solid; mp: 215–217 °C; ¹H NMR (400 MHz, DMSO-*d*₆) δ 8.83 (d, J = 23.3 Hz, 1H), 8.33 – 7.84 (m, 2H), 7.79 – 7.61 (m, 2H), 7.50 (ddd, J = 21.6, 12.0, 6.7 Hz, 2H), 7.39 – 7.17 (m, 5H), 7.14 – 6.91 (m, 3H), 5.63 – 5.31 (m, 2H), 4.03 (q, J = 7.1 Hz, 1H), 2.03 – 1.85 (m, 2H), 1.17 (t, J = 7.1 Hz, 1H).; ¹³C NMR (100 MHz, DMSO-*d*₆) δ 170.80, 159.63, 159.18, 156.43, 156.27, 151.52, 137.27, 133.13, 131.31, 128.49, 125.19, 123.71, 123.21, 121.60, 114.24, 112.33, 112.12, 110.58, 104.62, 60.23, 25.13, 21.24, 18.60, 16.59, 14.55.; HRMS-ESI+ calculated for C₂₅H₂₂F₂N₅ [M+H]⁺ 430.1843, found: 430.1845.

4.2.2.36 (Z)-2-((E)-1-(1-(4-(tert-butyl)benzyl)-1H-indol-3-yl)-3-phenylallylidene)hydrazine-1-carboximidamide (5d)

Yield 86 %, yellow solid; mp: 242–244 °C; ¹H NMR (400 MHz, DMSO-*d*₆) δ 10.19 (s, 1H), 9.61 (s, 1H), 8.33 – 8.08 (m, 1H), 7.94 (dd, J = 24.7, 13.2 Hz, 2H), 7.73 (d, J = 10.5 Hz, 4H), 7.58 – 7.47 (m, 3H), 7.34 – 7.31 (m, 3H), 7.18 (d, J = 8.2 Hz, 1H), 7.09 (dd, J = 16.2, 7.2 Hz, 1H), 5.43 (dd, J = 51.3, 35.7 Hz, 2H), 3.24 – 2.78 (m, 1H), 1.97 (d, J = 4.5 Hz, 2H), 1.89 (s, 3H), 1.30 – 1.21 (m, 6H).; ¹³C NMR (100 MHz, DMSO-*d*₆) δ 170.13, 159.68, 159.27, 156.55, 156.37, 155.00, 150.36, 137.34, 135.12, 133.32, 129.11, 128.45, 127.77, 127.54, 127.31, 127.27, 126.19, 125.78, 125.71, 113.88, 49.49, 34.65, 31.56, 31.53, 31.44, 25.13, 21.23, 18.70, 16.71.; HRMS-ESI+ calculated for C₂₉H₃₂N₅ [M+H]⁺ 450.2658, found: 450.2657.

4.2.2.37 (Z)-2-((E)-3-phenyl-1-(1-(4-(trifluoromethyl)benzyl)-1H-indol-3-yl)allylidene)hydrazine-1-carboximidamide (5e)

Yield 89 %, brown solid; mp: 231–233 °C; ¹H NMR (400 MHz, DMSO-*d*₆) δ 8.82 (d, J = 28.2 Hz, 1H), 8.26 (dd, J = 32.0, 19.4 Hz, 1H), 8.09 – 7.97 (m, 1H), 7.82 (s, 2H), 7.71 (s, 2H), 7.60 (d, J = 33.0 Hz, 2H), 7.48 (s, 1H), 7.40 (dd, J = 22.1, 7.2 Hz, 2H), 7.27 (s, 1H), 7.19 (s, 2H), 7.07 – 7.01 (m, 1H), 6.97 – 6.86 (m, 1H), 5.61 (dd, J = 50.9, 35.0 Hz, 2H), 4.69 (s, 1H), 2.00 – 1.84 (m, 2H).; ¹³C NMR (100 MHz, DMSO-*d*₆) δ 170.15, 163.93, 163.73, 159.62, 159.16, 158.79, 156.42, 156.27, 155.12, 151.60, 137.33, 133.38, 129.14, 128.62, 128.48, 128.10, 126.04, 123.22, 121.61, 114.26, 110.78, 49.30, 25.13, 21.21, 18.60, 16.61.; HRMS-ESI+ calculated for C₂₆H₂₃F₃N₅ [M+H]⁺ 462.1906, found: 462.1910.

4.2.2.38 (Z)-2-((E)-1-(1-(3,5-bis(trifluoromethyl)benzyl)-1H-indol-3-yl)-3-phenylallylidene)hydrazine-1-carboximidamide (5f)

Yield 87 %, yellow solid; mp: 226–228 °C; ¹H NMR (400 MHz, DMSO-*d*₆) δ 9.00 – 8.22 (m, 2H), 8.19 – 8.07 (m, 1H), 8.04 – 7.80 (m, 3H), 7.58 (dd, J = 30.6, 22.8 Hz, 3H), 7.45 – 7.37 (m, 1H), 7.31 – 7.13 (m, 4H), 6.89 (d, J = 123.6 Hz, 2H), 6.12 – 5.34 (m, 2H), 4.85 – 4.44 (m, 1H), 2.43 (s, 1H), 1.99 – 1.89 (m, 1H).; ¹³C NMR (100 MHz, DMSO-*d*₆) δ 159.62, 156.47, 156.42, 156.29, 155.10, 151.51, 141.60, 137.22, 133.22, 131.10, 130.77, 129.13, 128.47, 127.35, 125.26, 123.84, 123.39, 121.96, 121.78, 114.53, 110.67, 48.76, 25.12, 21.21, 18.59, 16.61, 14.54.; HRMS-ESI+ calculated for C₂₇H₂₂F₆N₅ [M+H]⁺ 530.1782, found: 530.1788.

4.2.2.39 (Z)-2-((E)-1-(1-(2,5-difluorobenzyl)-1H-indol-3-yl)-3-phenylallylidene)hydrazine-1-carboximidamide (5g)

Yield 84 %, yellow solid; mp: 231–233 °C; ¹H NMR (400 MHz, DMSO-*d*₆) δ 8.35 – 7.80 (m, 3H), 7.71 – 7.48 (m, 3H), 7.26 (tdd, J = 38.3, 30.1, 17.6 Hz, 8H), 6.79 (dd, J = 66.3, 49.9 Hz, 2H), 5.54 (dd, J = 54.4, 36.6 Hz, 2H), 3.32 – 2.90 (m, 1H), 2.49 – 1.62 (m, 2H).; ¹³C NMR (100 MHz, DMSO-*d*₆) δ 158.81, 156.24, 140.85, 136.93, 133.41, 133.18, 132.91, 129.42, 129.17, 128.60, 128.40, 127.46, 125.16, 123.30, 121.67, 121.40, 119.85, 117.87, 116.90, 116.66, 116.37, 62.31, 49.05, 43.82, 16.56.; HRMS-ESI+ calculated for C₂₅H₂₂F₂N₅ [M+H]⁺ 430.1843, found: 430.1850.

4.2.2.40 (Z)-2-((E)-1-(1-(4-fluoro-2-(trifluoromethyl)benzyl)-1H-indol-3-yl)-3-phenylallylidene)hydrazine-1-carboximidamide (5h)

Yield 81 %, yellow solid; mp: 226–228 °C; ¹H NMR (400 MHz, DMSO-*d*₆) δ 8.84 (d, J = 49.5 Hz, 2H), 8.39 – 7.87 (m, 1H), 7.90 – 6.30 (m, 14H), 4.96 – 3.98 (m, 2H), 1.99 – 1.84 (m, 2H).; ¹³C NMR (100 MHz, DMSO-*d*₆) δ 170.15, 169.90, 159.71, 159.24, 156.89, 156.51, 156.41, 156.37, 155.05, 151.36, 148.70, 137.31, 133.59, 129.41, 125.32, 123.50, 121.83, 120.53,

120.37, 117.11, 114.55, 43.44, 25.13, 21.23, 18.68, 16.69.; HRMS-ESI+ calculated for $C_{26}H_{22}F_4N_5$ [M+H]⁺ 480.1811, found: 480.1814.

4.2.2.41 (Z)-2-((E)-1-(1-(4-methylbenzyl)-1H-indol-3-yl)-3-phenylallylidene)hydrazine-1-carboximidamide (5i)

Yield 78 %, yellow solid; mp: 231–233 °C; ¹H NMR (400 MHz, DMSO-*d*₆) δ 11.15 (s, 1H), 8.36 – 8.03 (m, 2H), 8.03 – 7.68 (m, 3H), 7.52 (ddd, J = 31.5, 28.4, 13.8 Hz, 3H), 7.40 – 6.74 (m, 8H), 5.52 – 5.16 (m, 2H), 2.41 (s, 2H), 2.25 (d, J = 10.3 Hz, 3H), 2.00 – 1.86 (m, 1H).; ¹³C NMR (100 MHz, DMSO-*d*₆) δ 170.14, 159.63, 159.18, 156.25, 151.70, 137.31, 137.18, 135.00, 133.31, 129.71, 129.59, 129.52, 128.48, 127.73, 127.54, 125.37, 125.30, 123.60, 122.97, 121.40, 113.84, 110.96, 49.69, 21.22, 21.11, 16.59.; HRMS-ESI+ calculated for $C_{26}H_{26}N_5$ [M+H]⁺ 408.2188, found: 408.2198.

4.2.2.42 (Z)-2-((E)-1-(1-(2-cyanobenzyl)-1H-indol-3-yl)-3-phenylallylidene)hydrazine-1-carboximidamide (5j)

Yield 91 %, yellow solid; mp: 226–228 °C; ¹H NMR (400 MHz, DMSO-*d*₆) δ 8.30 – 8.01 (m, 1H), 7.99 – 7.86 (m, 1H), 7.86 – 7.66 (m, 2H), 7.64 – 7.55 (m, 1H), 7.52 – 7.36 (m, 3H), 7.28 (ddd, J = 24.4, 18.8, 10.8 Hz, 3H), 7.20 – 7.14 (m, 1H), 7.13 – 7.06 (m, 1H), 6.97 (d, J = 15.2 Hz, 1H), 6.85 – 6.41 (m, 1H), 4.03 (q, J = 7.1 Hz, 1H), 3.37 (s, 2H), 2.06 – 1.87 (m, 1H), 1.29 – 1.08 (m, 2H), 0.96 – 0.79 (m, 1H).; ¹³C NMR (100 MHz, DMSO-*d*₆) δ 170.82, 156.16, 156.11, 155.77, 152.33, 137.59, 129.95, 129.38, 129.23, 128.91, 128.78, 128.69, 128.50, 128.40, 128.28, 128.05, 125.84, 124.60, 122.76, 121.04, 114.22, 112.14, 60.23, 21.21, 16.36, 14.56.; HRMS-ESI+ calculated for $C_{26}H_{21}N_6$ [M+H]⁺ 417.1872, found: 417.1875.

4.2.2.43 (Z)-2-((E)-1-(1-([1,1'-biphenyl]-4-ylmethyl)-1H-indol-3-yl)-3-phenylallylidene)hydrazine-1-carboximidamide (5k)

Yield 93 %, yellow solid; mp: 208–210 °C; ¹H NMR (400 MHz, DMSO-*d*₆) δ 8.36 – 8.07 (m, 2H), 7.68 (d, J = 15.9 Hz, 2H), 7.66 – 7.57 (m, 6H), 7.52 (dd, J = 13.2, 8.2 Hz, 2H), 7.44 (dd, J = 15.2, 7.9 Hz, 3H), 7.39 – 7.29 (m, 4H), 7.28 – 7.09 (m, 3H), 5.54 (d, J = 16.5 Hz, 2H), 2.43 (s, 2H), 1.98 – 1.88 (m, 1H).; ¹³C NMR (100 MHz, DMSO-*d*₆) δ 170.16, 159.57, 159.13, 156.20, 151.73, 140.12, 139.89, 137.38, 137.26, 133.40, 129.46, 129.37, 128.31, 128.22, 128.09, 127.94, 127.54, 127.38, 127.30, 127.08, 125.31, 123.66, 123.20, 123.09, 121.56, 121.49, 113.99, 110.97, 49.55, 21.22, 16.58.; HRMS-ESI+ calculated for $C_{31}H_{28}N_5$ [M+H]⁺ 470.2345, found: 470.2466.

4.2.2.44 (Z)-2-((E)-1-(1-(4-chlorobenzyl)-1H-indol-3-yl)-3-phenylallylidene)hydrazine-1-carboximidamide (5l)

Yield 89 %, yellow solid; mp: 258–260 °C; ¹H NMR (400 MHz, DMSO-*d*₆) δ 11.13 (s, 1H), 8.36–7.87 (m, 2H), 7.60 (d, J = 45.8 Hz, 4H), 7.53–7.47 (m, 1H), 7.40 (dt, J = 22.4, 10.2 Hz, 3H), 7.27 (d, J = 8.5 Hz, 2H), 7.23–6.94 (m, 3H), 5.48 (s, 2H), 2.42 (s, 3H), 2.00–1.89 (m, 1H); ¹³C NMR (100 MHz, DMSO-*d*₆) δ 170.15, 159.58, 159.14, 156.39, 156.22, 151.65, 137.25, 137.09, 133.30, 132.76, 132.60, 129.47, 129.39, 129.16, 129.06, 125.30, 123.68, 123.12, 121.54, 114.08, 110.87, 49.13, 21.22, 18.58, 16.58.; HRMS-ESI+ calculated for C₂₅H₂₃ClN₅ [M+H]⁺ 428.1774, found: 428.1779.

4.2.2.45 (Z)-2-((E)-1-(1-(3-(benzyloxy)benzyl)-1H-indol-3-yl)-3-phenylallylidene)hydrazine-1-carboximidamide (5m)

Yield 96 %, yellow solid; mp: 258–260 °C; ¹H NMR (400 MHz, DMSO-*d*₆) δ 11.18–10.95 (m, 1H), 10.12 (d, J = 9.4 Hz, 1H), 9.55 (s, 1H), 8.31–7.87 (m, 2H), 7.78 (d, J = 13.3 Hz, 1H), 7.64 (s, 3H), 7.59–7.51 (m, 2H), 7.48 (d, J = 7.9 Hz, 1H), 7.38 (s, 1H), 7.36 (s, 1H), 7.33 (d, J = 5.2 Hz, 1H), 7.31–7.27 (m, 1H), 7.24 (d, J = 8.4 Hz, 1H), 7.20–7.15 (m, 1H), 7.15–7.07 (m, 1H), 6.92 (s, 1H), 6.80 (dd, J = 20.6, 11.7 Hz, 1H), 5.59–5.22 (m, 2H), 5.15–4.94 (m, 2H), 1.97 (d, J = 8.3 Hz, 3H), 1.90 (s, 1H); ¹³C NMR (100 MHz, DMSO-*d*₆) δ 170.15, 159.60, 159.16, 158.94, 156.42, 156.23, 155.11, 151.70, 139.65, 137.30, 133.39, 130.23, 128.87, 128.46, 128.32, 128.29, 128.26, 125.25, 123.62, 123.05, 121.46, 119.87, 114.41, 113.93, 113.84, 110.93, 69.64, 49.76, 25.14, 21.22, 18.61, 16.61.; HRMS-ESI+ calculated for C₃₂H₃₀N₅O [M+H]⁺ 500.2450, found: 500.2480.

4.2.2.46 (Z)-2-((E)-1-(1-(4-bromobenzyl)-1H-indol-3-yl)-3-phenylallylidene)hydrazine-1-carboximidamide (5n)

Yield 76 %, yellow solid; mp: 208–210 °C; ¹H NMR (400 MHz, DMSO-*d*₆) δ 11.12 (d, J = 56.3 Hz, 1H), 10.12 (s, 1H), 9.56 (s, 1H), 8.29–8.22 (m, 1H), 7.80 (d, J = 11.8 Hz, 1H), 7.66 (s, 2H), 7.52 (d, J = 3.7 Hz, 1H), 7.50 (s, 1H), 7.46 (d, J = 7.9 Hz, 1H), 7.20 (d, J = 8.4 Hz, 4H), 7.17 (dd, J = 4.2, 1.3 Hz, 1H), 7.13 (d, J = 6.9 Hz, 1H), 5.46 (s, 2H), 2.41 (s, 1H), 1.97 (d, J = 7.0 Hz, 2H), 1.90 (s, 1H); ¹³C NMR (100 MHz, DMSO-*d*₆) δ 170.15, 159.63, 159.18, 156.45, 156.28, 155.09, 151.60, 137.52, 137.23, 133.31, 131.96, 129.73, 125.28, 123.68, 123.11, 121.53, 121.10, 114.07, 110.87, 49.18, 25.13, 21.22, 18.68, 18.64, 16.63.; HRMS-ESI+ calculated for C₂₅H₂₃BrN₅ [M+H]⁺ 472.1137, found: 474.1329.

4.2.2.47 (Z)-2-((E)-1-(1-(3,5-dimethoxybenzyl)-1H-indol-3-yl)-3-phenylallylidene)hydrazine-1-carboximidamide (5o)

Yield 72 %, yellow solid; mp: 226–228 °C; ¹H NMR (400 MHz, DMSO-*d*6) δ 11.24 – 11.01 (m, 1H), 8.87 (s, 1H), 8.36 – 7.98 (m, 1H), 7.81 (d, J = 6.4 Hz, 1H), 7.63 (d, J = 15.8 Hz, 3H), 7.49 (dd, J = 15.0, 7.2 Hz, 1H), 7.27 – 7.10 (m, 7H), 6.59 – 6.28 (m, 2H), 5.57 – 5.16 (m, 1H), 3.87 – 3.51 (m, 6H), 2.41 (d, J = 3.8 Hz, 1H), 1.97 (d, J = 7.5 Hz, 2H).; ¹³C NMR (100 MHz, DMSO-*d*6) δ 161.08, 159.63, 156.44, 156.26, 155.68, 155.09, 151.68, 140.35, 137.42, 133.44, 129.14, 128.44, 125.22, 123.61, 123.04, 121.46, 113.91, 110.95, 105.91, 105.81, 99.06, 55.65, 49.86, 25.13, 21.22, 18.63, 16.62.; HRMS-ESI+ calculated for C₂₇H₂₈N₅O₂ [M+H]⁺ 454.2259, found: 454.2266.

4.2.2.48 (Z)-2-((E)-1-(1-(4-fluorobenzyl)-1H-indol-3-yl)-3-phenylallylidene)hydrazine-1-carboximidamide (5p)

Yield 71 %, yellow solid; mp: 231–233 °C; ¹H NMR (400 MHz, DMSO-*d*6) δ 11.71 – 10.95 (m, 1H), 8.83 (t, J = 20.9 Hz, 1H), 8.21 (td, J = 24.1, 7.5 Hz, 1H), 8.08 – 7.88 (m, 1H), 7.80 (dd, J = 23.2, 15.7 Hz, 1H), 7.64 (dd, J = 19.8, 12.0 Hz, 2H), 7.58 – 7.46 (m, 2H), 7.41 – 7.26 (m, 3H), 7.18 (ddd, J = 17.4, 13.1, 7.2 Hz, 4H), 7.13 – 7.03 (m, 1H), 7.00 – 6.75 (m, 1H), 5.77 – 5.16 (m, 2H), 2.42 (s, 1H), 2.03 – 1.85 (m, 2H).; ¹³C NMR (100 MHz, DMSO-*d*6) δ 159.61, 156.41, 156.24, 155.12, 151.66, 137.23, 134.29, 133.25, 129.71, 129.62, 129.15, 128.63, 128.51, 128.46, 125.30, 123.66, 123.08, 121.50, 115.98, 115.76, 114.02, 49.10, 25.14, 18.60, 16.59.; HRMS-ESI+ calculated for C₂₅H₂₃FN₅ [M+H]⁺ 412.1937, found: 412.1966.

4.2.2.49 (Z)-2-((E)-1-(1-(2-fluorobenzyl)-1H-indol-3-yl)-3-phenylallylidene)hydrazine-1-carboximidamide (5q)

Yield 73 %, yellow solid; mp: 242–244 °C; ¹H NMR (400 MHz, DMSO-*d*6) δ 11.27 (dd, J = 129.2, 47.1 Hz, 1H), 10.15 (d, J = 12.4 Hz, 1H), 9.56 (s, 1H), 8.88 (s, 1H), 8.17 – 7.87 (m, 1H), 7.83 – 7.75 (m, 1H), 7.66 – 7.60 (m, 1H), 7.57 – 7.49 (m, 1H), 7.49 – 7.40 (m, 1H), 7.35 (ddd, J = 9.6, 5.8, 3.3 Hz, 1H), 7.31 – 7.25 (m, 1H), 7.25 – 7.21 (m, 1H), 7.20 – 7.16 (m, 1H), 7.15 – 7.11 (m, 1H), 7.11 – 6.58 (m, 2H), 5.65 – 5.36 (m, 1H), 4.29 – 3.39 (m, 2H), 1.97 (d, J = 7.6 Hz, 1H), 1.89 (s, 2H).; ¹³C NMR (100 MHz, DMSO-*d*6) δ 170.14, 159.64, 159.19, 156.45, 156.29, 155.08, 151.53, 137.34, 133.28, 130.39, 128.63, 128.48, 125.16, 123.69, 123.17, 121.56, 116.08, 115.87, 114.14, 110.62, 43.94, 25.13, 21.22, 18.64, 16.62.; HRMS-ESI+ calculated for C₂₅H₂₃FN₅ [M+H]⁺ 412.1968, found: 412.1971.

4.2.2.50 (Z)-2-((E)-1-(1-(4-bromo-2-fluorobenzyl)-1H-indol-3-yl)-3-phenylallylidene)hydrazine-1-carboximidamide (5r)

Yield 94 %, yellow solid; mp: 198–200 °C; ¹H NMR (400 MHz, DMSO-*d*₆) δ 11.11 (s, 1H), 8.36 – 7.93 (m, 2H), 7.68 (s, 2H), 7.65 – 7.56 (m, 2H), 7.54 – 7.42 (m, 2H), 7.36 (dt, J = 19.1, 9.5 Hz, 2H), 7.27 – 7.10 (m, 3H), 7.08 – 6.89 (m, 2H), 5.51 (s, 2H), 2.40 (s, 2H), 2.03 – 1.88 (m, 1H).; ¹³C NMR (100 MHz, DMSO-*d*₆) δ 161.47, 159.58, 158.98, 156.22, 151.53, 137.30, 133.20, 131.34, 131.30, 128.38, 128.35, 125.18, 124.57, 124.42, 123.73, 123.26, 121.71, 121.65, 119.54, 119.29, 114.30, 110.58, 60.23, 43.63, 16.56.; HRMS-ESI+ calculated for C₂₅H₂₂BrFN₅ [M+H]⁺ 492.1217, found: 492.1218.

4.2.2.51 (Z)-2-((E)-1-(1-(2,5-dichlorobenzyl)-1H-indol-3-yl)-3-phenylallylidene)hydrazine-1-carboximidamide (5s)

Yield 89 %, yellow solid; mp: 214–216 °C; ¹H NMR (400 MHz, DMSO-*d*₆) δ 9.06 – 8.05 (m, 2H), 8.03 – 7.75 (m, 2H), 7.66 (ddd, J = 14.5, 10.6, 6.5 Hz, 2H), 7.60 – 7.55 (m, 1H), 7.54 – 7.47 (m, 1H), 7.47 – 7.41 (m, 1H), 7.41 – 7.34 (m, 1H), 7.34 – 7.23 (m, 1H), 7.19 (ddd, J = 23.6, 10.8, 5.6 Hz, 2H), 7.10 – 6.67 (m, 2H), 5.77 – 5.28 (m, 1H), 4.87 – 4.12 (m, 1H), 3.46 (d, J = 7.3 Hz, 2H), 2.05 – 1.82 (m, 2H).; ¹³C NMR (100 MHz, DMSO-*d*₆) δ 170.14, 159.63, 159.17, 156.43, 156.31, 155.09, 137.54, 137.38, 133.33, 132.54, 131.83, 131.03, 129.72, 128.37, 128.22, 125.17, 123.46, 121.80, 114.49, 47.44, 25.14, 21.22, 18.68, 18.63, 16.64.; HRMS-ESI+ calculated for C₂₅H₂₂Cl₂N₅ [M+H]⁺ 462.1252, found: 462.1273.

4.2.2.52 (Z)-2-((E)-1-(1-(4-nitrobenzyl)-1H-indol-3-yl)-3-phenylallylidene)hydrazine-1-carboximidamide (5t)

Yield 88 %, yellow solid; mp: 209–211 °C; ¹H NMR (400 MHz, DMSO-*d*₆) δ 10.11 (d, J = 23.6 Hz, 1H), 9.57 (s, 1H), 8.89 (s, 2H), 8.10 – 7.89 (m, 1H), 7.78 (d, J = 40.8 Hz, 1H), 7.66 (s, 1H), 7.52 (dd, J = 10.6, 5.3 Hz, 1H), 7.22 (s, 8H), 6.94 (d, J = 5.6 Hz, 1H), 4.02 (dd, J = 14.2, 7.1 Hz, 2H), 2.00 – 1.93 (m, 1H), 1.92 – 1.83 (m, 2H).; ¹³C NMR (100 MHz, DMSO-*d*₆) δ 170.15, 159.19, 156.27, 151.68, 138.06, 137.35, 133.37, 129.12, 129.06, 127.97, 127.68, 127.49, 127.34, 125.28, 123.63, 123.03, 121.45, 113.93, 110.93, 49.87, 49.05, 25.13, 21.23, 18.62, 16.62.; HRMS-ESI+ calculated for C₂₅H₂₆N₇O₂ [M+H]⁺ 456.2148, found: 456.2113.

4.2.2.53 (Z)-2-((E)-1-(1-(3-bromobenzyl)-1H-indol-3-yl)-3-phenylallylidene)hydrazine-1-carboximidamide (5u)

Yield 90 %, yellow solid; mp: 252–254 °C; ¹H NMR (400 MHz, DMSO-*d*₆) δ 11.06 (d, J = 52.5 Hz, 1H), 8.33 – 8.14 (m, 1H), 8.06 – 7.84 (m, 1H), 7.84 – 7.65 (m, 2H), 7.65 – 7.52 (m, 2H), 7.52 – 7.42 (m, 3H), 7.40 – 7.27 (m, 2H), 7.26 – 7.15 (m, 3H), 7.15 – 7.08 (m, 1H), 7.07 – 6.97 (m, 1H), 6.96 – 6.51 (m, 1H), 5.60 – 5.31 (m, 2H), 3.17 (s, 1H), 2.42 (s, 1H), 1.99 –

1.89 (m, 1H).; ^{13}C NMR (100 MHz, DMSO-*d*6) δ 170.15, 159.59, 159.15, 156.23, 151.63, 140.87, 137.27, 133.32, 131.31, 130.89, 130.19, 126.58, 125.27, 123.71, 123.19, 122.31, 121.59, 114.16, 110.85, 49.11, 49.05, 25.14, 21.22, 18.60, 16.60.; HRMS-ESI+ calculated for $\text{C}_{25}\text{H}_{23}\text{BrN}_5$ [M+H] $^{+}$ 472.1137, found: 474.1143.

4.2.2.54 (Z)-2-((E)-1-(1-(3-cyanobenzyl)-1H-indol-3-yl)-3-phenylallylidene)hydrazine-1-carboximidamide (5v)

Yield 84 %, yellow solid; mp: 262–264 °C; ^1H NMR (400 MHz, DMSO-*d*6) δ 11.56 – 10.98 (m, 1H), 8.97 – 8.65 (m, 1H), 8.38 – 8.08 (m, 1H), 8.04 – 7.89 (m, 1H), 7.89 – 7.70 (m, 2H), 7.59 (dd, $J = 27.8, 19.2$ Hz, 2H), 7.45 (ddd, $J = 26.5, 14.9, 6.5$ Hz, 2H), 7.36 – 7.26 (m, 1H), 7.25 – 7.10 (m, 2H), 7.04 (t, $J = 23.3$ Hz, 2H), 6.96 – 6.45 (m, 1H), 5.53 (dd, $J = 41.5, 22.0$ Hz, 1H), 4.85 – 4.12 (m, 2H), 3.14 (d, $J = 22.4$ Hz, 1H), 2.38 (d, $J = 32.5$ Hz, 1H), 2.00 – 1.88 (m, 1H).; ^{13}C NMR (100 MHz, DMSO-*D*6) δ 167.47, 159.65, 158.82, 156.45, 156.29, 155.65, 155.08, 148.74, 146.79, 138.70, 137.32, 136.98, 133.35, 131.58, 129.43, 129.14, 128.93, 128.75, 128.45, 128.19, 128.10, 49.04, 25.13, 18.64, 16.64, 14.60.; HRMS-ESI+ calculated for $\text{C}_{26}\text{H}_{23}\text{N}_6$ [M+H] $^{+}$ 419.1925, found: 419.1921.

4.2.2.55 (Z)-2-((E)-1-(1-(4-cyanobenzyl)-1H-indol-3-yl)-3-phenylallylidene)hydrazine-1-carboximidamide (5w)

Yield 74 %, yellow solid; mp: 226–228 °C; ^1H NMR (400 MHz, DMSO-*d*6) δ 8.96 – 8.22 (m, 1H), 8.21 – 7.84 (m, 2H), 7.83 – 7.60 (m, 2H), 7.59 – 7.45 (m, 2H), 7.39 (dd, $J = 33.2, 6.7$ Hz, 2H), 7.27 (dd, $J = 19.1, 7.3$ Hz, 2H), 7.20 – 7.09 (m, 2H), 6.95 (dd, $J = 41.1, 35.5$ Hz, 2H), 6.83 – 6.24 (m, 1H), 4.90 – 3.82 (m, 1H), 3.39 (s, 2H), 3.17 (s, 1H), 2.41 (d, $J = 4.6$ Hz, 1H), 1.40 – 0.76 (m, 1H).; ^{13}C NMR (100 MHz, DMSO-*d*6) δ 159.57, 156.19, 152.24, 151.67, 137.59, 137.34, 133.37, 130.06, 129.96, 129.92, 129.28, 129.10, 128.81, 128.57, 128.30, 128.08, 127.92, 127.65, 127.29, 123.67, 122.77, 121.06, 49.06, 16.50, 16.40, 14.62.; HRMS-ESI+ calculated for $\text{C}_{26}\text{H}_{23}\text{N}_6$ [M+H] $^{+}$ 419.1984, found: 419.1900.

4.2.2.56 (Z)-2-((E)-1-(1-(4-isopropylbenzyl)-1H-indol-3-yl)-3-phenylallylidene)hydrazine-1-carboximidamide (5x)

Yield 79 %, yellow solid; mp: 234–236 °C; ^1H NMR (400 MHz, DMSO-*d*6) δ 11.13 (d, $J = 46.7$ Hz, 1H), 8.90 (s, 2H), 8.29 – 8.22 (m, 1H), 8.02 – 7.92 (m, 1H), 7.66 (dd, $J = 16.4, 8.1$ Hz, 2H), 7.53 – 7.47 (m, 2H), 7.41 – 7.38 (m, 1H), 7.19 (s, 2H), 7.18 (s, 3H), 7.16 (s, 1H), 7.13 (d, $J = 6.9$ Hz, 1H), 7.08 – 7.02 (m, 1H), 5.52 – 5.31 (m, 2H), 2.41 (s, 1H), 1.99 – 1.90 (m, 2H), 1.14 (dd, $J = 10.9, 6.9$ Hz, 6H).; ^{13}C NMR (100 MHz, DMSO-*D*6) δ 159.66, 156.47, 156.28, 155.05, 151.65, 148.14, 137.34, 135.48, 133.32, 128.48, 127.79, 127.55, 126.99, 126.94, 126.87, 125.32, 125.25, 123.61, 123.00, 121.40, 113.87, 110.94, 49.60, 33.54, 25.13,

24.28, 18.66, 16.65.; HRMS-ESI+ calculated for C₂₈H₃₀N₅ [M+H]⁺ 436.2501, found: 436.2502.

4.2.2.57 (Z)-2-((E)-3-(2,3-dimethoxyphenyl)-1-(1-(4-(trifluoromethoxy)benzyl)-1H-indol-3-yl)allylidene)hydrazine-1-carboximidamide (6a)

Yield 84 %, yellow solid; mp: 228–230 °C; ¹H NMR (400 MHz, DMSO-*d*₆) δ 11.10 (d, J = 57.7 Hz, 1H), 8.86 (s, 1H), 8.31 – 8.24 (m, 1H), 7.74 (d, J = 64.1 Hz, 3H), 7.52 (dd, J = 10.5, 6.7 Hz, 2H), 7.41 – 7.28 (m, 4H), 7.23 – 7.11 (m, 2H), 5.51 (d, J = 10.1 Hz, 2H), 4.71 (s, 1H), 3.42 (s, 6H), 2.41 (s, 1H), 1.98 – 1.88 (m, 2H).; ¹³C NMR (100 MHz, DMSO-*d*₆) δ 170.15, 159.63, 159.17, 156.43, 156.27, 155.66, 155.09, 151.60, 148.73, 148.05, 137.61, 137.27, 133.29, 129.37, 125.27, 123.70, 123.16, 121.73, 121.56, 119.19, 114.15, 110.83, 48.99, 25.13, 21.21, 18.67, 18.61, 16.61.; HRMS-ESI+ calculated for C₂₈H₂₇F₃N₅O₃ [M+H]⁺ 538.2066, found: 538.2036.

4.2.2.58 (Z)-2-((E)-1-(1-(3-bromobenzyl)-1H-indol-3-yl)-3-(3-phenoxyphenyl)allylidene)hydrazine-1-carboximidamide (6b)

Yield 93 %, yellow solid; mp: 231–233 °C; ¹H NMR (400 MHz, DMSO-*d*₆) δ 11.10 (d, J = 53.1 Hz, 1H), 10.20 (d, J = 45.4 Hz, 1H), 9.70 – 9.26 (m, 1H), 8.87 (s, 2H), 8.33 – 8.10 (m, 1H), 7.74 (d, J = 65.9 Hz, 4H), 7.54 – 7.38 (m, 3H), 7.35 – 7.13 (m, 4H), 7.11 – 6.92 (m, 3H), 5.50 (d, J = 7.8 Hz, 1H), 4.71 (s, 2H), 2.41 (s, 1H), 1.98 – 1.89 (m, 2H).; ¹³C NMR (100 MHz, DMSO-*d*₆) δ 170.16, 159.64, 159.18, 156.44, 156.28, 155.67, 155.09, 151.60, 148.74, 146.80, 140.86, 137.25, 133.32, 131.30, 130.88, 130.18, 126.58, 125.25, 123.70, 123.18, 122.30, 121.58, 114.14, 110.84, 49.10, 25.13, 21.22, 18.68, 18.63, 16.64, 15.35.; HRMS-ESI+ calculated for C₃₁H₂₇BrN₅O [M+H]⁺ 564.1399, found: 566.1330.

4.2.2.59 (Z)-2-((E)-3-(4-(tert-butyl)phenyl)-1-(1-(2,4-difluorobenzyl)-1H-indol-3-yl)allylidene)hydrazine-1-carboximidamide (6c)

Yield 92 %, yellow solid; mp: 242–244 °C; ¹H NMR (400 MHz, DMSO-*d*₆) δ 11.09 (d, J = 54.1 Hz, 1H), 10.14 (s, 1H), 9.56 (s, 1H), 8.87 (s, 1H), 8.15 (s, 1H), 7.82 (s, 1H), 7.66 (s, 1H), 7.32 (d, J = 2.5 Hz, 1H), 7.30 – 7.28 (m, 1H), 7.27 – 7.25 (m, 1H), 7.24 (d, J = 1.2 Hz, 1H), 7.22 (s, 1H), 7.20 (d, J = 1.4 Hz, 1H), 7.18 – 7.17 (m, 1H), 7.14 (d, J = 7.0 Hz, 1H), 7.07 – 7.02 (m, 1H), 5.50 (s, 2H), 2.39 (s, 2H), 1.99 – 1.85 (m, 9H).; ¹³C NMR (100 MHz, DMSO-*d*₆) δ 170.17, 159.62, 159.17, 156.43, 156.27, 155.66, 155.11, 151.51, 148.76, 137.24, 133.15, 131.33, 125.16, 123.70, 123.20, 121.60, 121.26, 114.19, 112.37, 112.15, 110.58, 104.88, 104.62, 43.51, 25.13, 21.22, 18.68, 18.63, 16.62.; HRMS-ESI+ calculated for C₂₉H₃₀F₂N₅ [M+H]⁺ 486.2469, found: 486.2423.

4.2.2.60 (Z)-2-((E)-1-(1-(4-(trifluoromethyl)benzyl)-1H-indol-3-yl)-3-(4-(trifluoromethyl)phenyl)allylidene)hydrazine-1-carboximidamide (6d)

Yield 75 %, yellow solid; mp: 228–230 °C; ¹H NMR (400 MHz, DMSO-*d*₆) δ 10.12 (d, J = 24.0 Hz, 1H), 9.57 (s, 1H), 8.97 (d, J = 24.6 Hz, 1H), 8.14 (t, J = 84.0 Hz, 1H), 7.85 – 7.65 (m, 3H), 7.64 – 7.48 (m, 2H), 7.48 – 7.37 (m, 1H), 7.27 (s, 3H), 7.16 (dd, J = 17.6, 8.2 Hz, 2H), 4.01 (s, 2H), 2.06 – 1.70 (m, 4H).; ¹³C NMR (100 MHz, DMSO-*d*₆) δ 170.17, 159.67, 159.58, 159.23, 159.18, 156.45, 156.30, 155.67, 155.11, 151.57, 148.75, 142.91, 137.27, 133.49, 128.68, 128.11, 125.99, 125.26, 123.71, 123.21, 121.61, 114.23, 110.81, 25.13, 21.22, 18.64, 16.66.; HRMS-ESI+ calculated for C₂₇H₂₂F₆N₅ [M+H]⁺ 530.1742, found: 530.1745.

4.2.2.61 (Z)-2-((E)-1-(1-(3,5-dimethoxybenzyl)-1H-indol-3-yl)-3-(3,4-dimethoxyphenyl)allylidene)hydrazine-1-carboximidamide (6e)

Yield 73 %, yellow solid; mp: 216–218 °C; ¹H NMR (400 MHz, DMSO-*d*₆) δ 11.06 (dd, J = 42.7, 13.8 Hz, 1H), 10.13 (s, 1H), 9.56 (s, 1H), 8.87 (s, 1H), 8.30 – 8.18 (m, 1H), 7.72 (s, 1H), 7.65 (s, 1H), 7.50 (dt, J = 26.1, 11.7 Hz, 2H), 7.17 (ddd, J = 14.9, 14.0, 7.0 Hz, 4H), 6.39 (s, 2H), 5.38 (s, 1H), 3.91 – 3.45 (m, 12H), 1.97 – 1.89 (m, 3H).; ¹³C NMR (100 MHz, DMSO-*d*₆) δ 170.19, 170.16, 161.07, 159.74, 159.62, 159.17, 156.43, 156.25, 155.11, 151.69, 148.76, 140.34, 137.41, 133.45, 125.21, 123.61, 123.04, 121.46, 113.89, 110.95, 105.84, 105.80, 99.05, 55.65, 49.86, 25.13, 21.22, 18.63, 16.62.; HRMS-ESI+ calculated for C₂₉H₃₂N₅O₄ [M+H]⁺ 514.2412, found: 514.2409.

4.2.2.62 (Z)-2-((E)-1-(1-([1,1'-biphenyl]-4-ylmethyl)-1H-indol-3-yl)-3-(4-(tert-butyl)phenyl)allylidene)hydrazine-1-carboximidamide (6f)

Yield 91 %, yellow solid; mp: 228–230 °C; ¹H NMR (400 MHz, DMSO-*d*₆) δ 11.09 (d, J = 49.2 Hz, 1H), 8.86 (s, 1H), 8.36 – 7.93 (m, 3H), 7.60 (d, J = 8.0 Hz, 5H), 7.53 (d, J = 8.0 Hz, 1H), 7.43 (t, J = 7.6 Hz, 3H), 7.35 (d, J = 2.5 Hz, 1H), 7.33 (d, J = 1.3 Hz, 1H), 7.32 (d, J = 3.6 Hz, 1H), 7.18 (ddd, J = 14.9, 14.0, 6.9 Hz, 3H), 5.52 (s, 2H), 4.72 (s, 1H), 3.42 (s, 9H), 2.43 (s, 1H), 1.98 – 1.90 (m, 2H).; ¹³C NMR (100 MHz, DMSO-*d*₆) δ 170.16, 159.61, 159.44, 159.16, 156.42, 156.24, 155.65, 155.11, 151.69, 148.77, 140.11, 139.87, 137.37, 137.26, 133.40, 129.36, 128.16, 128.09, 127.93, 127.37, 127.07, 125.31, 123.67, 123.08, 121.49, 113.99, 110.97, 56.48, 49.54, 25.13, 21.22, 19.03, 18.68, 18.60, 16.62.; HRMS-ESI+ calculated for C₃₅H₃₆N₅ [M+H]⁺ 526.2931, found: 526.2928.

4.2.2.63 (Z)-2-((E)-1-(1-(4-(tert-butyl)benzyl)-1H-indol-3-yl)-3-(3,4-difluorophenyl)allylidene)hydrazine-1-carboximidamide (6g)

Yield 89 %, yellow solid; mp: 216–218 °C; ¹H NMR (400 MHz, DMSO-*d*₆) δ 11.09 (d, J = 54.1 Hz, 1H), 10.14 (s, 1H), 9.56 (s, 1H), 8.87 (s, 1H), 8.15 (s, 1H), 7.82 (s, 1H), 7.66 (s, 1H),

7.32 (d, $J = 2.5$ Hz, 1H), 7.30 – 7.28 (m, 1H), 7.27 – 7.25 (m, 1H), 7.24 (d, $J = 1.2$ Hz, 1H), 7.22 (s, 1H), 7.20 (d, $J = 1.4$ Hz, 1H), 7.18 – 7.17 (m, 1H), 7.14 (d, $J = 7.0$ Hz, 1H), 7.07 – 7.02 (m, 1H), 5.50 (s, 2H), 2.39 (s, 2H), 1.99 – 1.85 (m, 9H).; ^{13}C NMR (100 MHz, DMSO-*d*6) δ 170.17, 159.62, 159.17, 156.43, 156.27, 155.66, 155.11, 151.51, 148.76, 137.24, 133.15, 131.33, 125.16, 123.70, 123.20, 121.60, 121.26, 114.19, 112.37, 112.15, 110.58, 104.88, 104.62, 43.51, 25.13, 21.22, 18.68, 18.63, 16.62.; HRMS-ESI+ calculated for $\text{C}_{29}\text{H}_{30}\text{F}_2\text{N}_5$ $[\text{M}+\text{H}]^+$ 486.2408, found: 486.2411.

4.2.2.64 (Z)-2-((E)-3-(4-(benzyloxy)phenyl)-1-(1-(4-methylbenzyl)-1H-indol-3-yl)allylidene)hydrazine-1-carboximidamide (6h)

Yield 87 %, yellow solid; mp: 224–226 °C; ^1H NMR (400 MHz, DMSO-*d*6) δ 11.07 (d, $J = 45.9$ Hz, 1H), 10.12 (s, 1H), 9.55 (s, 1H), 8.29 – 8.19 (m, 1H), 7.65 (s, 1H), 7.55 – 7.51 (m, 2H), 7.47 (d, $J = 5.4$ Hz, 1H), 7.45 (s, 2H), 7.40 (t, $J = 7.5$ Hz, 3H), 7.34 (dd, $J = 7.1, 1.5$ Hz, 1H), 7.19 – 7.15 (m, 2H), 7.11 (d, $J = 8.1$ Hz, 2H), 6.96 (d, $J = 8.6$ Hz, 1H), 6.33 (s, 1H), 5.42 (d, $J = 13.1$ Hz, 2H), 5.07 (d, $J = 5.7$ Hz, 2H), 2.41 (s, 1H), 2.24 (s, 1H), 1.98 – 1.95 (m, 2H), 1.90 (s, 3H).; ^{13}C NMR (100 MHz, DMSO-*d*6) δ 170.14, 159.60, 159.16, 158.52, 156.42, 156.23, 155.10, 151.70, 137.47, 137.30, 137.18, 135.00, 133.33, 130.22, 129.59, 128.89, 128.32, 128.29, 127.54, 125.28, 123.60, 122.97, 121.40, 114.55, 113.82, 110.96, 69.71, 49.69, 25.13, 21.22, 21.12, 18.61, 16.59.; HRMS-ESI+ calculated for $\text{C}_{33}\text{H}_{32}\text{N}_5\text{O}$ $[\text{M}+\text{H}]^+$ 514.2554, found: 514.2559.

4.2.2.65 (Z)-2-((E)-1-(1-(2,5-difluorobenzyl)-1H-indol-3-yl)-3-(4-isopropylphenyl)allylidene)hydrazine-1-carboximidamide (6i)

Yield 89 %, yellow solid; mp: 208–210 °C; ^1H NMR (400 MHz, DMSO-*d*6) δ 11.17 (s, 1H), 10.13 (s, 1H), 9.56 (s, 1H), 8.88 (s, 1H), 8.30 – 8.17 (m, 1H), 7.81 (d, $J = 9.9$ Hz, 1H), 7.66 (s, 1H), 7.52 (dd, $J = 9.5, 4.4$ Hz, 2H), 7.34 – 7.27 (m, 2H), 7.25 – 7.23 (m, 1H), 7.21 (d, $J = 1.3$ Hz, 1H), 7.19 (d, $J = 4.4$ Hz, 1H), 7.16 (dd, $J = 9.3, 2.3$ Hz, 1H), 6.95 (ddd, $J = 8.9, 5.6, 3.2$ Hz, 1H), 5.52 (s, 2H), 4.04 – 3.92 (m, 1H), 2.40 (s, 2H), 1.98 – 1.89 (m, 6H).; ^{13}C NMR (100 MHz, DMSO-*d*6) δ 170.14, 159.72, 159.62, 159.18, 156.44, 156.29, 155.08, 151.50, 148.74, 137.24, 133.19, 125.14, 123.73, 123.28, 121.66, 117.77, 117.53, 116.82, 116.67, 116.38, 116.13, 114.32, 110.56, 43.76, 25.13, 21.22, 18.63, 16.62.; HRMS-ESI+ calculated for $\text{C}_{28}\text{H}_{28}\text{F}_2\text{N}_5$ $[\text{M}+\text{H}]^+$ 472.2274, found: 472.2270.

4.2.2.66 (Z)-2-((E)-1-(1-(4-fluorobenzyl)-1H-indol-3-yl)-3-(4-(trifluoromethyl)phenyl)allylidene)hydrazine-1-carboximidamide (6j)

Yield 93 %, yellow solid; mp: 217–219 °C; ^1H NMR (400 MHz, DMSO-*d*6) δ 11.13 (s, 1H), 10.11 (s, 1H), 9.64 – 9.21 (m, 1H), 8.33 – 7.90 (m, 2H), 7.65 (s, 2H), 7.60 – 7.40 (m, 3H), 7.32

(dd, $J = 8.6, 5.5$ Hz, 2H), 7.24 – 7.00 (m, 4H), 5.54 – 5.40 (m, 2H), 2.41 (s, 1H), 1.96 – 1.89 (m, 2H).; ^{13}C NMR (100 MHz, DMSO- d_6) δ 170.16, 163.16, 160.74, 159.60, 159.15, 156.40, 156.23, 151.66, 137.22, 134.28, 134.25, 133.24, 129.70, 129.62, 125.29, 123.65, 123.07, 121.49, 115.97, 115.75, 114.01, 110.90, 49.09, 21.21, 18.59, 16.58.; HRMS-ESI+ calculated for $\text{C}_{26}\text{H}_{22}\text{F}_4\text{N}_5$ $[\text{M}+\text{H}]^+$ 480.1811, found: 480.1762.

4.2.2.67 (Z)-2-((E)-3-(2,4-difluorophenyl)-1-(1-(2-fluorobenzyl)-1H-indol-3-yl)allylidene)hydrazine-1-carboximidamide (6k)

Yield 92 %, yellow solid; mp: 213–215 °C; ^1H NMR (400 MHz, DMSO- d_6) δ 11.15 (d, $J = 45.7$ Hz, 1H), 8.94 (s, 2H), 8.29 – 8.16 (m, 1H), 7.48 (d, $J = 8.1$ Hz, 1H), 7.26 (d, $J = 4.4$ Hz, 5H), 7.20 (d, $J = 6.4$ Hz, 1H), 7.17 (s, 1H), 7.15 – 7.11 (m, 1H), 7.08 (dd, $J = 11.2, 5.5$ Hz, 1H), 5.53 (s, 2H), 2.40 (s, 1H), 1.97 – 1.89 (m, 3H).; ^{13}C NMR (100 MHz, DMSO- d_6) δ 159.65, 156.49, 156.33, 155.05, 151.49, 137.33, 133.28, 130.39, 130.31, 129.81, 125.19, 125.15, 124.85, 124.70, 123.69, 123.16, 121.56, 116.07, 115.86, 114.13, 110.61, 43.93, 25.13, 18.68, 16.66.; HRMS-ESI+ calculated for $\text{C}_{25}\text{H}_{21}\text{F}_3\text{N}_5$ $[\text{M}+\text{H}]^+$ 448.1749, found: 448.1712.

4.2.2.68 (Z)-2-((E)-1-(1-(4-bromobenzyl)-1H-indol-3-yl)-3-(4-(tert-butyl)phenyl)allylidene)hydrazine-1-carboximidamide (6l)

Yield 73 %, yellow solid; mp: 204–206 °C; ^1H NMR (400 MHz, DMSO- d_6) δ 11.16 (s, 1H), 8.86 (s, 1H), 8.28 (d, $J = 7.4$ Hz, 1H), 8.23 (s, 1H), 7.65 (s, 1H), 7.52 (d, $J = 8.4$ Hz, 3H), 7.46 (d, $J = 7.6$ Hz, 1H), 7.21 (s, 2H), 7.19 (s, 2H), 7.17 (dd, $J = 3.9, 1.2$ Hz, 1H), 7.14 (d, $J = 6.9$ Hz, 1H), 5.46 (s, 2H), 4.57 (d, $J = 101.4$ Hz, 3H), 3.33 (dd, $J = 88.1, 6.9$ Hz, 6H), 2.41 (s, 3H), 1.98 – 1.96 (m, 1H).; ^{13}C NMR (100 MHz, DMSO- d_6) δ 159.62, 156.43, 156.36, 156.34, 156.26, 155.09, 151.67, 151.61, 137.51, 137.47, 137.32, 137.24, 133.31, 131.97, 129.82, 129.72, 125.29, 123.74, 123.69, 123.12, 121.54, 121.11, 114.08, 110.87, 49.18, 25.14, 18.69, 18.62, 16.62.; HRMS-ESI+ calculated for $\text{C}_{29}\text{H}_{31}\text{BrN}_5$ $[\text{M}+\text{H}]^+$ 528.1763, found: 530.1689.

4.2.2.69 (Z)-2-((E)-3-(4-(tert-butyl)phenyl)-1-(1-(4-fluorobenzyl)-1H-indol-3-yl)allylidene)hydrazine-1-carboximidamide (6m)

Yield 96 %, yellow solid; mp: 182–184 °C; ^1H NMR (400 MHz, DMSO- d_6) δ 11.12 (d, $J = 48.4$ Hz, 1H), 10.15 (s, 1H), 9.57 (s, 1H), 8.91 (s, 2H), 8.28 – 8.24 (m, 1H), 7.67 (s, 2H), 7.50 (d, $J = 8.1$ Hz, 1H), 7.35 – 7.33 (m, 1H), 7.31 (d, $J = 5.5$ Hz, 1H), 7.25 (s, 3H), 7.19 (s, 1H), 7.17 (s, 1H), 7.15 (s, 1H), 7.14 – 7.11 (m, 1H), 5.46 (s, 2H), 2.41 (s, 1H), 2.02 – 1.83 (m, 9H).; ^{13}C NMR (100 MHz, DMSO- d_6) δ 170.14, 163.15, 160.73, 159.64, 159.20, 156.47, 156.29, 155.70, 155.06, 151.60, 137.21, 134.29, 133.26, 129.71, 129.68, 129.63, 125.28, 123.65, 123.06, 121.48, 115.96, 115.75, 113.99, 110.90, 49.08, 25.13, 21.23, 18.65, 16.65.; HRMS-ESI+ calculated for $\text{C}_{29}\text{H}_{31}\text{FN}_5$ $[\text{M}+\text{H}]^+$ 468.2563, found: 468.2564.

4.2.2.70 (Z)-2-((E)-1-(1-([1,1'-biphenyl]-4-ylmethyl)-1H-indol-3-yl)-3-(3,4-dimethoxyphenyl)allylidene)hydrazine-1-carboximidamide (6n)

Yield 92 %, yellow solid; mp: 252-254°C; ¹H NMR (400 MHz, DMSO-*d*₆) δ 11.14 (s, 1H), 8.85 (s, 1H), 8.36 – 8.19 (m, 2H), 7.75 – 7.69 (m, 1H), 7.61 (d, J = 8.3 Hz, 5H), 7.54 (d, J = 8.1 Hz, 1H), 7.44 (dd, J = 10.3, 4.8 Hz, 3H), 7.36 – 7.30 (m, 3H), 7.26 – 7.09 (m, 3H), 5.54 (d, J = 17.5 Hz, 2H), 3.89 – 3.41 (m, 6H), 2.43 (s, 3H), 1.99 – 1.89 (m, 1H).; ¹³C NMR (100 MHz, DMSO-*d*₆) δ 170.14, 159.67, 159.60, 159.16, 156.41, 156.23, 155.10, 151.76, 151.69, 140.12, 139.88, 137.37, 137.27, 133.40, 129.44, 129.36, 128.17, 128.09, 127.93, 127.89, 127.38, 127.08, 125.31, 123.67, 123.08, 121.49, 113.99, 110.97, 49.55, 25.13, 21.22, 18.60, 16.61.; HRMS-ESI+ calculated for C₃₃H₃₂N₅O₂ [M+H]⁺ 530.2556, found: 530.2568.

4.2.2.71 (Z)-2-((E)-1-(1-(4-(tert-butyl)benzyl)-1H-indol-3-yl)-3-(4-(tert-butyl)phenyl)allylidene)hydrazine-1-carboximidamide (6o)

Yield 82 %, yellow solid; mp: 218-220°C; ¹H NMR (400 MHz, DMSO-*d*₆) δ 11.11 (d, J = 47.1 Hz, 1H), 10.14 (s, 1H), 9.56 (s, 1H), 8.92 (s, 2H), 8.24 (d, J = 10.2 Hz, 1H), 7.66 (s, 2H), 7.51 (d, J = 8.0 Hz, 1H), 7.33 (s, 1H), 7.31 (s, 1H), 7.25 (s, 3H), 7.19 (s, 1H), 7.16 (d, J = 7.6 Hz, 1H), 7.12 (d, J = 7.0 Hz, 1H), 5.42 (s, 2H), 2.41 (s, 2H), 1.98 – 1.89 (m, 9H), 1.30 – 1.15 (m, 9H).; ¹³C NMR (100 MHz, DMSO-*d*₆) δ 170.14, 159.70, 159.68, 159.61, 159.19, 156.46, 156.27, 155.07, 151.66, 150.37, 137.34, 135.11, 133.33, 127.31, 127.26, 127.21, 125.85, 125.79, 125.48, 125.23, 123.60, 123.00, 121.40, 113.86, 110.94, 49.49, 34.66, 31.52, 25.13, 21.22, 18.68, 18.65, 16.64.; HRMS-ESI+ calculated for C₃₃H₄₀N₅ [M+H]⁺ 506.3284, found: 506.3284.

4.2.2.72 (Z)-2-((E)-1-(1-(3-(benzyloxy)benzyl)-1H-indol-3-yl)-3-(4-(benzyloxy)phenyl)allylidene)hydrazine-1-carboximidamide (6p)

Yield 85 %, yellow solid; mp: 240-242°C; ¹H NMR (400 MHz, DMSO-*d*₆) δ 11.30 – 10.95 (m, 1H), 10.10 (d, J = 27.4 Hz, 1H), 9.51 (d, J = 49.3 Hz, 1H), 8.84 (d, J = 59.6 Hz, 2H), 8.33 – 7.87 (m, 2H), 7.74 (dd, J = 32.5, 23.8 Hz, 4H), 7.53 (dd, J = 7.9, 5.7 Hz, 1H), 7.49 – 7.43 (m, 2H), 7.39 (dd, J = 10.2, 4.2 Hz, 2H), 7.36 – 7.31 (m, 2H), 7.31 – 7.22 (m, 4H), 7.21 – 7.12 (m, 2H), 7.05 (dd, J = 28.6, 8.2 Hz, 1H), 6.98 – 6.89 (m, 2H), 6.81 (d, J = 7.6 Hz, 1H), 5.54 – 5.31 (m, 1H), 5.14 – 4.99 (m, 2H), 4.66 (s, 2H), 2.41 (s, 1H), 1.98 – 1.89 (m, 2H).; ¹³C NMR (100 MHz, DMSO-*d*₆) δ 170.13, 159.62, 159.20, 158.93, 158.50, 156.46, 156.28, 155.06, 154.46, 151.66, 139.65, 137.47, 137.43, 137.36, 137.30, 133.38, 130.23, 128.92, 128.89, 128.86, 128.33, 128.31, 128.25, 125.25, 123.62, 123.04, 121.45, 119.87, 114.50, 114.41, 113.92, 113.83, 110.93, 69.63, 49.76, 25.13, 21.23, 18.64, 16.64.; HRMS-ESI+ calculated for C₃₉H₃₆N₅O₂ [M+H]⁺ 606.2905, found: 606.2909.

4.2.2.73 (Z)-2-((E)-1-(1-(4-butylbenzyl)-1H-indol-3-yl)-3-(4-**(trifluoromethyl)phenyl)allylidene)hydrazine-1-carboximidamide (6q)**

Yield 89 %, yellow solid; mp: 241-243°C; ¹H NMR (400 MHz, DMSO-*d*6) δ 11.14 (s, 1H), 8.86 (s, 1H), 8.33 – 8.10 (m, 2H), 7.66 (s, 4H), 7.55 – 7.42 (m, 2H), 7.19 (dd, J = 10.7, 3.8 Hz, 2H), 7.15 (s, 2H), 7.13 (d, J = 3.2 Hz, 2H), 7.11 (s, 1H), 5.41 (s, 2H), 2.41 (s, 2H), 1.99 – 1.86 (m, 2H), 1.53 – 1.39 (m, 2H), 1.30 – 1.15 (m, 2H), 0.84 (t, J = 7.3 Hz, 3H).; ¹³C NMR (100 MHz, DMSO-*d*6) δ 170.15, 159.62, 159.17, 156.43, 156.24, 155.10, 151.69, 142.10, 137.33, 135.27, 133.33, 128.99, 128.93, 127.59, 127.49, 125.26, 123.60, 122.99, 121.41, 113.84, 110.94, 49.65, 34.88, 33.55, 25.13, 22.18, 21.22, 18.62, 16.61, 14.20.; HRMS-ESI+ calculated for C₃₀H₃₁F₃N₅ [M+H]⁺ 518.2569, found: 518.2573.

4.2.2.74 (Z)-2-((E)-3-(4-(tert-butyl)phenyl)-1-(1-(4-(trifluoromethyl)benzyl)-1H-indol-3-yl)allylidene)hydrazine-1-carboximidamide (6r)

Yield 88 %, yellow solid; mp: 241-243°C; ¹H NMR (400 MHz, DMSO-*d*6) δ 11.03 (d, J = 16.9 Hz, 1H), 8.87 (d, J = 14.8 Hz, 1H), 7.79 – 7.59 (m, 3H), 7.54 – 7.46 (m, 1H), 7.33 – 7.26 (m, 2H), 7.23 – 7.17 (m, 1H), 7.16 – 7.10 (m, 2H), 7.09 – 7.04 (m, 1H), 7.00 (d, J = 8.7 Hz, 2H), 6.77 – 6.71 (m, 1H), 6.20 (ddd, J = 6.5, 5.1, 2.9 Hz, 1H), 5.66 – 5.53 (m, 2H), 3.86 – 3.40 (m, 9H), 2.22 (s, 1H), 1.94 (dd, J = 25.7, 8.1 Hz, 2H).; ¹³C NMR (100 MHz, DMSO-*d*6) δ 170.13, 159.60, 159.16, 156.41, 156.32, 156.16, 155.09, 153.01, 147.74, 147.65, 147.60, 139.49, 129.24, 128.91, 128.86, 128.67, 128.26, 121.77, 121.58, 121.48, 119.23, 116.32, 108.59, 61.31, 56.22, 51.90, 25.13, 21.21, 18.60, 16.98.; HRMS-ESI+ calculated for C₃₀H₃₀F₃N₅Na [M+Na]⁺ 540.2251, found: 540.2244.

4.2.2.75 (Z)-2-((E)-1-(1-([1,1'-biphenyl]-4-ylmethyl)-1H-indol-3-yl)-3-(3-phenoxyphenyl)allylidene)hydrazine-1-carboximidamide (6s)

Yield 85 %, yellow solid; mp: 241-243°C; ¹H NMR (400 MHz, DMSO-*d*6) δ 8.84 (d, J = 13.7 Hz, 1H), 8.39 – 8.19 (m, 1H), 7.92 – 7.80 (m, 1H), 7.76 – 7.68 (m, 1H), 7.65 – 7.58 (m, 4H), 7.54 (d, J = 7.9 Hz, 2H), 7.46 – 7.41 (m, 4H), 7.36 – 7.32 (m, 3H), 7.27 – 7.10 (m, 7H), 7.07 – 6.93 (m, 4H), 5.57 (dd, J = 25.4, 9.4 Hz, 2H), 2.44 (s, 1H).; ¹³C NMR (100 MHz, DMSO-*d*6) δ 159.58, 156.21, 151.71, 140.13, 140.08, 139.89, 137.38, 137.27, 136.74, 136.66, 133.40, 130.58, 129.37, 129.12, 128.93, 128.34, 128.27, 128.09, 127.98, 127.94, 127.51, 127.39, 127.10, 127.08, 125.32, 123.85, 123.67, 123.09, 122.51, 121.49, 119.06, 118.94, 118.66, 114.00, 110.97, 49.55, 16.60.; HRMS-ESI+ calculated for C₃₇H₃₂N₅O [M+Na]⁺ 562.2607, found: 562.2603.

4.2.2.76 (Z)-2-((E)-3-(4-(benzyloxy)phenyl)-1-(1-(4-butylbenzyl)-1H-indol-3-yl)allylidene)hydrazine-1-carboximidamide (6t)

Yield 89 %, yellow solid; mp: 241-243°C; ¹H NMR (400 MHz, DMSO-*d*₆) δ 11.18 (s, 1H), 8.95 (s, 2H), 8.29 – 8.21 (m, 2H), 7.73 (s, 1H), 7.51 – 7.45 (m, 2H), 7.28 (s, 6H), 7.20 (d, J = 1.1 Hz, 1H), 7.19 (d, J = 0.9 Hz, 1H), 7.18 – 7.16 (m, 1H), 7.15 (s, 2H), 7.13 (s, 2H), 7.11 (d, J = 2.4 Hz, 1H), 5.41 (s, 2H), 4.49 (s, 2H), 2.41 (s, 2H), 1.98 – 1.82 (m, 2H), 1.52 – 1.41 (m, 2H), 1.30 – 1.17 (m, 2H), 0.84 (t, J = 7.3 Hz, 3H).; ¹³C NMR (100 MHz, DMSO-*d*₆) δ 170.13, 159.69, 159.61, 159.41, 159.21, 156.34, 156.29, 151.66, 142.13, 142.09, 137.38, 137.33, 135.37, 135.28, 133.39, 133.32, 129.00, 128.92, 127.59, 127.49, 125.26, 123.67, 123.60, 123.05, 122.98, 121.44, 121.40, 113.85, 110.93, 49.65, 34.88, 33.54, 22.17, 21.22, 16.64, 14.20.; HRMS-ESI+ calculated for C₃₆H₃₈N₅O [M+Na]⁺ 556.3076, found: 556.3029.

4.2.2.77 (Z)-2-((E)-1-(1-(4-butylbenzyl)-1H-indol-3-yl)-3-(2,5-dimethoxyphenyl)allylidene)hydrazine-1-carboximidamide (6u)

Yield 92 %, yellow solid; mp: 241-243°C; ¹H NMR (400 MHz, DMSO-*d*₆) δ 11.17 (s, 1H), 8.93 (s, 2H), 8.29 – 8.20 (m, 2H), 7.69 (d, J = 14.9 Hz, 1H), 7.49 (d, J = 8.0 Hz, 1H), 7.26 (s, 5H), 7.20 (dd, J = 7.1, 1.1 Hz, 1H), 7.17 (d, J = 1.0 Hz, 1H), 7.15 (s, 1H), 7.13 (s, 1H), 7.12 – 7.10 (m, 1H), 5.41 (s, 2H), 4.39 (d, J = 87.6 Hz, 6H), 2.48 (s, 1H), 2.41 (s, 2H), 1.52 – 1.42 (m, 2H), 1.31 – 1.18 (m, 2H), 0.85 (t, J = 7.3 Hz, 3H).; ¹³C NMR (100 MHz, DMSO-*d*₆) δ 159.59, 156.32, 156.26, 156.22, 151.66, 142.14, 142.09, 137.41, 137.33, 135.34, 135.28, 133.39, 133.32, 129.01, 128.93, 127.57, 127.49, 125.30, 125.26, 123.61, 122.98, 121.40, 113.85, 111.01, 110.94, 49.64, 34.89, 33.55, 22.18, 16.63, 14.20.; HRMS-ESI+ calculated for C₃₁H₃₉N₆O₂ [M+NH₄]⁺ 527.3157, found: 527.3162.

4.3 *In-vitro* Evaluation

4.3.1 Pyrrol-2-yl-phenyl allylidene hydrazine carboximidamide analogues

The AChE and BACE 1 inhibitory activities of pyrrol-2-yl-phenyl allylidene hydrazine carboximidamides against AChE and BACE 1 were evaluated by the Ellman assay and Fluorescence resonance energy transfer (FRET) assay, respectively using donepezil and β -Secretase Inhibitor IV as reference standards. The results are shown in **Table 23-25**.

Table 23 indicates the results for compounds **1a-1ak** of the first series where ring A was substituted with electron-withdrawing and donating substituents and ring B was unsubstituted. Overall, the results indicate that the hypothesis that the extension of our reported compound could result in dual inhibition of AChE and BACE 1 was correct. The compounds were active against both enzymes; however, with the introduction of AChE inhibition, the BACE 1 inhibitory potential was decreased.

It was found that strong electron-withdrawing substituents like 4-nitro or 2,4-dichloro on ring A enhanced the AChE inhibition but decreased BACE 1 inhibitory activity. Conversely, the substitution of electron donating groups on ring A enhanced the BACE 1 inhibitory potential but decreased the AChE inhibitory potency of compounds. It was noticed that substituting ring A alone with either electron donating or electron withdrawing moieties was not favorable for BACE 1 inhibition, and compared to the earlier reported compound, the activity was decreased. However, if phenyl is replaced with pyridine at ring A, BACE 1 inhibition is not impacted much as it exhibited an IC_{50} of 13.74 μ M but affects AChE inhibition as the activity against AChE was poor.

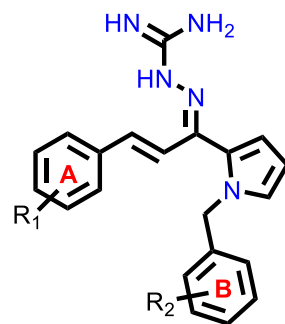
In the second series (compounds **2a-2y**), ring A was not substituted, and ring B was substituted with various electron-withdrawing and donating substituents. It was observed that as compared to ortho, the para substitution of electron-withdrawing groups on ring B (compounds **2o**, **2r**, **2t**, and **2u**) was favorable for AChE inhibition. Also, for BACE 1 inhibition, the substitution of electron-donating substituents on ring B was favored (compounds **2a**, **2d**, **2i**, and **2m**). Increasing the bulk at the 4-position of ring B favored AChE inhibition but compromised BACE 1 inhibition, as seen in compounds **2q**, **2x**, and **2y**. Overall, it can be noted that the electron-withdrawing substitution on ring B favors AChE inhibition, and electron-donating groups promote BACE 1 inhibition.

In the previous two series, electron withdrawing group substitution on any of the rings favored AChE inhibition, and electron-donating substituents on ring A or B were favorable to BACE 1 inhibition. Also, the substitution of bulky groups had impacted the activity. Therefore, in the third series, both the rings (A and B) were substituted, and in particular, the effect of bulky or

electron-withdrawing substituents was studied. It was expected that the substitution on both rings may potentiate the AChE inhibition. However, not much change in AChE inhibition was observed by substituting bulky or electron-withdrawing substituents on both rings. Compound **3s** with tert-butyl substituent on both the rings was the most potent AChE inhibitor of all these compounds, showing an IC₅₀ value of 48.06 μM. However, it did affect BACE 1 inhibition, and the IC₅₀ values increased, indicating that bulky or electron-withdrawing substituents on any ring or both rings were unfavorable for BACE 1 inhibition.

Structure-Activity Relationship

Based on the compounds' AChE and BACE 1 inhibitory activity, their structure-activity relationship was analyzed. The potential of the compounds to inhibit AChE and BACE 1 varied with respect to the substitutions on the rings A and B. In the case of molecular modeling studies of AChE, ring B occupies the CAS site of AChE, while ring A is anchored to the PAS site. This same binding pattern is mainly driven by hydrogen bonding and π - π stacking interactions, in which the aromatic ring B of the *N*-benzyl interacts with the Trp86 of CAS, ring A interacts with Trp286 of PAS, pyrrole interacts with residue Tyr337 Tyr341, Phe338 and guanidine interacts with the catalytic amino acid residues of AChE (Ser203, Glu202 and His447). The presence of substitution (**1j** and **1k**) on ring A resulted in better AChE inhibition in comparison to their unsubstituted counterparts (**1a**). As represented in **Tables 10** and **11**, this might have provided additional binding stability to the ligand through enhanced hydrophobic interactions with the CAS and PAS of AChE. When conducting modeling studies on BACE 1, it is observed that ring B occupies the S1 region, ring A is anchored to the S3 site, and the guanidine group can form H-bonding interactions with catalytic aspartate dyad that is, Asp32 and Asp228, respectively. When ring A alone was replaced with pyridine (compounds **1h**), it was observed that compound **1h** had a high docking score and strong inhibition. One possible explanation could be attributed to the robust interactions that were observed during the docking simulation: (i) ring B occupied S1 active site region with the pyrrole scaffold π - π stacked to Phe108; (ii) aminoguanidinium nitrogen formed hydrogen bonding interactions with catalytic aspartate dyad (Asp228 and Asp32). Introducing EDG and EWG on ring A alone gave less potent molecules, probably due to weaker interactions with the enzymatic active site of BACE 1. Placing 4-butyl and 2-CF₃,4-F on ring B (**2q** and **2o**), although showed good interactions in docking, were more favorable for balanced AChE/BACE 1 dual inhibition, which may be attributed to strong hydrophobic interactions in S1 and S3 region of BACE 1, occupying CAS and PAS of AChE and interacts with the catalytic amino acid residues of BACE 1 and AChE (Asp32/Asp228 and Glu202).

Table 23. Inhibitory potential of compounds **1a-1a**, **1aa-1ak** (Series I) against AChE and BACE 1

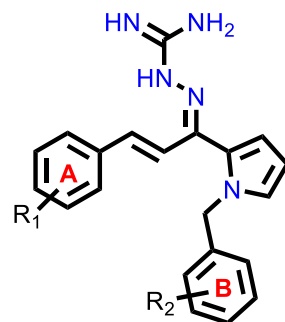
Compound Code	R ₁	R ₂	Mol. Wt.	EeAChE IC ₅₀ (μM) ± SD	EeAChE PIC ₅₀ (μM)	hBACE 1 IC ₅₀ (μM) ± SD	hBACE 1 PIC ₅₀ (μM)
1a	-H	-H	343.43	215.30 ± 0.14	4.11	169.90 ± 1.27	4.14
1b	4-Cl	-H	377.88	167.90 ± 2.40	4.37	171.30 ± 0.57	4.01
1c	4-F	-H	361.17	183.25 ± 0.49	4.11	175.45 ± 1.91	4.23
1d	3-phenylacetaldehyde	-H	357.46	209.85 ± 0.35	3.83	141.95 ± 1.77	4.93
1e	3-phenylpropionaldehyde	-H	371.49	186.45 ± 2.47	3.86	173.30 ± 2.26	3.93
1f	5-methoxy indole	-H	412.50	241.35 ± 0.92	4.17	164.60 ± 0.14	4.05
1g	furan-2-yl	-H	333.40	249.55 ± 1.63	4.11	147.65 ± 1.91	4.05
1h	pyridin-2-yl	-H	344.42	222.60 ± 2.40	4.18	13.74 ± 0.77	4.82
1i	2-Cl	-H	377.88	173.95 ± 0.92	4.14	183.75 ± 0.92	4.01
1j	4-NO ₂	-H	388.43	43.25 ± 0.41	4.21	194.30 ± 0.99	4.14

1k	2,4-di-Cl	-H	411.10	55.45 ± 0.91	3.73	207.95 ± 1.91	3.88
1l	3-benzyloxy	-H	449.22	210.75 ± 0.07	4.22	219.20 ± 0.71	5.03
1m	2-NO ₂	-H	388.43	179.10 ± 1.56	3.83	210.50 ± 1.13	4.89
1n	3-NO ₂	-H	388.43	163.45 ± 2.76	3.67	208.90 ± 1.27	4.91
1o	biphenyl-4-yl	-H	419.21	204.80 ± 1.56	3.90	178.20 ± 0.57	4.89
1p	3,4-di-Cl	-H	412.32	203.90 ± 0.99	4.31	195.95 ± 1.34	3.87
1q	3-F	-H	361.42	182.85 ± 0.49	4.08	186.90 ± 2.69	4.78
1r	4-CN	-H	368.44	211.85 ± 1.20	4.33	177.90 ± 0.14	3.69
1s	3-CN	-H	368.44	199.80 ± 1.41	3.84	144.95 ± 2.33	3.69
1t	2,5-di-F	-H	379.41	176.90 ± 1.98	4.33	177.05 ± 2.19	3.70
1u	2,4-di-F	-H	379.41	1950 ± 2.55	4.25	187.20 ± 2.55	3.99
1v	2-F	-H	361.42	172.30 ± 1.56	4.25	174.45 ± 1.48	4.15
1w	4-CH ₃	-H	357.46	194.70 ± 2.83	3.77	168.60 ± 1.56	3.85
1x	4-OCH ₃	-H	373.46	139.15 ± 0.35	4.36	173.05 ± 1.06	3.71
1y	4-CF ₃	-H	411.43	144.25 ± 2.47	4.37	175.85 ± 0.99	3.67
1z	3,4-di-F	-H	379.41	172.65 ± 2.47	4.26	179.10 ± 0.99	4.08
1aa	3-phenoxy	-H	435.53	181.50 ± 0.99	4.20	177.60 ± 1.56	3.84
1ab	4-tertbutyl	-H	399.54	174.50 ± 0.14	4.37	161.30 ± 0.14	3.73
1ac	3,4-di-OCH ₃	-H	403.49	145.90 ± 2.40	4.12	114.20 ± 1.70	3.75
1ad	4-isopropyl	-H	385.52	203.80 ± 1.70	4.42	107.55 ± 1.20	3.65
1ae	3-OCH ₃	-H	373.46	206.65 ± 0.49	4.66	134.05 ± 0.21	3.70

1af	2,6-difluoro,4-bromo	-H	458.31	211.00 ± 0.14	4.78	154.45 ± 0.92	3.70
1ag	4-benzyloxy	-H	449.56	223.35 ± 0.78	3.71	162.60 ± 1.70	4.11
1ah	4-Dimethylamino	-H	386.50	213.35 ± 1.48	3.84	151.85 ± 0.49	3.97
1ai	3-Br	-H	422.23	243.65 ± 0.78	3.78	151.35 ± 1.91	4.09
1aj	4-Br	-H	422.33	262.15 ± 2.62	3.81	161.70 ± 0.71	3.75
1ak	2,5-di-OCH ₃	-H	403.49	218.70 ± 1.70	4.25	178.25 ± 0.92	3.75
Donepezil			-	0.04 ± 0.01	7.40		
β-Secretase Inhibitor IV			-			0.02 ± 0.01	7.70

*Results are presented as mean ± SD, n=3, eeAChE indicates AChE from electric eel, and hBACE 1 indicates human BACE 1.

Table 24. Inhibitory activities of compounds **2a-2y** (Series-II) against AChE and BACE 1



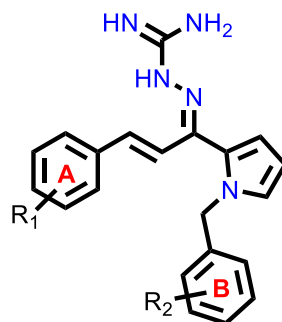
Compound Code	R ₁	R ₂	Mol. Wt.	EeAChE IC ₅₀ (μM) ± SD	EeAChE PIC ₅₀ (μM)	hBACE 1 IC ₅₀ (μM) ± SD	hBACE 1 PIC ₅₀ (μM)
2a	-H	3,5-di-OCH ₃	403.49	231.00 ± 2.26	4.33	95.75 ± 3.45	3.70

2b	-H	4-Cl	377.88	248.35 ± 0.78	4.25	140.75 ± 0.92	3.99
2c	-H	4-Br	422.33	204.55 ± 1.48	4.25	131.10 ± 1.13	4.15
2d	-H	4-OCF ₃	427.43	231.60 ± 1.27	3.77	86.19 ± 0.38	3.85
2e	-H	biphenyl-4-yl	419.53	246.40 ± 4.67	4.36	135.00 ± 0.14	3.71
2f	-H	4-CF ₃	411.43	203.10 ± 3.96	4.37	139.85 ± 1.34	3.67
2g	-H	4-F	361.42	172.35 ± 1.48	4.26	134.60 ± 2.83	4.08
2h	-H	2-CN	368.44	203.35 ± 2.90	4.20	135.50 ± 0.28	3.84
2i	-H	4-OCHF ₂	409.44	195.80 ± 0.99	4.37	15.35 ± 0.24	3.73
2j	-H	2,5-di-F	379.41	153.30 ± 1.98	4.12	107.45 ± 3.04	3.75
2k	-H	4-bromo,2-fluoro	440.32	183.20 ± 1.27	3.54	201.75 ± 1.48	3.63
2l	-H	2,5-di-Cl	412.32	75.57 ± 3.09	4.26	178.25 ± 0.92	3.49
2m	-H	4-CH ₃	357.46	176.75 ± 0.64	3.96	85.74 ± 2.43	4.39
2n	-H	2-F	361.42	163.35 ± 3.18	4.10	100.80 ± 0.57	4.28
2o	-H	4-F-2-CF ₃	429.42	57.09 ± 3.91	3.06	74.24 ± 1.80	4.19
2p	-H	3,5-bis-CF ₃	479.43	77.56 ± 0.66	3.95	139.1 ± 1.13	3.60
2q	-H	4-butyl	399.54	55.36 ± 4.19	4.25	132.75 ± 1.20	3.28
2r	-H	2,4-di-F	379.41	61.00 ± 1.48	4.98	133.40 ± 1.84	4.09
2s	-H	4-NO ₂	388.43	43.57 ± 0.66	3.67	193.35 ± 0.07	4.16
2t	-H	3-Br	422.33	51.14 ± 0.20	3.56	134.40 ± 3.11	3.50
2u	-H	4-CN	368.44	56.05 ± 1.87	4.13	112.00 ± 0.71	3.67
2v	-H	3-CN	368.44	75.42 ± 1.03	3.97	147.80 ± 0.28	4.28

2w	-H	5-F,2-CH ₃	375.45	80.13 ± 0.16	4.03	145.00 ± 0.28	3.96
2x	-H	4-tertbutyl	399.54	48.52 ± 0.23	3.28	167.50 ± 0.71	4.29
2y	-H	4-isopropyl	385.52	50.37 ± 0.91	3.86	191.20 ± 1.41	3.59
Donepezil			-	0.04 ± 0.01	7.40		
β-Secretase Inhibitor IV			-			0.02 ± 0.01	7.70

*Results are presented as mean ± SD, n=3, eeAChE indicates AChE from electric eel and hBACE 1 indicates human BACE 1.

Table 25. Inhibitory activities of compounds **3a-3s** (Series-III) against AChE and BACE 1



Compound	R ₁	R ₂	Mol. Wt.	EeAChE	EeAChE	hBACE 1	hBACE 1
				IC ₅₀ (μM) ± SD	PIC ₅₀ (μM)	IC ₅₀ (μM) ± SD	PIC ₅₀ (μM)
3a	4-Cl	4-Br	456.77	123.40 ± 3.11	4.25	192.35 ± 1.77	3.99
3b	4-F	4-Br	440.32	86.09 ± 0.30	4.25	165.65 ± 1.34	4.15
3c	4-CF ₃	4-Br	490.33	149.50 ± 1.41	3.77	197.00 ± 1.98	3.85
3d	4-CH ₃	4-Br	436.36	170.15 ± 3.04	4.36	178.25 ± 0.92	3.71
3e	4-CF ₃	4-butyl	467.54	57.35 ± 1.10	4.37	204.60 ± 0.42	3.67

3f	4-tertbutyl	4-OCF ₃	483.54	261.50 ± 1.56	4.26	209.15 ± 1.91	4.08
3g	4-CF ₃	4-CF ₃	479.43	154.40 ± 1.41	4.20	212.45 ± 1.91	3.84
3h	2,3-di-OCH ₃	4-CH ₃	417.51	86.18 ± 1.89	4.37	217.20 ± 0.57	3.73
3i	3,4-di-OCH ₃	4-F,2-CF ₃	489.47	57.09 ± 0.44	4.12	74.24 ± 2.33	3.75
3j	2,3-di-OCH ₃	4-OCF ₃	487.48	133.95 ± 1.34	4.42	215.40 ± 3.25	3.65
3k	4-tertbutyl	2,4-di-F	435.52	221.80 ± 1.27	4.66	104.30 ± 0.14	3.70
3l	3,4-di-OCH ₃	3,5-di-OCH ₃	463.54	57.23 ± 2.47	4.78	162.20 ± 2.40	3.70
3m	3,4-di-F	4-tertbutyl	435.52	126.00 ± 0.71	3.71	135.90 ± 0.71	4.11
3n	4-tertbutyl	4-biphenyl	475.64	76.08 ± 0.79	3.84	185.40 ± 1.84	3.97
3o	4-tertbutyl	4-CF ₃	505.67	71.17 ± 0.49	3.78	179.00 ± 2.26	4.09
3p	4-isopropyl	3,6-di-F	421.50	149.55 ± 1.06	3.58	187.00 ± 0.28	3.58
3q	4-tertbutyl	4-Br	478.44	83.94 ± 0.74	4.56	193.40 ± 2.12	4.56
3r	3,4-di-OCH ₃	4-tertbutyl	459.59	69.60 ± 1.51	3.36	177.20 ± 2.83	3.27
3s	4-tertbutyl	4-tertbutyl	455.65	48.06 ± 0.52	3.86	178.25 ± 0.92	4.39
Donepezil			-	0.04 ± 0.01	7.40		
β-Secretase Inhibitor IV			-			0.02 ± 0.01	7.70

*Results are presented as mean ± SD, n=3, eeAChE indicates AChE from electric eel and hBACE 1 indicates human BACE 1

4.3.2. Indol-3-yl-phenyl allylidene hydrazine carboximidamide analogues analogues

The inhibitory activities of indol-3-yl-phenyl allylidene hydrazine carboximidamide hybrids **4a-4z**, **4aa-4af**, **5a-5x**, and **6a-6u** against AChE and BACE 1 were evaluated by the Ellman technique and Fluorescence resonance energy transfer (FRET) assay, respectively using donepezil and β -Secretase Inhibitor IV as reference standards. The results are shown in **Tables 26-28**.

Table 26 indicates the results for compounds **4a-4af** of the first series where ring A was substituted with electron-withdrawing and donating substituents and ring B was unsubstituted. Overall, the results validate the hypothesis that the extension of our reported compound could result in pronounced dual inhibition of AChE and BACE 1. The compounds were active against both enzymes; however, with the introduction of AChE inhibition, the BACE 1 inhibitory potential was decreased. It was found that electron-donating substituents like 4-tertbutyl (**4c**) and 2-methyl (**4af**) on ring A showed good AChE inhibition but decreased BACE 1 inhibitory activity. Conversely, the substitution of electron-withdrawing groups on ring A retained the BACE 1 inhibitory potential but affected the AChE inhibitory potency of compounds. It was also observed that the bulky substituent on ring A reduces the AChE inhibitory potential. Compound **4o**, which had *p*-cyano, showed good AChE and BACE 1 inhibition activities and can be called the most active of the series.

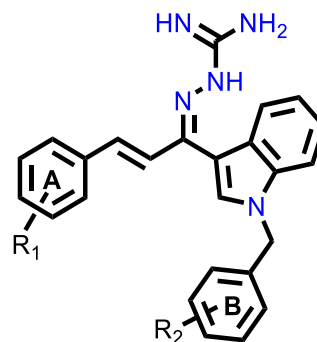
In the second series (compounds **5a-5x**), ring B was substituted with various electron-withdrawing and donating substituents while keeping ring A unsubstituted. It was observed that compared to ortho, the para substitution of electron-withdrawing groups on ring B was favorable for AChE inhibition. Compound **5f** showed comparable AChE and BACE 1 inhibition. Overall, it can be noted that the electron-withdrawing substitution on ring B favors AChE inhibition. However, in general, substitution on ring B reduces BACE 1 inhibitory potential, as shown in **Table 27**.

In the previous two series, electron withdrawing group substitution on any of the rings favored AChE inhibition, and substitution on ring B was unfavorable for BACE 1 inhibition. Also, the substitution of bulky groups had impacted the activity. Therefore, in the third series (**Table 28**), both the rings (A and B) were substituted, and in particular, the effect of bulky or electron-withdrawing substituents was studied. It was expected that the substitution on both rings may potentiate the AChE inhibition and would also balance out the BACE 1 inhibition. However, substituting bulky or electron-withdrawing substituents on both rings significantly improved AChE inhibition but compromised BACE 1 inhibition. This can be observed with compound

6r, which had a bulky substituent on both rings and was the most potent AChE inhibitor of all compounds ($IC_{50} = 13.38 \mu\text{M}$).

Structure-Activity Relationship

Their structure-activity relationship was analyzed based on the compounds' AChE and BACE 1 inhibitory activity. The potential of the compounds to inhibit AChE and BACE 1 varied with respect to the substitutions on the rings A and B, respectively. In the case of molecular modeling studies of AChE, ring A occupies the CAS site of AChE, while ring B is anchored to the PAS site. This binding pattern is mainly driven by hydrogen bonding and π - π stacking interactions, in which the aromatic ring B of the *N*-benzyl interacts with the Trp86 of PAS, ring A interacts with Trp286 of CAS, pyrrole interacts with residue Tyr337 Tyr341, Phe338 and guanidine interacts with the catalytic amino acid residues of AChE (Ser203, Glu202 and His447). Also, for BACE 1, it is observed that ring A occupies the S1 region, ring B is anchored to the S3 site, and the guanidine group can form H-bonding interactions with catalytic aspartate dyad Asp32 and Asp228, respectively. When ring A alone was substituted with the *p*-cyano group (compound **4o**), it was observed that compound **4o** had a high docking score and maintained the BACE 1 inhibition as the parent compound [24] while also having AChE inhibition. One possible explanation could be attributed to the robust interactions that were observed during the docking simulation: (i) ring B occupied the S3 active site region with the indole scaffold π - π stacked to Tyr71 and Trp76; (ii) amino-guanidinium nitrogen formed hydrogen bonding interactions with catalytic aspartate dyad (Asp228 and Asp32).

Table 26. Inhibitory activities of compounds **4a-4z**, **4aa-4af** (Series-IV) against AChE and BACE 1

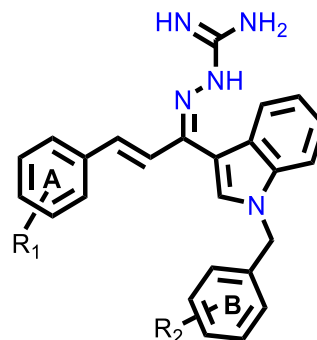
Compound Code	R ₁	R ₂	Mol. Wt.	EeAChE IC ₅₀ (μM) ± SD	EeAChE PIC ₅₀ (μM)	hBACE 1 IC ₅₀ (μM) ± SD	hBACE 1 PIC ₅₀ (μM)
4a	3,4-di-F	-H	429.47	77.24 ± 2.24	4.11	72.11 ± 0.01	4.14
4b	3-Phenoxy	-H	485.59	77.21 ± 3.04	4.37	178.25 ± 0.92	4.01
4c	4-tertbutyl	-H	449.60	42.95 ± 0.48	4.11	97.36 ± 1.36	4.23
4d	3,4-di-OCH ₃	-H	453.55	77.08 ± 1.54	3.83	59.51 ± 0.21	4.93
4e	4-isopropyl	-H	435.58	146.25 ± 3.18	3.86	11.73 ± 0.15	3.93
4f	3-OCH ₃	-H	423.52	137.80 ± 0.14	4.17	117.00 ± 0.57	4.05
4g	3-F	-H	411.48	67.01 ± 1.95	4.11	88.59 ± 0.32	4.05
4h	4-Benzyloxy	-H	499.62	82.04 ± 0.79	4.18	179.45 ± 1.91	4.82
4i	4-dimethylamino	-H	436.56	78.24 ± 2.28	4.14	89.02 ± 2.29	4.01
4j	3-Br	-H	472.39	66.27 ± 1.70	4.21	15.10 ± 0.74	4.14
4k	4-Br	-H	472.39	73.11 ± 2.07	3.73	97.83 ± 0.31	3.88

4l	2,5-di-OCH ₃	-H	453.55	60.96 ± 2.29	4.22	72.24 ± 1.76	5.03
4m	4-CH ₃	-H	407.52	185.50 ± 2.69	3.83	132.00 ± 0.28	4.89
4n	3-NO ₂	-H	438.49	57.11 ± 2.20	3.67	187.15 ± 1.06	4.91
4o	4-CN	-H	418.50	60.90 ± 2.53	3.90	9.38 ± 0.50	4.89
4p	2-F	-H	411.48	137.25 ± 0.49	4.31	207.20 ± 1.41	3.87
4q	2,4-di-F	-H	429.47	147.60 ± 3.11	4.08	12.81 ± 0.50	4.78
4r	-H	-H	393.49	146.15 ± 0.07	4.33	202.75 ± 2.05	3.69
4s	4-OCH ₃	-H	423.52	239.05 ± 2.76	3.84	213.60 ± 1.98	3.69
4t	2-NO ₂	-H	438.49	216.25 ± 3.61	4.33	12.35 ± 0.60	3.70
4u	4-CF ₃	-H	461.49	175.45 ± 4.31	4.25	221.05 ± 1.20	3.99
4v	2-Br,5-Cl	-H	506.83	159.45 ± 2.76	4.25	178.25 ± 0.92	4.15
4w	3-Benzyloxy	-H	499.62	126.60 ± 0.99	3.77	12.79 ± 0.42	3.85
4x	4-NO ₂	-H	438.49	80.26 ± 2.93	4.36	225.90 ± 0.99	3.71
4y	3-CN	-H	418.50	76.52 ± 1.29	3.58	210.20 ± 1.27	3.68
4z	2,5-di-F	-H	429.47	81.30 ± 4.24	4.28	227.80 ± 1.41	4.29
4aa	2,3-di-OCH ₃	-H	453.55	48.57 ± 1.51	3.31	134.25 ± 1.40	4.39
4ab	2,4-di-Cl	-H	462.38	159.00 ± 1.84	3.38	179.75 ± 1.34	3.48
4ac	4-Cl	-H	427.94	82.64 ± 1.92	3.06	16.40 ± 0.39	3.02
4ad	3,4-di-Cl	-H	462.38	79.24 ± 0.41	4.26	202.70 ± 2.40	3.29
4ae	4-F	-H	411.48	149.05 ± 1.20	4.89	174.60 ± 2.12	4.28
4af	2-CH ₃	-H	407.52	46.78 ± 1.83	3.58	206.35 ± 3.75	3.45

Donepezil	-	0.04 ± 0.01	7.40		
β-Secretase Inhibitor IV	-			0.02 ± 0.01	7.70

*Results are presented as mean ± SD, n=3, eeAChE indicates AChE from electric eel and hBACE 1 indicates human BACE 1.

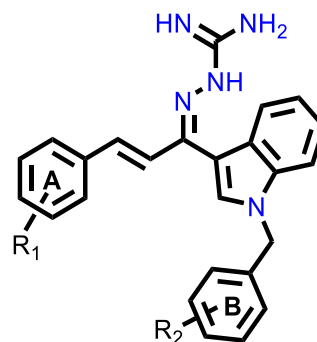
Table 27. Inhibitory activities of compounds **5a-5x** (Series-V) against AChE and BACE 1



Compound Code	R ₁	R ₂	Mol. Wt.	EeAChE IC ₅₀ (μM) ± SD	EeAChE PIC ₅₀ (μM)	hBACE 1 IC ₅₀ (μM) ± SD	hBACE 1 PIC ₅₀ (μM)
5a	-H	4-butyl	449.60	51.31 ± 0.71	3.69	210.45 ± 2.76	3.60
5b	-H	4-OCF ₃	477.49	79.28 ± 0.57	4.58	191.20 ± 1.56	3.69
5c	-H	2,4-di-F	429.47	46.40 ± 1.63	4.23	200.10 ± 1.98	4.53
5d	-H	4-tertbutyl	449.60	79.64 ± 0.26	3.39	192.95 ± 1.34	3.32
5e	-H	4-CF ₃	461.49	55.99 ± 2.44	3.68	102.05 ± 1.06	3.85
5f	-H	3,5-bis-CF ₃	529.49	56.58 ± 0.98	4.37	70.04 ± 0.87	3.59
5g	-H	2,5-di-F	429.47	59.60 ± 1.03	4.26	178.25 ± 0.92	4.28

5h	-H	4-F-2-CF ₃	479.48	168.55 ± 1.91	4.20	140.85 ± 1.06	3.84
5i	-H	4-CH ₃	407.52	47.85 ± 2.23	4.37	203.70 ± 2.26	3.73
5j	-H	2-CN	418.50	44.02 ± 0.19	4.12	196.70 ± 2.4	3.75
5k	-H	4- bromomethylbiphenyl	469.59	50.53 ± 0.71	3.54	211.40 ± 1.13	3.63
5l	-H	4-Cl	427.94	42.78 ± 2.79	4.26	213.00 ± 2.26	3.49
5m	-H	3-benzyloxy	499.62	155.40 ± 2.26	3.96	192.05 ± 0.07	4.39
5n	-H	4-Br	472.39	163.85 ± 1.34	4.10	217.30 ± 0.99	4.28
5o	-H	3,5-di-OCH ₃	453.55	55.57 ± 0.72	3.06	83.43 ± 1.90	4.19
5p	-H	4-F	411.48	40.54 ± 1.00	3.95	204.80 ± 2.83	3.60
5q	-H	2-F	411.48	62.86 ± 0.62	4.25	143.25 ± 0.21	3.28
5r	-H	4-Br-2-F	490.38	42.63 ± 1.58	4.98	185.95 ± 0.07	4.09
5s	-H	2,5-di-Cl	462.38	57.73 ± 0.83	3.67	223.40 ± 0.85	4.16
5t	-H	4-NO ₂	438.49	77.48 ± 2.91	3.56	204.85 ± 0.49	3.50
5u	-H	3-Br	472.39	72.91 ± 3.67	4.13	193.60 ± 3.25	3.67
5v	-H	3-CN	418.50	75.91 ± 0.32	3.97	178.25 ± 0.92	4.28
5w	-H	4-CN	418.50	77.38 ± 1.89	4.03	200.75 ± 0.35	3.96
5x	-H	4-isopropyl	435.58	45.23 ± 3.37	3.28	205.65 ± 1.91	4.29
Donepezil			-	0.04 ± 0.01	7.40		
β-Secretase Inhibitor IV			-			0.02 ± 0.01	7.70

*Results are presented as mean ± SD, n=3, eeAChE indicates AChE from electric eel, and hBACE 1 indicates human BACE 1.

Table 28. Inhibitory activities of compounds **6a-6u** (Series-VI) on AChE and BACE 1

Compound Code	R ₁	R ₂	Mol. Wt.	EeAChE IC ₅₀ (μM) ± SD	EeAChE PIC ₅₀ (μM)	hBACE 1 IC ₅₀ (μM) ± SD	hBACE 1 PIC ₅₀ (μM)
6a	2,3-di-OCH ₃	4-OCF ₃	537.54	56.89 ± 3.63	3.84	209.20 ± 2.12	3.69
6b	3-Phenoxy	3-Br	564.49	63.11 ± 1.12	4.33	178.85 ± 0.78	3.70
6c	4-tertbutyl	2,4-di-F	485.58	143.75 ± 4.03	4.25	204.45 ± 0.78	3.99
6d	4-CF ₃	4-CF ₃	529.49	38.41 ± 3.46	4.25	222.35 ± 0.49	4.15
6e	3,4-di-OCH ₃	3,5-di-OCH ₃	513.60	21.99 ± 0.65	3.77	197.55 ± 3.18	3.85
6f	4-tertbutyl	4-bromomethylbiphenyl	525.70	16.58 ± 1.04	4.36	200.90 ± 3.82	3.71
6g	3,4-di-F	4-tertbutyl	485.58	195.90 ± 1.70	4.37	76.87 ± 2.38	3.67
6h	4-benzyloxy	4-CH ₃	513.65	144.15 ± 1.77	4.26	107.10 ± 2.55	4.08
6i	4-isopropyl	2,5-di-F	471.56	166.60 ± 2.12	4.20	82.15 ± 2.74	3.84

6j	4-CF ₃	4-F	479.48	196.25 ± 2.62	4.37	191.40 ± 0.42	3.73
6k	2,4-di-F	2-F	447.47	57.52 ± 0.71	4.12	203.80 ± 1.70	3.75
6l	4-tertbutyl	4-Br	528.50	212.95 ± 2.90	4.42	189.65 ± 0.92	3.65
6m	4-tertbutyl	4-F	467.59	155.75 ± 2.62	4.66	178.25 ± 0.92	3.70
6n	3,4-di-OCH ₃	4- bromomethylbiphenyl	529.64	83.89 ± 2.49	4.78	203.65 ± 0.92	3.70
6o	4-tertbutyl	4-tertbutyl	505.71	67.94 ± 2.60	3.71	213.40 ± 2.26	4.11
6p	4-benzyloxy	3-benzyloxy	605.74	55.66 ± 3.17	3.84	179.15 ± 0.78	3.97
6q	4-tertbutyl	4-CF ₃	517.60	26.99 ± 0.13	3.78	189.05 ± 1.91	4.09
6r	4-CF ₃	4-butyl	517.60	13.38 ± 0.49	3.81	182.40 ± 1.41	3.75
6s	3-Phenoxy	4- bromomethylbiphenyl	561.69	207.10 ± 7.64	4.25	139.40 ± 1.98	3.75
6t	4-benzyloxy	4-butyl	555.73	126.85 ± 3.04	3.84	199.95 ± 1.91	3.69
6u	2,3-di-OCH ₃	4-butyl	509.65	146.35 ± 2.33	4.33	165.20 ± 0.85	3.70
Donepezil			-	0.04 ± 0.01	7.40		
β-Secretase Inhibitor IV			-			0.02 ± 0.01	7.70

*Results are presented as mean ± SD, n=3, eeAChE indicates AChE from electric eel, and hBACE 1 indicates human BACE 1.

4.4 Molecular dynamics simulations

4.4.1. The potent analogue from Pyrrol-2-yl-phenyl allylidene hydrazine carboximidamide series

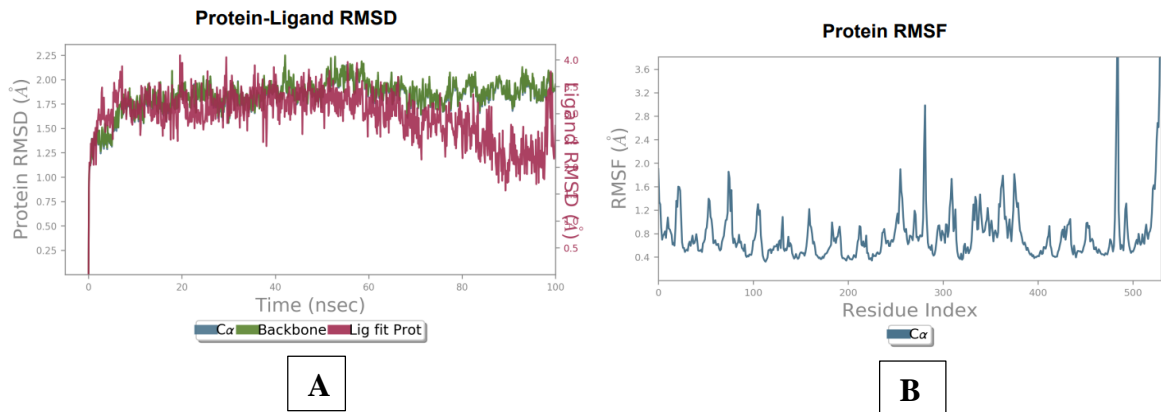
The stability of the binding of **31** with AChE and BACE 1 complex was analyzed through the molecular dynamics simulation study, utilizing the Desmond software developed by DE Shaw Research. The stability of the docked complex was assessed in the context of a flexible protein environment while considering the behavior of virtual water molecules in the vicinity. The docked complexes' root mean square deviations (RMSD) were calculated and compared to the reference protein backbone structures, with the values falling within a certain range. Analysis of the simulation trajectories revealed that the root mean square fluctuations (RMSF) values for the compound **31** in the AChE/BACE 1 complex remained relatively stable, indicating consistent trajectories for both the ligand and protein residues. Various methods were employed to thoroughly analyze the protein-ligand interaction, including histograms, graphical representations, and time-line visualizations. The proportion of protein residues that interacted with compound **31** was determined by examining the contacts between the protein and ligand. The findings of AChE molecular dynamics studies showed that compound **31** interacted considerably with PAS, and CAS residues of AChE formed hydrogen bonding interactions with compound **31**. Trp286, a CAS residue, interacted with the ring A and pyrrole scaffold of compound **31** with Phe297 and Trp86 by π - π stacking and charged interaction. The amino-guanidinium nitrogen atom of compound **31** displayed hydrogen bonding with the catalytic site His447, Tyr124, Glu202, and Ser203 residues, respectively. Also, the Tyr72, Trp286, Tyr337, Phe338, and Tyr341 residue formed the same interaction as that of Trp86 residue with compound **31** in the PAS region.

The BACE 1 molecular dynamics simulation results showed that Compound **31** established strong interactions with aspartate dyad residues (Asp32 and Asp228) with the least fluctuations. The amino-guanidinium functionality involved in H-bonding interaction with Asp32 accounted for throughout the trajectories. Asp228, one of the catalytic aspartate dyad residues, interacted with the *N*-atom of the amino-guanidinium core of compound **31** through the salt bridge. The MD findings suggested that compound **31** showed more stable and balanced interaction in AChE and BACE 1 active sites.



Figure 21. Molecular dynamics studies of **3I**-AChE (4EY7) docked complex. [A] Comparative RMSD of AChE (protein backbone) and compound **3I** in the protein-ligand complex throughout the simulation period of 100 ns. [B] Graphical representation showing protein RMSF throughout the simulation period of 100 ns. [C] Histogram showing interaction fractions

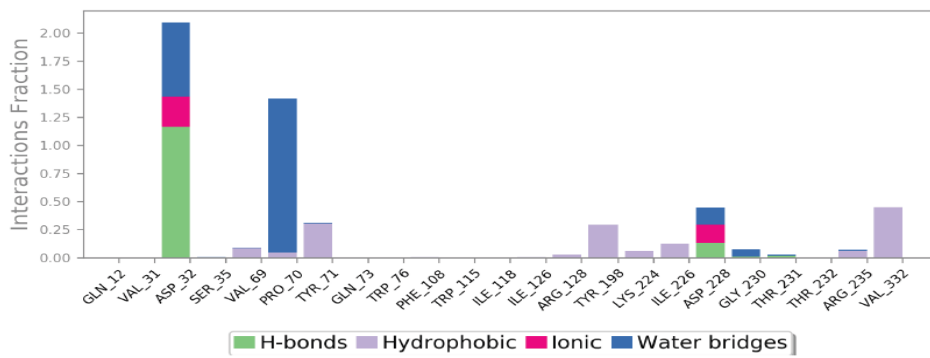
with active amino acid residues. [D and E] Timeline representation showing interaction with all the amino acid residues at each time frame.



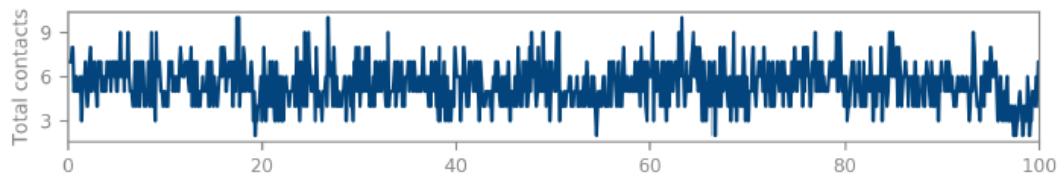
A

B

Protein-Ligand Contacts



C



D

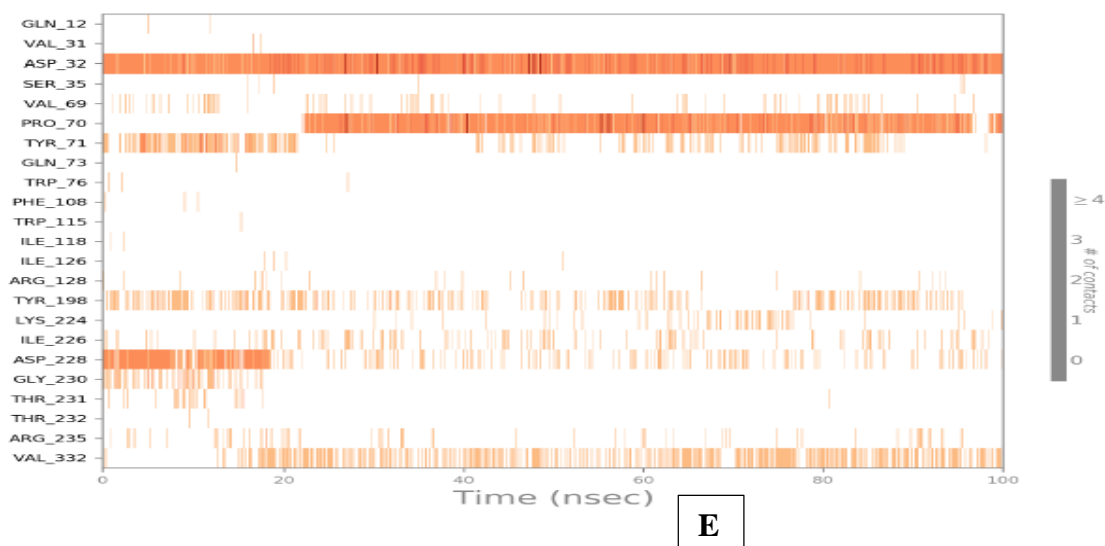


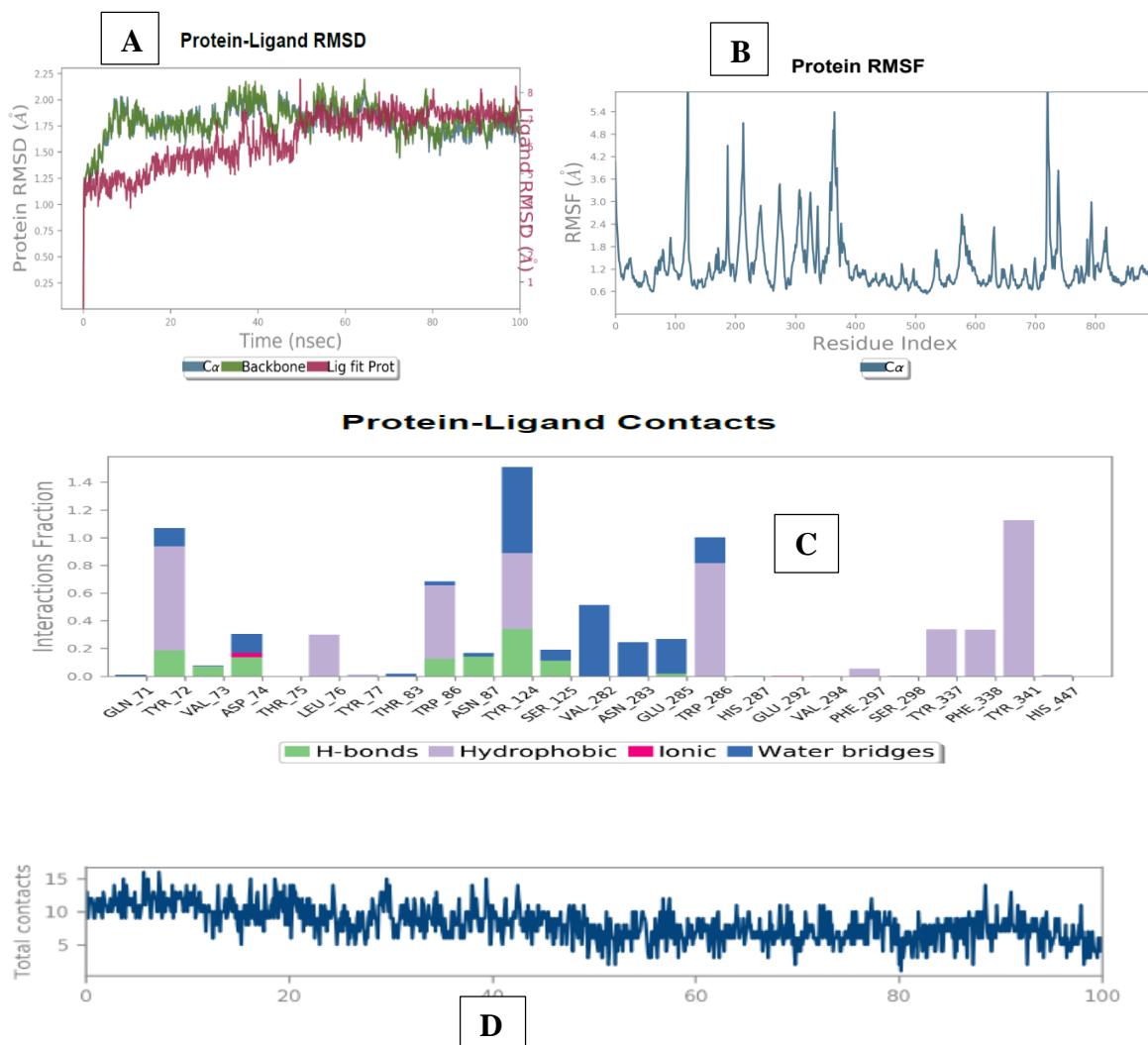
Figure 22. Molecular dynamics studies of **31**-BACE 1 (6UWP) docked complex [A] Comparative RMSD of BACE 1 (protein backbone) and compound **31** in the protein-ligand complex throughout the simulation period of 100 ns. [B] Graphical representation showing protein RMSF throughout the simulation period of 100 ns. [C] Histogram showing interaction fractions with active amino acid residues; [D, E] Timeline representation showing interaction with all the amino acid residues at each time frame.

4.4.2. The potent analogue from Indol-3-yl-phenyl allylidene hydrazine carboximidamide series

A molecular dynamics simulation study was conducted to analyze the binding stability between the compound **40**-AChE/BACE 1 complex. The results showed that the RMSF values remained relatively stable, indicating consistent trajectories for both the ligand and protein residues. It was observed that compound **40** exhibited significant interactions with PAS/CAS residues of AChE. Tyr341, a CAS residue, played a role in interacting with the indole scaffold of compound **40** through π - π stacking (51% of the time) and charged interactions. Furthermore, Tyr124 and Trp286 residue in the PAS region exhibited a similar interaction to Trp341 residue, with a time scale of 22% and 32%, respectively. The aminoguanidinium nitrogen atom of compound **40** formed hydrogen bonds with Tyr124 residue, with respective time scales of 28%. Tyr72 formed a π -cation interaction with -NH functionality of **40** (40%-time scale).

The molecular dynamics simulation with BACE 1 revealed that Compound **40** established strong and consistent interactions with the residues, namely Tyr71, Tyr198, and Arg235. The aminoguanidinium functionality of Compound **40** formed halogen bonding interaction with chlorine atom, accounting for 11% of the interactions observed throughout the simulation

trajectories. Tyr198 formed a π - π stacked interaction with ring B and indole nucleus of **4o** with a time scale of 15% and 7%. Tyr71 residue engaged in a π - π stacked interaction with the ring A core of Compound **4o**, representing 15% of the time scale. Furthermore, Arg235 residue exhibited a π cation interaction with ring A core of **4o**, with a time scale of 5%. Overall, the molecular dynamics simulation results indicated that Compound **4o** exhibited stable and well-balanced interactions within the active sites of both AChE and BACE 1.



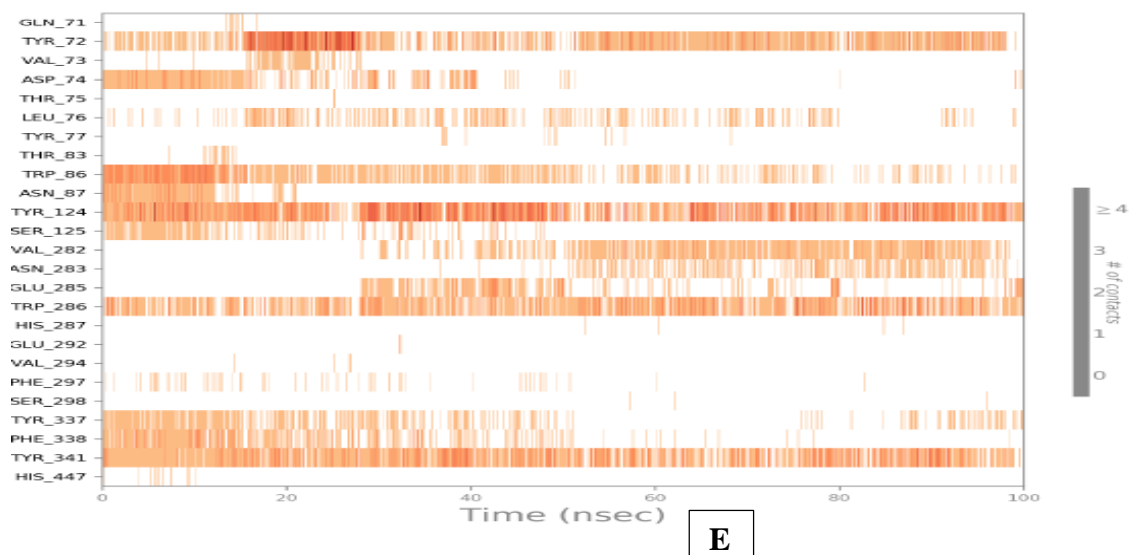
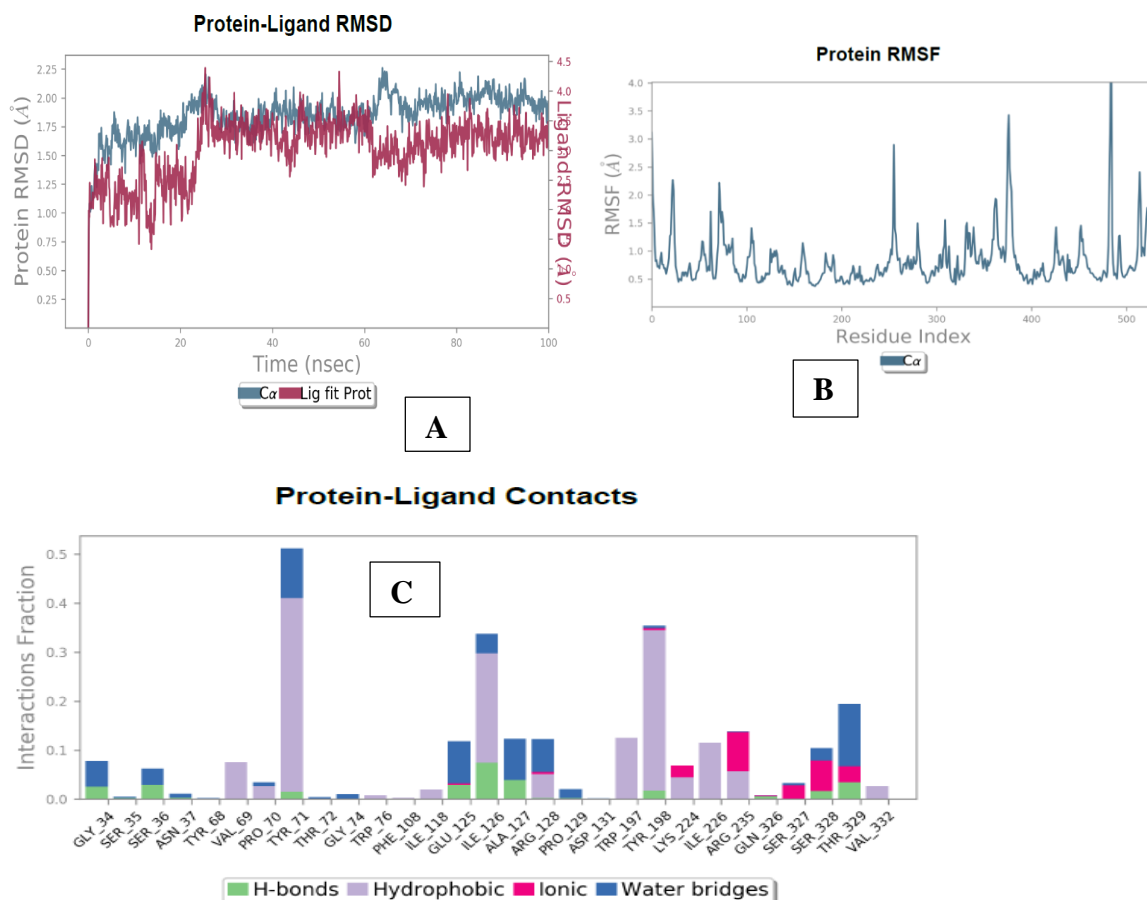


Figure 23. Molecular dynamics studies of compound **40**-AChE (4EY7) docked complex. [A] Comparative RMSD of AChE (protein backbone) and compound **40** in the protein-ligand complex throughout the simulation period of 100 ns. [B] Graphical representation showing interactions with active site amino acid residues of PAS and CAS; [C] Histogram showing interaction fractions with active amino acid residues; [D and E] Timeline representation showing interaction with all the amino acid residues at each time frame



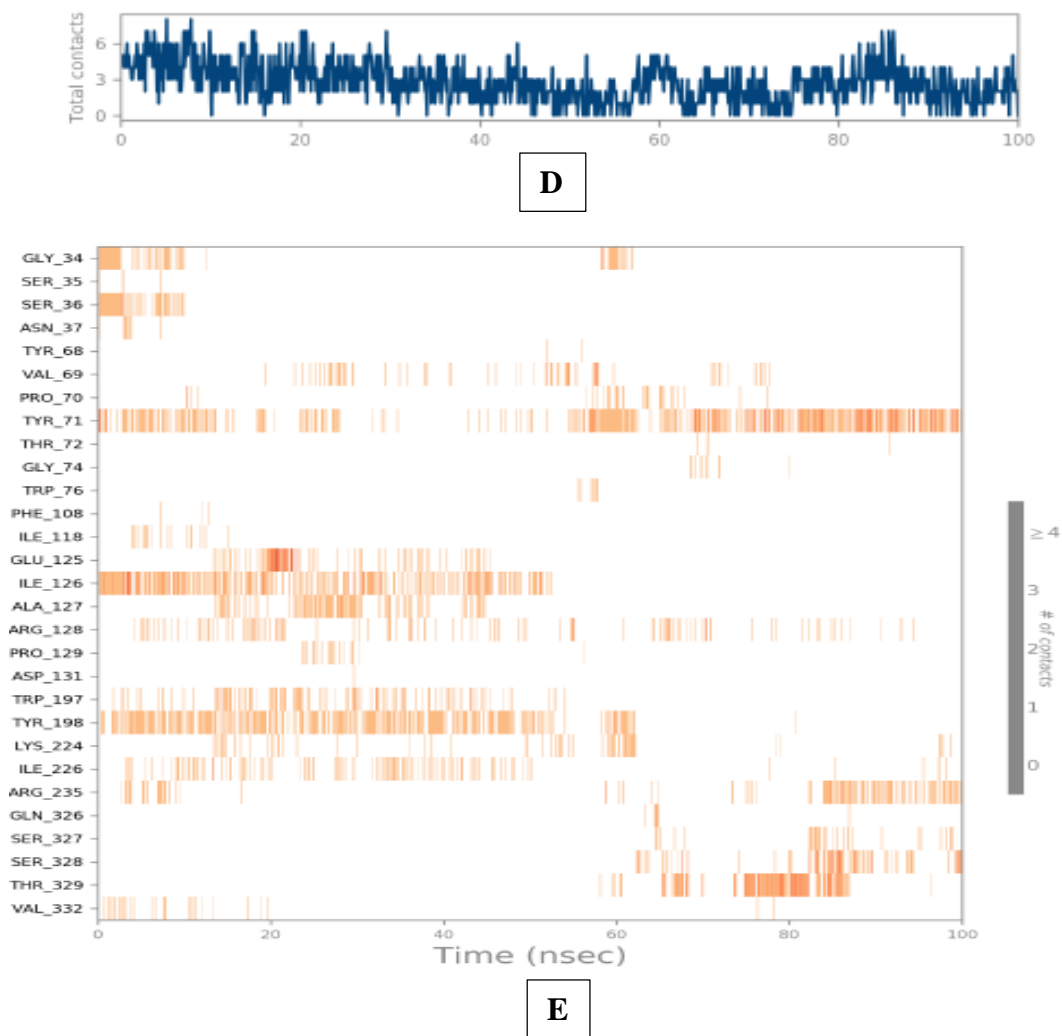


Figure 24. Molecular dynamics studies of compound **40**-BACE 1 (6UWP) docked complex. [A] Comparative RMSD of BACE 1 (protein backbone) and compound **40** in the protein-ligand complex throughout the simulation period of 100 ns. [B] Graphical representation showing interactions with active site amino acid residues (Aspartate dyad); [C] Histogram showing interaction fractions with active amino acid residues; [D, E] Timeline representation showing interaction with all the amino acid residues at each time frame.

From the molecular docking and dynamics studies, it was observed that the substitution of ring A does not affect binding with the BACE 1 active site but also makes the compound fit in the active site of AChE. However, when the ring B is substituted, the substitution pushes the compound out of the binding pocket of BACE 1, and hence, it does not show good BACE binding.

CHAPTER 5. SUMMARY AND CONCLUSION

Alzheimer's disease (AD) is a progressive neurodegenerative disorder that causes cognitive decline and memory loss. AD is the most common cause of dementia that slowly degrades thinking and social interactions as there is degradation of brain cells. Despite significant research, AD's underlying causes and precise molecular processes remain unclear. A key characteristic and pathological feature of Alzheimer's disease (AD) is the presence of senile plaques, primarily composed of the cytotoxic amyloid- β peptide (A β -42). The production and deposition of A β -42 are central events in the pathogenesis of AD. The amyloid- β peptide (A β -42) is generated by sequential actions involving the amyloid precursor protein (APP), where the β -secretase (BACE 1) cleaves at the β -site, followed by the γ -secretase cleaving at the γ -site of APP. BACE1 is a key target for therapies aiming to reduce amyloid plaque production or enhance clearance to slow AD progression. AChE is one of the most explored targets for the development of effective drug candidates for the treatment of AD. Available treatment primarily relies on acetylcholinesterase inhibitors (AChEIs) to restore acetylcholine levels and influence A β peptide aggregation, potentially alleviating AD symptoms.

Due to the complex nature of AD and the numerous factors contributing to its progression, focusing on a singular causative aspect is unlikely to result in a comprehensive cure or effectively impede the advancement of the disease. Hence, efforts are directed toward dual or multiple target inhibitors.

Based on previous work and work by the collaborator, modification of allylidene hydrazine carboximidamide was undertaken. It involved the replacement of one of the two aromatic rings separated by a linker by a nitrogen-containing hetero-aromatic ring system (pyrrole and indole). Thus, such designed analogues, with pharmacophoric features required for dual targeting, were expected to show potent inhibition of AChE and BACE 1. The aim was, therefore, to design, synthesize, and evaluate small molecular BACE 1 and AChE dual inhibitors.

Among the various crystal structures available for BACE 1 and AChE, 6UWP (PDB id for BACE 1) and 4EY7 (PDB id for AChE) were chosen. The protocol was validated and used further for docking of designed compounds. *In silico* ADMET prediction using QikProp (Schrodinger) was also performed. Pyrrol-2-yl-phenyl allylidene hydrazine carboximidamide derivatives were conceived in the first set of compounds. Docking studies revealed that these compounds generally occupy S1 active site region and formed hydrogen bonding interactions with Asp32 along with the occupancy of CAS and PAS region in AChE. Further, the series complied well with Lipinski's rule of five and did not display toxicity in *in silico* prediction. Consequently, a set of **81** compounds, incorporating both electron-withdrawing (EWG) and

electron-donating (EDG) groups, were synthesized. All target compounds showed weak to good inhibitory activity against AChE and BACE 1.

Strong electron-withdrawing substituents, such as 4-nitro or 2,4-dichloro, on ring A, were found to enhance inhibition of AChE but decrease inhibitory activity against BACE 1. Conversely, introducing electron-donating groups on ring A improved the potential for inhibiting BACE 1 while reducing the potency of AChE inhibition. It was observed that substituting ring A alone with either electron-donating or electron-withdrawing moieties was not favorable for BACE 1 inhibition compared to previously reported compounds, resulting in decreased activity. However, replacing the phenyl group at ring A with pyridine did not significantly impact BACE 1 inhibition but adversely affected AChE inhibition, showing poor activity against AChE. Increasing the bulk at the 4-position of ring B was advantageous for AChE inhibition but hindered BACE 1 inhibition, as evidenced by compounds **2q**, **2x**, and **2y**. Generally, electron-withdrawing substitutions on ring B supported AChE inhibition, whereas electron-donating groups encouraged BACE 1 inhibition. It was anticipated that substituting both rings would enhance AChE inhibition. However, there was minimal change in AChE inhibition when bulky or electron-withdrawing substituents were introduced on both rings. Compound **3s**, featuring tert-butyl substituents on both rings, emerged as the most potent AChE inhibitor among these compounds, with an IC_{50} value of 48.06 μ M. However, it adversely affected BACE 1 inhibition, as indicated by increased IC_{50} values, suggesting that bulky or electron-withdrawing substituents on either ring or both rings were not conducive to BACE 1 inhibition.

The docking and inhibition data from this series facilitated the conclusion that the *N*-containing heterocyclic ring (Pyrrole) acts as a compact linker, efficiently preventing the flipping of substituent rings. Therefore, the effect of bicyclic nitrogen heterocycle was also checked. *N*-benzyl indole was considered to replace the pyrrole ring, and a library of **77** indol-3-yl-phenyl allylidene hydrazine carboximidamide derivatives was designed, incorporating both electron-withdrawing (EWG) and electron-donating (EDG) groups. These groups were fully explored at each aromatic position, including a combination of ortho, meta, and para orientations. All the compounds displayed higher docking scores, revealing strong hydrogen bonding interactions with catalytic aspartate dyad and the aromatic rings properly accommodated in S1 and S3 of BACE 1 and AChE (CAS and PAS) substrate binding clefts. Also, these compounds obeyed Lipinski's rule of oral bioavailability and had better drug scores than the previous series, indicating no sign of toxicity, better solubility, and drug likeliness.

While the compounds demonstrated activity against both enzymes, an increase in AChE inhibition corresponded to a decrease in BACE 1 inhibitory potential. Electron-donating substituents like 4-tert-butyl (**4c**) and 2-methyl (**4af**) on ring A exhibited strong AChE inhibition but reduced BACE 1 inhibitory activity. Conversely, introducing electron-withdrawing groups on ring A maintained BACE 1 inhibitory potential but impacted the potency of AChE inhibition. Additionally, bulky substituents on ring A were found to diminish AChE inhibitory potential. Compound **4o**, featuring p-cyano, demonstrated notable AChE and BACE 1 inhibition activities, making it the most active compound in the series. It had BACE 1 inhibition (IC_{50} value of $9.38\mu\text{M}$). For AChE, it showed IC_{50} value of $60\mu\text{M}$. However, substituting bulky or electron-withdrawing substituents on both rings significantly improved AChE inhibition but compromised BACE 1 inhibition. This can be observed with compound **6r**, which had a bulky substituent on both rings and was the most potent AChE inhibitor of all compounds ($IC_{50} = 13.38\mu\text{M}$). Overall, the findings support the hypothesis that extending our previously reported compound could lead to significant dual inhibition of AChE and BACE 1.

In summary, the distinct contributions of this study can be outlined as follows:

- A. This study supports the hypothesis that the modification of our previously reported BACE 1 inhibitor could lead to significant dual inhibition of AChE and BACE 1.
- B. The increased IC_{50} value against BACE 1 indicates that bulkier substituents on both rings were unfavorable for BACE 1 inhibition
- C. The substitution of ring A does not affect binding with the BACE 1 active site but also makes the compound fit in the active site of AChE. However, when the ring B is substituted, the substitution pushes the compound out of the binding pocket of BACE 1, and hence, it does not show good BACE binding.
- D. This research may serve as a foundation for further development of smaller, low molecular weight dual inhibitors having the capability to inhibit both BACE 1 and AChE enzymes.
- E. Compound **4o** is a promising starting point for comprehensive modifications aimed at hit-to-lead conversion.

Future Perspectives

The primary focus of this study was on designing a new series of allylidene hydrazine carboximidamides having dual - acetyl cholinesterase and β -secretase- inhibition. Building upon this research, future studies may be devised as follows:

- A. In vivo studies in animal models could be undertaken to establish the efficacy and toxicity of these compounds.
- B. Examinations of specificity against alternative aspartyl proteases and cholinesterases could be carried out.
- C. Modifications to the active structures can be done to enhance potency and mitigate potential shortcomings.
- D. Based on the results, QSAR models can be developed to predict the dual activity of subsequent analogues.

CHAPTER 6. REFERENCES

6.1 References

- [1] Shanmugam, Jayanthi Venkatraman, Baskar Duraisamy, Blessy Chittattukarakkaran Simon, Preethi Bhaskaran. Alzheimer's disease classification using pre-trained deep networks. *Biomed. Signal Process. Control.* 71 (2022): 103217. <https://doi.org/10.1016/j.bspc.2021.103217>
- [2] <https://www.alz.org/alzheimers-dementia/facts-figures> Accessed (07 May 2024)
- [3] Domico, Matthew, Valerie Hill. What You Need to Know about Alzheimer's Disease. *Bloomsbury Publishing USA*, 2022. [https://doi.org/10.1016/S0002-9343\(97\)00262-3](https://doi.org/10.1016/S0002-9343(97)00262-3)
- [4] Galle, Sara A., Ilse K. Geraedts, Jan Berend Deijen, Maarten V. Milders, Madeleine L. Drent. The interrelationship between insulin-like growth factor 1, apolipoprotein E ϵ 4, lifestyle factors, and the aging body and brain. *J. Prev. Alzheimer's Dis.* 7 (2020): 265-273. <https://doi.org/10.14283/jpad.2020.11>
- [5] Olczak, Kaya J., Victoria Taylor-Bateman, Hannah L. Nicholls, Matthew Traylor, Claudia P. Cabrera, Patricia B. Munroe. Hypertension genetics past, present and future applications. *J. Intern. Med.* 290 (2021): 1130-1152. <https://doi.org/10.1111/joim.13352>
- [6] Sadiq, Idris Z. Free radicals and oxidative stress: Signaling mechanisms, redox basis for human diseases, and cell cycle regulation. *Curr. Mol. Med.* 23 (2023): 13-35. <https://doi.org/10.2174/1566524022666211222161637>
- [7] Thoe, Ewen Se, Ayesha Fauzi, Yin Quan Tang, Sunita Chamyuang, Adeline Yoke Yin Chia. A review on advances of treatment modalities for Alzheimer's disease. *Life Sci.* 276 (2021): 119129. <https://doi.org/10.1016/j.lfs.2021.119129>
- [8] Golde, Todd E. Disease-modifying therapies for Alzheimer's disease: More questions than answers. *Neurotherapeutics.* 19 (2022): 209-227. <https://doi.org/10.1007/s13311-022-01201-2>
- [9] Regier, Natalie G., Nancy A. Hodgson, Laura N. Gitlin. Characteristics of activities for persons with dementia at the mild, moderate, and severe stages. *Gerontol.* 57 (2017): 987-997. <https://doi.org/10.1093/geront/gnw133>
- [10] Vitek, Grace E., Boris Decourt, Marwan N. Sabbagh. Lecanemab (BAN2401): an anti-beta-amyloid monoclonal antibody for the treatment of Alzheimer disease. *Expert Opin. Investig. Drugs.* 32 (2023): 89-94. <https://doi.org/10.1080/13543784.2023.2178414>

-
- [11] Nasb M, Tao W, Chen N. Alzheimer's Disease Puzzle: Delving into Pathogenesis Hypotheses. *Aging Dis.* (2024); 15(1):43-73. [https://doi: 10.14336/AD.2023.0608](https://doi.org/10.14336/AD.2023.0608).
- [12] Lee, Gloria, Chad J. Leugers. Tau and tauopathies. *Prog. Mol. Biol. Transl. Sci.* 107 (2012): 263-293. <https://doi.org/10.1016/B978-0-12-385883-2.00004-7>
- [13] Craig, Laura A., Nancy S. Hong, Robert J. McDonald. Revisiting the cholinergic hypothesis in the development of Alzheimer's disease. *Neurosci. Biobehav. Rev.* 35 (2011): 1397-1409. <https://doi.org/10.1016/j.neubiorev.2011.03.001>
- [14] Li, Shaomin. The β -adrenergic hypothesis of synaptic and microglial impairment in Alzheimer's disease. *J. Neurochem.* (2023). <https://doi.org/10.1111/jnc.15782>
- [15] Cheng, Yu-Jung, Chieh-Hsin Lin, Hsien-Yuan Lane. Involvement of cholinergic, adrenergic, and glutamatergic network modulation with cognitive dysfunction in Alzheimer's disease. *Int. J. Mol. Sci.* 22 (2021): 2283. <https://doi.org/10.3390/ijms22052283>
- [16] Honarnejad, Kamran, Jochen Herms. Presenilins: role in calcium homeostasis. *Int. J. Biochem. Cell Biol.* 44 (2012): 1983-1986. <https://doi.org/10.1016/j.biocel.2012.07.019>
- [17] Khan, M. Firoze, Gangduo Wang. Environmental agents, oxidative stress and autoimmunity. *Curr. Opin. Toxicol.* 7 (2018): 22-27. <https://doi.org/10.1016/j.cotox.2017.10.012>
- [18] Hansen, David V., Jesse E. Hanson, Morgan Sheng. Microglia in Alzheimer's disease. *J. Cell Biol.* 217 (2018): 459-472. <https://doi.org/10.1083/jcb.201709069>
- [19] Chen, Li-Lin, Yong-Gang Fan, Ling-Xiao Zhao, Qi Zhang, Zhan-You Wang. The metal ion hypothesis of Alzheimer's disease and the anti-neuroinflammatory effect of metal chelators. *Bioorg. Chem.* 131 (2023): 106301. <https://doi.org/10.1016/j.bioorg.2022.106301>
- [20] Traikapi, Artemis, Nikos Konstantinou. Gamma oscillations in Alzheimer's disease and their potential therapeutic role. *Front. Syst. Neurosci.* 15 (2021): 782399. <https://doi.org/10.3389/fnsys.2021.782399>
- [21] Condello, Carlo, Gregory E. Merz, Atsushi Aoyagi, William F. DeGrado, Stanley B. Prusiner. A β and Tau Prions Causing Alzheimer's Disease. *In Alzheimer's Disease: Methods and Protocols*, 293-337. New York, NY: Springer US, 2022.

- [22] Fan, Liyuan, Chengyuan Mao, Xinchao Hu, Shuo Zhang, Zhihua Yang, Zhengwei Hu, Huifang Sun. New insights into the pathogenesis of Alzheimer's disease. *Front. Neurol.* 10 (2020): 1312. <https://doi.org/10.3389/fneur.2019.01312>
- [23] Korte, Nils, Ross Nortley, David Attwell. Cerebral blood flow decrease as an early pathological mechanism in Alzheimer's disease. *Acta Neuropathol.* 140 (2020): 793-810. <https://doi.org/10.1007/s00401-020-02215-w>
- [24] Pardo-Moreno, Teresa, Anabel González-Acedo, Antonio Rivas-Domínguez, Victoria García-Morales, Francisco Jose García-Cozar, Juan Jose Ramos-Rodríguez, Lucía Melguizo-Rodríguez. Therapeutic approach to Alzheimer's disease: Current treatments and new perspectives. *Pharmaceutics.* 14 (2022): 1117. <https://doi.org/10.3390/pharmaceutics14061117>
- [25] Pernecky, Robert, Frank Jessen, Timo Grimmer, Johannes Levin, Agnes Flöel, Oliver Peters, Lutz Froelich. Anti-amyloid antibody therapies in Alzheimer's disease. *Brain.* 146 (2023): 842-849. <https://doi.org/10.1093/brain/awad005>
- [26] Alexander, G. Caleb, Scott Emerson, Aaron S. Kesselheim. Evaluation of aducanumab for Alzheimer disease: scientific evidence and regulatory review involving efficacy, safety, and futility. *J. Am. Med. Assoc.* 325 (2021): 1717-1718. <https://doi.org/10.1001/jama.2021.3854>
- [27] Breijyeh, Zeinab, Rafik Karaman. Comprehensive review on Alzheimer's disease: Causes and treatment. *Molecules.* 25 (2020): 5789. <https://doi.org/10.3390/molecules25245789>
- [28] Sugimoto, Hachiro, Y. Yamanish, Youichi Iimura, Yoshiyuki Kawakami. Donepezil hydrochloride (E2020) and other acetylcholinesterase inhibitors. *Curr. Med. Chem.* 7 (2000): 303-339. <https://doi.org/10.2174/0929867003375191>
- [29] Marco-Contelles, José, Maria do Carmo Carreiras, Carolina Rodríguez, Mercedes Villarroya, Antonio G. García. Synthesis and pharmacology of galantamine. *Chem. Rev.* 106 (2006): 116-133. <https://doi.org/10.1021/cr040415t>
- [30] Anand, Preet, Baldev Singh. A review on cholinesterase inhibitors for Alzheimer's disease. *Arch. Pharm. Res.* 36 (2013): 375-399. <https://doi.org/10.1007/s12272-013-0036-3>
- [31] Lucey, Brendan P., Haiyan Liu, Cristina D. Toedebusch, David Freund, Tiara Redrick, Samir L. Chahin, Kwasi G. Mawuenyega. Suvorexant acutely decreases tau phosphorylation and A β in the human CNS. *Ann. Neurol.* (2023). <https://doi.org/10.1002/ana.26641>

- [32] Schneider, Lon S., Francesca Mangialasche, Niels Andreasen, Howard Feldman, Ezio Giacobini, Roy Jones, Valentina Mantua. Clinical trials and late-stage drug development for Alzheimer's disease: an appraisal from 1984 to 2014. *J. Intern. Med.* 275 (2014): 251-283. <https://doi.org/10.1111/joim.12191>
- [33] Jeremic, Danko, Lydia Jiménez-Díaz, Juan D. Navarro-López. Past, present and future of therapeutic strategies against amyloid- β peptides in Alzheimer's disease: A systematic review. *Ageing Res. Rev.* 72 (2021): 101496. <https://doi.org/10.1016/j.arr.2021.101496>
- [34] Kim, JiMin, Hanna Jeon, Hye Yun Kim, YoungSoo Kim. Failure, Success, and Future Direction of Alzheimer Drugs Targeting Amyloid- β Cascade: Pros and Cons of Chemical and Biological Modalities. *Chembiochem.* 24 (2023): e202300328. <https://doi.org/10.1002/cbic.202300328>
- [35] Ghosh, Sudeshna, Rafat Ali, Sandeep Verma. A β -oligomers: A potential therapeutic target for Alzheimer's disease. *Int. J. Biol. Macromol.* (2023): 124231. <https://doi.org/10.1016/j.ijbiomac.2023.124231>
- [36] Athar T, Al Balushi K, Khan SA. Recent advances on drug development and emerging therapeutic agents for Alzheimer's disease. *Mol Biol Rep.* (2021); 48(7):5629-5645. [https://doi: 10.1007/s11033-021-06512-9](https://doi.org/10.1007/s11033-021-06512-9).
- [37] Decourt B, Wilson J, Ritter A, Dardis C, DiFilippo FP, Zhuang X, Cordes D, Lee G, Fulkerson ND, St Rose T, Hartley K, Sabbagh MN. MCLENA-1: A Phase II Clinical Trial for the Assessment of Safety, Tolerability, and Efficacy of Lenalidomide in Patients with Mild Cognitive Impairment Due to Alzheimer's Disease. *Open Access J Clin Trials.* (2020); 12:1-13. [https://doi: 10.2147/oajct.s221914](https://doi.org/10.2147/oajct.s221914).
- [38] Vossel K, Ranasinghe KG, Beagle AJ, La A, Ah Pook K, Castro M, Mizuiri D, Honma SM, Venkateswaran N, Koestler M, Zhang W, Mucke L, Howell MJ, Possin KL, Kramer JH, Boxer AL, Miller BL, Nagarajan SS, Kirsch HE. Effect of Levetiracetam on Cognition in Patients With Alzheimer Disease With and Without Epileptiform Activity: A Randomized Clinical Trial. *JAMA Neurol.* (2021); 78(11):1345-1354. [https://doi: 10.1001/jamaneurol.2021.3310](https://doi.org/10.1001/jamaneurol.2021.3310).
- [39] Yao W, Yang H, Yang J. Small-molecule drugs development for Alzheimer's disease. *Front Aging Neurosci.* (2022); 14:1019412. [http://doi: 10.3389/fnagi.2022.1019412](http://doi.org/10.3389/fnagi.2022.1019412).

- [40] Maccacchini, Maria L., Mee Young Chang, Catherine Pan, Varghese John, Henrik Zetterberg, Nigel H. Greig. Posiphen as a candidate drug to lower CSF amyloid precursor protein, amyloid- β peptide and τ levels: target engagement, tolerability and pharmacokinetics in humans. *J. Neurol. Neurosurg. Psychiatry.* 83 (2012): 894-902. <http://dx.doi.org/10.1136/jnnp-2012-302589>
- [41] <https://www.alz.org/> (Accessed 30 May 2024).
- [42] Cummings, Jeffrey L., Kate Zhong, Jefferson W. Kinney, Chelcie Heaney, Joanne Moll-Tudla, Abhinay Joshi, Michael Pontecorvo, Michael Devous, Anne Tang, James Bena. Double-blind, placebo-controlled, proof-of-concept trial of bexarotene in moderate Alzheimer's disease. *Alzheimer's Res. Ther.* 8 (2016): 1-9. <https://doi.org/10.1186/s13195-016-0173-2>
- [43] Hey, John A., Jeremy Y. Yu, Mark Versavel, Susan Abushakra, Petr Kocis, Aidan Power, Paul L. Kaplan, John Amedio, Martin Tolar. Clinical pharmacokinetics and safety of ALZ-801, a novel prodrug of tramiprosate in development for the treatment of Alzheimer's disease. *Clin. Pharmacokinet.* 57 (2018): 315-333. <https://doi.org/10.1007/s40262-017-0608-3>
- [44] Kutzsche, Janine, Dagmar Jürgens, Antje Willuweit, Knut Adermann, Carola Fuchs, Stefanie Simons, Manfred Windisch. Safety and pharmacokinetics of the orally available antiprionic compound PRI-002: A single and multiple ascending dose phase I study. *Alzheimer's Dement. Transl. Res. Clin.* 6 (2020): e12001. <https://doi.org/10.1002/trc2.12001>
- [45] Lannfelt L, Blennow K, Zetterberg H, Batsman S, Ames D, Harrison J, Masters CL, Targum S, Bush AI, Murdoch R, Wilson J, Ritchie CW; PBT2-201-EURO study group. Safety, efficacy, and biomarker findings of PBT2 in targeting Abeta as a modifying therapy for Alzheimer's disease: a phase IIa, double-blind, randomised, placebo-controlled trial. *Lancet Neurol.* (2008); 7(9):779-86. [https://doi: 10.1016/S1474-4422\(08\)70167-4](https://doi: 10.1016/S1474-4422(08)70167-4).
- [46] Scheltens, Philip, Merja Hallikainen, Timo Grimmer, Thomas Duning, Alida A. Gouw, Charlotte E. Teunissen, Alle Meije Wink. Safety, tolerability and efficacy of the glutaminy cyclase inhibitor PQ912 in Alzheimer's disease: results of a randomized, double-blind, placebo-controlled phase 2a study. *Alzheimer's Res. Ther.* 10 (2018): 1-14. <https://doi.org/10.1186/s13195-018-0431-6>
- [47] Spurrier, Joshua, LaShae Nicholson, Xiaotian T. Fang, Austin J. Stoner, Takuya Toyonaga, Daniel Holden, Timothy R. Siegert. Reversal of synapse loss in Alzheimer mouse

models by targeting mGluR5 to prevent synaptic tagging by C1Q. *Sci. Transl. Med.* 14 (2022): eabi8593. <https://doi.org/10.1126/scitranslmed.abi8593>

[48] Izzo, Nicholas J., Carla M. Yuede, Kelsie M. LaBarbera, Colleen S. Limegrover, Courtney Rehak, Raymond Yurko, Lora Waybright. Preclinical and clinical biomarker studies of CT1812: A novel approach to Alzheimer's disease modification. *Alzheimers. Dement.* 17 (2021): 1365-1382. <https://doi.org/10.1002/alz.12302>

[49] Kellar, Derek, Thomas Register, Samuel N. Lockhart, Paul Aisen, Rema Raman, Robert A. Rissman, James Brewer, Suzanne Craft. Intranasal insulin modulates cerebrospinal fluid markers of neuroinflammation in mild cognitive impairment and Alzheimer's disease: A randomized trial. *Sci. Rep.* 12 (2022): 1346. <https://doi.org/10.1038/s41598-022-05165-3>

[50] Wang, H-Y., Z. Pei, K-C. Lee, E. Lopez-Brignoni, B. Nikolov, C. A. Crowley, M. R. Marsman, R. Barbier, N. Friedmann, Lindsay H. Burns. PTI-125 reduces biomarkers of Alzheimer's disease in patients. *J. Prev. Alzheimer's Dis.* 7 (2020): 256-264. <https://doi.org/10.14283/jpad.2020.6>

[51] Iwatsubo, Takeshi. Molecular pathogenesis and disease-modifying therapies of Alzheimer's disease and related disorders. *JMA j.* 5 (2022): 307-313. <https://doi.org/10.31662/jmaj.2022-0079>

[52] Khezri, Mohammad Rafi, Mehdi Mohebalizadeh, Morteza Ghasemnejad-Berenji. Therapeutic potential of ADAM10 modulation in Alzheimer's disease: a review of the current evidence. *Cell Commun. Signal.* 21 (2023): 60. <https://doi.org/10.1186/s12964-023-01072-w>

[53] Miranda A, Montiel E, Ulrich H, Paz C. Selective Secretase Targeting for Alzheimer's Disease Therapy. *J Alzheimers Dis.* (2021); 81(1):1-17. <https://doi: 10.3233/JAD-201027>. PMID: 33749645.

[54] Zhang, Yun, Huaqiu Chen, Ran Li, Keenan Sterling, Weihong Song. Amyloid β -based therapy for Alzheimer's disease: Challenges, successes and future. *Signal Transduct. Target. The.* 8 (2023): 248. <https://doi.org/10.1038/s41392-023-01484-7>

[55] Roselli, Sandra, Tugce Munise Satir, Rafael Camacho, Stefanie Fruhwürth, Petra Bergström, Henrik Zetterberg, Lotta Agholme. APP-BACE1 Interaction and Intracellular Localization Regulate A β Production in iPSC-Derived Cortical Neurons. *Cell. Mol. Neurobiol.* (2023): 1-16. <https://doi.org/10.1007/s10571-023-01374-0>

- [56] Yen YC, Kammeyer AM, Tirlangi J, Ghosh AK, Mesecar AD. A Structure-Based Discovery Platform for BACE2 and the Development of Selective BACE Inhibitors. *ACS Chem Neurosci.* (2021); 12(4):581-588. <https://doi.org/10.1021/acscchemneuro.0c00629>.
- [57] Evin G. Future Therapeutics in Alzheimer's Disease: Development Status of BACE Inhibitors. *BioDrugs.* (2016); 30(3):173-94. <https://doi.org/10.1007/s40259-016-0168-3>. PMID: 27023706.
- [58] Iraj, Aida, Mahsima Khoshneviszadeh, Omidreza Firuzi, Mehdi Khoshneviszadeh, Najmeh Edraki. Novel small molecule therapeutic agents for Alzheimer disease: Focusing on BACE1 and multi-target directed ligands. *Bioorg. Chem.* 97 (2020): 103649. <https://doi.org/10.1016/j.bioorg.2020.103649>
- [59] Gehlot, Pinky, Sunil Kumar, Vivek Kumar Vyas, Bhanwar Singh Choudhary, Manish Sharma, Ruchi Malik. Guanidine-based β amyloid precursor protein cleavage enzyme 1 (BACE 1) inhibitors for the Alzheimer's disease (AD): A Review. *Bioorg. Med. Chem.* (2022): 117047. <https://doi.org/10.1016/j.bmc.2022.117047>
- [60] Haass, Christian, Christoph Kaether, Gopal Thinakaran, Sangram Sisodia. Trafficking and proteolytic processing of APP. *Cold Spring Harb. perspect. med.* 2 (2012). <https://doi.org/10.1101/2012.03.006270>
- [61] Nie P, Vartak A, Li YM. γ -Secretase inhibitors and modulators: Mechanistic insights into the function and regulation of γ -Secretase. *Semin Cell Dev Biol.* (2020); 105:43-53. <https://doi.org/10.1016/j.semcdb.2020.03.002>.
- [62] Hur JY. γ -Secretase in Alzheimer's disease. *Exp Mol Med.* (2022); 54(4):433-446. <https://doi.org/10.1038/s12276-022-00754-8>.
- [63] Henley DB, Sundell KL, Sethuraman G, Dowsett SA, May PC. Safety profile of semagacestat, a gamma-secretase inhibitor: IDENTITY trial findings. *Curr Med Res Opin.* (2014): 2021-32. <https://doi.org/10.1185/03007995.2014.939167>.
- [64] Wang D, Xu J, Liu B, He X, Zhou L, Hu X, Qiao F, Zhang A, Xu X, Zhang H, Wicha MS, Zhang L, Shao ZM, Liu S. IL6 blockade potentiates the anti-tumor effects of γ -secretase inhibitors in Notch3-expressing breast cancer. *Cell Death Differ.* (2018) ;25(2):330-339. <https://doi.org/10.1038/cdd.2017.162>.

- [65] Nordvall G, Lundkvist J, Sandin J. Gamma-secretase modulators: a promising route for the treatment of Alzheimer's disease. *Front Mol Neurosci.* (2023); 16:1279740. [https://doi:10.3389/fnmol.2023.1279740](https://doi.org/10.3389/fnmol.2023.1279740).
- [66] Bush, Ashley I., Rudolph E. Tanzi. Therapeutics for Alzheimer's disease based on the metal hypothesis. *Neurother.* 5 (2008): 421-432. <https://doi.org/10.1016/j.nurt.2008.05.001>
- [67] Ribeiro, Marta, Cátia A. Sousa, Manuel Simões. Harnessing microbial iron chelators to develop innovative therapeutic agents. *J. Adv. Res.* 39 (2022): 89-101. <https://doi.org/10.1016/j.jare.2021.10.010>
- [68] Siemers, E. Drug Development in AD: Point of View from the Industry. *J. Prev. Alzheimer's Dis.* 2 (2015): 216-218. <https://doi.org/10.14283/jpad.2015.80>
- [69] Henley, David B., Karen L. Sundell, Gopalan Sethuraman, Sherie A. Dowsett, Patrick C. May. Safety profile of semagacestat, a gamma-secretase inhibitor: IDENTITY trial findings. *Curr. Med. Res. Opin.* 30 (2014): 2021-2032. <https://doi.org/10.1185/03007995.2014.939167>
- [70] Becker, Robert E., Nigel H. Greig. Increasing the success rate for Alzheimer's disease drug discovery and development. *Expert Opin. Drug Discov.* 7 (2012): 367-370. <https://doi.org/10.1517/17460441.2012.672409>
- [71] Atri, Alireza, José L. Molinuevo, Ole Lemming, Yvonne Wirth, Irena Pulte, David Wilkinson. Memantine in patients with Alzheimer's disease receiving donepezil: new analyses of efficacy and safety for combination therapy. *Alzheimer's Res. Ther.* 5 (2013): 1-11. <https://doi.org/10.1186/alzrt160>
- [72] Barabási, Albert-László, Natali Gulbahce, Joseph Loscalzo. Network medicine: a network-based approach to human disease. *Nat. Rev. Genet.* 12 (2011): 56-68. <https://doi.org/10.1038/nrg2918>
- [73] Albertini, Claudia, Alessandra Salerno, Pedro de Sena Murteira Pinheiro, Maria L. Bolognesi. From combinations to multitarget-directed ligands: A continuum in Alzheimer's disease polypharmacology. *Med. Res. Rev.* 41 (2021): 2606-2633. <https://doi.org/10.1002/med.21699>
- [74] Li, Feifei, Changqi Zhao, Lili Wang. Molecular-targeted agents combination therapy for cancer: developments and potentials. *Int. J. Cancer.* 134 (2014): 1257-1269. <https://doi.org/10.1002/ijc.28261>

- [75] Maramai, Samuele, Mohamed Benchekroun, Moustafa T. Gabr, Samir Yahiaoui. Multitarget therapeutic strategies for Alzheimer's disease: Review on emerging target combinations. *Biomed. Res. Int.* 2020 (2020). <https://doi.org/10.1155/2020/5120230>
- [76] Ramsay, Rona R., Marija R. Popovic-Nikolic, Katarina Nikolic, Elisa Uliassi, Maria Laura Bolognesi. A perspective on multi-target drug discovery and design for complex diseases. *Clin. Transl. Med.* 7 (2018): 1-14. <https://doi.org/10.1186/s40169-017-0181-2>
- [77] Zhou, Junting, Xueyang Jiang, Siyu He, Hongli Jiang, Feng Feng, Wenyuan Liu, Wei Qu, Haopeng Sun. Rational design of multitarget-directed ligands: strategies and emerging paradigms. *J. Med. Chem.* 62 (2019): 8881-8914. <https://doi.org/10.1021/acs.jmedchem.9b00017>
- [78] Malafaia, Daniela, Hélio MT Albuquerque, Artur MS Silva. Amyloid- β and tau aggregation dual-inhibitors: A synthetic and structure-activity relationship focused review. *Eur. J. Med. Chem.* 214 (2021): 113209. <https://doi.org/10.1016/j.ejmech.2021.113209>
- [79] Mishra, Pankaj, Amit Kumar, Gautam Panda. Anti-cholinesterase hybrids as multi-target-directed ligands against Alzheimer's disease (1998–2018). *Bioorg. Med. Chem.* 27 (2019): 895-930. <https://doi.org/10.1016/j.bmc.2019.01.025>
- [80] Najafi, Zahra, Mina Saeedi, Mohammad Mahdavi, Reyhaneh Sabourian, Mahnaz Khanavi, Maliheh Barazandeh Tehrani, Farshad Homayouni Moghadam. Design and synthesis of novel anti-Alzheimer's agents: Acridine-chromenone and quinoline-chromenone hybrids. *Bioorg. Chem.* 67 (2016): 84-94. <https://doi.org/10.1016/j.bioorg.2016.06.001>
- [81] Deng, Youchao, Yuren Jiang, Xiongjie Zhao, Jinlian Wang. Design, Synthesize and Bio-Evaluate 1, 2-Dihydroisoquinolin-3 (4H)-One Derivates as Acetylcholinesterase and β -Secretase Dual Inhibitors in Treatment with Alzheimer's Disease. *J. Biosci. Med.* 4 (2016): 112. <https://doi.org/10.4236/jbm.2016.41014>
- [82] Kumar, Naveen, Vijay Kumar, Piyush Anand, Vinay Kumar, Ashish Ranjan Dwivedi, Vinod Kumar. Advancements in the development of multi-target directed ligands for the treatment of Alzheimer's disease. *Bioorg. Med. Chem.* 61 (2022): 116742. <https://doi.org/10.1016/j.bmc.2022.116742>

- [83] Sang, Zhipei, Keren Wang, Jiangong Dong, Lei Tang. Alzheimer's disease: updated multi-targets therapeutics are in clinical and in progress. *Eur. J. Med. Chem.* 238 (2022): 114464. <https://doi.org/10.1016/j.ejmech.2022.114464>
- [84] Kogen, Hiroshi, Narihiro Toda, Keiko Tago, Shinji Marumoto, Kazuko Takami, Mayuko Ori, Naho Yamada. Design and synthesis of dual inhibitors of acetylcholinesterase and serotonin transporter targeting potential agents for Alzheimer's disease. *Org. Lett.* 20 (2002): 3359-3362. <https://doi.org/10.1021/ol026418e>
- [85] He, Feng, Yingying Ran, Xiaoyang Li, Defeng Wang, Qiuqiong Zhang, Jiahui Lv, Chenggong Yu. Design, synthesis and biological evaluation of dual-function inhibitors targeting NMDAR and HDAC for Alzheimer's disease. *Bioorg. Chem.* 103 (2020): 104109. <https://doi.org/10.1016/j.bioorg.2020.104109>
- [86] Kaur, Sukhvir, Yogita Bansal. Design, molecular Docking, synthesis and evaluation of xanthoxylin hybrids as dual inhibitors of IL-6 and acetylcholinesterase for Alzheimer's disease. *Bioorg. Chem.* 121 (2022): 105670. <https://doi.org/10.1016/j.bioorg.2022.105670>
- [87] Lv, Peng, Chun-Li Xia, Ning Wang, Zhen-Quan Liu, Zhi-Shu Huang, Shi-Liang Huang. Synthesis and evaluation of 1, 2, 3, 4-tetrahydro-1-acridone analogues as potential dual inhibitors for amyloid-beta and tau aggregation. *Bioorg. Med. Chem.* 26 (2018): 4693-4705. <https://doi.org/10.1016/j.bmc.2018.08.007>
- [88] Iraj, Aida, Mahsima Khoshneviszadeh, Omidreza Firuzi, Mehdi Khoshneviszadeh, Najmeh Edraki. Novel small molecule therapeutic agents for Alzheimer disease: Focusing on BACE1 and multi-target directed ligands. *Bioorg. Chem.* 97 (2020): 103649. <https://doi.org/10.1016/j.bioorg.2020.103649>
- [89] Luo, Zonghua, Jianfei Sheng, Yang Sun, Chuanjun Lu, Jun Yan, Anqiu Liu, Hai-bin Luo, Ling Huang, Xingshu Li. Synthesis and evaluation of multi-target-directed ligands against Alzheimer's disease based on the fusion of donepezil and ebselen. *J. Med. Chem.* 56 (2013): 9089-9099. <https://doi.org/10.1021/jm401047q>
- [90] Rodríguez-Soacha, Diego Alejandro, Matthias Scheiner, Michael Decker. Multi-target-directed-ligands acting as enzyme inhibitors and receptor ligands. *Eur. J. Med. Chem.* 180 (2019): 690-706. <https://doi.org/10.1016/j.ejmech.2019.07.040>

- [91] Leon, Rafael, Antonio G. Garcia, José Marco-Contelles. Recent advances in the multitarget-directed ligands approach for the treatment of Alzheimer's disease. *Med. Res. Rev.* 33 (2013): 139-189. <https://doi.org/10.1002/med.20248>
- [92] Dorababu, Atukuri. Promising heterocycle-based scaffolds in recent (2019–2021) anti-Alzheimer's drug design and discovery. *Eur. J. Pharmacol.* 920 (2022): 174847. <https://doi.org/10.1016/j.ejphar.2022.174847>
- [93] Zhou, Junting, Xueyang Jiang, Siyu He, Hongli Jiang, Feng Feng, Wenyuan Liu, Wei Qu, Haopeng Sun. Rational design of multitarget-directed ligands: strategies and emerging paradigms. *J. Med. Chem.* 62 (2019): 8881-8914. <https://doi.org/10.1021/acs.jmedchem.9b00017>
- [94] Blaikie, Laura, Graeme Kay, Paul Kong Thoo Lin. Current and emerging therapeutic targets of alzheimer's disease for the design of multi-target directed ligands. *MedChemComm.* 10 (2019): 2052-2072. <https://doi.org/10.1039/c9md00337a>
- [95] Dolles, Dominik, Michael Decker. Dual-acting compounds acting as receptor ligands and enzyme inhibitors. In *Design of hybrid molecules for drug development*, pp. 137-165. Elsevier, 2017. <https://doi.org/10.1016/B978-0-08-101011-2.00005-2>
- [96] Alcaro, Stefano, Maria Laura Bolognesi, Alfonso T. García-Sosa, Simona Rapposelli. Multi-target-directed ligands (MTDL) as challenging research tools in drug discovery: From design to pharmacological evaluation. *Front. Chem.* 7 (2019): 71. <https://doi.org/10.3389/fchem.2019.00071>
- [97] Benchekroun, Mohamed, Samuele Maramai. Multitarget-directed ligands for neurodegenerative diseases: real opportunity or blurry mirage? *Future Med. Chem.* 11 (2019): 261-263. <https://doi.org/10.4155/fmc-2018-0249>
- [98] Talevi, Alan. Multi-target pharmacology: possibilities and limitations of the “skeleton key approach” from a medicinal chemist perspective. *Front. pharmacol.* 6 (2015): 205. <https://doi.org/10.3389/fphar.2015.00205>
- [99] Ramsay, R. R., M. R. Popovic-Nikolic, K. Nikolic, E. Uliassi, M. L. Bolognesi. A perspective on multi-target drug discovery and design for complex diseases. *Clin. Transl. Med.* 7 (2018). <https://doi.org/10.1186/s40169-017-0181-2>

- [100] Agis-Torres, Angel, Monica Sollhuber, Maria Fernandez, JM3915347 Sanchez-Montero. Multi-target-directed ligands and other therapeutic strategies in the search of a real solution for Alzheimer's disease. *Curr. Neuropharmacol.* 12 (2014): 2-36. <https://doi.org/10.2174/1570159X113116660047>
- [101] Csermely, Peter, Vilmos Agoston, Sandor Pongor. The efficiency of multi-target drugs: the network approach might help drug design. *Trends Pharmacol. Sci.* 26 (2005): 178-182. <https://doi.org/10.1016/j.tips.2005.02.007>
- [102] Arooj, Mahreen, Sugunadevi Sakkiah, Guang Ping Cao, Keun Woo Lee. An innovative strategy for dual inhibitor design and its application in dual inhibition of human thymidylate synthase and dihydrofolate reductase enzymes. *PloS one.* 8 (2013): e60470. <https://doi.org/10.1371/journal.pone.0060470>
- [103] Morphy, Richard, Zoran Rankovic. Designed multiple ligands. An emerging drug discovery paradigm. *J. Med. Chem.* 48 (2005): 6523-6543. <https://doi.org/10.1021/jm058225d>
- [104] Zhang, Pengfei, Shengtao Xu, Zheyang Zhu, Jinyi Xu. Multi-target design strategies for the improved treatment of Alzheimer's disease. *Eur. J. Med. Chem.* 176 (2019): 228-247. <https://doi.org/10.1016/j.ejmech.2019.05.020>
- [105] Baptista, Filipa I., Ana G. Henriques, Artur MS Silva, Jens Wiltfang, Odete AB da Cruz e Silva. Flavonoids as therapeutic compounds targeting key proteins involved in Alzheimer's disease. *ACS Chem. Neurosci.* 5 (2014): 83-92. <https://doi.org/10.1021/cn400213r>
- [106] To, Dao Cuong, Manh Hung Tran, Sang Ho Oh, Jeong Ah Kim, Md Yousof Ali, Mi-Hee Woo, Jae Sue Choi, Byung Sun Min. Isolation of cholinesterase and β -secretase 1 inhibiting compounds from *Lycopodiella cernua*. *Bioorg. Med. Chem.* 23 (2015): 3126-3134. <https://doi.org/10.1016/j.bmc.2015.04.080>
- [107] Nuthakki, Vijay K., Ankita Sharma, Ajay Kumar, Sandip B. Bharate. Identification of embelin, a 3-undecyl-1, 4-benzoquinone from *Embelia ribes* as a multitargeted anti-Alzheimer agent. *Drug Dev. Res.* 80 (2019): 655-665. <https://doi.org/10.1002/ddr.21544>
- [108] Paudel, Pradeep, Su Hui Seong, Yajuan Zhou, Manh Tuan Ha, Byung Sun Min, Hyun Ah Jung, Jae Sue Choi. Arylbenzofurans from the root bark of *Morus alba* as triple inhibitors of cholinesterase, β -site amyloid precursor protein cleaving enzyme 1, and glycogen synthase

kinase-3 β : Relevance to Alzheimer's disease. *ACS omega*. 4 (2019): 6283-6294. <https://doi.org/10.1021/acsomega.9b00198>

[109] Panche, Archana N., Sheela Chandra, A. D. Diwan. Multi-target β -protease inhibitors from *Andrographis paniculata*: in silico and in vitro studies. *Plants*. 8 (2019): 231. <https://doi.org/10.3390/plants8070231>

[110] Jannat, Susoma, Anand Balupuri, Md Yousof Ali, Seong Su Hong, Chun Whan Choi, Yun-Hyeok Choi, Jin-Mo Ku. Inhibition of β -site amyloid precursor protein cleaving enzyme 1 and cholinesterases by pterosins via a specific structure– activity relationship with a strong BBB permeability. *Exp. Mol. Med.* 51 (2019): 1-18. <https://doi.org/10.1038/s12276-019-0205-7>

[111] Lee, Jinhyuk, Mira Jun. Dual BACE1 and cholinesterase inhibitory effects of phlorotannins from *Ecklonia cava*—An in vitro and in silico study. *Mar. Drugs*. 17 (2019): 91. <https://doi.org/10.3390/md17020091>

[112] Omar, Syed Haris, Christopher J. Scott, Adam S. Hamlin, Hassan K. Obied. Biophenols: Enzymes (β -secretase, Cholinesterases, histone deacetylase and tyrosinase) inhibitors from olive (*Olea europaea* L.). *Fitoterapia*. 128 (2018): 118-129. <https://doi.org/10.1016/j.fitote.2018.05.011>

[113] Xu, Qing-Xia, Ying Hu, Gui-Yang Li, Wei Xu, Ying-Tao Zhang, Xiu-Wei Yang. Multi-target anti-Alzheimer activities of four prenylated compounds from *Psoralea Fructus*. *Molecules*. 23 (2018): 614. <https://doi.org/10.3390/molecules23030614>

[114] Blaikie, Laura, Graeme Kay, Paul Kong Thoo Lin. Current and emerging therapeutic targets of alzheimer's disease for the design of multi-target directed ligands. *MedChemComm*. 10 (2019): 2052-2072. <https://doi.org/10.1039%2Fc9md00337a>

[115] Wang, Huan, Haiyan Zhang. Reconsideration of anticholinesterase therapeutic strategies against Alzheimer's disease. *ACS Chem. Neurosci.* 10 (2018): 852-862. <http://dx.doi.org/10.1021/acchemneuro.8b00391>

[116] Camps, Pelayo, Xavier Formosa, Carles Galdeano, Diego Munoz-Torrero, Lorena Ramirez, Elena Gómez, Nicolás Isambert. Pyrano [3, 2-c] quinoline– 6-chlorotacrine hybrids as a novel family of acetylcholinesterase-and β -amyloid-directed anti-Alzheimer compounds. *J. Med. Chem.* 52 (2009): 5365-5379. <https://doi.org/10.1021/jm900859q>

- [117] Fernández-Bachiller, María Isabel, Concepción Pérez, Leticia Monjas, Jörg Rademann, María Isabel Rodríguez-Franco. New Tacrine–4-Oxo-4 H-chromene hybrids as multifunctional agents for the treatment of alzheimer’s disease, with cholinergic, antioxidant, and β -amyloid-reducing properties. *J. Med. Chem.* 55 (2012): 1303-1317. <https://doi.org/10.1021/jm201460y>
- [118] Zha, Xiaoming, Dorian Lamba, Lili Zhang, Yinghan Lou, Changxu Xu, Di Kang, Li Chen. Novel tacrine–benzofuran hybrids as potent multitarget-directed ligands for the treatment of Alzheimer’s disease: design, synthesis, biological evaluation, and X-ray crystallography. *J. Med. Chem.* 59 (2016): 114-131. <https://doi.org/10.1021/acs.jmedchem.5b01119>
- [119] Viayna, Elisabet, Tània Gómez, Carles Galdeano, Lorena Ramírez, Míriam Ratia, Albert Badia, M. Victòria Clos. Novel Huprine Derivatives with Inhibitory Activity toward β -Amyloid Aggregation and Formation as Disease-Modifying Anti-Alzheimer Drug Candidates. *ChemMedChem*. 5 (2010): 1855-1870. <https://doi.org/10.1002/cmdc.201000322>
- [120] Gabr, Moustafa T., Mohammed S. Abdel-Raziq. Design and synthesis of donepezil analogues as dual AChE and BACE 1 inhibitors. *Bioorg. Chem.* 80 (2018): 245-252. <https://doi.org/10.1016/j.bioorg.2018.06.031>
- [121] Costanzo, Paola, Luca Cariati, Doriana Desiderio, Roberta Sgammato, Anna Lamberti, Rosaria Arcone, Raffaele Salerno, Monica Nardi, Mariorosario Masullo, Manuela Oliverio. Design, synthesis, and evaluation of donepezil-like compounds as AChE and BACE 1 inhibitors. *ACS Med. Chem. Lett.* 7 (2016): 470-475. <http://dx.doi.org/10.1021/acsmedchemlett.5b00483>
- [122] Sharma, Piyooosh, Avanish Tripathi, Prabhash Nath Tripathi, Santosh Kumar Prajapati, Ankit Seth, Manish Kumar Tripathi, Pavan Srivastava, Vinod Tiwari, Sairam Krishnamurthy, Sushant Kumar Shrivastava. Design and development of multitarget-directed N-Benzylpiperidine analogs as potential candidates for the treatment of Alzheimer’s disease. *Eur. J. Med. Chem.* 167 (2019): 510-524. <https://doi.org/10.1016/j.ejmech.2019.02.030>
- [123] Zhu, Yiping, Kun Xiao, Lanping Ma, Bin Xiong, Yan Fu, Haiping Yu, Wei Wang. Design, synthesis and biological evaluation of novel dual inhibitors of acetylcholinesterase and

β -secretase. *Bioorg. Med. Chem.* 17 (2009): 1600-1613.
<https://doi.org/10.1016/j.bmc.2008.12.067>

[124] Tripathi, Avanish, Priyanka Kumari Choubey, Piyooosh Sharma, Ankit Seth, Poorvi Saraf, Sushant Kumar Shrivastava. Design, synthesis, and biological evaluation of ferulic acid based 1, 3, 4-oxadiazole hybrids as multifunctional therapeutics for the treatment of Alzheimer's disease. *Bioorg. Chem.* 95 (2020): 103506.
<https://doi.org/10.1016/j.bioorg.2019.103506>

[125] Tripathi, Avanish, Priyanka Kumari Choubey, Piyooosh Sharma, Ankit Seth, Prabhash Nath Tripathi, Manish Kumar Tripathi, Santosh Kumar Prajapati, Sairam Krishnamurthy, Sushant Kumar Shrivastava. Design and development of molecular hybrids of 2-pyridylpiperazine and 5-phenyl-1, 3, 4-oxadiazoles as potential multifunctional agents to treat Alzheimer's disease. *Eur. J. Med. Chem.* 183 (2019): 111707.
<https://doi.org/10.1016/j.ejmech.2019.111707>

[126] Belluti, Federica, Angela De Simone, Andrea Tarozzi, Manuela Bartolini, Alice Djemil, Alessandra Bisi, Silvia Gobbi. Fluorinated benzophenone derivatives: balanced multipotent agents for Alzheimer's disease. *Eur. J. Med. Chem.* 78 (2014): 157-166.
<https://doi.org/10.1016/j.ejmech.2014.03.042>

[127] Mphahlele, Malose J., Emmanuel N. Agbo, Samantha Gildenhuis. Synthesis and evaluation of the 4-substituted 2-hydroxy-5-iodochalcones and their 7-substituted 6-iodoflavonol derivatives for inhibitory effect on cholinesterases and β -secretase. *Int. J. Mol. Sci.* 19 (2018): 4112. <https://doi.org/10.3390/ijms19124112>

[128] Mphahlele, Malose J., Samantha Gildenhuis, Emmanuel N. Agbo. *In Vitro* Evaluation and Docking Studies of 5-oxo-5 H-furo [3, 2-g] chromene-6-carbaldehyde Derivatives as Potential Anti-Alzheimer's Agents. *Int. J. Mol. Sci.* 20 (2019): 5451.
<https://doi.org/10.3390/ijms20215451>

[129] Mphahlele, Malose J., Emmanuel N. Agbo, Samantha Gildenhuis, Itumeleng B. Setshedi. Exploring biological activity of 4-oxo-4 H-furo [2, 3-h] chromene derivatives as potential multi-target-directed ligands inhibiting cholinesterases, β -secretase, cyclooxygenase-2, and lipoxygenase-5/15. *Biomolecules.* 9 (2019): 736. <https://doi.org/10.3390/biom9110736>

[130] Mohamed, Tarek, Jacky CK Yeung, Maryam S. Vasefi, Michael A. Beazely, Praveen PN Rao. Development and evaluation of multifunctional agents for potential treatment of

Alzheimer's disease: application to a pyrimidine-2, 4-diamine template. *Bioorganic Med. Chem. Lett.* 22 (2012): 4707-4712. <https://doi.org/10.1016/j.bmcl.2012.05.077>

[131] Huang, Wenhai, Li Tang, Ying Shi, Shufang Huang, Lei Xu, Rong Sheng, Peng Wu, Jia Li, Naiming Zhou, Yongzhou Hu. Searching for the multi-target-directed ligands against Alzheimer's disease: discovery of quinoxaline-based hybrid compounds with AChE, H3R and BACE 1 inhibitory activities. *Bioorg. Med. Chem.* 19 (2011): 7158-7167. <https://doi.org/10.1016/j.bmc.2011.09.061>

[132] Sun, Zhi-Qing, Li-Xiang Tu, Feng-Juan Zhuo, Song-Xia Liu. Design and discovery of Novel Thiazole acetamide derivatives as anticholinesterase agent for possible role in the management of Alzheimer's. *Bioorganic Med. Chem. Lett.* 26 (2016): 747-750. <https://doi.org/10.1016/j.bmcl.2016.01.001>

[133] Jain P, Wadhwa PK, Rohilla S, Jadhav HR. Rational design, synthesis and in vitro evaluation of allylidene hydrazinecarboximidamide derivatives as BACE-1 inhibitors. *Bioorg Med Chem Lett.* (2016); 26(1):33-7. <https://doi: 10.1016/j.bmcl.2015.11.044>.

[134] Sharma A, Bharate SB. Synthesis and Biological Evaluation of Coumarin Triazoles as Dual Inhibitors of Cholinesterases and β -Secretase. *ACS Omega.* (2023); 8(12):11161-11176. <https://doi: 10.1021/acsomega.2c07993>.

[135] Ellman, George L., K.Diane Courtney, Valentino Andres, and Robert M. Featherstone. A New and Rapid Colorimetric Determination of Acetylcholinesterase Activity. *Biochemical Pharmacology*, (1961): 88-95. [https://doi.org/10.1016/0006-2952\(61\)90145-9](https://doi.org/10.1016/0006-2952(61)90145-9).

7. Appendixes

List of publications

- **Amit Sharma**, Santosh Rudrawar, Ankita Sharma, Sandip B. Bharate and Hemant R. Jadhav. "Design, synthesis, *in-silico*, and *in-vitro* evaluation of pyrrol-2-yl-phenyl allylidene hydrazine carboximidamide derivatives as AChE/BACE 1 dual inhibitors." *RSC Advances*, 2024, 14, 26703-26722.
- **Amit Sharma**, Santosh Rudrawar, Ankita Sharma, Sandip B. Bharate and Hemant R. Jadhav. "Unveiling the potential of novel indol-3-yl-phenyl allylidene hydrazine carboximidamide derivatives as AChE/BACE 1 dual inhibitors: A combined *in-silico*, synthesis and *in-vitro* studies." *RSC Advances*, 2024, 14, 23853-23872.
- **Amit Sharma**, Santosh Rudrawar, and Hemant R. Jadhav. "Butadiene Sulfone-catalyzed Monobromination of Arenes with NBS as the Bromination Source: A Simple, Mild, Efficient, and Chemoselective Protocol." *Letters in Organic Chemistry*, 2023, 21 (2), 201-208.
- **Amit Sharma**, Jadhav R. Hemant, Rai Anubhav, Lakkaniga Rajiv Naga, Chandramoorthy C. Harish, Kamli Mohammed Hossam, Alshahrani Y. Mohammad and Rajagopalan Prasanna. "A Comprehensive Review of Systemic Targeted Therapies in Cancer Treatment." *Current Cancer Therapy Reviews*, 2023, doi: 10.2174/0115733947261058231017170056.
- **Amit Sharma**, Santosh Rudrawar, Sandip B. Bharate and Hemant R. Jadhav. "Recent advancements in the therapeutic approaches for Alzheimer's disease treatment: Current and future perspective." *RSC Medicinal Chemistry* **{Under Revision}**
- **Amit Sharma**, Sonali J. Jain, Prabhat Nath Jha, Santosh Rudrawar, Sandip B. Bharate and Hemant R. Jadhav. "Unfolding the potential of pyrrole and indole-based guanidine derivatives as antimicrobial agents: Design, synthesis, and *in-vitro* evaluation." **{Under communication}**

List of Workshops/ Symposium/Conferences/Presentation attended

- Amit Sharma, Sonali J. Jain, Prabhat Nath Jha and Hemant R. Jadhav, Poster presentation on “Discovery of novel allylidene hydrazine carboximidamide as potent antimicrobial agents” at RTCDD 2023, organized by BITS, PILANI.
- Participated in the Lab India Analytical Instruments Pvt. Ltd. Bangalore sponsored workshop on “Applications of FTIR and 2D NMR in Pharmaceutical Research”, held at Birla Institute of Technology and Science, Pilani, 2022.
- Attended virtual workshop on “Introduction to Pharmacophore Modelling and Protein-Ligand Interactions: SeeSAR Software”, held at Birla Institute of Technology and Science, Pilani, 2022.
- Successfully completed workshop on “Biosafety and Biohazards” conducted by Institute Biosafety Committee, held at Birla Institute of Technology and Science, Pilani, 2022.
- Attended “Virtual Conference on Pharmacy: Always trusted for your health” organized by Department of Pharmacy, held at Birla Institute of Technology and Science, Pilani, 2021.
- Participated in the “International virtual conference on Computer-Aided Drug Design” organized by Department of Pharmacy, BITS Pilani, Pilani campus, held on 2020.
- Participated in the “International Virtual Conference on Drug Discovery and Delivery “ organized by Department of Pharmacy, BITS Pilani, Pilani campus, held on 2020.
- Attended a webinar on “The People and The Principles Behind Nature- The What, The Why and The How” organized by Springer Nature in collaboration with INFLIBNET Centre, held on 2020.
- Participated in the “Virtual Conference on Regulatory Aspects and Intellectual Property Rights in Pharmaceuticals “ organized by Department of Pharmacy, BITS Pilani, Pilani campus, held on 2020.
- Successfully completed 3 days’ workshop on “Drug Discovery, Designing and Development” conducted by IIT Kharagpur, held at Department of Pharmaceutical Sciences and Technology, Birla Institute of Technology, Mesra, Ranchi, 2019.

BRIEF BIOGRAPHY OF THE SUPERVISOR

Dr. Hemant R Jadhav is presently working as a Professor at the Department of Pharmacy, BITS Pilani, Pilani Campus. He received his M.S. (Pharm) and Ph.D. degrees from the National Institute of Pharmaceutical Education and Research (NIPER), Mohali, India. He has been involved in research for the last 24 years and in teaching for the last 20 years. His research area is Pharmaceutical Chemistry, particularly the design, synthesis, and evaluation of anti-Alzheimer, anti-cancer, anti-HIV compounds and compounds for diabetic cardiomyopathy. He has successfully completed several research projects sponsored by DST, UGC, and the industry. Presently, he has a SERB CRG and an ICMR project as Principal Investigator. He is also a co-investigator in a DBT BUILDER project worth 9.2 crores. He has supervised seven Ph. D students, and seven students are pursuing Ph.D. under his guidance. He has authored more than 70 research papers and 3 book chapters and has edited one book (Principles of Research Methodology and Ethics in Pharmaceutical Sciences: An Application Guide for Students and Researchers). His work is presented at more than 50 national and international conferences. He is a member of the Board of Studies, a member of the Academic Council, and an external DRC member of various Universities. He also is an expert reviewer of many national and international journals. At BITS Pilani, Pilani campus, he has served in various administrative positions such as Head of the department, Associate dean, Academic Research (Ph. D. Programme) division, and sponsored research and consultancy division for many years.

BRIEF BIOGRAPHY OF THE CO-SUPERVISOR

Dr. Santosh Rudrawar is presently the Group Leader, Menzies Health Institute Queensland, Griffith University, Australia and Program Director – Bachelor of Pharmacology and Toxicology at Griffith University. Before joining Griffith, he was ARC DECRA Fellow and Lecturer, The University of Sydney from 2014 to 2015.

He did his Masters in 2001 and joined Discovery Research at Dr Reddy's Laboratories for two years. After that, he did Ph.D. from NIPER Mohali followed by postdoctoral fellowships from 2008-2013. He has more than 45 publications to his credit.

BRIEF BIOGRAPHY OF THE CANDIDATE

Amit Sharma is pursuing Ph.D. in Medicinal Chemistry from Birla Institute of Technology and Sciences, Pilani (BITS Pilani), Pilani campus, Rajasthan, India. He has completed B. Pharmacy in 2017, from Dr. A.P.J Abdul Kalam Technical University, Lucknow. He completed his M.Pharm. in Pharmaceutical Chemistry from Birla Institute of Technology, Mesra (BIT Mesra), Mesra campus, Jharkhand, India, 2019. In Masters, he has worked in the field of antimicrobial drug design and development under the supervision of Prof. Swastika Ganguly, Professor, Ex. Head, Department of Pharmaceutical Sciences, BIT, Mesra, Ranchi, India. He joined Ph.D. programme at BITS Pilani, Pilani Campus, under the supervision of Prof. Hemant R. Jadhav, Professor, Department of Pharmacy, BITS Pilani, Pilani Campus in the year 2019. He is availing Institute research fellowship from BITS Pilani. His research interest includes the use of molecular modelling tools in the design of analogues, synthetic medicinal chemistry for the treatment of neurodegeneration. He has published numerous articles in peer reviewed journals.